Recombinant expression and characterization of a prokaryotic lipoxygenase from *Pseudomonas aeruginosa.* Investigations into the biological role of this enzyme

Inaugural-Dissertation
to obtain the academic degree
Doctor rerum naturalium (Dr. rer. nat.)
submitted to the Department of Biology, Chemistry and Pharmacy
of Freie Universität Berlin

by
SWATHI BANTHIYA
from Bangalore, India

2017

This work was carried out between 01.01.2014 and 16.02.2017 at the Institute for Biochemistry, Universitätsmedizin Berlin Charitè, under the supervision of Prof. Dr. sc. Med. Hartmut Kühn.

1st Reviewer: Prof. Rudolf Tauber
2nd Reviewer: Prof. Hartmut Kühn

Date of defence: 22.06.2017

ACKNOWLEDGEMENT

None of us got to where we are alone. Whether the assistance we received was obvious or subtle, acknowledging someone's help is a big part of understanding the importance of saying thank you. - Harvey Mackay

It has been a wholly gratifying experience, but the vast majority of it were the joy I received by working with Prof. Hartmut Kühn. He has been a great mentor. I am honored to have worked under him. He is an amazing teacher who made the journey of my doctoral studies enjoyable and at the same time extremely productive. I have learnt a lot from him that will stay with me for the rest of my life. He was always there when we needed his time and made sure we always excelled in anything we attempted to venture into.

Prof. Rudolf Tauber actively took interest in the progress of my project throughout. His valuable feedback and suggestions always motivated me to work better. I am grateful for his assistance and being a catalyst for achieving my goal. I am thankful to Dr. Dagmar Heydeck, Dr. Astrid Borchert and Dr. Christoph Ufer for their excellent scientific guidance throughout the tenure of my doctoral study and for constantly encouraging me in the most optimistic manner towards achieving my goals. A special mention goes to Mrs. Sabine Stehling, for her excellent technical guidance and for always patiently guiding me with new techniques. A memorable note to Maria, Marlena, Eugenia, Felix, Sajad, Sophia, and Ilya for being a part of and sharing my learning experiences.

In addition, I extend my thanks to Dr. Patrick Scheerer, Jacqueline Kalms, Etienne Galemou Yoga, Dr. Valerie O'Donnell, Dr. Maceler Aldrovandi, Prof. Mats Hamberg, Prof. Dr. Hermann-Georg Holzhütter and Dr. Igor Ivanov for their successful collaboration throughout the duration of my study.

To my parents, Dr. Ummed Singh Banthiya and Mrs. Surajkala Banthiya, I am forever indebted. My biggest supporters, Sandeep and Shruthi, a huge applause. To my husband, Aakash, my north star, I don't have enough words to express my gratitude to him. Lots of love to my nephews for being the best stress-busters ever. There are a lot more people who have helped me to reach where I am today and I would like to include all of them in my grace for being a part of my life and fueling my ambition.

TABLE OF CONTENTS

LIST OF ABBREVIATIONS

Abbreviation	Full form
Å	Angstrom, unit of Length
AA	Arachidonic acid
ALOX5	Arachidonate 5-lipoxygenase
ALOX12	Arachidonate 12-lipoxygenase
ALOX12B	Arachidonate 12-Lipoxygenase, 12R type
ALOX15	Arachidonate 15-lipoxygenase
ALOX15B	Arachidonate 15-lipoxygenase type 2
ALOXE3	Arachidonate lipoxygenase 3
bp	Base pairs
BSA	Bovine serum albumin
C	Carbon
cDNA	Complementary DNA
CL	Cardiolipin
COX	Cyclooxygenase
CP-HPLC	Chiral phase-HPLC
Da	Dalton (atomic mass unit) 1kDa = 1000Da
DGLA	Dihomo-γ-linolenic acid
DHA	Docosahexaenoic acid
DNA	Deoxyribonucleic acid
E.coli	*Escherichia coli*
EDTA	Ethylenediaminetetraacetic acid
EPA	Eicosapentaenoic acid
ESI	Electronspray ionisation
Fe	Iron
FLAP	5-lipoxygenase-activating protein
FPLC	Fast protein liquid chromatography
GC/MS	Gas chromatography/Mass spectroscopy
HEPES	2-[4-(2-hydroxyethyl)piperazin-1-yl]ethanesulfonic acid
5-HETE	5-Hydroxy-6*E*,8Z,11Z,14Z-eicosatetraenoic acid
5, 6- DiHETE	5,6-dihydroxy-8Z,11Z,14Z,17Z-eicosatetraenoic acid
5, 15-DiHETE	5,15-dihydroxy-6E,8Z,10Z,13E-eicosatetraenoic acid
8-HETE	8-Hydroxy-5Z,9E,11Z,14Z-eicosatetraenoic acid
11-HETE	11-hydroxy-5Z,8Z,12E,14Z-eicosatetraenoic acid
12-HETE	12-Hydroxy-5Z,8Z,10E,14Z-eicosatetraenoic acid
15-HETE	15-Hydroxy-5Z,8Z,11Z,13E-eicosatetraenoic acid
5-H(p)ETE	5-Hydroperoxy-6*E*,8Z,11Z,14Z-eicosatetraenoic acid

8-H(p)ETE	8-Hydroperoxy-5Z,9E,11Z,14Z-eicosatetraenoic acid
11-H(p)ETE	11-hydroperoxy-5Z,8Z,12E,14Z-eicosatetraenoic acid
12-H(p)ETE	12-Hydroperoxy-5Z,8Z,10E,14Z-eicosatetraenoic acid
15-H(p)ETE	15-Hydroperoxy-5Z,8Z,11Z,13E-eicosatetraenoic acid
9-HODE	9-hydroxy-10E,12Z-octadecadienoic acid
13-HODE	13-hydroxy-9Z,11E-octadecadienoic acid
HPLC	High pressure liquid chromatography
9-H(p)ODE	9-hydroperoxy-10E,12Z-octadecadienoic acid
13-H(p)ODE	13-hydroperoxy-9Z,11E-octadecadienoic acid
IC_{50}	Half maximal inhibitory concentration
IgG	Immunoglobulin G
IPTG	Isopropyl β-D-1-thiogalactopyranoside
15-KETE	15-oxo-5Z,8Z,11Z,13E-eicosatetraenoic acid
LA	Linoleic acid
LB	Luria Bertani-Medium
LC/MS	Liquid chromatography/Mass spectrometry
LDL	Low density lipoprotein
LOX	Lipoxygenase
LTs	Leukotrienes
LTA4	5S-trans-5,6-oxido-7E,9E,11Z,14Z-eicosatetraenoic acid
LTB4	5S,12R-dihydroxy-6Z,8E,10E,14Z-eicosatetraenoic acid
LTC4	5S-hydroxy-6R-(S-glutathionyl)-7E,9E,11Z,14Z-eicosatetraenoic acid
LTD4	5S-hydroxy-6R-(S-cysteinylglycinyl)-7E,9E,11Z,14Z-eicosatetraenoic acid
LTE4	5S-hydroxy-6R-(S-cysteinyl)-7E,9E,11Z,14Z-eicosatetraenoic acid
Lx	Lipoxin
M	Molar
MW	Molecular weight
m/z	Mass to charge ratio
NF-κB	nuclear factor kappa-light-chain-enhancer of activated B cells
OD	Optical density
opt	Optimum
PA	*Pseudomonas aeruginosa*
PAGE	Polyacrylamide gel electrophoresis
PBS	Phosphate buffered saline
PC	Phosphatidylcholine
PCR	Polymerase chain reaction

PDB	Protein data bank
8PE	(2R)-3-{[(S)-(2-aminoethoxy)(hydroxy)phosphoryl]oxy}-2-(tetradecanoyloxy)propyl octadecanoate
PE	Phosphatidylethanolamine
PEG	Polyethylene glycol
PI	Phosphatidylinositol
PLAT	Polycystin-1, Lipoxygenase, Alpha-Toxin
PS	Phosphatidylserine
PUFA	Polyunsaturated fatty acid
R_{free}	Free R-factor
RMSD	Root mean square deviation
R_{work}	Reliability factor
RP-HPLC	Reverse phase-HPLC
rpm	Rotations per minute
SDS	Sodium dodecyl sulfate
SEM	Standard error of the mean
SOC	Super optimal broth with catabolite repression
SP-HPLC	Straight phase-HPLC
TAE	Tris/Acetate/EDTA
TCA	Trichloroacetic acid
TEMED	Tetramethylethylenediamine
TLR	Toll-like-receptor
TMS	Trimethylsyl derivative
T_{opt}	Optimum temperature
Tris	2-Amino-2-(hydroxymethyl)-1,3-propanediol
TX-100	Triton X-100
UV	Ultra-violet
v/v	Volume per volume
WT	Wildtype
w/v	Weight per volume
ZPE	-(2R)-3-{[(S)-(2-aminoethoxy)(hydroxy) phosphoryl]oxy}-2-(tetradec-5-enoyloxy)propyl (11Z)-octadec-11-enoate

In addition to the abbreviations listed above, further symbols and units corresponding to the international unit system have been used.

1. INTRODUCTION

The integrity of cells depends on both, the functionality of membranes that separate its inside from the environment but also on the properties of the membranes that limit intracellular organelles. Typical biomembranes are composed of membrane proteins, membrane lipids and a minor share of carbohydrates (glycocallix in case of plasma membranes). The lipid compartment of biomembranes mainly consists of glycerophospholipids, sphingolipids and cholesterol. Glycerophospholipids are amphiphilic molecules containing two hydrophobic fatty acids attached to a glycerol. This glycerol moiety is connected via a phosphodiester bond to a polar head group. The phosphate and the polar head group constitute the hydrophilic part of the phospholipid molecule (Watson, 2015). The fatty acids of the membrane lipids are not only an important source of energy, but they also function as substrates for the biosynthesis of lipid hormones (Neitzel, 2010). Eicosanoids form such a class of bioactive lipid mediators (Dennis and Norris, 2015) and the oxygenation of polyunsaturated fatty acids into their hydroperoxy derivatives is the first step in the biosynthetic cascade of these compounds. Cyclooxygenases (COXs), cytochrome P450 isoenzymes (P450) and lipoxygenases (LOXs) (Dennis and Norris, 2015) have been identified as key enzymes in the biosynthesis of these mediators and inhibitors of these biocatalysts (COX1, COX2, ALOX5) are currently available for prescription for the treatment of inflammatory (Harel, 2004) and hypercoagulative disorders (Schafer, 1995). Arachidonic acid, one of the most abundant polyenoic fatty acids in humans, is converted to prostaglandins, prostacyclins and thromboxanes via the COX pathway (Dubois et al., 1998), to lipid epoxides and fatty acid diols by cytochrome P450 isoenzymes (Spector and Kim, 2015) and to leukotrienes (Savari et al., 2014), lipoxins (Romano, 2010), resolvins (Yoo et al., 2013), maresins (Serhan et al., 2012) and protectins (Serhan and Petasis, 2011) via the LOX pathway.

1.1. Lipoxygenases

1.1.1. History of lipoxygenases

LOXs, originally known to function as carotene oxidases, were discovered in plants, more than 80 years ago. In 1932, Andre and Hou identified an enzyme in

dried soybeans capable of oxidizing polyunsaturated fatty acids. They called this enzyme lipoxidase (Andre and Hou, 1932). In 1940, it was reported that the two catalytic activities (carotene oxidase and lipoxidase) are exhibited by one and the same enzyme (Sumner and Sumner, 1940). Finally, in 1947, Theorell et al. first characterized this enzyme and crystallized it (Theorell et al., 1947). Although LOXs were discovered quiet early, the progress of LOX research was rather slow. The major reason for this delay was the unclear biological function of these enzymes. Lipid peroxidation was generally considered a deleterious process, which leads to cellular dysfunction and even cell death. It remained totally unclear why nature would have introduced enzymes to catalyse lipid peroxidation. However, the interest in plant lipoxygenases continued over the years at low levels since these proteins could be used as bleaching enzymes in food- and agro-chemistry (Eskin et al., 1977).

For years, the presence of LOXs was considered to be restricted to plants and lipid peroxidation in animal tissues had been related to non-enzymatic heme-catalysed reactions (Tappel et al., 1953). In 1955 Rapoport and co-workers described in the cytosol of immature red blood cells (rabbit reticulocytes) a heat-labile catalytic activity capable of destroying mitochondrial membranes during *in vitro* incubations and named the corresponding enzyme as "mitochondrial lysis factor" (MLF) (Rapoport and Gerischer-Mothes, 1955). However, at that time it remained unclear what kind of enzyme MLF actually represented and from the chemical composition of biomembranes (membranes mainly consist of lipids and proteins), it was concluded that MLF might constitute a protease or a lipase. LOXs were not identified in animal tissues at that time and thus, MLF were not tested for LOX-activity. During the next couple of years MLF was purified and characterized with respect to its protein-chemical properties but its catalytic activity could not be identified. In the early 1970's, lipid peroxidation products were isolated when human blood platelets were incubated with arachidonic acid. Although the corresponding enzyme was not characterized at that time it was called a platelet type 12-LOX (Hamberg and Samuelsson, 1974). Several months later, Nugteren identified a soluble protein in the cytosol of blood platelets of several mammalian species capable of oxidizing arachidonic acid and other polyenoic fatty acids to hydroxylated derivatives and he called this enzyme platelet arachidonate lipoxygenase (Nugteren, 1975). These two reports marked

the starting point of animal LOX research, which developed into a major research area in biochemistry, pharmacology and medicine. Since biomembranes contain polyenoic fatty acids as essential structural components, Rapoport and co-workers explored whether MLF might exhibit lipoxygenase activity. These experiments were successful and in 1975 it was reported that rabbit reticulocytes contain a cytosolic LOX capable of oxidizing unsaturated phospholipids of mitochondrial membranes, which leads to a loss of membrane integrity and thus, to structural and functional decomposition of mitochondria (Schewe et al., 1975). After this, there was no looking back and during the subsequent years, LOXs have been identified in a large number of animal cells and tissues. Today we know that LOXs occur in two (eucarya, bacteria) of the three kingdoms of terrestrial life but the search for corresponding enzymes in archaea was not yet successful (Horn et al., 2015).

1.1.2. Distribution of lipoxygenases in terrestrial life

As indicated above LOX sequences have been detected in two of the three domains of terrestrial life (bacteria, eukarya) and more detailed information on different organisms containing LOX-like sequences are provided by Table 1.

In viruses, LOX-like sequences have been identified. However, most of them are either heavily truncated or lack amino acids (iron liganding residues) that are essentially required for the catalytic activity of functional enzymes. In the genome of the giant virus *Acanthamoeba polyphaga mimivirus,* a full length LOX sequence has recently been identified (Horn et al., 2015). However, expression of the recombinant protein indicated a lack of both, the catalytic non-heme iron and LOX activity (Gehring et al., unpublished data). Thus, for the time being no functional LOXs has been identified in viruses.

Although LOX-like sequences have been identified in several archaea species (third domain of terrestrial life) like *Halorubrum kocurii* and *Methanococcus voltae*, until date, no convincing data is available indicating the expression of catalytically active LOXs by these organisms. Like in viruses, most of these sequences are either strongly truncated or lack amino acids that are essentially required for the catalytic activity (Horn et al., 2015).

As it was in the case for animal LOX, it was believed for a long time that these enzymes do not occur in bacteria.

Table 1: Distribution of LOX-sequences in the three domains of life (modified from Ivanov et al., 2010; Hansen et al., 2013).
?? – Indicate ALOX-like sequences the functionality of which has not been tested.

Archaea

?? Methanococcus jannaschii
?? Methanococcus voltae
?? Halorubrum kocurii

Bacteria

Cyanobacteria: *Variovorax sp. CF313, Thiocapsa marina 5811, Cyanothece sp. ATCC 51142, Acaryochloris marina MBIC11017, Nostoc punctiforme PCC 73102, Nostoc sp. PCC 7120, Calothrix sp. PCC 63, Rivularia sp. PCC 7116, Oscillatoria acuminata PCC 6304, Anabaena cylindrica PCC 7122, Anabaena flos-aque, Cylindrospermum stagnale PCC 7417, Leptolyngbya sp. PCC 7375, Leptolyngbya sp. PCC 7376, Synechococcus sp. PCC 7335, Chamaesiphon minutus PCC 6605, Coleofasciculus chthonoplastes PCC 7420, Microcoleus vaginatus FGP-2, Microcystis aeruginosa PCC 9808, Oscillatoria nigro-viridis PCC 7112*
Proteobacteria: *Shewanella woodyi ATCC 51908, Shewanella woodyi ATCC 51908, Shewanella violacea DSS12, Shewanella denitrificans OS217, Pseudomonas aeruginosa 42 A2 NCIMB 40045, Myxococcus xanthus DK 1622, Nitrosomonas europaea ATCC 19718, Photobacterium profundum 3TCK, Burkholderia thailandensis E264, Burkholderia thailandensis Bt4, Citromicrobium bathyomarinum JL354, Corallococcus coralloides DSM 2259, Nitrosococcus watsonii C-113, Nitrosospira multiformis ATCC 25196, Plesiocystis pacifica SIR-1*
Bacteroidete: *Indibacter alkaliphilus LW1*

Eucarya

Animalia

Chordata
Ascidiace: *Cione intestinalis*
Leptocardii: *Branchiostoma floridae*
Actinopterygii: *Danio rerio, Salmo salar, Takifugu rubripes, Gasterosieus aculeatus*
Amphibia: *Ambystoma mexico, Xenopus laevis,*
Reptilia: *Anolis carolinensis*
Aves: *Gallus gallus*
Mammalia: *Bos Taurus, Tursiops truncates, Myotis lucifugus, Felis catus, Macropus eugenii, Omithorhyncus anatinus, Erinaceus europaeus, Choleopus hoffmanni, Loxodonta africana, Mus musculus, Equus caballus, Sus scrofa, Oryctolagus cuniculus, Homo sapiens*
Invertebrata
Placozoa: *Trichoplax adhaerens*
Cnidaria: *Gersemia fruticosa, Nematostella vectensis, Clavuraria viridis, Plexaura homomalla, Hydra magnipapillata*
Echinodermata: *Stronglycocentrus purpuratus*
Plathyhelminthes: *Schistosoma mansoni*
Arthropoda: *Ixodes scapularis*
Hemichordata: *Saccoglossus kowalevskii*

Plantae

Angiosperms/ Magnoliophyta
Monocots: *Oryza sativa, Sorghum bicolor, Triticum aestivum*
Eudicots: *Glycine max, Olea europsea, Betula pendula, Prunus persica, Vitis vinifera, Nicotiana tabacum, Arabidopsis thaliana, Camellia sinensis, Persea americana, Populus trichocarpa, Cucumis sativus, Citrus jambhiri*
Bryophyta: *Physcomitrella patens*

Protista

Rhodophyta: *Porphyra purpurea*
Chlorophyta: *Chlamydomonas reinhardtii , Ostreococcus lucimarinus*
Heterokontophyta: *Phytophtora infestans*
Mycetozoa: *Dictyostelium discoideum*

Fungi

Ascomycota: *Neurospora crassa, Aspergillus fumigatus, Sclerotinia sclerotiorum, Haematonectria*
Basidomycota: *Laccaria bicolor*

The major reason for this assumption was that the genome of the bacterial model organism *Escherichia coli* does not contain LOX-like sequences. However, the first bacterial lipoxygenase described was that of *Pseudomonas aeruginosa* (Shimahara, 1964; Shimahara and Hashizume, 1973) and at present this enzyme is the most comprehensively studied bacterial LOX. A systematic search of currently available genomic bacterial sequences (~13,000 bacterial genomes) for potential LOX-like sequences only revealed 60 hits, indicating that LOXs are not widely (<0.5 %) distributed among bacteria (Horn et al., 2015). This data indicates that LOX might not be essential for bacterial survival and pathology. In fact, most bacteria that cause infections in humans lack LOX genes (Horn et al., 2015).

In eukarya, functional lipoxygenases have been characterized in a wide variety of organisms. Functional LOXs have been identified in algae (red algae, green algae), (Zimmerman and Vick, 1973) and fungi (Su and Oliw, 1998). However, some human pathogenic fungi, such as *Candida albicans*, as well as the fungi model organism *Saccharomyces cerevisiae* do not carry functional LOX genes. In plants, numerous LOX isoforms have been characterized in both, lower plants like mosses (Siedow, 1991; Senger et al., 2005) and in large variety of higher flowering plants (eudicots and monocots) (Siedow, 1991).

In animals, functional LOX genes have been identified in many species that range from protozoans via metazoans to mammals including higher primates (Horn et al., 2015). In invertebrates functional LOX-isoforms have been characterized in lower marine organisms such as coral (Brash et al., 1996), sea urchin (Hawkins and Brash, 1987), starfish (Brash et al., 1991) and mussel (Hada et al., 1997; Coffa and Hill, 2000). However, *Drosophila melanogaster* and *Caenorhabditis elegans,* which are frequently employed as invertebrate model organisms do not carry functional LOX genes (Horn et al., 2015). Among lower cordata, genomic LOX-like sequences occasionally occur but functional characterization of the corresponding enzymes from *Florida lancelet*, sea squirts and sea lamprey is still pending. In higher cordates LOX-like sequences are more common and such sequences have been identified in the elephant shark (cartilaginous fish), zebra fish (bony fish), amphibians (Western clawed frog, African claw toads and bull frogs), reptiles (American alligator and snakes) and birds (chickens, turkey) (Horn et al., 2015). In mammals, functional LOX-genes have been described in rats, mice, hedgehogs, rabbits, pigs, cattle, rhesus monkeys, baboons, gibbons,

orangutans, chimpanzees as well as in recent (*H. sapiens*) and extinct (*H. neandertalenis*, *H. denisovan*) human subspecies (Ivanov et al., 2010; Horn et al., 2015). Completion of the human genome project indicated the existence of six functional LOX-genes (*ALOX15, ALOX15B, ALOX12, ALOX12B, ALOXE3, ALOX5*), which encode for the six functional LOX-isoforms. In addition, a corrupted pseudogene (*ALOXE12*) is present. Among these, *ALOX5* was localized on the short arm of chromosome 10, while the remaining ALOX genes were mapped to a joint LOX gene cluster located on the short arm of chromosome 17. The mouse genome involves single orthologs for all human LOX genes but in this species the *aloxe12* gene is functional (Funk et al., 2002).

1.1.3. Lipoxygenase reaction

LOXs are classified as a family of dioxygenases that catalyse the bioconversion of polyunsaturated fatty acids to their hydroperoxy derivatives. These enzymes contain one ion of non-heme iron at the catalytic center, which is essential for its enzymatic activity. When the iron is present in its ferrous (Fe^{2+}) form, LOXs are catalytically silent and need to be activated to function as catalyst. This activation is achieved by oxidizing the iron into its ferric form (Fe^{3+}) and a number of oxidizing agents are capable to do so (Pistorius and Axelrod, 1974; Funk et al., 1990b). In addition to iron-containing LOXs, there are manganese enzymes. The LOX from the fungus *Gäumannomyces graminis*, possess a manganese ion and for this enzyme a similar switch in the valency state of the transition metal has been implicated in the oxygenase reaction (Su and Oliw, 1998).

Formally, the LOX reaction (Figure 1) can be subdivided in four catalytic steps: 1) Hydrogen abstraction: The activated ferric (Fe^{3+}) LOX abstracts a hydrogen atom from a bisallylic methylene of the polyunsaturated fatty acid. Thus, for a fatty acid to be a substrate for LOX, it has to carry a minimum of two double bonds spaced by a methylene group. Hydrogen abstraction is the rate-limiting step of the LOX reaction and proceeds as electron coupled proton tunnelling (Lehnert and Solomon, 2003). 2) Radical rearrangement: The electron of the abstracted hydrogen reduces the enzyme-bound iron from the Fe^{3+} to Fe^{2+} and the proton is buffered by the medium. The resulting carbon-centred fatty acid radical can rearrange, which is associated with the formation of a *cis-trans* conjugated diene system. The direction of the radical rearrangement (n+2, rearrangement in

direction of the methyl terminus of the substrate; n-2 rearrangement in direction of the carboxylic terminus of the substrate) depends on the specificity of the enzyme.
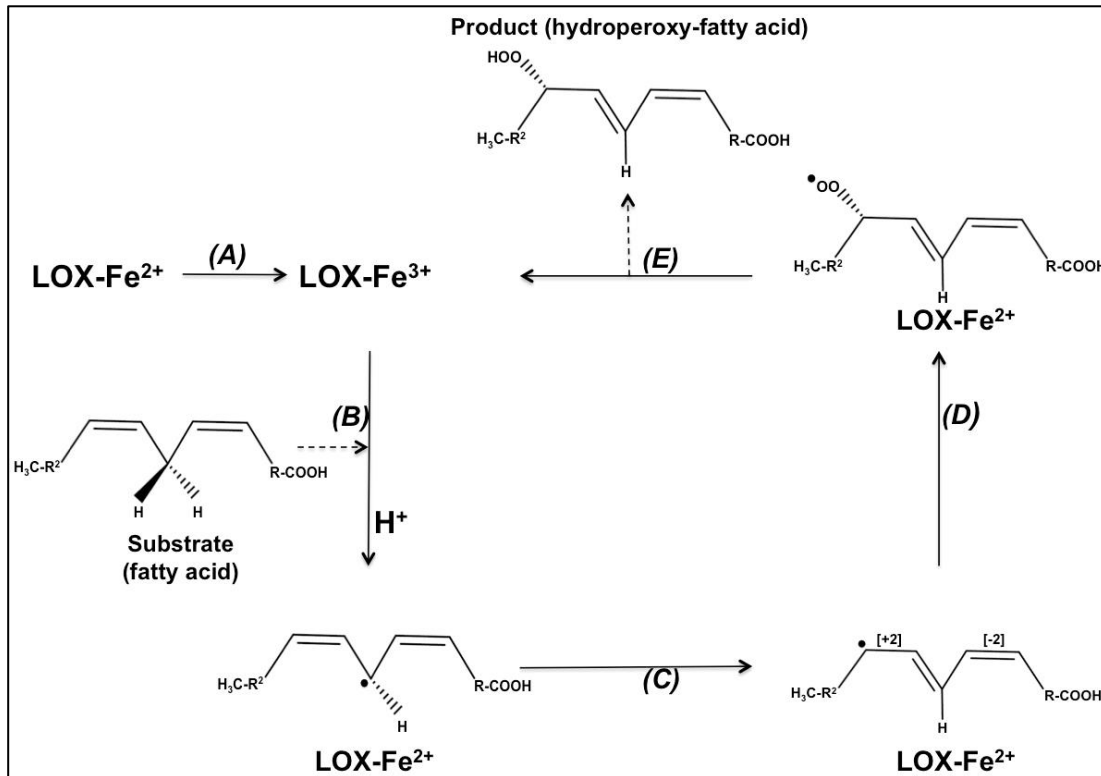
Figure 1: Steps involved in a lipoxygenase-catalyzed reaction. A) peroxide dependent activation of ferrous-LOX to ferric-LOX B) abstraction of hydrogen C) radical rearrangement D) oxygen insertion E) peroxy radical reduction (modified from Ivanov et al., 2015).

3) Oxygen insertion: The carbon-centred fatty acid radical then combines with atmospheric dioxygen to form an oxygen-centred peroxy radical. 4) Reduction of the peroxy radical: This peroxy radical is then reduced to the peroxy anion by picking up an electron from the enzyme-bound ferrous iron, which is re-oxidized to its ferric form. The peroxy anion is subsequently protonated (addition of a proton from the buffer) which completes the catalytic cycle (Haeggström and Funk, 2011).

1.1.4. Nomenclature of lipoxygenases

The nomenclature of lipoxygenases is very variable and somewhat confusing. Previously, the different animal lipoxygenase-isoforms were classified with respect to the position at which the oxygen molecule was inserted when

arachidonic acid is used as a substrate. According to this nomenclature 5-, 8-, 11-, 12- or 15-LOXs were differentiated. This method of classification was simple but had been discontinued because of several reasons (Ivanov et al., 2010, 2015). 1) For many non-mammalian lipoxygenases, arachidonic acid is not a good substrate; instead they prefer other polyenoic acids like linoleic acid as substrates (Porta and Rocha-Sosa, 2002). 2) Evolutionarily related LOX-isoforms of various species exhibit different positional specificities and thus, they are differently classified according to the specificity-based classification concept. This problem can be visualized if one compares human and mouse ALOX15. Both enzymes are functional orthologs, but exhibit different positional specificities. Human ALOX15 oxygenates arachidonic acid mainly at carbon 15 of arachidonic acid (Sloane et al., 1991b) while mouse alox15 catalyses arachidonic acid 12-lipoxygenation (Sun and Funk, 1996). Similarly, human ALOX15B and the corresponding mouse ortholog (alox15b) exhibit different reaction specificity although they are also functional orthologs. On the other hand, human ALOX15 and human ALOX15B exhibit similar reaction specificities although they are evolutionary far distant. To overcome these problems a similarity-based nomenclature concept was suggested, which classifies LOX isoforms according to their amino acid sequence homology with the corresponding human enzymes. This method of classification works well for all mammalian LOXs, but does not work properly for classification of evolutionary more distant organisms owing to a low degree of amino acid sequence conservation. For example, although a number of LOX genes have been identified in zebrafish, neither of them shares a high degree of amino acid conservation with human ALOX15 (Haas et al., 2011; Jansen et al., 2011).

In summary, despite the numerous attempts, a universally accepted nomenclature of LOXs is currently not available (Ivanov et al., 2010, 2015).

1.2. Biological role of LOX-isoforms

1.2.1. In mammals

Arachidonic acid (AA) and linoleic acid (LA) are the two most abundant polyenoic fatty acids found in mammalian cells that serve as efficient substrates for the different LOX-isoforms. Other LOX fatty acid substrates are alpha- and gamma-linolenic acid, eicosapentaenoic acid (EPA) and docosahexaenoic acid (DHA)

(Kuhn et al., 2015). Mammalian LOXs exhibit their biological function via three different proposed mechanistic approaches:

1) The primary products of the LOX reaction constitute reaction intermediates in the biosynthesis of lipid mediators such as leukotrienes (LTs) (Savari et al., 2014), lipoxins (Romano, 2010), hepoxins (Pace-Asciak, 2009), eoxins (Sachs-Olsen et al., 2010), resolvins (Yoo et al., 2013), protectins (Serhan and Petasis, 2011) and others. LTs are typical pro-inflammatory mediators that are produced from arachidonic acid via the ALOX5 pathway in leukocytes and other immune cells (Haeggström and Funk, 2011). Along this pathway arachidonic acid is first converted to 5S-H(p)ETE and then to leukotriene A4 (LTA4) by the catalytic activity of ALOX5 (Rådmark et al., 2007). The unstable LTA4 is further converted either to cysteinyl LTs (LTC4, LTD4, LTE4) by LTC4 synthase or cysteine-free LTs (LTB4) by LTA4 hydrolase. There are also additional non-LT ALOX5 products formed via the ALOX5 pathway such as 5-HETE and 5-oxo-ETE (Powell and Rokach, 2013) and these metabolites may also exhibit bioactivities. The cysteinyl LTs play essential roles in allergic disorders like allergic rhinitis (Cobanoğlu et al., 2013), pulmonary dysfunction (bronchial asthma) (Singh et al., 2013) and allergic diseases of the eye (Gane and Buckley, 2013). LTB4 is one of the most powerful pro-inflammatory stimulator of the innate immune response (Le Bel et al., 2014). After injury, it stimulates cellular aggregation, vascular permeability, chemotaxis, neutrophil adherence to the vessel wall (Palmblad et al., 1981) and activation of several pro-inflammatory cells (M1 macrophages) by initiating G-protein coupled intracellular signaling cascades when binding to cell surface receptors of target cells (Hicks et al., 2007; Yokomizo, 2011). Anti-inflammatory lipid mediators such as lipoxins (formed from AA) (Romano, 2010), resolvins and protectins (formed from EPA and DHA) (Serhan and Petasis, 2011) induce pro-resolving responses. They modify the cellular composition in the inflamed tissue by decreasing diapedesis of neutrophils. They normalize vascular permeability and induce apoptosis in neutrophils. Moreover, pro-inflammatory M1 macrophages are replaced with anti-inflammatory M2 cells aimed at cleaning up the inflamed tissue (Ereso et al., 2009; Ohira et al., 2010; El Kebir and Filep, 2013).

2) Several LOX-isoforms are capable of oxidizing complex lipid-protein assemblies (like biomembranes or lipoproteins) altering their structural and

functional properties in physiological processes like erythropoiesis (ALOX15) (Schewe et al., 1977) and epidermal differentiation (mice alox12b and aloxe3) (Epp et al., 2007; Krieg et al., 2013).
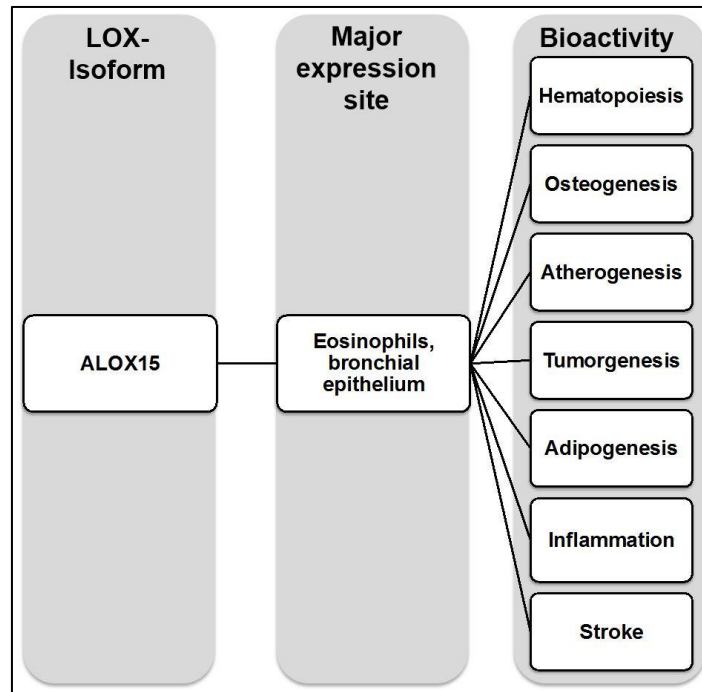
Figure 2: The bioactivity of mammalian ALOX15 isoforms. (Kelavkar et al., 2001; Zhao and Funk, 2004; Krönke et al., 2009a, 2009b; Pallast et al., 2010; Cole et al., 2013; Kuhn et al., 2015).

3) As lipid peroxidizing enzymes, LOXs modify the cellular redox-state. Regulation of cell proliferation and gene expression is governed by the maintenance of cellular redox equilibrium indicating that the LOXs activity may in turn modify the functional phenotype of the mammalian cells (Kuhn et al., 2015). Since the expression of several proto-oncogenes and tumor suppressor genes is also redox-dependent, LOX have also been implicated in carcinogenesis. In fact, various LOX-isoforms have been reported to exhibit both pro- and anti-carcinogenic properties especially in colorectal (ALOX5) (Wasilewicz et al., 2010) and prostrate carcinoma (ALOX5, ALOX12, ALOX15, ALOX15B) (Gupta et al., 2001; Kandouz et al., 2003; Kelavkar et al., 2006). Figure 2 indicates the physiological roles of mammalian ALOX15 isoforms. Although detailed clinical trials are yet to be carried out, the different mammalian LOX-isoforms seem to play active roles in the pathogenesis of several cardiovascular (ALOX5, ALOX15,

ALOX15B) and neurological (ALOX15) disorders (Kuhn et al., 2015).

1.2.2. In plants

Linoleic acid and linolenic acid are two major fatty acids in plant tissues and these fatty acids serve as efficient substrates for plant LOXs. The diversity of LOX products in plants has been related to the multiplicity of LOX-isoforms and to the variability of the peroxide metabolism (Porta and Rocha-Sosa, 2002). The predominant factors that induce expression of LOX genes in plants include infections (fungal or microbial), water deficiency, wounding, thermal injury (both heat and cold), ozone stress, mechanical treatment and ultraviolet irradiation (Grechkin, 1998). The fatty acid hydroperoxides derived from plant LOXs are further metabolized into oxylipins such as jasmonates (Mosblech et al., 2009), which regulate a number of physiological and patho-physiological processes:

1) Defense reaction in plant infection: LOX-derived hydroperoxy fatty acids, such as 13-H(p)ODE and 9-H(p)ODE, of *Arachis hypogaea* (peanuts) function as inhibitors and inducers for mycotoxin synthesis but the detailed mechanism remains elusive (Burow et al., 2000).

2) Vegetative growth and ripening: Plants LOXs (e.g. potato tubers LOXs) are essential in the development and growth of tubers by catalyzing the formation of oxylipins that play important roles in regulating cell growth during the formation of tubers (Kolomiets et al., 2001). The different LOX-isoforms in tomatoes are involved in fruit ripening and in the synthesis of C6 aldehydes that contribute to the taste and aroma of tomatoes. In addition, tomato fruit LOXs have been implicated in the degradation of the thylakoid membranes during the transition of chloroplast to chromoplast in tomatoes (Griffiths et al., 1999). Some LOXs (eg. in soybean leaves) are used as vegetative storage proteins (VSPs) that store excessive nitrogen (for the production of chlorophyll) and are completely different from the storage proteins found in plant seeds (Tranbarger et al., 1991; Fischer et al., 1999).

3) Wounds and herbivore attacks: Oxylipins synthesized by plant LOXs are essential for defense mechanisms. Among others are jasmonic acid and phytodienoic acid that behave as signaling molecules during wounding and pathogen attack (Siedow, 1991; Porta and Rocha-Sosa, 2002). Also, plant LOXs provides protection against herbivores (insects) by releasing several defense

molecules (eg. (Z)-3-hexenyl acetate) that in turn attract herbivore predators (Alborn, 1997).

4) Pathogen attack: Plants LOXs also provide defense against pests. Several LOX products (colneleic and colnelenic acid) of potatoes exhibit anti-microbial activities during infections (Weber et al., 1999).

1.2.3. In prokaryotes

Although a number of catalytically active LOX-isoforms have been identified in bacteria, their biological roles are largely unknown (Hansen et al., 2013). The absence of LOXs in most bacterial species and sequence comparison with eukaryotic LOXs suggested that there has not been a continuous development of bacterial LOXs. In fact, bacteria have acquired LOX sequences from eukaryotes via horizontal gene transfer (Porta and Rocha-Sosa, 2001) and have retained them as functional genes since then. Thus, for these bacterial species, there appears to be an evolutionary pressure on these sequences that has prevented inactivating mutations. Bacteria containing LOXs have been hypothesized to facilitate the dynamic plasticity of membranes that might provide a selective advantage for the bacteria during the colonization to different ecological niches. In order to maintain the plasticity and the functionality of bacterial membranes, it is important to maintain a (poly) unsaturated fatty acid containing environment around the bacteria (Hansen et al., 2013). Cyanobacteria are aquatic and photosynthetic bacteria that occur in many terrestrial ecosystems such as fresh water, marine environments, rocks or damp soil (Cohen and Gurevitz, 2006). It has been hypothesized that cyanobacterial LOXs might be involved in the metabolism of chloroplasts (Koeduka et al., 2007). Chloroplasts are rich in polyunsaturated fatty acids, making them suitable substrates candidates for LOXs. Polyenoic fatty acids have been proven to be efficient substrates for both plant and animal LOXs (Porta and Rocha-Sosa, 2002; Kuhn et al., 2015).

However, some bacterial species like *Pseudomonas aeruginosa* (PA) are devoid of polyenoic fatty acids and thus, they do not contain classical LOX substrates. In fact, the major fatty acids of many *P. aeruginosa* strains involve mono-unsaturated fatty acids, such as C18:1 (46.2 %), C16:1 (34.4%) and C16:0 (16.9 %) (Oliver and Colwell, 1973). These data suggest that the substrates for the

secreted *Pseudomonas aeruginosa*-lipoxygenase (PA-LOX) should come from its hosts' cells. PA-LOX is a secreted arachidonate 15-LOX that was discovered many years ago. Unfortunately, its biological roles still remains unknown (Vance et al., 2004). Based on the currently available data, the following biological roles of PA-LOX have been postulated:

1) PA-LOX might modulate host's inflammatory response: Although the PA-LOX activity is predominantly restricted to the periplasmic space of *P. aeruginosa*, significant amounts of active PA-LOX was also secreted to the surrounding medium via the Xcp type II secretion pathway. *P. aeruginosa* infections frequently occur in lung diseases, such as bronchial asthma and cystic fibrosis. Thus, it is possible that this bacterium produces lipoxins via the 15-LOX pathway to suppress host derived-inflammation and in turn provide itself with a favorable environment to survive throughout the chronic disorder in immunocompromised patients (Vance et al., 2004).

2) PA-LOX might increase the invasive capacity of *P. aeruginosa*: Interaction of LOX sufficient and deficient *P. aeruginosa* strains with human lung epithelial cells indicated that the introduction of LOX in the genome of *P. aeruginosa* increases the invasive capacity making the bacteria more infectious (Garreta et al., 2013). However, whether this effect on the *P. aeruginosa* virulence is due to the direct modification of the host cells' membrane integrity or by modulation of the host's inflammatory response via interference with the arachidonic acid cascade remains unknown.

3) PA-LOX might promote biofilm growth: A recent study has implicated PA-LOX in biofilm formation. However, PA-LOX was not required for biofilm growth in abiotic *in vitro* systems. The authors suggest that PA-LOX alters lipid signaling during host-pathogen interaction, which might impact the biofilm growth (Deschamps et al., 2016). Nonetheless, the molecular basis for this prediction and the PA-LOX products that trigger the biofilm formation still needs to be addressed in a more detail. Moreover, LOX-deficient bacteria such as *E. coli* are also capable of forming biofilms following alternative mechanisms (eg. autotransporter adhesins) (Beloin et al., 2008). Thus, the authors' interpretation that PA-LOX is required for biofilm growth requires further clarification with respect to bacteria that exhibit this ability in the absence of LOX.

1.3. Properties of lipoxygenases

Enzymes are proteins that catalyze a large number of chemical reactions in biological systems and the rates of these reactions depend on the structural characteristics of the proteins.

1.3.1. Protein-chemical properties of lipoxygenases

1.3.1.1. Structural properties of lipoxygenases

The open reading frame of the different mammalian LOX-isoforms indicated proteins in the range of ~600-700 amino acids (Brash, 1999; Haeggström and Funk, 2011). In contrast, soybean lipoxygenase is a protein with ~850 amino acids (Boyington et al., 1993). From the amino acid sequence data, the protein chemical properties of these enzymes can be concluded. The molecular mass of LOXs in animals range between 75-80 kDa, while in plants, it is in the range of 94-104 kDa (Brash, 1999). The recently described prokaryotic LOXs have their molecular masses in the range of 61-111 kDa (Hansen et al., 2013). Previous studies have indicated that although the molecular weight of human ALOX15 (74.67 kDa) is slightly lower when compared to rabbit ALOX15 (75.26 kDa), the human enzyme runs somewhat slower on the SDS-PAGE gel. The theoretical isoelectric point for human 15-LOX is 6.8 and 6.7 for rabbit enzyme. However, under native conditions, these two enzymes exhibited an isoelectric point of 5.5 (Rapoport et al., 1978; Kühn et al., 1993). Interestingly, a study done on the different LOX-isozymes in soybean leaves have identified one class of isozymes that exhibit neutral isoelectric points (ranging from pH 6.8 to 7.2) and another class of isozymes exhibiting rather acidic isoelectric points (ranging from pH 4.7 to 5.6) (Saravitz and Siedow, 1995).

The crystal structure of several LOXs has been solved. The first plant and mammalian LOXs whose crystal structures were solved were soybean LOX (Boyington et al., 1993) and rabbit ALOX15 respectively (Gillmor et al., 1997). Most lipoxygenases constitute a single polypeptide chain, which is folded into a two-domain structure. The N-terminal β- barrel domain consists of several parallel and anti-parallel β-strands but the larger C-terminal domain is mostly helical and involves the substrate-binding pocket. Figure 3 indicates the two domains in the structure of human ALOX15B.
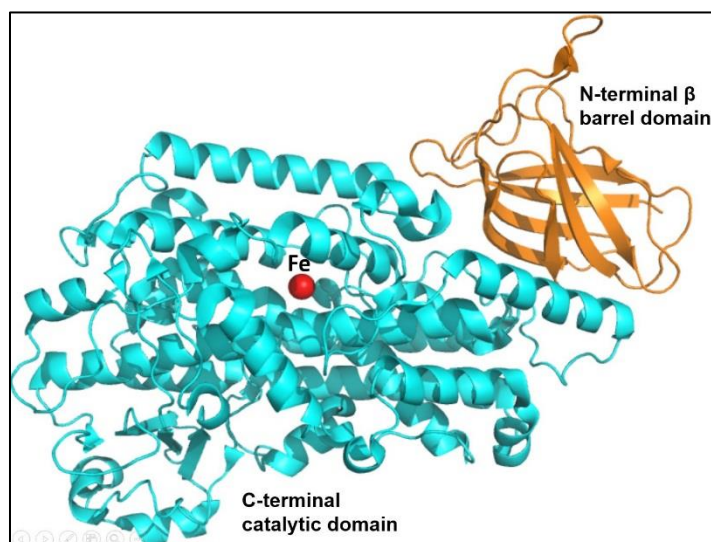
Figure 3. Structure of human ALOX15B (PDB ID: 4NRE) (Kobe et al., 2014). Orange: N-terminal β- barrel domain; cyan: C-terminal catalytic domain; red sphere: iron atom.

The structure of rabbit ALOX15 and coral 8*R*-LOX resembles an elliptic cylinder while the soybean LOX1 resembles an elliptic spheroid (Ivanov et al., 2010). In lower organisms LOXs can also occur as fusion proteins (Koljak et al., 1997; Lõhelaid et al., 2008). For soybean LOX1 and rabbit ALOX15, the β-domain consists of first N-terminal 146 and 110 amino acids respectively. Because of its similarity to the C2-domain of lipases, the N-terminal domain of both plants and animal LOXs has been implicated in membrane binding and in activity regulation. A study on several truncated mammalian-LOXs indicated that the N-terminal domain may not be essential for catalytic activity of all LOXs and has hardly any impact on reaction specificity of LOXs (Walther et al., 2011). The two domains of eukaryotic LOXs are typically interconnected by a flexible oligopeptide (Ivanov et al., 2010; Kuhn et al., 2015). The C-terminal catalytic domain involves the non-heme iron located in the putative substrate-binding pocket. The C-terminal core of the soybean LOX1 represents a multi-helix bundle with two anti-parallel β-sheets (Minor et al., 1996). The catalytic domain of rabbit ALOX15 on the other hand consists of 21 helices interrupted by a small β-sheet sub-domain (Gillmor et al., 1997). The crystal structures of various LOXs indicated that the non-heme iron is octahedrally coordinated by 6 ligands. These include water molecule or hydroxyl group and five amino acid side chains. Three conserved histidines, the largely conserved C-terminal isoleucine and a variable amino acid that differs in the LOXs from different species (Brash, 1999).

Pseudomonas aeruginosa lipoxygenase (PA-LOX) was the first bacterial LOX that was crystallized (Garreta et al., 2011) and detailed investigations have indicated remarkable structural and functional differences to the eukaryotic isoforms. In place of the N-terminal β-barrel domain of the eukaryotic LOXs, PA-LOX has an insertion of ~100 amino acids. These amino acids form a pair of long anti-parallel helices that act as a lid to its large substrate-binding pocket. Also, the crystal structure of PA-LOX indicated a bifurcated substrate-binding pocket that was big enough to accommodate a complete phosphatidylethanolamine molecule with a C18 (at sn-1 position) and a C14/16 (at sn-2-position) fatty acid linked to the polar head group. This phospholipid was spontaneously incorporated into the holoenzyme during recombinant expression of the protein and was retained at the active site throughout the entire purification procedure (Garreta et al., 2013). Similar to plants, the iron ligands for PA-LOX also included three histidines, one aspargine, a C-terminal isoleucine and a water/hydroxyl molecule (Garreta et al., 2013).

1.3.1.2. Mutant variants of lipoxygenases

Human ALOX15 (Kühn et al., 1993) and the ALOX15 orthologs of rabbits (Bryant et al., 1982) and orangutans (Vogel et al., 2010) convert arachidonic acid to 12*S*- and 15*S*-H(p)ETE in a ratio of 1:10. On the contrary, the mouse (Freire-Moar et al., 1995), rat (Watanabe and Haeggström, 1993), pig (Yoshimoto et al., 1990), cattle (De Marzo et al., 1992) and rhesus monkey ALOX15 orthologs (Vogel et al., 2010) form an inverse product pattern (12- and 15-H(p)ETE in a ratio of 10:1). The molecular basis of the different reaction specificities of ALOX15 orthologs has been extensively studied (Ivanov et al., 2010). Multiple sequence alignment of various 12- and 15-lipoxygenating enzymes have indicated that when the amino acids at positions 416, 417 and 418 of human ALOX15 (15-lipoxygenating) were mutated to smaller residues, a 12-lipoxygenating ALOX15 variant was created. This data suggested that the region around these amino acids might impact the substrate alignment at the active site (Sloane et al., 1991a). Similar strategies were also employed for rabbit and mouse ALOX15 orthologs and the data of these experiments led to the development of the triad concept of positional specificity (Borngräber et al., 1996, 1999). According to this hypothesis, the triad amino acids consisting of Phe353 (Borngräber-1 determinant), Ile418/Met419

(Sloane determinants) (Sloane et al., 1991a, 1995) and Ile593 (Borngräber-2 determinant) (Borngräber et al., 1999) (numbers according to rabbit ALOX15) contribute to the positional specificity of ALOX15 orthologs. These residues were suggested to occupy the bottom of the substrate-binding pocket so that the geometry of their side-chains directly impacts the volume of the active site. Insertion of smaller residues at these positions in the 15-lipoxygenating human ALOX15 enables arachidonic acid to penetrate deeper into the pocket, which favors arachidonate 12-lipoxygenation (Sloane et al., 1991a; Vogel et al., 2010). Inversely, the 12-lipoxygenating mouse alox15 can be converted to a 15-lipoxygenating enzyme by a Leu353Phe (insertion of a bulkier residue) exchange (Borngräber et al., 1996). Multiple site directed mutagenesis studies carried out for the 12- and 15-lipoxygenating ALOX15 orthologues of pig (Suzuki et al., 1994), man (Sloane et al., 1995), rabbit (Borngräber et al., 1999), rhesus monkey (Vogel et al., 2010), orangutan (Vogel et al., 2010), rat (Pekárová et al., 2015) and gibbon (Adel et al., 2016) indicate that these orthologs follow this concept.

The triad concept explains the reaction specificities of mammalian ALOX15 orthologs, of human ALOX12 and of human ALOX5 (Vogel et al., 2010). However, it is not applicable to human and mouse ALOX15B (Vogel et al., 2010) and mouse alox12b (Meruvu et al., 2005). Human ALOX15B exhibits a single positional specificity converting arachidonic acid predominantly to 15S-H(p)ETE (Brash et al., 1997). On the other hand, the mouse enzyme which shares a high degree of sequence conservation with the human ortholog, oxygenates arachidonic acid to 8S-H(p)ETE (Jisaka et al., 1997). Site directed mutagenesis of Asp602 and Val603 (Jisaka determinants) of human ALOX15B to the corresponding amino acids present at these positions in the mouse ortholog, Asp602Tyr+Val603His, resulted in a complete shift in the positional specificity of human ALOX15B. The double mutant exhibited a positional specificity of 70 % 8S-H(p)ETE and 30 % 15S-H(p)ETE. Similarly, when the 8-LOX mouse residues were mutated to the corresponding residues present in human ALOX15B (Try603Asp+His604Val), its positional specificity was converted from 8S- to 90 % 15S-arachidonic acid oxygenation (Jisaka et al., 2000). When the sequences of different mammalian ALOX15B orthologs (chimpanzee, gorilla, orangutan, rhesus monkey, pigs, baboon, rats) was compared, an Asp-Val/Asp-Ile motif was

found. These sequence data suggest that the ALOX15B orthologs of these species exhibit arachidonic acid 15-lipoxygenating activities (Kuhn et al., 2015). The regio-specificity of LOXs has been an area of focus of many studies and recent publications have hypothesized several factors that contribute to the mechanisms of the stereo-specificity that control a LOX-catalyzed reaction. The depth of the substrate binding pocket and the head-to-tail orientation of the substrate are both important factors (Coffa and Brash, 2004). A single amino acid residue controls the mechanism underlying the *R*- and *S*-stereospecificity exhibited by LOXs. Multiple sequence alignment of several LOX sequences suggested that most *S*-lipoxygenating enzymes carry an alanine (Ala) residue at a critical position (so-called 'Coffa site') in their primary structure. On the contrary, most *R*-lipoxygenating enzymes carry a glycine (Gly) at this site (Table 2). Several mutagenesis studies showed that an Ala to Gly exchange induced significant alterations in the enantioselectivity and positional specificity of several LOX-isoforms (Coffa and Brash, 2004; Coffa et al., 2005b; Schneider et al., 2007). After Ala to Gly exchange, human ALOX15B that converted arachidonic acid exclusively to 15*S*-HETE as wildtype enzyme now formed a 1.5:1 mixture of both 11*R*-HETE and 15*S*-HETE. On the contrary, after the Gly441Ala exchange, the human ALOX12B that only produced 12*R*-HETE as wildtype enzyme now converted arachidonic acid to 8*S*-HETE and 12*R*-HETE in a ratio of 1.4:1 (Coffa and Brash, 2004).

Recombinant mini-LOX from cyanobacterium *Nostoc (Anabaena) sp.* PCC7120 carries an alanine at the position, which aligns with the 'Coffa site'. However, it converted linoleic acid to 9*R*-HODE (Lang et al., 2008; Zheng et al., 2008) (Table 2). Interestingly, a substitution of this alanine by a larger valine resulted in a linoleic acid 13*S*-lipoxygenation (Zheng et al., 2008). Also, the *S*-lipoxygenating mouse alox12 carries a serine at this position instead of an alanine (Coffa and Brash, 2004). However, there is no experimental data yet to confirm if the exchange of the serine to a glycine alters the reaction specificity of this isoform. Although the molecular basis behind the observed specificity alterations is not yet clear, the amino acid side chain geometry has been postulated to impact intra-enzyme oxygen diffusion (Schneider et al., 2007). However, final proof of this concept is still pending.It should be stressed that only minor alterations in the reaction specificity were observed when the Ala-to-Gly exchanges were carried

out in ALOX15 orthologs (rabbit, rhesus monkeys, mice, human and orangutans) (Jansen et al., 2011).

Table 2: The amino acid residue at the Coffa positions of different LOX isoforms (modified from Coffa and Brash, 2004).

Organism	S/R-LOX	Amino acid residue at the Coffa site	Reference
Human ALOX5	S	Alanine	(Funk et al., 1989)
Human ALOX12	S	Alanine	(Funk et al., 1990a)
Human ALOX15	S	Alanine	(Sigal et al., 1988)
Human ALOX15B	S	Alanine	(Brash et al., 1997)
Mouse alox5	S	Alanine	(Chen et al., 1995)
Mouse alox12e	S	Alanine	(Kinzig et al., 1997)
Mouse alox15	S	Alanine	(Martínez-Clemente et al., 2010)
Rabbit ALOX15	S	Alanine	(Schewe et al., 1981)
Soybean LOX-1	S	Alanine	(Van Os et al., 1981)
Barley LOX-2	S	Alanine	(Bachmann et al., 2002)
Human ALOX12B	R	Glycine	(Boeglin et al., 1998)
Mouse alox12b	R	Glycine	(Krieg et al., 1999)
Coral 8-LOX	R	Glycine	(Brash et al., 1996)
Mouse alox12	S	Serine	(Siebert et al., 2001)
Zebrafish LOX1	S	Glycine	(Jansen et al., 2011)
Anabaena sp. PCC7120 mini LOX	R	Alanine	(Zheng et al., 2008)

Moreover, the zebrafish LOX-2, which carries a glycine at this position, was predicted to catalyze *R*-oxygenation. However, the recombinant protein converts arachidonic acid mainly to 12*S*-HETE (Haas et al., 2011; Jansen et al., 2011) indicating that this LOX-isoform does not adhere to the Ala-vs.-Gly concept.

Pseudomonas aeruginosa is a gram-negative bacterial pathogen, which is known for its high intrinsic resistance to antibiotics and for its ability to cause a wide spectrum of opportunistic infections (Gellatly and Hancock, 2013). A lipoxygenase from this pathogen (PA-LOX) has been successfully expressed as a recombinant protein and a number of studies explored the enzymatic properties

of this enzyme (Vance et al., 2004; Vidal-Mas et al., 2005; Garreta et al., 2013; Lu et al., 2013; Deschamps et al., 2016). However, identification of key amino acid residues that might contribute to the reaction specificity of PA-LOX is still pending. Multiple sequence alignment of PA-LOX with several eukaryotic LOXs reveal that the amino acids Glu369, Met434, Phe435 and Leu612, might constitute the triad determinants. Glu604 and Lys605 might be the Jisaka determinants of this enzyme. Additionally, PA-LOX converts arachidonic acid exclusively to 15*S*-HETE, and carries an alanine at its "Coffa site". Thus, mutagenesis of the above mentioned residues might provide valuable information on the applicability of the currently available concepts explaining the reaction specificity of other LOX-isoforms.

1.3.2. Enzymatic properties of lipoxygenases

1.3.2.1. Reaction conditions favored by different LOX-isoforms

Several studies have suggested that the reaction conditions have a great impact on the catalytic properties of LOXs. For instance, oxygenation of fatty acid substrates is pH-dependent. The different isoforms of soybean LOX show a pH optimum ranging between 6.5 to 9.0 with a maximum activity at a pH 9.0 for soybean LOX1 (Siedow, 1991; Baysal and Demirdoven, 2007). The pH optimum for human ALOX15 was 7.0 in the presence of 0.2 % sodium cholate and a Km for linoleic acid oxygenation of 3 µM was determined (Kühn et al., 1993). The recombinant human ALOX15 was expressed at high levels in the baculovirus/insect cell system, and purified to an apparent electrophoretic homogeneity with a yield of 25 – 30 mg of pure protein/liter of liquid culture. Its molecular turnover rate for linoleic acid oxygenation (13*S*-H(p)ODE) ranges between 8 – 25 s^{-1} (Kühn et al., 1993) depending on the quality of the enzyme preparation. Recombinant human ALOX12 expressed in the baculovirus/insect cell system exhibited a pH optimum in the range of 7.5 - 8.0 (in the presence of 0.006 % Tween-20) and had a Km value of 10 µM for both arachidonic acid and linoleic acid. The molecular turnover rate (k$_{cat}$) of arachidonic acid oxygenation was 250 s^{-1} (Chen et al., 1993). An arachidonate 15-lipoxygenting enzyme detected in human neonatal foreskin cultured keratinocytes exhibited its maximum activity in the pH range of 6.7 - 7.3 in the presence of > 2 mM calcium.

Its efficiency to metabolize both arachidonic acid (Km: 10.6 µM) and linoleic acid (Km: 9.5 µM) was very similar (Burrall et al., 1988) but for the time being it remains unclear which human gene (ALOX15 vs. ALOX15B) encodes for this enzyme. For native rabbit ALOX15 prepared from the lysate of a reticulocyte-rich blood cell population, the pH optimum ranged between 7.0 - 7.4. The molecular turnover ratio for linoleic acid (13S-H(p)ODE) oxygenation ranges between 5 – 50 s^{-1} with a temperature optimum between 20 – 25 °C. An activation energy of 12 kJ/mol was determined. In the absence of substrate, rabbit ALOX15 is stable for long time periods at temperatures <10 °C, however, it undergoes structural fluctuations and becomes inactive at temperatures >20 °C (Mei et al., 2008). Among prokaryotes, the LOXs from cyanobacteria, *Nostoc sp.* PCC 7120 exhibits a broad pH optimum between pH 7 - 10 and oxygenates linoleic acid exclusively to 9R-H(p)ODE (Lang et al., 2008). Two isoforms of LOXs have been described in *Anabaena sp*, *Nostoc punctiforme*, that convert linoleic acid to 13S-H(p)ODE with an optimum activity at a pH 7.0 (Koeduka et al., 2007).

A LOX-like enzyme has been reported in the *Pseudomonas aeruginosa* strain 42A2. For this enzyme, periplasmic (Guerrero et al., 1997; Busquets et al., 2004) and/or secreted expression has been described (Vance et al., 2004; Vidal-Mas et al., 2005; Lu et al., 2013; Deschamps et al., 2016). When intact *P. aeruginosa* bacteria were incubated with oleic acid, the bacteria were capable to oxidize this substrate to (E)-10-hydroxy-8-octadecenoic acid, (E)-10-hydroperoxy-8-octadecenoic acid and (E)-7,10-dihydroxy-8-octadecenoic acid. In an attempt to find out whether this bioconversion was cell bound or extracellular, the cell culture supernatant and different subcellular fractions (outer membrane, periplasm, cytoplasmic membrane, and cytoplasm) were tested for enzymatic activity. From gas chromatographic analyses of the reaction products it was concluded that a LOX-like enzyme present in the periplasmic space of the bacterium was responsible for the biotransformation of oleic acid (Guerrero et al., 1997). Busquets et al. later confirmed this by isolating the native protein from the periplasmic space of *P. aeruginosa*. This protein had a molecular weight of 45 kDa. A pH range of 8.5 - 9 and temperatures 25 – 30 °C seemed to be optimal for this periplasmic LOX. Interestingly, this enzyme oxygenated linoleic acid more efficiently (100 %, Km=0.66 mM) than linolenic (60 %, Km=0.73 mM:) and oleic acids (46 %, Km=0.74 mM), although the substrate affinities seemed similar

(Busquets et al., 2004). However, the chemical identity of this enzyme, in particular the amino acid sequence has not been clarified. Later, in 2004, a secreted lipoxygenase from *P. aeruginosa* (PA-LOX) was recombinantly expressed that converted arachidonic acid to 15*S*-HETE (Vance et al., 2004). This recombinant enzyme had a molecular weight of 70 kDa and converted linoleic acid predominantly to 13*S*-HODE (Km=48.9 µM). It exhibited a maximal catalytic activity at pH 7.5 and 25 °C (Lu et al., 2013). In a recent study, PA-LOX was expressed as a recombinant His-tag fusion protein (without the secretion signal). It exhibited a molecular weight of 76 kDa and converted arachidonic acid (Km=12 µM) to 15*S*-H(p)ETE and linoleic acid to 13*S*-H(p)ODE. This enzyme exhibited its maximum activity at pH 6.5 in the presence of 0.01 % TX-100 at 25 °C (Deschamps et al., 2016). Guerrero et al. were the first to test for a LOX-like activity in *P. aeruginosa* cell culture supernatant (Guerrero et al., 1997). However, they were unsuccessful because of two reasons: 1) Large amounts of PA-LOX is required for biotransformation of oleic acid (Vidal-Mas et al., 2005). 2) Secreted PA-LOX oxygenates polyenoic acids such as arachidonic and linoleic acids more efficiently when compared to oleic acid (Vance et al., 2004; Vidal-Mas et al., 2005; Deschamps et al., 2016).

1.3.2.2. Substrate specificity of lipoxygenases

Most mammalian LOXs prefer free polyenoic fatty acids as substrates but they are also capable of further converting the products of fatty acid oxygenation to secondary products such as epoxy leukotrienes, double oxygenation products and glutathione conjugates (Ivanov et al., 2015). Leukotrienes constitute the most comprehensively characterized secondary LOX products and their biosynthetic pathway involves two critical steps catalyzed by LOX: 1) Formation of hydroperoxy polyenoic fatty acids and 2) Formation of epoxy leukotrienes from the hydroperoxy derivative. The second reaction involves both, a hydrogen abstraction from a bisallylic methylene and the homolytic cleavage of the hydroperoxide bond, which leads to the formation of an oxygenated fatty acid biradical. This biradical is subsequently stabilized by the formation of epoxy leukotrienes, such as LTA4 (Haeggström and Funk, 2011; Ivanov et al., 2015). This reaction sequence has been postulated for ALOX5 (5,6-LTA4) (Rådmark and Samuelsson, 2010) and ALOX15 (14,15-LTA4) (Bryant et al., 1985). These

epoxy leukotrienes can then be conjugated with glutathione leading to the formation of LTC4 (Hammerström and Samuelsson, 1980) and eoxins (Sachs-Olsen et al., 2010).

Anti-inflammatory mediators like lipoxins can in principle be synthesized via two major pathways: 1) Triple oxygenation pathway: Arachidonic acid is first converted to 15-H(p)ETE by ALOX15. The 15-H(p)ETE is oxygenated once again by these LOXs to 14,15-DiH(p)ETE that is then oxygenated by ALOX5 to 5,14,15-TriH(p)ETE (lipoxin B4). Lipoxin A4 can be synthesized via an alternative pathway. ALOX5 first converts arachidonic acid to 5-H(p)ETE, which is subsequently double and triple oxygenated to 5,6,15-TriHETE via the catalytic activity of different LOX-isoforms. 2) Epoxy leukotriene pathway: The archidonate-oxygenation products of ALOX5 (5S-H(p)ETE) and ALOX15 (15S-H(p)ETE) are first converted to 5,6- or 14,15-epoxy leukotrienes that are hydrolyzed to vincinal diols like 5,6-DiHETE or 14,15-DiHETE. These diols are then further oxygenated to lipoxins. For instance, the 5,6-DiHETE is oxygenated to lipoxin A4 by human and rabbit ALOX15. On the other hand, 14,15-DiHETE originating from the hydrolysis of 14,15-LTA4 may be converted to lipoxin B4 by ALOX5 catalyzed oxygenation (Ivanov et al., 2015). For PA-LOX, the lipoxin synthase activity was also tested but the authors concluded that this enzyme does not exhibit such catalytic property (Deschamps et al., 2016).

Some LOX-isoforms are also capable of oxygenating phospholipids, cholesterol esters and even complex substrates like biomembranes and lipoproteins (Schewe et al., 1975; Belkner et al., 1991; Takahashi et al., 1993; Pekárová et al., 2015). Rabbit ALOX15 is capable of oxygenating both polyenoic fatty acid containing phospholipids (Schewe et al., 1975) and cholesterol esters (Belkner et al., 1991). In fact, the ability of rabbit ALOX15 to attack phospholipids led to its discovery (Schewe et al., 1975). However, its phospholipid oxygenase capability is more than one order of magnitude lower than its fatty acid oxygenase capability, indicating that free fatty acids are the preferred substrates (Ivanov et al., 2015). Molecular docking of a phospholipid to the active site of rabbit ALOX15 indicated that it is impossible for a phospholipid molecule to bind at its substrate-binding pocket without steric clashes. Thus, this ability of rabbit ALOX15 to oxygenate phospholipids can only be explained if the enzyme exhibits a high degree of motional flexibility during phospholipid interaction that causes its

structure to undergo sizeable rearrangements (Ivanov et al., 2015). Side by side experiments with different LOXs indicated that porcine ALOX15 behaves similarly. It is capable of oxygenating arachidonic acid containing phospholipids to 12S-HETE containing products. In contrast, human ALOX12 was not able to do so (Takahashi et al., 1993). Among the plant LOXs, soybean LOX1 is also capable of oxygenating phosphatidylcholines in the presence of detergents (Brash et al., 1987). Interestingly, a recent study on bacterial LOXs has indicated that the mini-LOX of *Anabaena sp.* PCC7120 (fusion protein) also oxygenated linoleic acid containing phosphatidylcholines to 9R-HODE. However, similar to eukaryotic LOXs, phospholipids are not a good substrate for this bacterial species since the reaction rate was much lower (Zheng et al., 2008). The ALOX15 orthologs of humans (Kühn et al., 1993), rabbits (Kuhn et al., 1990) and pig (Takahashi et al., 1993) are capable of oxygenating complex lipid-protein assemblies such as biomembranes and lipoproteins. Rabbit ALOX15 oxygenates various biological membranes including rat liver mitochondrial and endoplasmic membranes, beef heart submitochondrial particles and erythrocyte plasma membranes to 15S-HETE and 13S-HODE containing ester lipids (Kuhn et al., 1990). This ability of rabbit ALOX15 suggested a role of this enzyme in the maturational breakdown of mitochondria and other intracellular organelles during the maturation of red blood cells (Schewe et al., 1975, 1986a; Kuhn et al., 1990). A more recent study indicated that the 12-lipoxygenating alox15 of rat and its 15-lipoxygenating Leu353Phe mutant are also capable of oxygenating the ester lipids of mitochondrial membranes and lipoproteins to 13S-HODE and 12S-HETE (wildtype) and 13S-HODE and 15S-HETE (Leu353Phe mutant) (Pekárová et al., 2015).

The structure of PA-LOX has been solved at a resolution of 1.75 Å. Unlike most eukaryotic LOXs, the substrate-binding cavity of this enzyme is much bigger and bifurcated. The structure also contains a complete phosphatidylethanolamine bound to its substrate-binding pocket. The sn-1 fatty acid of this phospholipid occupies the catalytic cavity containing the non-heme iron and the sn-2 fatty acid occupies the second cavity of the enzyme (Garreta et al., 2013). These data suggest a high binding affinity of the enzyme for phospholipids. Thus, it might be possible that PA-LOX, when secreted from the bacteria during *P. aeruginosa* infections is capable of oxygenating the membrane phospholipids of the

surrounding host cells. However, so far no direct experimental evidence is available indicating the capability of the enzyme to oxygenate membrane bound phospholipids without the preceding activity of lipid hydrolyzing enzymes.

1.3.2.3. Reaction stereochemistry of lipoxygenases

The LOX reaction is initiated by a stereospecific hydrogen removal from a CH_2 between two *cis* double bonds after which molecular dioxygen is covalently inserted at the opposite face of the fatty acid substrate. This stereo chemical arrangement as indicated in Figure 4 is called "antarafacial character" of the LOX reaction and has been reported for a number of LOX isoforms (Hamberg and Samuelsson, 1967a, 1967b; Egmond et al., 1972; Brash et al., 2012). Stereospecifically labeled fatty acids containing a tritium at either the pro *R-* or the pro *S*-position of a bisallylic methylene was first prepared by Schroepfer and Bloch in 1965 (Schroepfer and Bloch, 1965). Since then, usage of these substrates has proved to be an efficient strategy to investigate the chemical reactions catalyzed by lipoxygenases and other eicosanoid synthesizing enzymes (Brash et al., 2012). Due of the difference in mass of a hydrogen and a deuterium or even a tritium, it is easier to break a C-H bond when compared with a C-^{2}H or a C-^{3}H-bond (Brash et al., 2012).
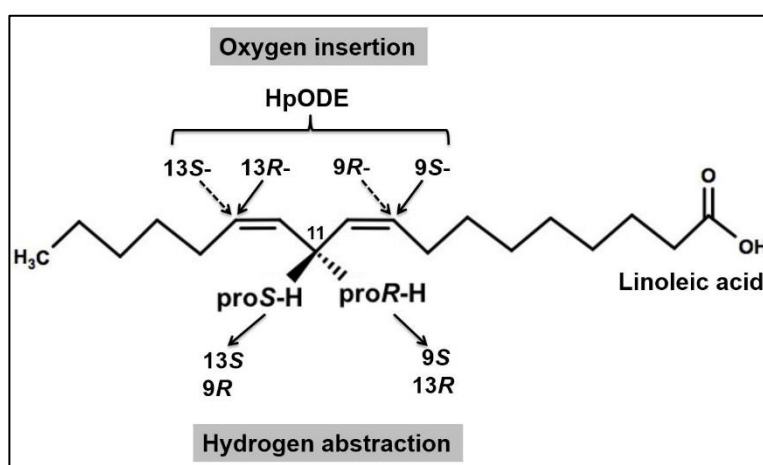
Figure 4: Antarafacial relationship between hydrogen abstraction and oxygen insertion with linoleic acid as a substrate (modified from Kuhn et al., 2005).

Since hydrogen abstraction is the rate-limiting step in LOX catalyzed reactions, the above-mentioned difference translates into a kinetic isotope effect (KIE) (Brash et al., 2012). M. Hamberg and B. Samuelsson were the first to describe

the stereo-chemical features of a LOX-catalyzed reaction. When soybean LOX was incubated with stereospecifically labeled [13D-^{3}H] (pro$R$) and [13L-^{3}H] (pro$S$) 8, 11, 14- eicosatrienoic acid (ω6), only the pro$S$-hydrogen at C13 was removed by the soybean LOX to form a 15L$_s$-hydroperoxide. Thus, the abstraction of hydrogen from the methylene group at C13 was strictly stereospecific (Hamberg and Samuelsson, 1967a). Among others, similar analysis of LOXs' stereochemistry was carried out for other LOX isoforms including plant 9S-LOX (Hamberg and Samuelsson, 1967a; Hamberg, 1971), human ALOX5 (Borgeat et al., 1976; Corey and Lansbury, 1983), human ALOX12 (Hamberg and Samuelsson, 1974; Hamberg and Hamberg, 1980) and soybean LOX1 (Coffa et al., 2005b). Among the prokaryotic LOXs, the stereochemistry of the LOXs only from *Anabaena sp.* PCC7120 has been established so far. These LOXs also exhibit the antarafacial relationship between the hydrogen abstraction and oxygenation while forming 9R-HODE from the stereospecifically labeled [11-^{3}H] linoleic acids (Zheng et al., 2008). An exception to this concept is the manganese containing fungal-LOX from *Gäumannomyces graminis.* It exhibits a suprafacial relationship between the hydrogen abstraction and oxygen insertion and oxygenates linoleic acid to 11S-HODE (Hamberg et al., 1998). Although it has been established that PA-LOX converts arachidonic acid to 15S-HETE and linoleic acid to 13S-HODE (Vance et al., 2004; Vidal-Mas et al., 2005), the reaction stereochemistry behind the catalysis is yet to be elucidated.

1.4. Aims of this project

Lipoxygenases (LOXs) are fatty acid dioxygenases that catalyze the conversion of polyunsaturated fatty acids to their hydroperoxy derivatives. They frequently occur in plants and mammals but have also been detected in several bacteria. *Pseudomonas aeruginosa* lipoxygenase (PA-LOX) is a secreted arachidonate 15-LOX, which has been implicated in the pathogenesis of PA infections. For this dissertation, PA-LOX was overexpressed as a recombinant N-terminal His_6-tagged fusion protein and purified to apparent electrophoretic homogeneity by a combination of various chromatographic techniques. The expression strategy was optimized and the purified enzyme was characterized with respect to its protein chemical properties (molecular weight, iron content). With the purified enzyme preparation, two sets of experiments have been carried out aiming at:

1) Characterization of basic enzymatic properties (temperature dependence, activation energy, kinetic constants, stereochemistry of the reaction products, substrate specificity, thermo stability). PA-LOX will then be crystallized to solve the 3D-structure of the enzyme-substrate complex in order to obtain more detailed information on the alignment of substrate lipids at the active site. Functionally relevant amino acids will identified and site-directed mutagenesis studies will be carried out to explore the functional consequences of selected enzyme mutants. Relevant mutants will then be crystallized to explore the structural basis for the observed functional changes.

2) Investigations into the biological relevance of PA-LOX as possible pathogenicity factor of the bacterium. Here the capability of PA-LOX to synthesize pro- (leukotreines) and anti-inflammatory (lipoxins) mediators will be quantified. Since PA-LOX is a secreted protein, it might contribute to attack host cells by oxidizing their membrane lipids. This possibility will be tested by incubating pure PA-LOX *in vitro* with different types of eukaryotic cells (erythrocytes, cultured lung epithelial cells) and by analyzing the amounts and structures of the oxygenated lipids employing a lipidomic approach (HPLC, LC-MS/MS).

2. MATERIALS AND METHODS

2.1. Materials

2.1.1. Chemicals

Chemical name	Company (City, country)
Acetic acid	Carl Roth GmbH (Karlsruhe, Germany)
Acetonitrile	Thermo Scientific (Schwerte, Germany)
Ammonium acetate	Sigma Aldrich (Taufkirchen, Germany)
Arachidonic acid	Sigma Aldrich (Taufkirchen, Germany)
Cardiolipin (from bovine heart, sodium salt)	Sigma Aldrich (Taufkirchen, Germany)
Chloroform	Baker (Deventer, Netherlands)
Disodium hydrogen phosphate	Carl Roth GmbH (Karlsruhe, Germany)
EDTA	Sigma Aldrich (Taufkirchen, Germany)
Glucose	Sigma Aldrich (Taufkirchen, Germany)
Glycerol	Carl Roth GmbH (Karlsruhe, Germany)
HEPES	Sigma Aldrich (Taufkirchen, Germany)
HPLC grade water	VWR Chemicals (Radnor, USA)
Hydrocholoric acid	Carl Roth GmbH (Karlsruhe, Germany)
Imidazole	Carl Roth GmbH (Karlsruhe, Germany)
Isopropanol	Carl Roth GmbH (Karlsruhe, Germany)
Kanamycin	Carl Roth GmbH (Karlsruhe, Germany)
LB-Agar	Carl Roth GmbH (Karlsruhe, Germany)
LB-Medium	Carl Roth GmbH (Karlsruhe, Germany)
Magnesium chloride	Merck (Darmstadt, Germany)
Magnesium sulfate	Sigma Aldrich (Taufkirchen, Germany)
Methanol	VWR Chemicals (Radnor, USA)
n-Hexane	Carl Roth GmbH (Karlsruhe, Germany)
Polyethylene glycol	Sigma Aldrich (Taufkirchen, Germany)
Ponceau S	Sigma Aldrich (Taufkirchen, Germany)
Potassium chloride	Merck (Darmstadt, Germany)
Potassium Hydroxide	Merck (Darmstadt, Germany)
Potassium dihyrodgen phosphate	Merck (Darmstadt, Germany)
Restriction enzyme *Nde*I	Thermo Scientific (Schwerte, Germany)
Restriction enzyme *Hin*dIII	Thermo Scientific (Schwerte, Germany)
SDS	Serva (Heidelberg, Germany)
Sodium borohydride	Life Technologies, Inc. (Eggenstein, Germany)
Sodium chloride	Carl Roth GmbH (Karlsruhe, Germany)

Soybean lipoxygenase	Sigma Aldrich (Taufkirchen, Germany)
Tris(hydroxymethyl)aminomethane	Sigma Aldrich (Taufkirchen, Germany)
Tris	Carl Roth GmbH (Karlsruhe, Germany)
Tryptone	Sigma Aldrich (Taufkirchen, Germany)
Tween 20	Sigma Aldrich (Taufkirchen, Germany)
Yeast extract	Becton Dickinson and Co. (Heidelberg, Germany)

2.1.2. Fatty acid substrates

Fatty acid	Company (City, country)
C18:Δ9 (cis) Octadecenoic acid	Sigma Aldrich (Taufkirchen, Germany)
C18:Δ11 (cis) Octadecenoic acid	
C18:Δ9,12 (all cis) Octadecadienoic acid (Linoleic acid)	
C18:Δ6,9,12 (all cis) Octadecadienoic acid	
C18:Δ9,12,15 (all cis) Octadecadienoic acid	
C18:Δ6,9,12,15 (all cis) Octadecatetraenoic acid	
C20:Δ5,8,11 (all cis) Eicosatrieneoic acid	
C20:Δ11,14 (all cis) Eicosadienoic acid	
C20:Δ8,11,14 (all cis) Eicosatrienoic acid	
C20:Δ5,8,11,14 (all cis) Eicosatetraenoic acid (Arachidonic acid)	
C20:Δ8,11,14,17 (all cis) Eicosatetraenoic acid	
C20:Δ5,8,11,14,17 (all cis) Eicosapentaenoic acid	
C22:Δ4,7,10,13,16,19 (all cis) Docosahexaenoic acid	

2.1.3. Phospholipid substrates

Phospholipids	Company (City, country)
1-palmitoyl-2-linoleoyl phosphatidylcholine	Santa Cruz (Texas, USA)
1-palmitoyl-2-linoleoyl phosphatidylethanolamine	
1-palmitoyl-2- linoleoyl phosphotidylionositol	
1-palmitoyl-2-linoleoyl phosphatidylserine	Avanti Polar Lipids (Alabaster, USA)
1,2-dilinoleoyl-*sn*-glycero-3-phosphoethanolamine	

2.1.4. HPLC-standards

Standard	Company (City, country)
5(±)-HETE	Cayman Chemical company (distributed by Biomol, Hamburg, Germany)
11R-HETE	
12S-HETE	
12(±)-HETE	
15S-HETE	
15(±)-HETE	
9R-HODE	Cascade Biochem Ltd. (London, United Kingdom)
13S-HODE	Cayman Chemical company (distributed by Biomol, Hamburg, Germany)
13(±)-HODE	

2.1.5. Lipoxin and Leukotriene synthesis

Standard	Company (City, country)
5S-HETE	Cayman Chemical company (distributed by Biomol, Hamburg, Germany)
5S,6S-DiHETE	
5S,6R-DiHETE	
15-H(p)ETE	

2.1.6. Cells and media

Competent bacteria and media

Purpose	Type of cells	Company (city, country)
Generation of mutants	*E. coli* XL-1 Blue cells	Stratagene (La Jolla, USA)
Protein expression	*E. coli* BL21 (DE3) cells	Invitrogen (Carlsbad, USA)

SOC medium

20 g/L trypton, 5 g/L yeast extract, 10 mM sodium chloride, 2.5 mM potassium chloride, 10 mM magnesium chloride, 10 mM magnesium sulfate and 20 mM glucose

Eukaryotic cells and cell culture media

Eukaryotic cells	Company (city, country)
Human epithelial adenocarcinoma cells (Caco-2 cells)	ATCC (Manassas, USA)
Adenocarcinomic human alveolar basal epithelial cells (A549 cells)	

Cell culture media	Company (city, country)
Eagle's Minimum Essential Medium (EMEM) – for Caco-2 cells	Lonza (Basel, Switzerland)
Dulbecco's Modified Eagle Medium (DMEM) – for A549 cells	PAN-Biotech (Aidenbach, Germany)

Red blood cells (RBCs)

5 ml of blood was taken from a healthy volunteer into a tube containing 250 µl of 0.5 M EDTA (pH 8.0). The collected blood was centrifuged at 700 $x\,g$ for 5 min at 4 °C and the supernatant, which is the plasma, was recovered. The pellet containing the RBCs was re-suspended in 20 ml of PBS and centrifuged at 200 $x\,g$ for 15 min at 4 °C. The supernatant was discarded and the RBCs were recovered. The above step was repeated once again in order to thoroughly wash the RBCs and to get rid of any remaining plasma in the sample. The supernatant was discarded completely and the RBC pellet was now ready for the assay.

2.1.7. Rabbit ALOX15

The native rabbit ALOX15 that was used for comparative measurements was previously prepared according to (Rapoport et al., 1978). It was purified to apparent electrophoretic homogeneity from a reticulocyte-rich hemolysate supernatant by sequential ammonium sulfate precipitation, anion exchange chromatography and preparative isoelectric focusing in a sucrose gradient.

2.1.8. Buffers

Technique	Buffer name	Composition
PA-LOX assay	10XPBS	137 nM NaCl, 2.7 mM KCl, 1.5 mM KH_2PO_4, 6.5 mM Na_2HPO_4 in 1 L water, pH 7.4. Dilute 1:10 to make 1XPBS
Protein purification	Wash buffer 1	0.1 M Tris/HCl, 300 mM NaCl, 10 mM imizadole, pH 8.0
	Wash Buffer 2	0.1 M Tris/HCl, 300 mM NaCl, 25 mM imizadole, pH 8.0
	Elution buffer	0.1 M Tris/HCl, 300 mM NaCl, 200 mM imizadole, pH 8.0
SDS page	Stacking gel buffer	0.5 M Tris/HCl, 0.4 % (v/v) SDS, pH 6.75
	Resolving gel buffer	1.5 M Tris/HCl, 0.6 % (v/v) SDS, pH 8.8
	Running buffer	25 mM Tris/HCl, 192 mM Glycine, 0.1 % (v/v) SDS, pH 8.3
Western Blot	Membrane buffer	1X Rapid transfer buffer (Amresco, Solon, USA)
	Wash Buffer	PBS/0.3 % (v/v) Tween 20 solution
Agarose gel electrophoresis	TAE buffer	40 mM Tris, 2 mM EDTA-Na salt, 29.6 mM Acetic acid, pH 8.5

2.1.9. Kits

Purpose	Kit name	Company (city, country)
DNA amplification	MIDI-preparation kit	Macherey Nagel (Düren, Germany)
Site-directed mutagenesis	QuikChange site-directed mutagenesis Kit	Agilent technologies (Santa Clara, USA)
Protein expression	Enpresso B kit	BioSilta Ltd. (St. Ives, Great Britain)

2.2. Methods

2.2.1. Site directed mutagenesis

Selection of primers

Forward and reverse primers were designed and the primers included the desired mutation. Primers comprising single mutants were around 30 bases long and those comprising double mutants were around 36 bases long. Each amino acid exchange was preceded and followed by at least 10 - 12 bases of the template DNA.

Performing PCR

Polymerised chain reaction (PCR) reaction mixture (25 µl) involved the template DNA, the forward and reverse primers for the respective mutants, variable amounts of 2-fold concentrated *Pfu* Master-Mix (Agilent technologies, Santa Clara, USA) and sterile water. The mixture was prepared on ice as suggested by the manufacturer. In most cases the wildtype-PA-LOX in pET-28a(+) was used as our template.

Digestion of the template DNA

The un-mutated parental DNA template was then digested with FastDigest *Dpn*I (Thermo Scientific, Massachusetts, USA) for 30 min at 37 °C. The degrading enzyme was then deactivated by incubating the mixture at 80 °C for 5 min.

Transformation of competent *E. coli* XL1-Blue cells

8 µl of the PCR mixture were then added to 100 µl of *E. coli* XL-1 Blue cells. The mixture was gently mixed and incubated on ice for 30 min. The cells were then subjected to heat shock by incubating them at 42 °C for 45 s. This made the competent cells porous allowing the DNA to pass the membranes. To prevent further damage to the *E. coli* cells, they were placed back on ice for 3 min. 300 µl of SOC medium was then added to the cells and incubated for 1 h on a shaker at 37 °C and 180 rpm shaking frequency. 100 – 200 µl of this mixture was then plated on kanamycin containing agar plates (50 µg/ml) and incubated overnight at 37 °C. After 24 h, 2 - 5 clones were picked for each mutant and re-suspended in 4 ml of LB medium containing 50 µg/ml kanamycin. After overnight culture, the plasmids were then prepared as per the instructions of the NucleoSpin Plasmid Easy Pure (Macherey-Nagel, Düren, Germany).

Agarose gel electrophoresis

To exclude that the mutagenesis strategy did not induce major structural alterations, an aliquot of mutant DNA was subjected to restriction digestion by *Nde*I and *Hin*dIII in FD fast digest buffer (Thermo Scientific, Schwerte, Germany). The mixture was incubated at 37 °C for 1 h and then run on agarose gel (1 % (w/v)) electrophoresis. The gels were then viewed on BioDocAnalyze software coupled with a transilluminator (Biometra, Göttingen, Germany).

Confirmation of successful mutation by DNA sequencing

DNA sequencing was carried out by Eurofins Genomics (Ebersberg, Germany) to confirm the successful amino acid exchange. The different mutants generated

included: PA-LOX Val189Arg, Val189Tyr, Glu369Ala, Glu373Asp, Glu373Leu, Met374Ala, Leu378Phe, Leu378Tyr, Ala420Gly, Leu425Phe, Leu425Tyr, Ile431Ala, Ile431Glu, Ile431Phe, Ile431Tyr, Met434Ala, Met434Val, Phe435Ala, Phe435Leu, Met434Val+Phe435Leu, Glu604Tyr+Lys605His, Tyr609Ala and Leu612Val

2.2.2. Protein expression

Transformation of competent *E. coli* BL21 (DE3) cells

The prokaryotic expression plasmid pET28a(±) containing the coding sequence of PA-LOX (without secretory sequence) was kindly provided by Prof. Xavi Carpena (Institut de Biologia Molecular, Parc Científic de Barcelona, Baldiri Reixac 10, 08028 Barcelona, Spain). This plasmid was amplified for further analysis in *E. coli* XL-1 Blue cells and extracted using the MIDI-preparation kit. PA-LOX (wildtype and mutants) was expressed in *E. coli* employing the Enpresso B kit. 200 ng of the plasmid-DNA was added to 100 µl of *E. coli* BL21 (DE3) cells, gently tap-mixed, and incubated on ice for 30 min. The cells were then subjected to heat shock at 42 °C for 45 s after which they were cooled down on ice for 2 min. Then 500 µl of SOC medium was added to this mixture and incubated on a shaker at 37 °C and 180 rpm shaking frequency for 1 h. 200 µl of this mixture was then plated on kanamycin containing agar plates and incubated overnight at 37 °C.

Pre-culture and main culture

2 ml of a bacterial pre-culture (LB medium with 50 µg/ml kanamycin) were inoculated and grown at 37 °C on a shaker for 6 – 8 h at 180 rpm shaking frequency. Once the required optical density (OD_{600}) was attained, the 2 ml pre-culture was then added to 50 ml main culture medium as suggested by the vendor. The main culture was grown overnight on a shaker at 30 °C and 250 rpm shaking frequency in Ultra Yield flasks (BioSilta Ltd., St. Ives, Great Britain). The expression of the recombinant enzyme was induced by adding 1 mM (final concentration) IPTG to the main culture after which the culture was incubated over night on a shaker at 25 °C and 250 rpm shaking frequency.

Cell harvest and enzyme purification

Bacteria suspension was centrifuged at 3000 *x g* at 4 °C for 10 min after which the cells were reconstituted in 20 ml PBS. The suspended cells were centrifuged

once again at 3000 x g and 4 °C for 10 min, the supernatant was discarded and the cells were reconstituted in 5 ml PBS. They were then lysed by sonication (digital sonifier, W-250D Microtip Max 70 % Amp, Model 102C (CE); Branson Ultraschall, Fürth, Germany) to release the intracellular proteins. Cell debris were then pelleted by centrifugation at 15,000 x g for 20 min at 4 °C and the resulting lysate supernatant was employed for further enzyme purification.

An aliquot of 200 µl of the cell lysate was stored away for SDS-PAGE. The His_6-tag containing recombinant protein was then purified by nickel agarose affinity chromatography using Protino Ni-NTA-agarose suspension (Machery Nagel, Düren, Germany). For this, 5 ml of cell lysate supernatant was incubated with 500 µl of the Ni-NTA beads on a rotator, rotamix RMI (ELMI, Riga, Latvia), for 1 h, at 4 °C. The gel beads were then transferred to an open bed chromatography column (Bio-Rad, München, Germany). Purification involved washes with three kinds of buffers with varying imidazole concentrations. To remove nonspecifically bound proteins, the column was first eluted thrice with 800 µl wash buffer 1 containing 10 mM imidazole. Next, the column was washed thrice with 800 µl wash buffer 2 containing 25 mM imidazole to elute weakly bound proteins. Finally, rinsing the column seven times with 300 µl of elution buffer containing 200 mM imidazole eluted the desired recombinant protein. This high concentration of imidazole competes with the His_6-tag of the recombinant protein for binding at the Ni-ions. As result of this competition, the protein is eluted from the column. Usually, the majority of the PA-LOX was recovered in the elution fractions 1, 2 and 3.

Desalting, concentration and gel filtration of the protein preparation

The imidazole ions present in the elution fractions of the affinity chromatography were removed by size exclusion chromatography using Econo-Pac 10DG desalting columns (Bio-Rad, California, USA). The columns were first washed two times with 20 ml of PBS. Once the buffer had drained out completely, 3 ml of the protein sample was loaded on the column. The first effluent was discarded. 4 ml of PBS was then allowed to run down the column and the effluent was collected as it contained the desired protein.

The desalted protein solution was subsequently concentrated to the required protein concentrations by centrifugation at 3000 x g through an Amicon Ultra-15 10K centrifugal filter (Millipore, Massachusetts, USA). 10 % (v/v) of glycerol was

added to the protein as cryoprotectant and the solution was stored at - 80 °C until further use.

When required, aliquots of the desalted protein were further purified by gel filtration using a Superdex 200 10/300 GL FPLC column (GE Healthcare, Uppsala, Sweden). The column was eluted with 20 mM Tris-HCl buffer at pH 8.0 (flow: 0.5 ml/min). The purified PA-LOX obtained from the FPLC was then concentrated for further use by centrifugation at 3000 x g through an Amicon Ultra-15 10K centrifugal filter.

2.2.3. Quantification of protein concentration and of the degree of purity

Protein determination by Bradford assay

Quantification of the protein concentrations in the enzyme solutions of different purity was determined by the Bradford assay (Bradford, 1976). The assay was carried out in polystyrene cuvettes (10 x 4 x 45 mm, Sarstedt AG & Co, Nümbrecht, Germany) with a final volume of 1 ml and measured on the Biophotometer plus (Eppendorf, Hamburg, Germany). The photometer was calibrated for a range of 0 – 10 µg/ml and from the absorbance at 595 nm the final concentration of the protein could be quantified.

SDS-PAGE

The degree of purity of the lysate, elution fractions and of the concentrated LOX preparations was estimated by SDS polyacrylamide gel electrophoresis (SDS-PAGE). The protein was denatured prior to loading the solution on the gel by incubating aliquots of the enzyme with 4-fold concentrated loading buffer (Carl Roth GmBH, Karlsruhe, Germany) and 20-fold concentrated reducing agent (Lonza, Basel, Switzerland) at 95 °C for 3 min. The samples were then centrifuged at 12,000 x g for one min and the supernatants were loaded on the gel. The SDS gel involved a 4 % stacking gel and 10 % resolving gel (suitable for proteins whose molecular weights ranged between 20 - 300 kDa). The SDS-PAGE gel was run in a Bio-Rad chamber (California, USA) at a current of 25 - 30 mA in the running buffer. After the separation of the different proteins according to their molecular weights, the gels were first washed three times (5 min each) with distilled water and then stained with Coomasie blue (Thermo Scientific, Schwerte, Germany) for 30 min on a shaker or used directly for western blot analysis.

Western-blot

Once the proteins have been separated according to their molecular weights on the SDS-PAGE, they were transferred on the nitrocellulose membrane. This transfer was achieved at 75 V for 20 min in 1X rapid transfer buffer (Amresco, Solon, USA). Preliminary visualization of the transferred protein bands (before treatment with antibodies) was carried out by staining the gels with 0.2 % (v/v) Ponceau S in 3 % (v/v) TCA. In order to prevent nonspecific binding of antibodies to the membrane surface, the membrane was first blocked with 5 % (w/v) dry milk solution (Bio-Rad, Hercules, USA) in PBS. To visualize His$_6$-tag fusion proteins, the membrane was then incubated with anti-His$_6$-tag antibody (30 min), which was coupled to rabbit peroxidase as reporter enzyme producing the color for specific visualization of the histidine-tagged proteins. When PA-LOX specific antibodies, raised in rabbits, were employed (as a primary antibody), the membrane was incubated (for 1 h) with a secondary antibody (anti-rabbit IgG peroxidase conjugate (1:5000 dilution), that recognizes the primary antibody. Excess of unbound antibodies were removed by washes with PBS containing 0.3 % (v/v) Tween 20. The membranes were then incubated with a 1:1 diluted Western lightening oxidizing agent and Western lightening enhanced luminol (Perkin Elmer, Waltham, USA) for 1 min. The specific PA-LOX bands were then visualized with the Fujifilm imagining system (Fujifilm, Dusseldorf, Germany).

2.2.4. Interaction of PA-LOX with different classes of substrates

2.2.4.1. Fatty acid oxygenase activity

The fatty acid oxygenase activity of PA-LOX was tested with ten different fatty acids with variable chain lengths and numbers of double bonds, which have previously been shown to be suitable substrates for other LOX isoforms (Hamberg and Samuelsson, 1967a; Borgeat et al., 1976; Lang et al., 2008). For these tests an aliquot of the enzyme preparations was incubated with 0.1 mM of PUFAs in a total volume of 1 ml. The activity was monitored at 235 nm on the spectrophotometer for 180 s and the increase in absorbance was considered as suitable measure for the catalytic activity with the different fatty acid substrates. After the incubation period, the products were reduced with sodium borohydride and incubated on ice for 10 min. 100 µl of 100 % acetic acid were then added in order to adjust a pH of 3 in the reaction mixture. Then 1 ml of methanol was added

to precipitate the protein and the sample was further incubated on ice for 5 min. The protein precipitated was removed by centrifugation at 14,000 $x\,g$ and 8 °C for 10 min. Aliquots of the supernatant containing the fatty acid oxygenase products were then subjected to HPLC analysis.

2.2.4.2. Phospholipid oxygenase activity

Wildtype-PA-LOX that was previously crystallized contained a complete phospholipid at its active site that was spontaneously incorporated during enzyme expression and was not removed during the purification procedure (Garreta et al., 2013). This result suggested that PA-LOX might exhibit a high binding-affinity for phospholipids. Thus, it would be possible that the enzyme may be capable of oxygenating phospholipids and other complex fatty acid derivatives. To test this hypothesis, aliquots of recombinant PA-LOX and purified native rabbit ALOX15 were first incubated side-by-side at 25 °C with phospholipid preparations representing the four most abundantly occurring membrane glycerophospholipid classes (phosphatidylcholine, PC; phosphatidylethanolamine, PE; phosphatidylinositol, PI; phosphatidylserine, PS). After an incubation of 15 min, the reaction was stopped by the addition of sodium borohydride as peroxide reducing agent. The assay mixture was then acidified with 80 µl of acetic acid and the total lipids were extracted according to the Bligh-Dyer method (Bligh and Dyer, 1959). 2.5 ml methanol and 1.25 ml chloroform were added to the reaction mixture, which was vortexed vigorously for 1 min and then cooled down on ice for 15 min. Next, 1.25 ml of chloroform and 1.25 ml of water were added and the mixture was again vortexed for 1 min. The samples were subsequently centrifuged for phase separation (3,000 $x\,g$ for 1 min). The bottom chloroform phase was recovered, the solvents were evaporated and the remaining lipids were reconstituted in 850 µl of methanol. 150 µl of 40 % (v/v in water) KOH were added and the ester lipids were hydrolyzed under argon atmosphere for 20 min at 60 °C. The samples were then cooled down on ice for 5 min and acidified with 150 µl of acetic acid. After incubating the samples on ice for 20 min, precipitate was removed by centrifugation (10,000 $x\,g$ for 10 min at 4 °C). The free hydroxy fatty acids present in the supernatants were prepared by RP-HPLC and further analyzed by SP- and CP-HPLC.

2.2.4.3. Oxygenation of membrane bound phospholipids

This capability of PA-LOX to oxygenate biomembranes was determined by incubating aliquots of the enzyme preparations with vesicles of beef heart inner mitochondrial membranes (Crane et al., 1956) that were considered as bio-relevant model membranes. The volume of each activity assay was adjusted to 1 ml and membrane and enzyme concentrations (PA-LOX and rabbit ALOX15) were variable depending on the arachidonic acid oxygenase activity of the different enzyme preparations. The membrane oxygenase activity of the two enzyme preparations was followed oxygraphically using a Clark-type oxygen electrode (Helmut Saur Laborbedarf, Reutlingen, Germany). After an incubation period of 15 min, the reaction was stopped by the addition of sodium borohydride, which reduces the formed hydroperoxy fatty acids to the corresponding hydroxy derivatives. The assay mixture was then acidified with 80 µl of 100 % acetic acid and the total lipids were extracted according to the Bligh-Dyer method (Bligh and Dyer, 1959). The bottom chloroform phase was recovered, the solvents were evaporated and the remaining ester lipids were reconstituted in 1 ml of a 1:1 mixture of chloroform and methanol. Aliquots of this mixture were then either subjected to SP-HPLC separation (Robins and Patton, 1986) of the major phospholipid classes or to alkaline hydrolysis as described above. The hydrolysis products were then directly injected into RP-HPLC for quantification of the 13-HODE + 15-HETE/linoleic acid + arachidonic acid ratio, which constitutes a suitable measure to characterize the degree of oxidation of the membrane lipids.

2.2.4.4. Oxygenation of intact erythrocyte membranes

The ability of PA-LOX to oxygenate intact cells was determined by incubating isolated human erythrocytes with purified PA-LOX. The reaction mixture consisted of 100 µl of packed human RBCs re-suspended in 1 ml of PBS, which was incubated with different amounts of pure recombinant PA-LOX for different time intervals. The disruption of RBCs' cell membranes was quantified by determining the degree of hemolysis. After the different incubation periods, the intact RBCs were centrifuged down at 13,000 $x\ g$ for 5 min and the hemoglobin content of the supernatant was determined by measuring the absorbance of the Soret band at 410 nm. The assay mixture was then subjected to lipid extraction (Bligh and Dyer, 1959). Aliquots of the extracted lipids dissolved in methanol were

subjected to LC-MS/MS analysis to identify the structures of the oxygenated phospholipids. The remaining sample was subjected to alkaline hydrolysis as described above and analyzed by RP-HPLC to quantify the amounts of 13-HODE and 15-HETE.

2.2.4.5. Leukotriene and lipoxin synthesis

Leukotriene synthesis

The ability of PA-LOX to synthesize 14,15-leukotrienes was determined by incubating the purified enzyme with 15-H(p)ETE under anaerobic conditions. The reaction mixture consisted of 25 µM of 15-H(p)ETE in 1 ml of PBS to which an aliquot of PA-LOX was added. The mixture was incubated for 10 min at room temperature. The reaction was stopped by the addition of 1 ml of 0.1 M hydrochloric acid and incubated on ice for 15 min. This procedure induced acidic hydrolysis of the epoxy leukotriene to the corresponding diols. The entire procedure was carried out under argon atmosphere in order to avoid 15-H(p)ETE oxygenation to the corresponding double oxygenation products. Finally 2 ml of methanol were added and aliquots were analyzed for leukotriene A4 hydrolysis products by HPLC. Pure rabbit-ALOX15 was used as a positive control. The products (conjugated trienes) were analyzed by RP-HPLC by recording the absorbance at 270 nm.

Lipoxin synthesis

PA-LOX lipoxin synthase activity was tested using 5*S*-HETE and a 1:1 mixture of both, 5*S*,6*S*- and 5*S*,6*R*-DiHETE as its substrates in the presence of 3 µM linoleic acid serving as activator of the enzyme. The reaction mixture consisted of 30 µM of the above substrates in 500 µl of PBS. An aliquot of purified PA-LOX was incubated with the substrate mixture for 10 min. The reaction was stopped by the addition of sodium borohydrate and incubated on ice for 10 min. The mixture was acidified with 50 µl of acetic acid followed by addition of 500 µl methanol and again incubated on ice for 10 min. The protein precipitate was removed by centrifugation at 14,000 *x g* and 8 °C for 10 min. The supernatant was recovered and formation of conjugated tetraenes was monitored by RP-HPLC by recording the absorbance at 300 nm.

2.2.5. Activity assay

2.2.5.1. Spectrophotometric analysis

2.2.5.1.1. PA-LOX with different PUFAs

The catalytic activity of the PA-LOX with different fatty acid substrates was monitored spectrophotometrically using a Shimadzu instrument (Shimadzu UV-2102 PC spectrophotometer, Shimadzu, Duisburg, Germany). The 1 ml activity assays were carried out in precision cuvettes made of quartz suprasil, (Hellma, Tustin, USA). The time-dependence of product formation (conjugated dienes) was monitored at 235 nm at 25 °C for 180 s in triplicates. The kinetic progress curves (absorbance vs. time) were obtained for each fatty acid substrate at different substrate concentrations. From the linear portion of the kinetic progress curves, the kinetic parameters, Km (Michaelis constant) and Vmax (maximum rate) for each substrate were calculated according to the Lineweaver-Burk equation.

2.2.5.1.2. Temperature profile

The effect of temperature on the activity of PA-LOX was also assayed spectrophotometrically. The substrate, 165 µM linoleic acid in PBS, was first heated in the cuvette holder of the spectrophotometer to the respective temperature (5, 10, 15, 20, 25, 30, 35 and 40 °C) for 10 min. Then, an aliquot of PA-LOX was added and the activity assay was carried out in triplicates. The initial rates of the kinetic progress curves were used to plot the temperature-dependence profile. The catalytic activities obtained for PA-LOX between 5 - 35 °C were employed to construct the Arrhenius plot from which the activation energy for PA-LOX could be determined. As a positive control, here again, rabbit ALOX15 was used. However, because of the higher sensitivity of rabbit ALOX15 for heat denaturation, the Arrhenius plot for the rabbit-LOX was constructed using catalytic activities obtained between 5 – 25 °C.

2.2.5.1.3. Variable oxygen concentrations

Measurement of activity under normoxic and hyperoxic conditions

Molecular oxygen is an essential requirement for the LOX reaction since atmospheric dioxygen serves as second substrate for fatty acid oxygenation.

Here we explored the impact of variable oxygen concentrations on the rate of fatty acid oxygenation for wildtype-PA-LOX and its Ala420Gly mutant. For this purpose, the oxygenation rate of PA-LOX was determined at two concentrations of arachidonic acid (0.16 mM and 0.32 mM) at different oxygen concentrations. The oxygen concentrations were adjusted by mixing different amounts of anaerobic PBS (argon saturated) with different amounts of hyperoxic PBS (oxygen saturated) so that the final oxygen concentrations in the assay system varied between 0.08 mM to 1.2 mM. For this purpose, two tubes containing 30 ml PBS were flushed with pure oxygen or argon for a period of 3 h. The spectrophotometric cuvette was first filled with argon gas to remove oxygen. We then added aliquots of the anaerobic buffer (0 - 1.6 ml) to the cuvette under argon atmosphere. To prevent diffusion of oxygen into the cuvette, a plastic stopper containing two capillary holes was used to close the cuvette. To achieve the desired oxygen concentration, different aliquots of hyperoxic buffer were added through the capillary holes of the stopper to give a final volume of 1.6 ml. The desired volume of anaerobic arachidonic acid solution (18 µl) was added and the reaction was started by the addition of aliquots (0.1 - 0.5 µl) of partially anaerobised PA-LOX solution. The increase in absorbance at 235 nm was measured under each condition for 180 s at 25 °C in triplicates. The Km values for oxygen for both, wildtype and mutant PA-LOX were then determined from the Hill equation from the linear part of the kinetic progress curve as described below.

Determination of oxygen affinity of wildtype- and Ala420Gly-PA-LOX

Prof. Dr. Hermann-Georg Holzhütter (Institut für Biochemie, Charité - Universitätsmedizin Berlin, Germany) evaluated the reaction kinetics of wildtype-PA-LOX and its Ala420Gly mutant at different oxygen concentrations. When the results characterizing the oxygen affinity of wildtype-PA-LOX and its Ala420Gly-mutant were evaluated, the kinetic raw data obtained were first fitted to the Michaels-Menton equation (Hill coefficient n =1). Unfortunately, the degree of fitting was not satisfying so we fitted the data to the Hill-equation (mentioned below) and obtained a higher degree of fitting.

$$V = \frac{V_{max}\, O_2{}^n}{S_{0.5}{}^n + O_2{}^n}$$

Here, Vmax represents the maximal catalytic activity the enzyme exhibited under

oxygen saturation conditions. $S_{0.5}$ is the half-saturation concentration of oxygen at which half-maximal rate is reached and the coefficient n takes into account positive cooperativity reflected by the sigmoidal shape of the activity-oxygen relationship. Employing the boot-strap method, the mean values and variances of the three kinetic parameters were determined. By assigning to each oxygen concentration randomly a single activity measurement selected from the set of repetitive measurements, restricted data sets were generated. Numerical values for the kinetic parameters were estimated by fitting the model to the randomly chosen restricted data set by least-square minimisation. The bootstrap trials were repeated 50 times and based on the 50 bootstrap sets of parameter values (mean ± variances) were calculated.

2.2.5.1.4. Experiments with stereospecifically labeled substrates

LOX reactions are initiated by stereospecific hydrogen abstraction from a bisallylic methylene group of the fatty acid substrate. This initial elementary reaction is followed by oxygen insertion at the opposite face of the substrate molecule. Thus, there is an antarafacial relationship between the initial hydrogen abstraction and the subsequent oxygen insertion during the LOX reaction. To test whether PA-LOX follows this paradigm, it was incubated with linoleic acid carrying a deuterium either at the pro$S$- ([11S-^{2}H]) position or at the pro$R$- ([11(R)-^{2}H]) position at C11 (bisallylic methylene) of linoleic acid. The rate of oxygenation of the two-substrate isomers was determined by measuring the increase in absorbance at 235 nm and 25 °C and the relative reaction rates were calculated. After 5 min, the reaction was stopped and the products were analyzed by HPLC. Reaction products were prepared by RP-HPLC (no separation of 13- and 9-HODE) and further analyzed by normal phase- and chiral phase-HPLC. Retention of the deuterium label in the final reaction products was quantified by GC/MS. The pro$R$ linoleic acid and pro$S$ linoleic acid were a kind gift of Prof. Mats Hamberg (Department of Medical Biochemistry and Biophysics, Karolinska Institute, Stockholm, Sweden).

2.2.5.2. Oxygraphic activity assay

The abstraction of hydrogen in the LOX reaction is followed by the introduction of atmospheric dioxygen into the fatty acid molecule. Thus, consumption of oxygen

from the reaction mixture was considered as an additional read out parameter for the oxygenase activity of PA-LOX. These measurements were carried out on the oxygraph using a Clark-type oxygen electrode (Helmut Saur Laborbedarf, Reutlingen, Germany). The reaction mixture comprised of 1 ml PBS containing 165 µM arachidonic acid or linoleic acid incubated in the presence of rabbit ALOX15 and PA-LOX. After 5 min of incubation, the reaction was stopped by the addition of sodium borohydride. After acidification and addition of methanol, the products were then analyzed by HPLC. The membrane oxygenase activity of rabbit ALOX15 and PA-LOX was determined by incubating both the LOXs with 1 mg/ml beef heart mitochondrial membranes. After 15 min of incubation, the products were recovered by lipid extraction and alkaline hydrolysis and then analyzed on the HPLC.

2.2.5.3. HPLC quantification of reaction products

2.2.5.3.1. Reversed phase - HPLC (RP-HPLC)

Isocratic RP-HPLC

HPLC analyses were performed on Shimadzu instrument equipped with a Hewlett Packard diode array detector 1040 A. A Nucleodur C18 Gravity column (Marchery-Nagel, Düren, Germany; 250 x 4 mm, 5 µm particle size) coupled with a guard column (8 x 4 mm, 5 µm particle size) was used. A flow of 1 ml/min was maintained throughout the run. The respective products were detected at different absorbances and the corresponding solvents as indicated in **Fout! Ongeldige bladwijzerverwijzing.**.

Table 3: The absorbances and solvent systems used while detecting different LOX-derived products.

Products	Absorbance	Solvent system
Conjugated dienes	235 nm	85/15/0.1 (% v/v) of methanol/water/acetic acid
Conjugated trienes	270 nm	80/20/0.1 (% v/v) of methanol/water/acetic acid
Conjugated tetraenes	300 nm	380/620/1 (% v/v) of acetonitrile/water/acetic acid

RP-HPLC separation of mono- and double oxygenated phospholipids

Phospholipids containing a linoleic acid residue at both, the sn1- and the sn2-position can be oxygenated by PA-LOX to a mono- and a double-oxygenated phospholipid. To separate mono- and double oxygenated phospholipids, the reaction products were analysed on a gradient RP-HPLC system. An aliquot of PA-LOX was incubated side by side with 1-palmitoyl-2-linoleoyl-phosphatidylethanolamine and 1,2-dilinoleoyl-phosphatidylethanolamine. The lipids were extracted (Bligh and Dyer, 1959) and the oxygenated phospholipids were then directly analysed on a Shimadzu equipment and diode array detector. A Nucleodur C18 Gravity column (Marchery-Nagel, Düren, Germany; 250 x 4 mm, 5 µm particle size) was used. The two solvents employed with this system were: 1) Solvent A: methanol/acetonitrile/water in the ratio of 70/20/10 (% v/v) containing 1 mM ammonium acetate and 2) Solvent B: 100% Methanol containing 1 mM ammonium acetate. The gradient system was set up in the following manner: For the first 10 min, 100 % solvent A was employed. Due to the lower concentration of methanol in solvent A (compared to solvent B), the more polar compounds (di-oxygenated-PE) were first eluted. Then from 11-40 min, the solvent system was shifted from 100 % solvent A to 100 % solvent B (linear increase in solvent B concentration) to elute apolar compounds (mono-oxygenated PE). From 41 – 50 min, the system was run with 100 % solvent B. Finally, the solvent system was shifted back to 100 % solvent A within 10 min (between 51 – 60 min) by a linear gradient. Absorbance at 235 nm indicated the presence of conjugated diene containing phospholipids (mono-HODE-PE and di-HODE-PE).

2.2.5.3.2. Straight phase - HPLC (SP-HPLC)

The separation of crirical pairs of different HETE-isomers (e.g. 11- and 15-HETE, 12- and 8-HETE) and HODE-isomers (13- and 9-HODEs) is not possible by RP-HPLC under our analytical conditions and thus, normal phase-HPLC (SP-HPLC) was carried out to resolve these isomers. SP-HPLC was performed on a Nucleosil 100 - 5 column (Macherey/Nagel, Düren, Germany, 250 x 4 mm, 5 µm particle size). An isocratic solution system of n-hexane/2-propanol/ acetic acid in a ratio of 100/2/0.1 (% v/v) was employed at a flow rate of 1 ml/min. The products were

detected at an absorbance of 235 nm. Using authentic standards, the HPLC was calibrated and the products eluting at the respective retention times were collected for further analyses.

In case of the incubations with mitochondrial membranes, the major classes of phospholipids (PE, PS, PI, PC and cardiolipin (CL)) were separated by SP-HPLC on a Nucleosil 50 - 7 column (Macherey/Nagel, Düren, Germany). The solvent system employed here consisted of 2-propanol/n-hexane/ethanol/25 mM phosphate buffer, pH 7.0/acetic acid in a ratio of 98/73.4/20/12.4/0.12 (% v/v) at a flow rate of 1 ml/min (isocratic elution). To avoid precipitation of the phosphate, the solvents were mixed in a particular order (Robins and Patton, 1986). The absorbance at 210 nm indicating the presence of PUFAs containing phospholipids and absorbance at 235 nm indicating the presence of conjugated diene in the phospholipids were simultaneously recorded. Unfortunately, the oxygenated phospholipids were not well separated from their non-oxygenated counterparts under these chromatographic conditions.

2.2.5.3.3. Chiral phase - HPLC (CP-HPLC)

The enantiomer composition or chirality of the oxygenation products was specified by CP-HPLC employing a Chiralcel OD column (Daicel Chem. Ind., Ltd., Osaka, Japan). A solvent system consisting of hexane/2-propanol/acetic acid (100/5/0.1 % v/v) and a flow rate of 1 - 1.5 ml/min was employed for this purpose (isocratic elution). The products were collected from either RP- or SP-HPLC, solvent was evaporated and the products were reconstituted in the CP-HPLC solvent for analysis.

2.2.6. Storage stability of purified enzyme

The stability of PA-LOX during long-term storage was explored under two conditions. The recombinant enzyme was incubated for different time sets (7 days) in the presence and absence of 10 % glycerol (v/v). After the respective time period, the enzymatic activity of PA-LOX was determined by measuring the catalytic activity of the enzymes using the spectrophotometric method.

2.2.7. Determination of iron content

Ms. Constanze Richter carried out the atom absorbance spectroscopy (AAS) at the Institute of Food Chemistry and Toxicology, Technical University Berlin, Germany, to quantify the iron content of PA-LOX. For the determination of iron content of wildtype-PA-LOX, the enzyme was first expressed and purified. Then the iron content of 5 mg/ml of enzyme was quantified by AAS on a Perkin-Elmer Life Sciences AA800 instrument equipped with an AS800 auto sampler (Massachusetts, United States). The iron content value obtained was related to the amount of enzyme that was measured spectrophotometrically (1 mg/ml of pure PA-LOX gives an absorbance of 1.1 at 280 nm).

2.2.8. GC/MS and LC/MS/MS analysis

2.2.8.1. Analysis of fatty acid oxygenation products of PA-LOX

The fatty oxygenation capacity of PA-LOX was tested with different polyenoic fatty acid substrates. The dominant conjugated dienes formed were prepared by RP-HPLC. The carboxylic groups were methylated, the hydroxy groups were silylated and the derivatives were analyzed by GC/MS to elucidate the chemical structure of the major oxygenation products. Our collaborator, Dr. Igor Ivanov (University of Rostock, Institute of pharmacology and toxicology, Rostock, Germany), carried these analyses out on a Hewlett Packard 5890 Series II Plus gas chromatograph coupled with Hewlett Packard 5971 detector and equipped with a 19091A 101HP-Ultra 1 column (12 m × 0.2 mm, coating thickness 0.33 µm). The temperature of the injector and the ion source was maintained at 280 °C and 200 °C, respectively. The following temperature program was followed for the elution of the derivatized fatty acids from the gas chromatographic column: isothermally at 70 °C for 3 min and then from 70 °C to 300 °C at a rate of 30 °C/min.

2.2.8.2. Analysis of products with stereospecifically labeled substrates

Prof. Mats Hamberg (Department of Medical Biochemistry and Biophysics, Karolinska Institute, Stockholm, Sweden) performed the GC/MS analysis of the reaction products obtained when PA-LOX was interacted with stereospecifically labeled linoleic acid (Hamberg, 1998, 2011). To determine whether the pro*S*- or pro*R*-hydrogen of the bisallylic methylene was abstracted by PA-LOX, both the

wildtype and Ala420Gly-PA-LOX were incubated with stereospecifically labeled linoleic acid. The activity of this interaction was monitored on the spectrophotometer after which the products were separated on SP-HPLC. The retention of deuterium in the products (13-HODE in wildtype and 13-HODE and 9-HODE in Ala420Gly-PA-LOX) was determined by GC/MS analysis. Since the mass of deuterium is higher than that of hydrogen, the C-^{2}H bonds of the linoleic acid are broken more slowly compared to the C-H bonds (Brash et al., 2012). This difference is translated into a strong kinetic isotope effect (KIE).

2.2.8.3. Oxidized lipids of PA-LOX treated RBCs

Dr. Maceler Aldrovandi, (Institute of Infection and Immunity, Cardiff University, United Kingdom) performed the LC/MS/MS analysis of the PA-LOX treated human erythrocytes. The membrane oxygenase activity of PA-LOX was tested by incubating the enzyme with intact erythrocytes for 12 h and 24 h. After the incubation period, the assay mixture was subjected to lipid extraction and the extracts were used to identify the oxygenated phospholipid species by reverse-phase LC/MS/MS. Lipid extracts (10 µl) were analyzed on a LUNA RP C18 column (150 x 2.1 mm, 3 µm particle size) (LUNA, Cheshire, United Kingdom) using a binary solvent gradient of mobile phase A (methanol/acetonitrile/water of 60/20/20 % v/v, 1 mM ammonium acetate) and B (methanol 100 %, 1mM ammonium acetate) at a flow rate 0.2 ml/min over 50 min. The elution gradient of B (%) over time was: 50 – 100 % for 10 min, 100 % for 30 min, reduced to 50 % in 2 min and held at 50 % for next 8 min. Products were monitored by LC/MS/MS in negative ion mode, on a 6500 Q-Trap (Sciex, Cheshire, United Kingdom) using the specific parent to daughter transitions (transitions specified in each graph in Figure 31 of the results section 3.3.4.2.). Optimized ESI-MS/MS conditions were: source temperature 500 °C, GS1 40, GS2 30, curtain gas (CUR) 35, ion spray voltage (IS) -4500 V, first quadrupole (Q1) at low resolution, third quadrupole (Q3) at unit resolution, dwell time 75 s, de-clustering potential (DP) -50 V, entrance potential (EP) -10 V, collision energy (CE) -38 V and collision cell exit potential (CXP) at -11 V. 1,2-dipentadecanoyl-sn-glycero-3-phosphocholine (15:0/15:0) (Avanti Polar Lipids, Alabaster, USA) and 1,2-dipentadecanoyl-sn-glycero-3-phosphoethanolamine (15:0/15:0) (Avanti Polar Lipids, Alabaster, USA) internal

standards were added at 10 ng per sample. Lipids were normalized to internal standards to correct for extraction efficiencies.

2.2.9. Protein crystallization

The crystal trials, X-ray diffraction data collection, structural refinement and structural modeling of both the wildtype- and Ala420Gly-PA-LOX were carried out under the supervision of Dr. Patrick Scheerer by Jacqueline Kalms and Etienne Galemou Yoga (Institute of Medical Physics and Biophysics, Charité - Universitätsmedizin Berlin, Germany).

2.2.9.1. Wildtype- PA-LOX

Crystallization

PA-LOX was crystallized in two different crystallization buffers leading to two different crystal forms. Crystallizations were performed with the sitting-drop vapor diffusion method in 24-well Linbro plates (Jena Biosciences, Jena, Germany) and a protein concentration of about 15 mg/ml at 293 K. The first crystallization condition (crystal form 1) was obtained over a reservoir solution containing 10 % polyethylene glycol (PEG) 3350, 50 mM magnesium chloride and 100 mM HEPES buffer at pH 7.5. Precipitants and protein solution were mixed in a 1.5 : 2 µl ratio into micro-bridges (Hampton Research, Aliso Viejo, USA). After 6 – 8 weeks the needle shaped PA-LOX crystals were cryo-cooled in liquid nitrogen using 20 % glycerol (v/v). The reservoir solution of the second crystallization conditions (crystal form 2) contained 12 % PEG 3350, 0.2 M magnesium chloride and 0.1 M Tris(hydroxymethyl)-aminomethane at pH 7.1. Precipitants, protein solution and seeding stock were mixed into micro-bridges (Hampton Research, Aliso Viejo, USA) according to the Microseed Matrix Seeding (MMS) protocol from Hampton Research (Aliso Viejo, USA). After 3 – 6 weeks, the plate-shaped crystals were cryo-cooled in liquid nitrogen using 25 % glycerol (v/v) as cryo-protectant. The cryo-protectant was mixed to the crystallization buffer in 5 % steps (15, 20 and 25 %).

Data collection and structure analysis

Diffraction data were collected at 100 K using synchrotron X-ray sources from BESSY II (Berlin, Germany) (Mueller et al., 2015) and ESRF (Grenoble, France). The best diffraction datasets for the highest resolution of both PA-LOX crystal

forms were collected at synchrotron beamline ID23-1 (Nurizzo et al., 2006) at ESRF with a Pilatus 6M-F detector at 0.972 nm wavelength. The data collection and strategy software packages MxCuBE (Gabadinho et al., 2010) and EDNA (Incardona et al., 2009) were used. The data collection of the first crystal form (needle shape – crystal form 1) was performed with a crystal-to-detector distance of 284 mm and a rotation increment of 0.1 ° with 0.04 s exposure time for each frame (1200 images). 1500 images of the second crystal form (plate shape – crystal form 2) were collected with a crystal-to-detector distance of 215 mm and a rotation increment of 0.1 ° with an exposure time of 0.04 s for each frame. The images of each data set were indexed, integrated and scaled using the XDS (Kabsch, 2010) program package and the CCP4 program SCALA (Collaborative Computational Project, 1994; Evans, 2006). The crystal form 1 belongs to the orthorhombic space group $P2_12_12$ (approximately unit cell constants: a = 133.09 Å, b = 116.35 Å, c = 42.72 Å, α = β = γ= 90.00 °). The crystal form 2 belongs to the orthorhombic space group $C222_1$ (a = 83.74 Å, b = 97.39 Å, c = 153.84 Å, α = β = γ= 90.00 °).

Table 5 (Results section 3.1.3.2.) summarizes the statistics for crystallographic data collection and structural refinement. Initial phases for both crystal forms of wildtype-PA-LOX were obtained by the conventional molecular replacement protocol (rotation, translation, rigid-body fitting) using the crystal structure of a phospholipid-lipoxygenase complex from *Pseudomonas aeruginosa* (PDB entry 4G32), which was used in the program Phaser (McCoy et al., 2007) of the CCP4 software package (Collaborative Computational Project, 1994). A simulated-annealing procedure with the resulting models were performed using a slow-cooling protocol and a maximum likelihood target function, energy minimization and B-factor refinements by the program PHENIX (Adams et al., 2010), which were carried out in the resolution range of 43.8 - 1.9 Å for the crystal form 1 and 48.97 - 1.48 Å for the crystal form 2, respectively. After the first round of refinements, phospholipid substrates in the ligand-binding pockets were clearly visible in the electron density of both σ_A-weighted 2*Fo-Fc* maps, as well as in the σ_A-weighted simulated annealing omitted density maps for both crystal forms of PA-LOX. Both PA-LOX crystal forms were modeled with TLS refinement (TLS - Translation, Libration (small movements) and Screw-rotation of a group of atoms) using anisotropic temperature factors for all atoms (Winn et al., 2001).

Restrained, individual B-factors were refined, and the crystal structure was finalized by the CCP4 program REFMAC5 (Vagin et al., 2004) and other programs of the CCP4 suite (Collaborative Computational Project, 1994). The final model has agreement factors R_{free} and R_{cryst} of 18.2 % and 14.4 %, for wildtype-PA-LOX crystal form 1 and 15.5 % and 13.6 %, for wildtype-PA-LOX crystal form 2, respectively. Manual rebuilding of the wildtype-PA-LOX crystal form 1 and 2 models and electron density interpretation were performed after each refinement cycle using the program COOT (Emsley et al., 2010). Structure validation was performed with the programs PHENIX (Adams et al., 2010), RCSB PDB Validation server (Berman et al., 2000), MolProbity (Davis et al., 2007), SFCHECK (Vaguine et al., 1999), PROCHECK (Laskowski et al., 1993), WHAT_CHECK (Hooft et al., 1996) and RAMPAGE (Lovell et al., 2003). All crystal structure superpositions of backbone a-carbon traces were performed using the CCP4 program LSQKAB (Collaborative Computational Project, 1994). All molecular graphics representations in this work were created using the PyMol software package.

Structural modeling of enzyme substrate complexes

Both structures of the wildtype-PA-LOX enzyme present a phosphatidylethanolamine molecule in two connected hydrophobic pockets of which one is close to the active site (subcavity 1). The electron density of the endogenous ligand was used to model linoleic acid and arachidonic acid in both PA-LOX structures. Structures of arachidonic acid and linoleic acid were provided by the COOT library and were directly modeled into the (positive difference) *Fo-Fc* electron density map of the ZPE-ligand via several steps of rotation, translation and real space refinement. The model-complex structures were finalized using the restrained refinement procedure of the CCP4 program REFMAC5 and a last refinement of geometric restrains using COOT (Vagin et al., 2004). The structure of 5,8,11-eicosatrienoic acid was created with PyMOL using arachidonic acid as template, since both fatty acids only differ in the double bond between C14 and C15.

2.2.9.2. Ala420Gly-PA-LOX

Crystallization

Purified Ala420Gly mutant was crystallized with the sitting-drop vapor diffusion

method in 24-well Linbro plates (Jena Biosciences, Jena, Germany) at a protein concentration of about 15 mg/ml at 293 K. The reservoir solution contained 12 % polyethylene glycol 3350, 0.2 M magnesium chloride and 0.1 M Tris(hydroxymethyl)-aminomethane at pH 7.1. Precipitants, protein solution and seeding stock were mixed into micro-bridges (Hampton Research, Aliso Viejo, USA) according to the Microseed Matrix Seeding (MMS) protocol from Hampton Research. After 2-3 weeks, the plate-shaped crystals were cryo-cooled in liquid nitrogen using 25 % glycerol (v/v) as cryo-protectant. The cryo-protectant was mixed with the crystallization buffer in 5 % steps (15, 20 and 25 %).

Data collection and structure analysis

Diffraction data was collected at the synchrotron radiation facility ESRF in Grenoble, France. The best data set was collected at the tunable beamline ID 23-1 (Nurizzo et al., 2006) with a PILATUS 6M-F detector at a wavelength of λ = 0.972 Å using the data collection and strategy software packages *MxCube* (Gabadinho et al., 2010) and EDNA (Incardona et al., 2009). The collection was performed at 100 K, a crystal-to-detector distance of 261 mm and a rotation increment 0.15 ° with an exposure time of 0.04 s for each frame (1000 images). The images of the best data set were indexed, integrated and scaled using the XDS program package (Kabsch, 2010) and the CCP4 program SCALA (Collaborative Computational Project, 1994; Winn et al., 2011). Crystals belong to orthorhombic space group $C222_1$ (approximately unit cell constants: a = 84 Å, b=97 Å, c=156 Å; $\alpha=\beta=\gamma=90.00$ °). Initial phases for PA-LOX-Ala420Gly mutant were obtained by molecular replacement based on the crystal structure of the phospholipid-lipoxygenase complex from *Pseudomonas aeruginosa* (PDB entry 5IR4) as initial search model using the CCP4 program PHASER (McCoy et al., 2007). Subsequently, different refinement strategies (*inter alia* real-space refinement, B-factor refinements) and simulated-annealing (slow cooling protocol, maximum likelihood target function, energy minimization) were carried out. The search for water molecules was performed with the PHENIX program (Adams et al., 2010). The crystal structure was modeled with TLS refinement using anisotropic temperature factors for all atoms. The crystal structure was finalized with the CCP4 program REFMAC5 (Murshudov et al., 1997). Manual rebuilding of the PA-LOX-Ala420Gly mutant model and electron density interpretation was performed after each refinement cycle using the program

COOT (Emsley et al., 2010). The final model has agreement factors R_{free} / R_{work} of 17.1 % / 13.9 % (Brünger, 1992). Structure validations were performed with the programs of the RCSB PDB Validation server (Berman et al., 2000), MolProbity server (Davis et al., 2007) and WHAT IF server (Rodriguez et al., 1998). All molecular graphics representations were created using PyMOL. Table 13 (Results section 3.2.3.4.) summarizes the statistics for crystallographic data collection and structural refinement.

Structural modeling of enzyme substrate complexes

The crystal structure of the PA-LOX-Ala420Gly mutant described here contains a phosphatidylethanolamine molecule (namely ZPE in the PDB entry) bound at the substrate-binding pocket. The two fatty acid moieties of this endogenous ligand occupy two adjacent fatty acid binding sub-cavities, which are connected by a lobby, which harbors the polar head group of the phospholipid. The sub-cavity that contains the sn1 fatty acid involves the catalytic non-heme iron. Linoleic acid and arachidonic acid molecules were modeled into this sub-cavity on the basis of the endogenous ligand. Both structures of the two fatty acids were obtained from the COOT (Emsley and Cowtan, 2004) small molecule library and directly fitted manually into the position of the endogenous ligand via several steps of rotation; translation and geometry regularization refinement. The model-complex structure was finalized using the structure geometry optimization (idealization) procedure of the CCP4 program REFMAC5, following a refinement of geometric restrains in COOT.

Caver tunnel analysis

The Caver 3.0 (Chovancova et al., 2012) program was used as PyMOL plugin. The settings in the program have been changed manually. The C11 and C15 carbon atom of the docked arachidonic acid as well as the C9 and C13 of linoleic acid served as initial starting point in the crystal structures of both wild-type (PDB entry 5IR4) and Ala420Gly (PDB entry 5LC8) mutant PA-LOX. The shell depth (4 Å), shell radius (3 Å), cluster threshold (3.5 Å), the maximum distance (3 – 4 Å) and the desired radius (5 Å) were maintained constant for all calculations. The maximum distance specifies the maximal distance of the tunnel calculation starting point from the initial starting point. The minimum probe radius was defined by the largest value showing a tunnel within the given parameters.

3. RESULTS

3.1. Expression and characterization of PA-LOX

3.1.1. Sequence alignment

To compare the amino acid sequence of the PA-LOX variant expressed in this study (no secretory sequence) with the sequences from other 15-lipoxygenating isoforms (human ALOX15, human ALOX15B, rabbit ALOX15, soybean 15-LOX and mouse alox15, Table 4), sequence alignments were carried out using the EMBOSS Needle software from EMBL-EBI. To get accurate alignments, the software introduced gaps to compensate for the insertions and deletions.

Table 4: Pairwise alignment of PA-LOX with other LOX-isoforms.

LOX type	Identity (%)	Similarity (%)
Human ALOX15	25.6	38.8
Human ALOX15B	28.0	40.5
Rabbit ALOX15	22.3	34.7
Soybean 15-LOX1	22.9	34.0
Mouse alox15	24.9	38.5

PA-LOX shares a medium (25 % amino acid identity, 40.5 % amino acid similarity) degree of amino acid conservation with these five lipoxygenases. These data indicate that PA-LOX may not be closely related to these LOXs.

Summary: As prokaryotic LOXs, PA-LOX only shares a minor degree of amino acid homology with higher developed plant and animal LOXs.

3.1.2. Expression of PA-LOX as a recombinant protein

For construction of the expression plasmid the cDNA of PA-LOX lacking the secretion sequence was cloned into the pET 28a(±) expression plasmid, which contains a kanamycin resistant gene. Because of technical reasons the coding sequence of PA-LOX in the expression plasmid was preceded by a N-terminal His_6-tag followed by 11 additional amino acid residues originating from the pET 28a(±) vector. The construct was devoid of the first 18 N-terminal amino acids of

the native protein, which involves the signal peptide responsible for effective secretion (Vance et al., 2004). The recombinant protein begins with alanine at the 19th position (last amino acid of the signal peptide) of the sequence (arrow in Figure 5).
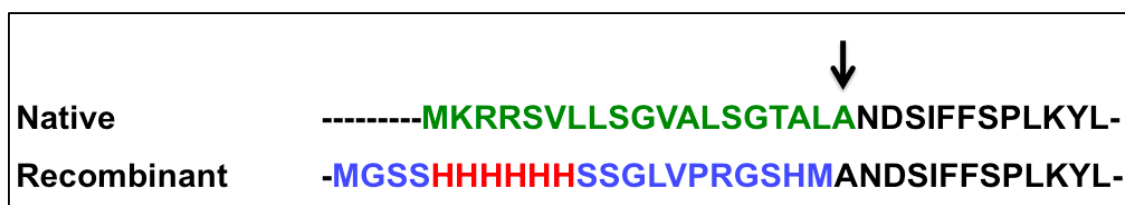
Figure 5: The predicted signal peptide region, His$_6$-tag and the vector sequence of the native and recombinantly expressed PA-LOX. Green: secretory sequence, black: protein sequence, blue: vector sequence and red: N-terminal His$_6$-tag; arrow: the start position of the coding sequence of signal sequence free PA-LOX.

PA-LOX was expressed as a recombinant protein in *E. coli* BL21 cells. After expression was induced with IPTG, the cells were grown overnight at 25 °C, bacteria were spun down, washed with PBS and the bacterial pellet was reconstituted in 5 ml of PBS. After sonication, PA-LOX was purified from the bacterial lysis supernatant by affinity chromatography on a nickel agarose column. From SDS-PAGE gels stained with coomasie blue, it was concluded that the majority of the recombinant protein was eluted in elution fractions 1-3 and that the LOX preparation was >80 % pure (Figure 6). The identity of the protein bands was confirmed by immunoblotting with an anti-His$_6$-tag antibody (not shown). In a culture volume of 50 ml, we got a total yield of 3.2 ± 0.3 mg (n=10) of purified recombinant protein. Therefore, ~63.3 ± 5 mg of pure PA-LOX can be obtained per liter of bacterial culture fluid. Another study has reported a total yield of 12 mg PA-LOX/L (Deschamps et al., 2016) using a different *E. coli* expression system. From SDS-PAGE (Figure 6), it became evident that the recombinant PA-LOX migrated at an apparent molecular weight of 70 kDa, which was consistent with previous literature data (Vidal-Mas et al., 2005). However, this value significantly differs from the PA-LOX isolated from the periplasmic space of *P. aeruginosa* bacteria, which showed a molecular weight of 45 kDa.
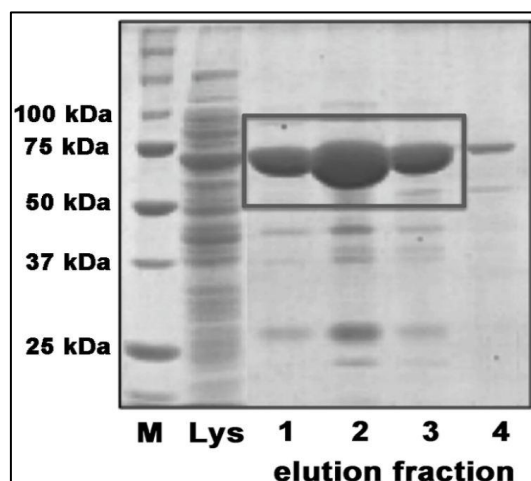
Figure 6: Bacterial PA-LOX expression. PA-LOX was expressed as a recombinant His6-tag-fusion protein in E. coli in a 50 ml culture. The cells were first washed and the bacterial pellet was re-suspended in 5 ml of PBS. After lysis by ultrasonication, an aliquot (500 µl) of the bacterial lysis supernatant was stored for further analysis. The remaining bacterial lysate was then purified on a nickel-agarose affinity chromatography column. The majority of the recombinant PA-LOX protein was eluted in the fractions 1, 2 and 3 when the column was eluted with 300 µl aliquots of the elution buffer containing 200 mM imidazole. An aliquot (1 µl) of the bacterial lysis supernatant (Lys) and aliquots (2 µl) of the different elution fractions 1,2,3 and 4 were analyzed by SDS-PAGE (Coomassie staining) to determine the degree of purity. M-Precision plus unstained marker (Biorad, California, USA) was used (Banthiya et al., 2016).

These data suggest that the native protein might have undergone post-translational proteolysis before or during its excretion into the periplasmic space (Busquets et al., 2004).

Summary: Recombinant PA-LOX was high level expressed in *E. coli* (63 mg/l liquid culture) as N-terminal His6-tag fusion protein and purified to electrophoretic homogeneity (80 % pure) by affinity chromatography on Ni-agarose.

3.1.2.1. Purification of PA-LOX using gel filtration

The PA-LOX preparation obtained from affinity chromatography was about 80 % pure exhibiting a molecular weight of 70 kDa. However, in addition to the PA-LOX band, two other major contaminating proteins were seen at molecular weights 25 kDa and 45 kDa. In an attempt to further purify PA-LOX, the elution fractions obtained from affinity chromatography were pooled and subjected to gel filtration.
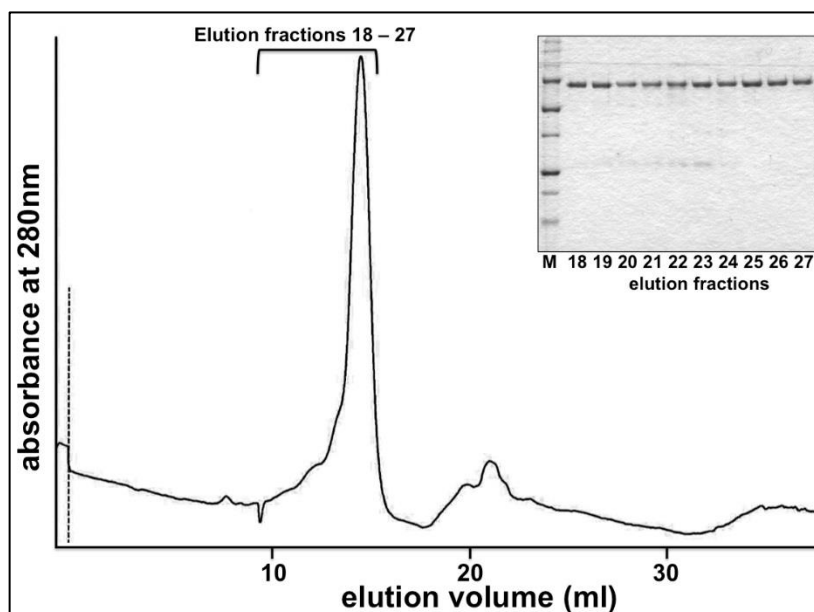
Figure 7: Purification of PA-LOX by gel filtration. Affinity purified enzyme (4 mg) was subjected to FPLC-gel filtration. Elution fractions of 500 µl were collected. Aliquots (0.8 µg) of fractions 18 – 27 (elution volume 9 – 14 ml) were then analyzed by SDS-PAGE (Coomassie staining) to determine the degree of purity. M: Precision plus unstained marker.

From Figure 7, it can be seen that a single major peak of PA-LOX exhibiting a molecular weight of 70 kDa was obtained on the FPLC. Aliquots of the major peak obtained from gel filtration were then analyzed on SDS-PAGE to determine the purity of the peak. As indicated in the inset of Figure 7, the contaminating bands seen in Figure 6 were now absent in these aliquots indicating a close to 100 % pure PA-LOX preparation.

Summary: When subjected to purification by gel filtration chromatography, a single major peak close to 100 % pure PA-LOX preparation was obtained.

3.1.3. Chemical properties of enzyme preparation

3.1.3.1. Iron content of PA-LOX

The iron content of the recombinantly expressed enzyme was 106 ± 3 mol % indicating that each molecule of enzyme carries one iron ion. Thus, the iron homeostasis of the expression system was sufficient to allow high yield expression of an iron containing recombinant protein. In a recent study, in which PA-LOX was expressed as 76 kDa version using a TOPO expression vector the

authors have identified an iron load of 67 % (Deschamps et al., 2016) indicating that 1 out of 3 enzyme molecules in this particular enzyme preparation did not contain iron and thus, was catalytically silent.

Summary: Recombinant PA-LOX contains 1 gram atom iron / mole enzyme.

3.1.3.2. Crystal structure of wildtype-PA-LOX

In previous studies on the structure-functionality relation of PA-LOX, the enzyme was crystallized (Garreta et al., 2013) and its 3D structure was solved at 1.75 Å resolution. In addition to this structure, two other sets of X-ray data have been provided for this enzyme. These included a wildtype-PA-LOX with a PDB entry 4G33 (2.0 Å) (Garreta et al., 2013) and Gly188Glu mutant of PA-LOX with a PDB entry 4RPE (1.6 Å). In all structures the active site of the enzyme involved a complete phospholipid molecule (phosphatidylethanolamine – ZPE, of PDB nomenclature), which contains different fatty acids: C14:1, C18:1 at its sn1 and sn2 positions (Garreta et al., 2013). In contrast, the Gly188Glu mutant of PA-LOX has been suggested to involve another type of phosphatidylethanolamine (8PE, of PDB nomenclature) at its active site which contained C14:0, C18:0 as its fatty acids (PDB entry: 4RPE). Thus, although the crystal structures of the proteins are almost identical the structures of the bound endogenous ligands are different. It should be stressed at this point that the electron density maps generated by X-ray crystallography at such resolutions can neither accurately predict the chain length of the attached fatty acids nor differentiate between single and double bonds. Therefore, four points need to be addressed in greater detail in order to obtain the precise structure of the endogenous ligand. 1) The number of carbon atoms of the fatty acid chains at sn1 and sn2 positions of the phospholipid, 2) The presence of double and/or single bonds in these fatty acids, 3) The positions of the double (if any) bonds and 4) The geometry (*cis*/*trans*) of the double bonds. More detailed chemical analysis of the enzyme bound lipids must be carried out to comprehensively identify the precise structure of the endogenous ligand.

We also solved the crystal structure of our recombinantly expressed PA-LOX and obtained two different forms of crystals with different geometry: 1) Crystal form 1:

at 1.9 Å resolution (PDB entry 5IR5; space group $P2_12_12$) 2) Crystal form 2: at 1.48 Å resolution (PDB entry 5IR4; space group $C222_1$).

Table 5 summarizes the details of data collection and the refinement statistics. Wildtype-PA-LOX is devoid of the N-terminal PLAT domain (Figure 8A), which is a typical element of most eukaryotic LOXs (Bateman and Sandford, 1999). Unlike the eukaryotic LOXs, the substrate-binding pocket of both our crystal forms is a bifurcated cavity, which involves a phosphatidylethanolamine molecule (ZPE of the PDB nomenclature).

Table 5: Methodological details of data collection and refinement statistics of PA-LOX crystals (Banthiya et al., 2016).

PDB entry	5IR5	5IR4
Beamline	ESRF; ID23-1 (Grenoble, France)	
Number of crystals	1	
Space group	$P2_12_12$	$C222_1$
Unit cell (a, b, c [Å]; α, β, γ [°])	133.09, 116.35, 42.72; 90.00, 90.00, 90.00	83.74, 97.39, 153.84; 90.00, 90.00, 90.00
Wavelength [Å]	0.97242	0.97242
Resolution [Å]	43.8 - 1.9 (2.0 – 1.9)	48.97 - 1.48 (1.56 – 1.48)
R_{pim}	0.034 (0.249)	0.035 (0.355)
R_{merge}	0.065 (0.471)	0.076 (0.774)
$I/\sigma (I)$	13.1 (2.8)	14.5 (2.0)
Completeness [%]	99.6 (99.8)	99.8 (99.0)
Redundancy	4.4 (4.4)	5.6 (5.6)
R_{work} [%]	14.4	13.6
R_{free} [%]	18.2	15.5
Ramachandran favoured [%]	94.2	94.7
Ramachandran allowed [%]	5.8	5.3
Ramachandran outlier [%]	0	0
RMSD superpose (LSQKAB)	0.118 (PDB entry 4G32)	0.364 (PDB entry 4G33)

Previous data suggested that the phospholipid head forms 2 ionic bonds with the protein. 1) Between the phosphate head group of the phospholipid and guanidinium group of Arg422 (Figure 8A) and 2) Between the terminal amino group of the phospholipid and the carboxylic group of Asp190. In addition to this, the side chain of Arg422 might also contribute to enzyme-phospholipid interaction (Garreta et al., 2013).
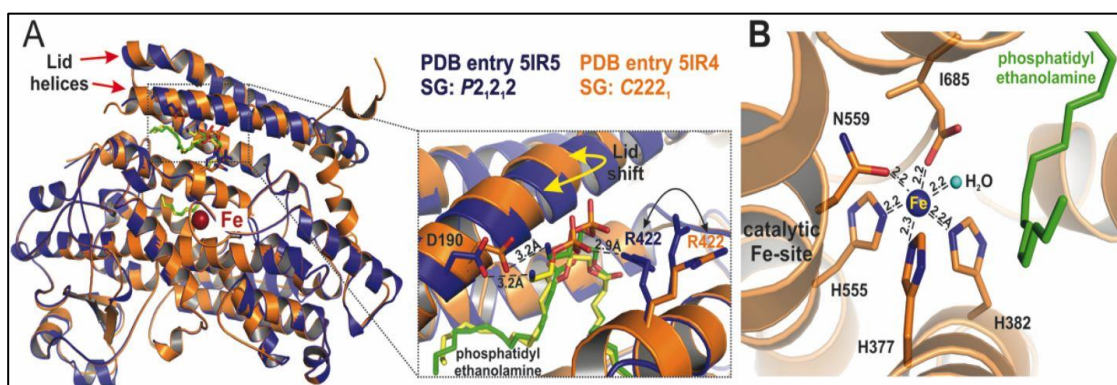
Figure 8: Comparison of wildtype-PA-LOX crystal structures: A) The two forms of PA-LOX crystals (crystal form 1 and 2) were superimposed on each other. Crystal form 1 is represented as a blue cartoon and the crystal form 2 as orange cartoon. The endogenous ligand (ZPE) is depicted by yellow and green sticks in crystal form 1 and 2 respectively. The non-heme iron atom is shown as a red sphere. Inset: Closer view of the substrate pocket which involves the endogenous ligand. The head group of the phosphatidylethanolamine ZPE in crystal form 1 is coordinated by the amino acids Asp190 and Arg422 via hydrogen bonds. In crystal form 2, the antiparallel lid helices are slightly shifted (by ~5 °) as indicated by the yellow arrow. Thus, the polar head group of the ligand does not have any interaction with Arg422 (depicted as a black arrow). B) The non-heme iron (blue sphere) is coordinated within an octahedral complex with five amino acids (depicted as orange sticks) as direct protein ligands and a water molecule (depicted as green sphere) (Banthiya et al., 2016).

The substrate-binding pocket of PA-LOX appears to be custom designed to efficiently bind a complete phospholipid molecule. The sn1 fatty acid of the phospholipid occupies the non-heme iron containing catalytic sub-cavity 1 while the sn2 fatty acid moiety occupies the sub-cavity 2, which is devoid of any direct access to the catalytic iron atom. The polar head group of the endogenous ligand occupies the active site "lobby". The catalytic centers of both the crystal forms contain the catalytic non-heme iron. The metal ion is complexed in an octahedral ligand sphere, in which three histidines (His377, His382 and His555), Asn559 and the C-terminal Ile685 function as direct protein iron ligands. As a sixth iron ligand, a water molecule or a hydroxyl group was identified (Figure 8B). The distance of the water (hydroxyl) molecule to the iron atom is 2.2 Å (hydrogen bond distance) and it also forms hydrogen bridges to the carboxylate oxygen of the C-terminal Ile685. The amino acids that line the substrate binding pocket include Glu373, Met374, Leu424, Phe430, Ile431, Met434, Phe435, Gln562, Ile608 and Tyr609. The catalytic subcavity-1 is separated from the catalytically silent subcavity-2 by a hydrophobic barrier formed by the amino acids Ile117,

Phe120, Val189, Ile192, Leu193, Ala196, Ser197, Phe430, Leu600, Leu603 and Glu604. The side chain of Ile608 limits the bottom of subcavity-2. Although the wildtype-PA-LOX lacks the N-terminal PLAT domain of the eukaryotic LOXs, it contains a pair of long-antiparallel helices that function as lid to the entrance of the substrate-binding pocket. These two alpha-helices occupy slightly different positions in the two crystal forms suggesting a certain degree of motional flexibility of this lid structure. Taken together, when our 3D-structure crystal forms was overlaid with the previously solved structures of the wildtype-PA-LOX (PDB entries: 4G32 and 4G33) (Garreta et al., 2013), there were only minor structural differences. Otherwise, the structures seemed virtually identical. However, the structure of the endogenous lipid ligand has not completely been solved

Summary: The wildtype-PA-LOX was successfully crystallized and the structure was solved to a resolution of 1.48 Å and 1.9 Å. Unlike eukaryotic LOXs, PA-LOX folds into a single domain structure and is devoid of the N-terminal PLAT domain.

3.1.4. Enzymatic properties of wildtype-PA-LOX

3.1.4.1. Oxidation of arachidonic and linoleic acid by PA-LOX

3.1.4.1.1. Product analysis

Arachidonic acid (AA) and linoleic acid (LA) are the two most frequently occurring polyenoic fatty acids in mammalian cells. The ability of PA-LOX to oxygenate these fatty acids was tested by incubating an aliquot of purified PA-LOX with the two fatty acid substrates. The catalytic activity was first monitored on the spectrophotometer for 3 min after which the products were prepared. RP-, SP- and CP-HPLC analysis of the prepared products indicated that PA-LOX converted arachidonic acid to 15S-HETE and linoleic acid to 13S-HODE (Figure 9 and Figure 10).
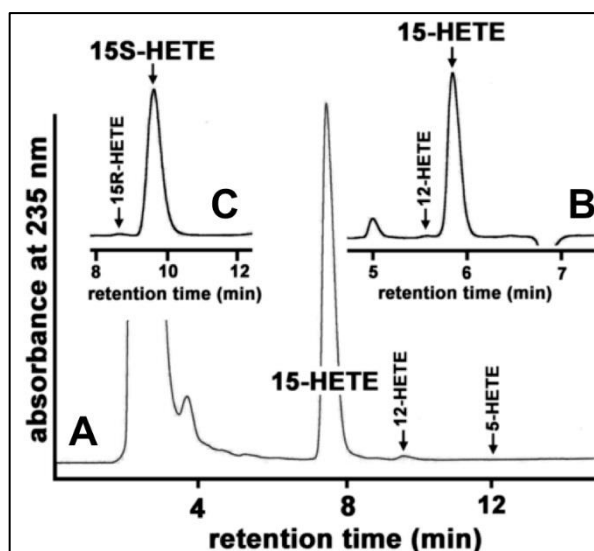
Figure 9: Product analysis of PA-LOX with arachidonic acid by HPLC. An aliquot (0.4 µg) of PA-LOX from the elution fraction 2 (obtained using nickel agarose affinity chromatography) was incubated with 165 µM of arachidonic acid in 1 ml of PBS (pH 7.4) for 3 min at 25 °C. The products were prepared and analyzed by HPLC. (A) RP-HPLC (B) SP-HPLC (C) CP-HPLC analysis. (Banthiya et al., 2016).

Thus, PA-LOX oxygenates the two fatty acids at the n-6th position irrespective of the chain length and number of double bonds present in the substrate fatty acid.
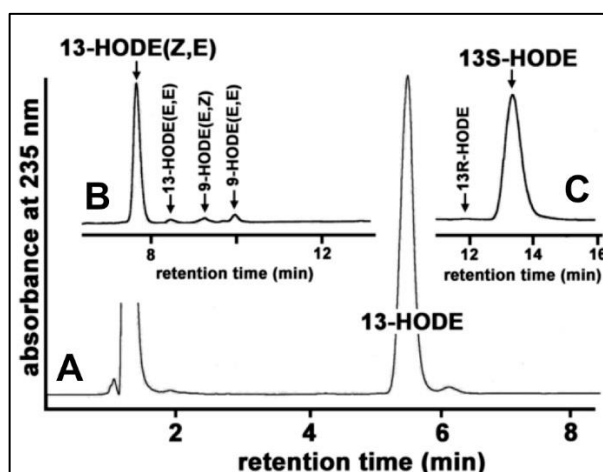
Figure 10: Product analysis of PA-LOX with linoleic acid on the HPLC. An aliquot (0.4 µg) of PA-LOX from the elution fraction 2 (obtained using nickel agarose affinity chromatography) was incubated with 165 µM of linoleic acid in 1 ml of PBS (pH 7.4) for 3 min at 25 °C. The products were prepared for product analysis on the HPLC. (A) RP-HPLC (B) SP-HPLC (C) CP-HPLC analysis. (Banthiya et al., 2016).

Summary: Recombinant PA-LOX converts arachidonic acid to 15*S*-HETE and linoleic acid to 13*S*-HODE suggesting an n-6 fatty acid oxygenase activity.

3.1.4.1.2. Quantification of kinetic parameters

Basic enzyme kinetic parameters for PA-LOX were determined both by spectrophotometrically assaying the increase in absorbance at 235 nm and oxygraphically measuring the oxygen uptake using a Clark-type oxygen electrode. On the oxygraph, a fresh preparation of PA-LOX exhibited a molecular turnover ratio of 162.4 ± 33.3 s^{-1} at 165 μM of linoleic acid in the absence of any detergent. In strictly comparative measurements under identical experimental conditions pure rabbit ALOX15 exhibited a linoleic acid molecular turnover ratio of 13.6 ± 2.6 s^{-1}. This value for rabbit ALOX15 is in fair agreement with the results of previous studies reporting molecular turnover rates of this enzyme for linoleic acid ranging between 5 – 50 s^{-1} (Schewe et al., 1986b; Borngräber et al., 1998).
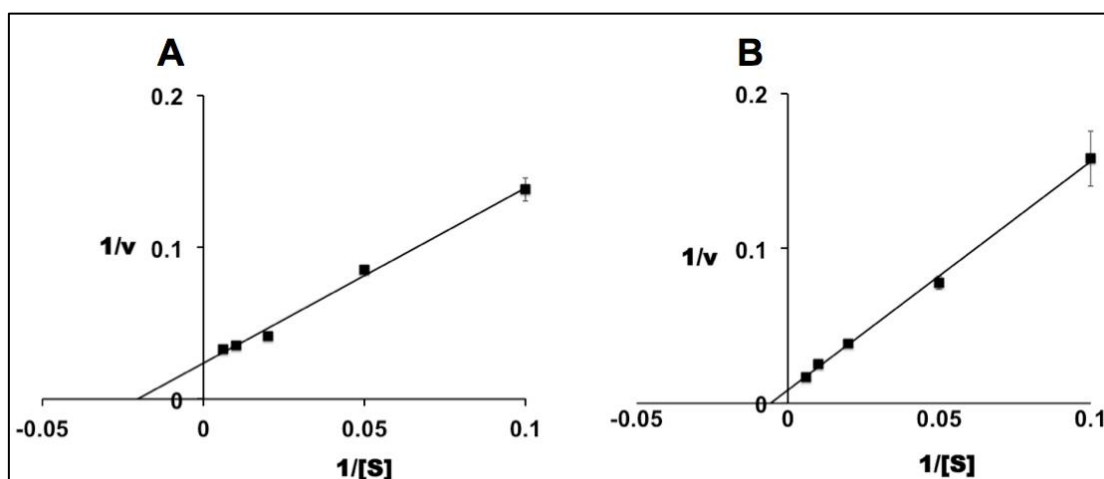
Figure 11: The Lineweaver-Burk plot for PA-LOX with arachidonic acid and linoleic acid as substrates. 2 μg of PA-LOX was incubated with five different substrate concentrations (10, 20, 50, 100 and 165 μM) at 25 °C for 3 min in 1 ml of PBS (pH 7.4). The increase in absorbance at 235 nm was measured in the absence of any detergent. The activity data was then used to construct the Lineweaver-Burk plot with A) arachidonic acid B) linoleic acid (Banthiya et al., 2016).

More detailed kinetic measurements were carried out for PA-LOX on the spectrophotometer to determine the substrate affinity (Km) of this enzyme. For this purpose an aliquot of PA-LOX was incubated with five different substrate concentrations and the increase in absorbance at 235 nm was monitored on the spectrophotometer. The linear parts of the kinetic progress curves were used to construct the Lineweaver-Burk plot (Figure 11) from which the basic kinetic parameters (Km, Vmax and Kcat) for each substrate were determined (Table

6).The wildtype-PA-LOX exhibited a higher affinity for arachidonic acid when compared to linoleic acid (Table 6). However, since the maximal rate of linoleic acid oxygenation was higher than that with arachidonic acid, the catalytic efficiency of PA-LOX with both the fatty acid substrates was very similar.

Table 6: Kinetic parameters of PA-LOX with arachidonic acid and linoleic acid as its substrates (Banthiya et al., 2016).

Substrate	Molecular turnover rate (s^{-1})	Km (μM)	Kcat/Km ($\mu M.s)^{-1}$
Arachidonic acid	23.5	48.9	0.48
Linoleic acid	65.4	174	0.38

The molecular turnover rate of PA-LOX with linoleic acid is almost 2.5-fold higher when oxygraphic measurements were carried out (162 s^{-1}) as compared with the measurements at the spectrophotometer (65.4 s^{-1}). Side by side experiments under strictly identical assay conditions using the same enzyme preparation indicated a molecular turnover rate of 145 ± 14 s^{-1} on the oxygraph and 76 ± 0.35 s^{-1} on the spectrophotometer. Therefore, a 2:1 stoichiometry between oxygen consumption (oxygraph) and conjugated diene formation (spectrophotometer) was observed. Oxygen consuming secondary reactions, which might contribute to the disappearance of conjugated dienes, may be discussed as reasons for this unusual stoichiometry. Previously, a 1.1 stoichiometry between oxygen uptake and conjugated diene formation has been reported for rabbit ALOX15 (Kühn et al., 1986).

Summary: The almost similar Kcat/Km ratios indicate that PA-LOX has no major preference for either arachidonic or linoleic acid as its substrate.

3.1.4.2. Substrate specificity of PA-LOX

Linoleic acid, alpha- and gama-linolenic acids, arachidonic acid, eicosapentaenoic acid and docosahexaenoic acid are the most abundant naturally occurring ALOX15 substrates (Ivanov et al., 2015). Since PA-LOX effectively oxygenates linoleic acid and arachidonic acid, it was important to find

out whether other n-6, n-3 and n-9 polyenoic fatty acids are suitable substrates for the enzyme. To answer this question PA-LOX was incubated spectrophotometrically with the different polyenoic fatty acids substrates indicated in Table 7. The catalytic activities with the different fatty acids were determined by measuring the increase in absorbance at 235 nm in triplicates on the spectrophotometer. The oxygenation products were prepared by RP-HPLC and then analyzed as trimethylsilyl derivatives by gas chromatography/mass spectroscopy.

Table 7 indicates that most of the fatty acids are oxygenated at the n-6th carbon atom irrespective of the chain length and of the number of double bonds. However, the ω-9 fatty acid, C20:Δ5,8,11 was not effectively oxygenated since no sizeable increase in absorbance at 235 nm could be measured using the spectrophotometer. Thus, it was impossible to quantify the kinetic constants. In order to explore the structure of small amounts of oxygenation products, which cannot be reliably detected by spectrophotometric measurements, are formed from this fatty acid, large-scale incubations were carried out with this fatty acid substrate. Then the oxygenation products were prepared by RP-HPLC (Figure 12A) and analyzed by GC/MS analysis. The key ions at m/z 261 (alpha-cleavage, relative abundance 100 %) and m/z 466 (molecular ion, relative abundance 0.2 %) indicated that the major product was a 5-hydro(pero)xy-derivative of this polyenoic fatty acid. These data indicate that, this polyenoic acid undergoes oxygenation at the n-16th carbon atom. Thus, with this fatty acid, PA-LOX exhibits a 5-lipoxygenating activity (Figure 12). The mechanistic basis for this unusual reaction specificity of the enzyme with 5,8,11-eicosatrienoic acid has not been explored in detail but the most plausible explanation for the observed 5-lipoxygenation may an inverse head-to-tail substrate orientation at the active site. It may be postulated that the fatty acid slides into the substrate-binding pocket with its carboxylic group ahead. Among the other fatty acids substrates tested, PA-LOX preferred dihomo-γ-linolenic acid (C20:Δ8,11,14; ω-6) followed by docosahexaenoic acid (C20:Δ4,7,10,13,16,19; ω-3), arachidonic acid (C20:Δ5,8,11,14; ω-6) linoleic acid (C18:Δ9,12; ω-6) and eicosapentaenoic acid (C20:Δ5,8,11,14,17; ω-3:) as indicated by their relative catalytic activities.

Table 7: Relative catalytic activities of PA-LOX with different polyenoic fatty acid substrates and GC/MS analysis of the corresponding oxygenated products (Banthiya et al., 2016).

Chain length	Class	Substrate fatty acid	Relative catalytic efficiency (%)	Position of oxygenation	Most informative key ions in MS m/z (rel. abundance)
C18	ω-6	C18:Δ9,12	50	n-6 (C_{13})	n.a.
		C18:Δ6,9,12	11	n-6 (C_{13})	173 (100), 367 (10.7) α-cleavage, 438 (0.1, M^+)
	ω-3	C18:Δ9,12,15	11	n-6 (C_{13})	171 (84.1), 369 (8.8), α-cleavage, 438 (0.4, M^+)
		C18:Δ6,9,12,15	6	n-6 (C_{13})	171 (82.3), 367 (2.0), α-cleavage, 436 (0.2, M^+)
C20	ω-9	C20:Δ5,8,11	n.d.	n-15 (C_5)	261 (100, α-cleavage), 466 (0.2, M^+)
	ω-6	C20:Δ11,14	66	n-6 (C_{15})	173 (100, α-cleavage), 468 (0.7, M^+)
		C20:Δ8,11,14	428	n-6 (C_{15})	173 (100, α-cleavage), 466 (0.7, M^+)
		C20:Δ5,8,11,14	100	n-6 (C_{15})	173 (90.9, α-cleavage), 464 (0.5, M^+)
	ω-3	C20:Δ8,11,14,17	39	n-6 (C_{15})	171 (90.9, α-cleavage), 464 (0.2, M^+)
		C20:Δ5,8,11,14,17	6	n-6 (C_{15})	171 (69.3, α-cleavage), 462 (0.4, M^+)
C22	ω-3	C22:Δ4,7,10,13,16,19	367	n-6 (C_{17})	171 (48.0, α-cleavage), 488 (0.2, M^+)

Eicosapentaenoic acid is well oxygenated by most mammalian ALOX15 orthologues (Haeggström and Funk, 2011), but for PA-LOX it is a rather poor substrate (relative catalytic activity of 6 %). In another study on substrate specificity of PA-LOX, it was reported that arachidonic acid was the most preferred substrate followed by linoleic acid, eicosapentaenoic acid, docosahexaenoic acid and dihomo-gamma-linolenic acid (Deschamps et al., 2016).
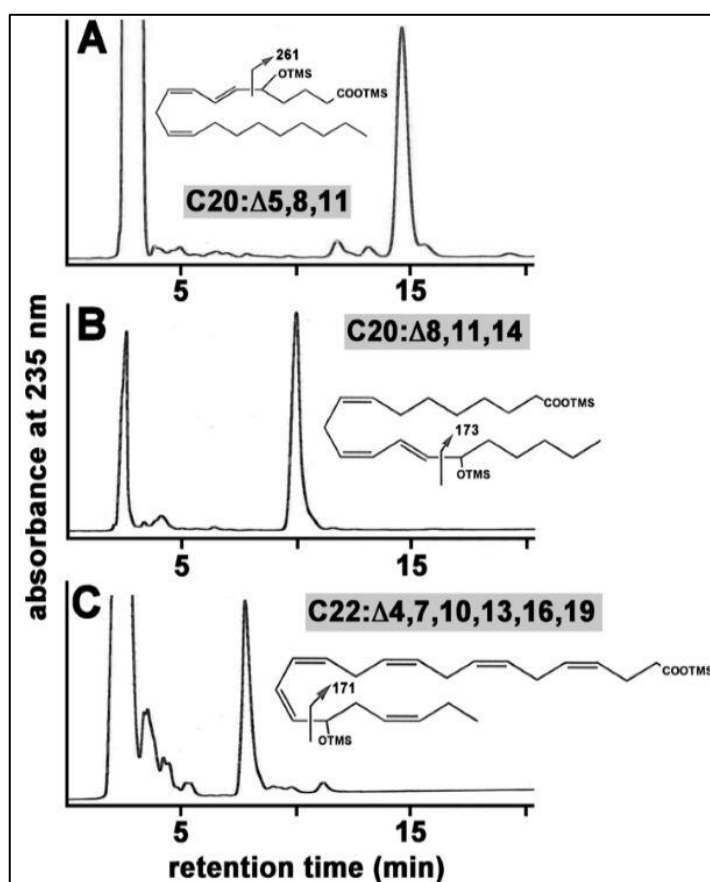
Figure 12: RP-HPLC analysis of selected polyenoic fatty acid substrates with PA-LOX. The bacterial lysate supernatant of PA-LOX ranging from 2-11 μg/ml was incubated in 1 ml of PBS (pH 7.4) containing 0.1 mM of different polyenoic fatty acids substrates with variable chain lengths and number of double bonds. The activity was monitored spectrophotometrically in triplicates. The major conjugated dienes were then prepared by RP-HPLC and analyzed as TMS-derivatives by GC/MS. The indicative fragmentation pattern is given in the insets. A) C20:Δ5,8,11 (ω-9), 11 μg; B) C20:Δ8,11,14 (ω-6), 5.5 μg; C) C22:Δ4,7,10,13,16,19 (ω-3), 2.2 μg (Banthiya et al., 2016).

The reason for these conflicting data remains unclear. However, the differences in the assay systems (different substrate concentrations: 10 μM in the Deschamps study vs. 100 μM in our study; different pH values: 7.0 in the

Deschamps study vs. 7.4 in our study) are likely to contribute to the different outcomes.

Summary: PA-LOX oxygenates most fatty acids at the n-6th position and dihomo-γ-linolenic acid and docosahexaenoic acid are its preferred fatty acid substrates.

3.1.4.2.1. Poor substrate behavior of C20:Δ5,8,11

As indicated in Table 7, arachidonic acid and linoleic acid are suitable substrates for PA-LOX while C20:Δ5,8,11 eicosatrienoic acid was hardly oxygenated. To determine the reason behind this substrate specificity we modeled the three substrates into the active site of PA-LOX on the basis of the endogenous ligand. Following the anatarafacial character of LOX, the pro*S* hydrogen of C13 of arachidonic acid and the pro*S*-hydrogen of C11 of linoleic acid are abstracted in PA-LOX catalyzed reaction (see section 3.2.3.3). Thus these atoms should be localized in close proximity to the non-heme iron.
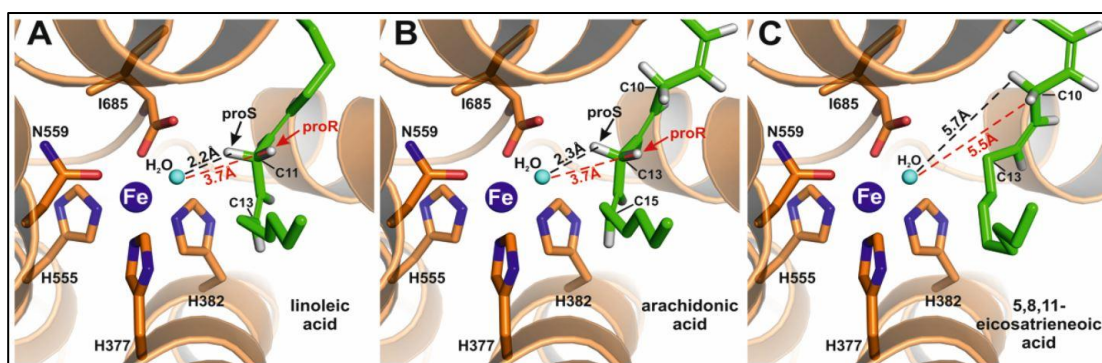
Figure 13: Structural modeling of wildtype-PA-LOX with three different polyenoic fatty acid substrates. The enzyme-substrate complexes were modeled into the substrate binding pocket on the basis of the X-ray coordinates of the endogenous ligand. The iron atom is indicated as a blue sphere, the water molecule completing the octahedral iron ligand sphere is given as cyan sphere, the iron liganding amino acids are represented by orange sticks, the remaining wildtype-PA-LOX protein as orange cartoon and the fatty acid substrates as green sticks. A) Linoleic acid, B) Arachidonic acid and C) C20:Δ5,8,11 eicosatrienoic acid were modeled at the position of the endogenous ligand of wildtype-PA-LOX (Banthiya et al., 2016).

The modeling data (Figure 13) indicate that the arachidonic acid backbone is oriented at the active site in such a way that its pro*S*-hydrogen at C13 of

arachidonic acid is closer (2.3 Å) to the water (hydroxyl) molecule while its pro*R* hydrogen is farther away (3.7 Å). With linoleic acid, a similar observation was made. Here the pro*S*-hydrogen at C11 of the hydrocarbon chain is closer (2.2 Å) to the water (hydroxyl) molecule than its pro*R*-hydrogen (3.7 Å). These data are consistent with preferential abstraction of the proS-hydrogen observed in the experiments with stereospecifically labeled linoleic acid as its substrate (section 3.2.3.3). In contrast, with C20:Δ5,8,11 eicosatrienoic acid the pro*R* and pro*S*-hydrogens of both its bisallylic methylenes (C7 and C10) were far away from the active site water (hydroxyl) molecule. The pro*S*-hydrogen at C10 was at a distance of 5.7 Å and the pro*R* at the same carbon atom was at a distance of 5.5 Å from the iron bound water. The two hydrogens at C7 were even farther away. Thus, our structural model of the fatty acid enzyme complexes explains the low oxygenation rate.

Summary: Both, spectrophotometric analysis and structural modeling studies indicate that C20:Δ5,8,11 eicosatrienoic is not a good substrate for PA-LOX.

3.1.4.3. Activation energy and thermal stability of PA-LOX

3.1.4.3.1. Temperature profile of PA-LOX

The effect of temperature on the catalytic efficiency of PA-LOX was explored by measuring the linoleic acid oxygenase activity of the enzyme at different temperatures. The activities were measured spectrophotometrically. Similar experiments were also performed with rabbit ALOX15 in order to compare the two temperature profiles and the activation energies for two the LOXs (Figure 14). From Figure 14A, it can be seen that the activity of PA-LOX increases gradually from 5 to 35 °C. At higher temperatures, there was a sudden drop in activity. This may be due to the thermal denaturation of the protein. Under identical experimental conditions rabbit ALOX15 exhibited maximal activity at 25 °C. Thus, it can be concluded that PA-LOX was more heat resistant than rabbit ALOX15. Previous studies on the temperature dependence of recombinant PA-LOX, suggested a T-optimum of PA-LOX at 25 °C (Lu et al., 2013; Deschamps et al., 2016). Thus, it can be concluded that our enzyme preparation is thermally

more stable than the preparations described before (Lu et al., 2013; Deschamps et al., 2016). From the Arrhenius-plot, an activation energy for the oxygenation of linoleic acid by PA-LOX of 33.8 kJ/mol x K was determined (Figure 14B).
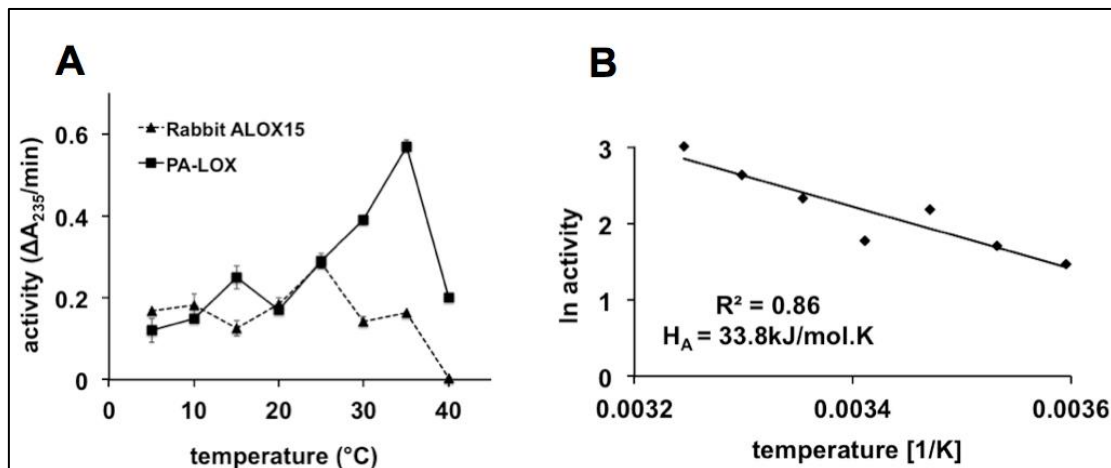
Figure 14: Temperature dependence on catalytic activity of PA-LOX and rabbit ALOX15. A) The linoleic acid oxygenase activities of purified PA-LOX and pure rabbit LOX were measured spectrophotometrically at temperatures ranging from 5 – 40 °C. The activities at each temperature were measured in triplicates. The linear parts of the kinetic progress curves were used to determine the catalytic activities and these values were plotted against the measuring temperature. B) The activity values for PA-LOX in the temperature range from 5 to 35 °C were used to construct the Arrhenius-plot in order to quantify the activation energy for linoleic acid oxygenation (Banthiya et al., 2016).

Native rabbit ALOX15 exhibited a significantly lower activation energy of 14.8 kJ/mol x K. The activation energy indicates the minimum amount of energy that is required to form the catalytic transition state (Krishtalik, 1985). Therefore, rabbit ALOX15 requires less energy to form its transition state. However, almost 2-fold higher energy levels are required to overcome the threshold for PA-LOX catalyzed reactions.

Summary: The maximum linoleic acid oxygenase activity of PA-LOX was seen at 35 °C and the enzyme exhibited an activation energy for linoleic acid oxygenation of 33.8 kJ/mol x K.

3.1.4.3.2. Thermo stability of PA-LOX

In order to explore the thermo stability of PA-LOX, a fresh enzyme preparation was incubated at 4 °C for an extended period of time in the presence and

absence of glycerol. Glycerol is frequently used as a stabilizing agent for protein preparations.
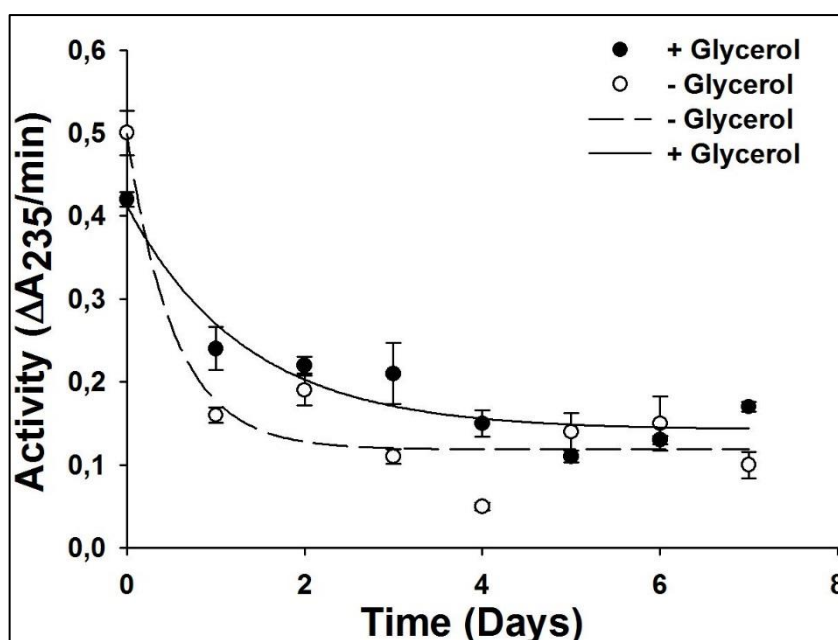
Figure 15: Thermo stability of PA-LOX. A fresh enzyme preparation was subjected to size exclusion chromatography to remove excessive imidazole from the nickel agarose purification and then concentrated to 16.7 mg/ml. This preparation was incubated at 4 °C for 7 days in the presence and absence of 10 % glycerol. Aliquots of the enzyme preparation were taken from the incubation sample at the different time points and activity assays were carried out using the spectrophotometer in triplicates (Banthiya et al., 2016).

The linoleic acid oxygenase activity of PA-LOX was determined at different time points on the spectrophotometer in triplicates. As indicated in Figure 15, PA-LOX loses about 60 % of its total linoleic acid oxygenase activity within the first 24 hours of incubation. This loss was more or less independent of the presence and absence of glycerol.

Summary: PA-LOX loses almost 3/4th of its activity in the first 24 hours of incubation at 4 °C and this loss is independent of the presence or absence of glycerol.

3.2. Concepts for the reaction specificity of LOXs

The reaction specificity of LOXs depends on their primary structure and site-directed mutagenesis of critical amino acids has been reported to alter the

reaction specificity of several LOX-isoforms (Sloane et al., 1991a, 1995, Borngräber et al., 1996, 1999). To test whether this may also be the case for PA-LOX, multiple site-directed mutagenesis were carried out and the reaction specificities of the mutant enzyme species were determined.

3.2.1. Triad concept

Multiple sequence alignments and mutagenesis data for several mammalian ALOX15 orthologs suggest that the amino acid regions around the Borngraber determinants, Phe353 and Ile593 (Borngräber et al., 1996, 1999) and the region around the Sloane determinants, Ile418 and Met419 (Sloane et al., 1991a, 1995) may play important roles for the positional specificity of the enzymes.

Table 8: PA-LOX does not follow the Triad concept. Triad determinants were mutated and the mutant enzyme species were expressed. Aliquots of the elution fraction 2 of nickle-agarose purification were used to assay the arachidonic acid (165 µM) oxygenase activity. The reaction products were prepared and analyzed by RP-HPLC and SP-HPLC (Banthiya et al., 2016). For direct comparison with other LOXs, the table also contains previously published data from rabbit ALOX15 (Borngräber et al., 1999).

The Triad determinants						
	Rabbit ALOX15			PA-LOX		
Deter-minant	LOX type	12-HETE (%)	15-HETE (%)	LOX type	12-HETE (%)	15-HETE (%)
	Wildtype	3	97	Wildtype	0	100
Born-gräber I	F353A	80	20	E369A	0	100
Sloane	I418A	92	8	M434V	0	100
Sloane	M419A	12	88	F435L	0	100
Born-gräber II	I593A	45	55	L612V	0	100

According to 3D models of rabbit ALOX15, these residues form the bottom of the putative substrate-binding pocket and their side chains have direct impact on the volume of the pocket. When they were mutated to smaller residues (such as alanine), the depth of the substrate-binding pocket increased so that arachidonic acid could penetrate deeper into the pocket. This alters the structure of the enzyme-substrate complex leading to arachidonic acid 12-lipoxygenation. On the contrary, 12-lipoxygenating ALOX15 orthologs can be converted to a 15-lipoxygenating enzyme by the targeted mutagenesis of the triad determinants. Several 15-lipoxygenating ALOX15 orthologs including human (Sloane et al.,

1995) and rabbit ALOX15 (Borngräber et al., 1999) as well as 12-lipoxygenating ALOX15 orthologs including the enzymes from pigs (Suzuki et al., 1994), rhesus monkeys (Vogel et al., 2010), mice (Borngräber et al., 1996) and rats (Pekárová et al., 2015) follow the triad concept. To test this concept for PA-LOX, we identified the corresponding triad determinants by multiple sequence alignment, generated the mutants and tested their reaction specificity.

As shown in Table 8, none of the mutants catalyzed arachidonic acid 12-ipoxygenation, indicating PA-LOX does not follow the triad concept. Similar data have previously been shown for human ALOX15B (Vogel et al., 2010) and mouse alox12b (Meruvu et al., 2005).

Summary: PA-LOX does not follow the classical triad concept that describes positional specificity exhibited by mammalian ALOX15 orthologs

3.2.2. Jisaka determinants

Previous studies on human ALOX15B indicate that this enzyme does not follow the triad concept (Vogel et al., 2010).

Table 9: The Jisaka determinants do not alter the positional specificity of PA-LOX. The Jisaka determinants were mutated and the mutant enzyme species were expressed. Aliquots of the elution fraction 2 of nickle-agarose purification were used to assay the arachidonic acid (165 µM) oxygenase activity. The reaction products were prepared and analyzed by RP-HPLC and SP-HPLC (Banthiya et al., 2016). For direct comparison with other LOXs, the table also contains previously published data from and human ALOX15B (Jisaka et al., 2000).

The Jisaka determinants					
Human ALOX15B			**PA-LOX**		
LOX-type	**8-HETE (%)**	**15-HETE (%)**	**LOX-type**	**8-HETE (%)**	**15-HETE (%)**
Wildtype	0	100	**Wildtype**	0	100
D602Y+V603H	70	30	**E604Y+K605H**	0	100

However, when Asp603 and Val604 of human ALOX15B were mutated to the corresponding residues of the mouse ortholog (this enzyme functions as arachidonic acid 8-lipoxygenase), the double mutant catalyzed arachidonic acid 8-lipoxygenation (Jisaka et al., 2000).

Following sequence alignment with human ALOX15B, Glu604 and Lys605 were the corresponding amino acid residues in PA-LOX. However as indicated in Table 9, when these residues were mutated (Glu604Tyr+Lys605His) in PA-LOX, there were no alterations in the reaction specificity of the enzyme. Thus, PA-LOX does not follow the Jisaka concept either.

Summary: Glu604Tyr+Lys605His-PA-LOX does not alter the reaction specificity of the enzyme indicating that Glu604Tyr and Lys605His cannot be classified as the Jisaka determinants of PA-LOX.

3.2.3. Ala vs. Gly concept

3.2.3.1. Product profile after Ala to Gly exchange

Multiple sequence alignments of various S- and R-lipoxygenases have previously indicated that an alanine residue is present at a critical position in most S-LOXs. In contrast, this amino acid is a glycine in most R-LOXs (Coffa and Brash, 2004; Coffa et al., 2005a; Schneider et al., 2007). When this Ala of an S-lipoxygenating enzyme was mutated to Gly, the product profile partly shifts from S- to R-lipoxygenation (Coffa and Brash, 2004). However, not all LOX isoforms follow this Ala-vs.-Gly concept. For instance, although the LOX1 of zebrafish contains a Gly at the critical position on the active site, it is a arachidonic acid 12S-lipoxygenating enzyme (Haas et al., 2011; Jansen et al., 2011). Moreover, only minor alterations (major product: 15S-HETE, minor product: 11R-HETE) in the reaction specificity was noted when similar mutagenesis was carried out for the ALOX15 orthologs from human, rabbits, rhesus monkeys and rats (Jansen et al., 2011).

Ala420 of PA-LOX aligns with the Coffa determinant of human ALOX15B Ala416. When this Ala420 was mutated to Gly, the Ala420Gly mutant of PA-LOX exhibited a dual reaction specificity. The mutant enzyme functions as a dominant arachidonic acid 11R-LOX (Figure 16B). The major products of arachidonic acid oxygenation, 11R-HETE and 15S-HETE, were formed in the ratio of 1.5:1.
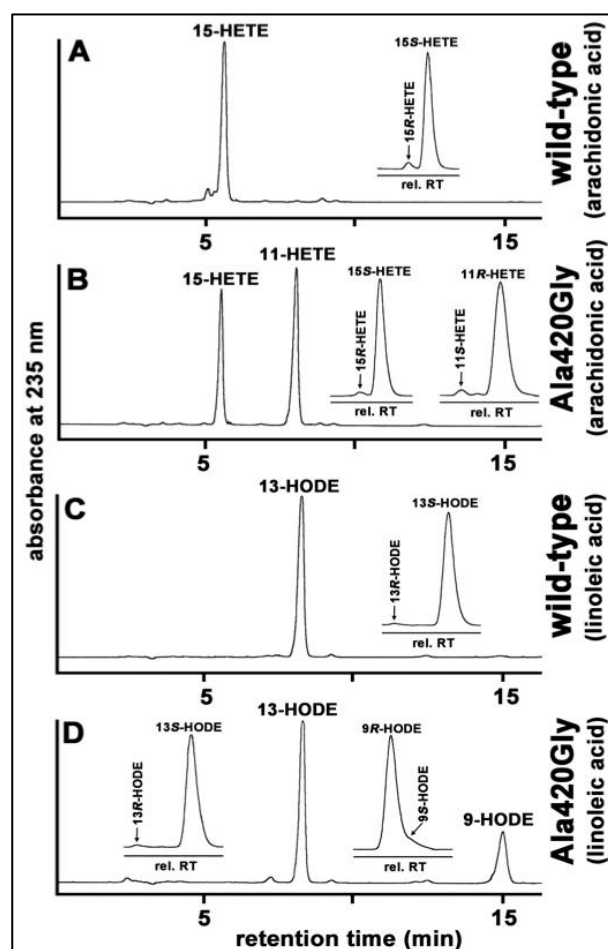
Figure 16: Ala420Gly alters the reaction specificity of PA-LOX. A final enzyme concentration of A) 3.7 µg/ml of wildtype-PA-LOX with arachidonic acid, B) 7.6 µg/ml of Ala420Gly-PA-LOX with arachidonic acid, C) 3.7 µg/ml of wildtype-PA-LOX with linoleic acid and D) 7.6 µg/ml of Ala420Gly-PA-LOX with linoleic acid were incubated for 3 min at 25 °C in 1 ml of PBS (pH 7.4). The final concentration of both arachidonic acid and linoleic acid was 165 µM. The reaction products were prepared by RP-HPLC and further analyzed by consecutive SP-(main traces) and CP-HPLC (insets) (Kalms et al., 2017).

A similar ratio of 1.5:1 (11R-HETE: 15S-HETE) has also been observed for Ala416Gly mutant of human ALOX15B (Coffa and Brash, 2004). With linoleic acid, as indicated in Figure 16D, the Ala420Gly-PA-LOX formed 13S-HODE and 9R-HODE in the ratio of 2.6:1.

Summary: The Ala420Gly exchange alters the positional and enantioselectivity of PA-LOX. It converts arachidonic acid to a 1.5:1 mixture of 11R- and 15S-HETE.

3.2.3.2. Ala420Gly lowers the catalytic efficiency of PA-LOX

As indicated above, Ala420Gly-mutant of PA-LOX exhibited different reaction specificity when compared with the wildtype enzyme. To explore whether other enzymatic properties were also altered, we compared the basic kinetic parameters between the mutant and the wildtype enzyme. For this, both the wildtype- and Ala420Gly-PA-LOX were incubated with arachidonic acid with five different substrate concentrations (10, 20, 50, 100 and 165 µM). The reaction rates were monitored spectrophotometrically and the linear parts of the kinetic progress curves were used to determine the kinetics of the reaction. From Table 10 it can be seen that there is a two-fold decrease in affinity for arachidonic acid with the Ala420Gly-PA-LOX when compared to the wildtype-PA-LOX.

Table 10: Kinetics of wildtype- and Ala420Gly-PA-LOX with arachidonic acid as its substrate.

Kinetics	Wildtype	Ala420Gly
Enzyme concentration (µM)	0.03	0.33
Km (µM)	38.2 ± 6	67.6 ± 17
Vmax (µM/min)	38.6 ± 2	31.3 ± 3
Molecular turn over rate (s^{-1})	21.45	1.6
Catalytic efficiency ($(µM.s)^{-1}$)	0.56	0.023

The molecular turnover rate of the mutant enzyme at substrate saturation was 13-fold lower than that of the wildtype enzyme (1.6 s^{-1} vs. 21.4 s^{-1}), indicating that the rate limiting step of the LOX reaction (hydrogen abstraction) catalyzed by the mutant enzyme was more than 1 order of magnitude lower. However, the enantiomer composition of the two major oxygenation products (15*S*-H(p)ETE, 11*R*-H(p)ETE) formed by the mutant enzyme indicated that the stereochemistry of the reaction is completely enzyme controlled.

Summary: The Ala420Gly exchange lowers the catalytic efficiency of PA-LOX.

3.2.3.3. The antarafacial relationship

The LOX reaction involves an antarafacial relationship between hydrogen abstraction and oxygen insertion (Haeggström and Funk, 2011). The major arachidonic acid and linoleic acid oxygenation products of wildtype-PA-LOX are

15*S*-H(p)ETE and 13*S*-H(p)ODE, respectively (Figure 9 and Figure 10) making PA-LOX an *S*-lipoxygenating enzyme. Thus, if PA-LOX reaction follows the antarafacial character, the pro*S* hydrogen at the bisallylic methylene C11 must be abstracted during incubations with linoleic acid. To test this hypothesis, we incubated wildtype-PA-LOX, its Ala420Gly mutant and rabbit ALOX15 (positive control) with 11*S*- (pro*S*) and 11*R*- (pro*R*) deuterated linoleic acids and measured the increase in absorbance at 235 nm. The results indicated that pro*R*-deuterated linoleic acid was more efficiently oxygenated when compared with the pro*S* deuterated substrate by both wildtype- and Ala420Gly-PA-LOX (Table 11).

Table 11: The reaction rates measured for the oxygenation of 11R- and 11S-deuterated linoleic acid by wildtype and mutant (Ala420Gly) PA-LOX as well as by rabbit ALOX15. The reaction rates measured with 11R-deuterated linoleic acid for each LOX were set 100 % (LA-linoleic acid).

LOX isoform	Product	Relative rate (%)		Kinetic isotope effect
		11*R*-^{2}H-LA	11*S*-^{2}H-LA	
Wildtype-PA-LOX	13*S*-H(p)ODE	100 ± 16.1	6.2 ± 3.3	16.1
Ala420Gly-PA-LOX	13*S*-H(p)ODE	100 ± 8.0	15.1 ± 3.9	6.6
	9*R*-H(p)ODE			
Rabbit ALOX15	13*S*-H(p)ODE	100 ± 33.0	6.9 ± 13.5	14.5

The observed primary kinetic isotopic effect, strongly suggests that the pro*S*-hydrogen is stereoselectively abstracted from C11 of linoleic acid. To confirm this conclusion, we analyzed the reaction products (13*S*-HODE, 9*R*-HODE) for retention or loss of the deuterium label by GC/MS. To do so, we first carried out SP-HPLC analysis of the reaction products and found that wildtype-PA-LOX and rabbit ALOX15 mainly produced 13*S*-H(p)ODE while for the Ala420Gly mutant a mixture of 13*S*-H(p)ODE and 9*R*-H(p)ODE was formed. The products were recovered from SP-HPLC and their deuterium content was determined by GC/MS. Table 12 indicates that with all the LOX variants tested, more than 95 % of the deuterium was lost in 13*S*-H(p)ODE and 9*R*-H(p)ODE when incubated with pro*S*-deuterated linoleic acid. On the other hand, more than 85 % of the deuterium was retained in these products when pro*R*-deuterated substrate was used. Taken together these results indicate that the formation of 9*R*-H(p)ODE

and 13*S*-H(p)ODE involves the abstraction of the pro*S* hydrogen from the bisallylic methylene at the C11 of linoleic acid.

Table 12: Retention of the deuterium label in the major reaction products. Wildtype and mutant (Ala420Gly) PA-LOX as well as rabbit ALOX15 was incubated with 11R- and 11S-deuterated linoleic acids. (LA-Linoleic acid).

LOX isoform	Product	Deuterium retention (%)	
		11*R*-^{2}H-LA	11*S*-^{2}H-LA
Wildtype-PA-LOX	13*S*-H(p)ODE	88.5 ± 1.5	3.3 ± 0.6
Ala420Gly-PA-LOX	13*S*-H(p)ODE	85.5 ± 5.5	2.5 ± 0.5
	9*R*-H(p)ODE	86.0 ± 1.0	3.5 ± 0.5
Rabbit ALOX15	13*S*-H(p)ODE	89.0 ± 0.0	3.0 ± 0.0

Together with the chirality analysis of the reaction products (stereoselective formation of 13*S*-H(p)ODE), these results indicate that fatty acid oxygenation catalyzed by PA-LOX involves an antarafacial character of initial hydrogen abstraction and subsequent oxygen insertion.

Summary: Both, the wildtype-PA-LOX and its Ala420Gly-mutant follow the antarafacial paradigm of LOX reaction.

3.2.3.4. Crystal structure of Ala420Gly mutant of PA-LOX

Wildtype-PA-LOX was previously crystallized to a resolution of 1.75 Å (PDB entry: 4G32, SG: *P*2$_1$2$_1$2) (Garreta et al., 2013). We improved the resolution of the wildtype-PA-LOX to 1.48 Å resolution (PDB entry 5IR4; SG:*C*222$_1$). Next, we aimed at identifying the structural reason behind the altered reaction specificity of the Ala420Gly mutant of PA-LOX. For this purpose, we crystallized this enzyme mutant and solved the structure to a resolution of 1.8 Å (PDB entry: 5LC8, SG: *C*222$_1$). Table 13 summarizes the details of data collection and the refinement statistics. Similar to the wildtype, the Ala420Gly also had a complete phosphatidylethanolamine (ZPE) at its active site (Figure 17A). The arachidonic acid molecular turnover rate of the Ala420Gly mutant was approximately 13-fold lower than that of the wildtype enzyme (Table 10) and this lowered activity can be explained by the orientation of the endogenous ligand (ZPE) at the active site of Ala420Gly mutant. When the ZPE of the wildtype-PA-LOX was superimposed

with that of the Ala420Gly mutant, the n-8 carbon (site of hydrogen removal) in the Ala420Gly mutant was displaced from the non-heme iron bound water by 0.6 Å (Figure 17B). The n-8 carbon of the endogenous ligand corresponds to the bisallylic C11 (linoleic acid) and C13 (arachidonic acid) from which the hydrogen is abstracted during the first step of a PA-LOX catalyzed reaction.

Table 13: Methodological details of data collection and refinement statistics of Ala420Gly-PA-LOX crystals. [a]Number of crystals for data set: 1; [b]highest resolution shell is shown in parenthesis; [c]R.m.s, root mean square; [d]as defined in the program RAMPAGE (Lovell et al., 2003)., (Kalms et al., 2017).

Ala420Gly-PA-LOX	Crystal form
PDB entry	5LC8
Beamline	ID 23-1 - ESRF (Grenoble, France)
Space group (SG)	$C222_1$
Cell dimensions (a, b, c [Å]; α, β, γ [°])	84.33, 97.42, 155.60; 90.00, 90.00, 90.00
Wavelength [Å]	0.972
Resolution (Å)	48.71 – 1.80 (1.90 – 1.80)[b]
R_{pim}	0.04 (0.36)[b]
R_{merge}	0.08 (0.67)[b]
$I/\sigma\ (I)$	10.9 (2.1)[b]
Completeness [%]	99.5 (99.6)[b]
Redundancy	4.5 (4.4)[b]
Wilson B factor ($Å^2$)	22.7
Resolution [Å]	48.71 – 1.80 (1.85 - 1.80)[b]
$R_{work}\ /R_{free}$ **[%]**	13.9 / 17.1 (25.9 / 30.0)[b]
Average B factor ($Å^2$)	28.4
R.m.s[c] deviations	
Bond lengths (Å)	0.008
Bond angles (º)	1.18
Ramachandran favored [%][d]	94.3
Ramachandran allowed [%][d]	5.7
Ramachandran outlier [%][d]	0

As discussed for wildtype-PA-LOX the pro*S*-hydrogen at C13 of arachidonic acid was localized in close proximity (2.2 Å) to the active site water (hydroxyl) when compared to the pro*R*-hydrogen (3.4 Å). Similar observations were also made with linoleic acid as substrate. Here (Figure 17C) the pro*S*-hydrogen at C11 was at a distance 2.2 Å from the water (hydroxyl) molecule, while the pro*R*-hydrogen was farther away (3.3 Å).
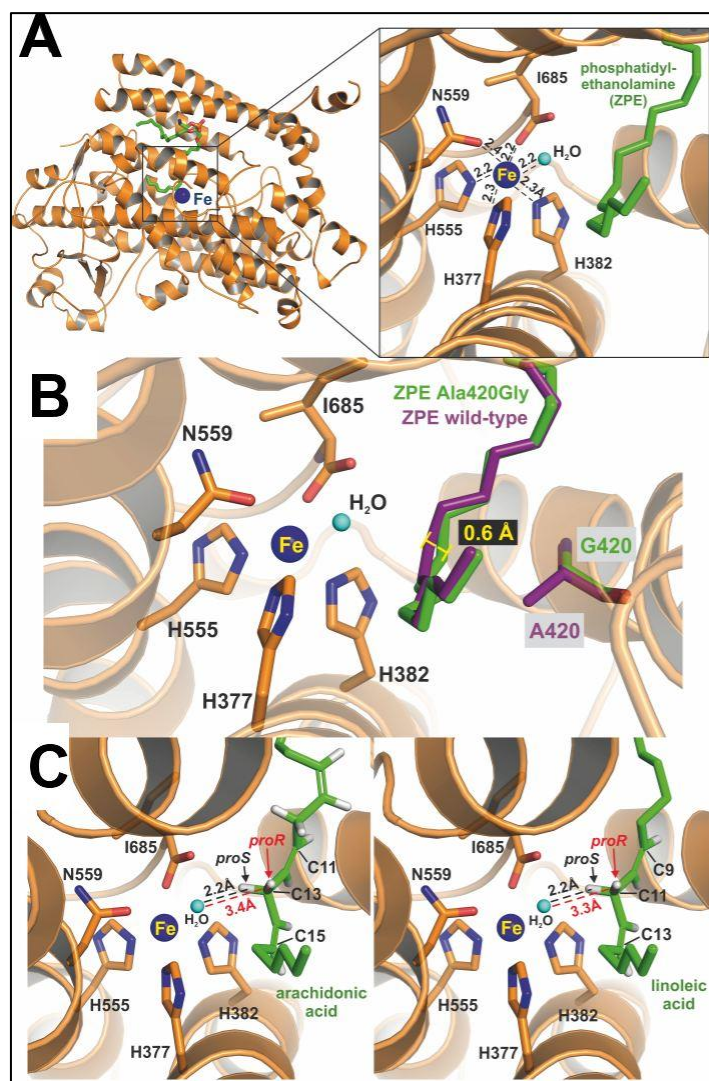
Figure 17: Structural analysis of the catalytic active center of Ala420Gly-mutant of PA-LOX. A) The overall structure of the Ala420Gly mutant is depicted as orange ribbon diagram. The inset is zoomed-in to view in detail the active site containing the non-heme iron (blue sphere). As for the wildtype-PA-LOX five amino acids (orange sticks) and a water molecule (cyan sphere) form the octahedral iron ligand sphere. The endogenous ligand (ZPE) is depicted as green stick model. B) The endogenous ligand of the Ala420Gly mutant (green sticks) and the wildtype-PA-LOX (purple sticks) superimposed. C) The PA-LOX substrates, arachidonic acid and linoleic acid (green sticks) modeled into the active site of the mutant. The amino acid iron ligands are depicted as orange sticks. The dashed lines indicate the distance between the proS- (black) and proR- (red) hydrogen of the fatty acid substrates and the water molecule (cyan sphere) (Kalms et al., 2017).

These structural data are consistent with preferential pro*S*-hydrogen abstraction observed in the experiments with the stereospecifically labeled linoleic acid as substrate (section 3.2.3.3). Thus, in principle the fatty acids substrates are aligned at the active site of mutant PA-LOX as it is the case for the wildtype enzyme. In other words, the structures of the enzyme-substrate complexes do

not explain the differences in reaction specificity we observed for the two enzyme variants.

Summary: The crystal structure of Ala420Gly-PA-LOX was solved at a resolution of 1.8 Å. The overall 3D-structure of the mutant enzyme resembled that of the wildtype-PA-LOX.

3.2.3.5. The putative oxygen channels

Because of the similarities of the enzyme-substrate complexes of wildtype-PA-LOX and its Ala420Gly mutant, the structural reasons for the different reaction specificities of the two enzyme species may not be related to differences in the initial hydrogen abstraction. Thus, subsequent elementary reactions (mechanism of radical rearrangement, stereochemistry of oxygen insertion) are likely to be impacted by the Ala420Gly exchange.

To explore these differences, we first investigated the cavity structure of both enzyme variants in the immediate surrounding of the catalytic center to identify potential oxygen access channels using the Caver 3.0 program (Chovancova et al., 2012). We identified a more or less continuous tunnel interconnecting the surface of the protein with the catalytic center. A similar tunnel has previously been identified for soybean LOX-1 and this cavity was suggested to function as oxygen transport channel (Minor et al., 1996; Knapp et al., 2001). Molecular dioxygen was hypothesized to employ this cavity system to travel from the periphery of the protein into the active site reaching the fatty acid substrate.

In the 3D-structure of wildtype-PA-LOX (Figure 18A), the side chain of the Ala420 blocks oxygen access to C11 of arachidonic acid and C9 of linoleic acid. In other words, all the oxygen molecules traveling along this tunnel are directed to C15 of arachidonic acid and C13 of linoleic acid, which explains the reaction specificity of wildtype-PA-LOX. When Ala420 is mutated to a Gly the blockage seen in the wildtype enzyme could not be observed any more.
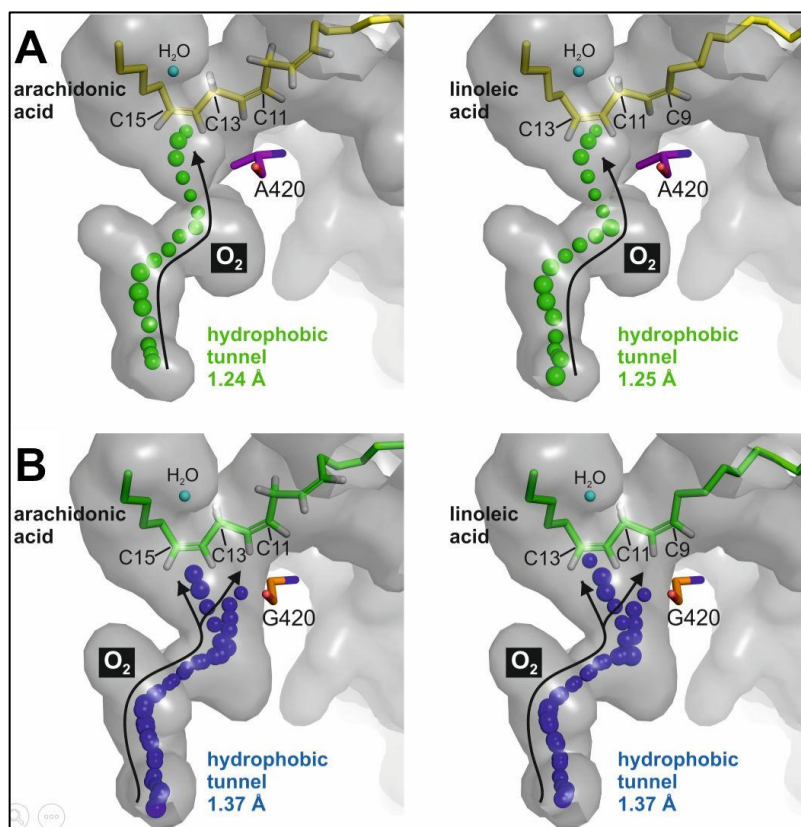
Figure 18: Comparison between the predicted oxygen access tunnel of the wildtype-PA-LOX and its Ala420Gly mutant. A) Structure of wildtype-PA-LOX fatty acid complexes. The fatty acids bound at the active site (right panel: linoleic acid; left panel: arachidonic acid) are indicated as yellow stick models. The surface of the cavities (calculated using PyMol) are colored in grey. The putative oxygen channel, which directs molecular dioxygen to C15 of arachidonic acid or C13 of linoleic acid is labelled by green spheres. The side chain of Ala420 blocks oxygen access to C11 of arachidonic acid and C9 of linoleic acid. B) Putative oxygen channels in the Ala420Gly mutant. The predicted oxygen access tunnel, which is labelled by blue spheres, directs molecular dioxygen to both C15 and C11 in arachidonic acid and C13 and C9 in linoleic acid. Black arrows in both A and B indicate the direction of the oxygen movement within the channel, which explains the singular positional specificity of wildtype-PA-LOX and the dual reaction specificity of its Ala420Gly mutant (Kalms et al., 2017).

Now it is possible for the oxygen molecules to reach C11 of arachidonic acid (in addition to C15), which explains the dual reaction specificity of the Ala420Gly mutant. A similar situation was observed for linoleic acid oxygenation (Figure 18B).

Summary: The Ala420Gly substitution bifurcates the putative oxygen access tunnel towards both C11 and C15 of arachidonic acid explaining the dual reaction specificity of the mutant enzyme.

3.2.3.6. Ala420Gly improves the oxygen affinity of PA-LOX

As indicated above (Table 10), Ala420Gly-mutant of PA-LOX exhibited a 13-fold lower molecular turnover rate when compared with the wildtype enzyme suggesting that the rate-limiting step of the oxygenase reaction (initial hydrogen abstraction) might be slowed down by this amino acid exchange. Next, we tested whether the 3rd elementary reaction of the catalytic cycle, the oxygen insertion, might also be impacted by this particular mutation. To answer this question we carried out activity assays at different oxygen concentrations and determined the Km for oxygen. For this purpose, anaerobic and oxygen saturated reaction buffers were mixed at 12 different volume ratios. The final oxygen concentrations in the assay mixtures varied in the range of 0.073 mM to 1.32 mM. After addition of enzyme, the arachidonate oxygenase activity of PA-LOX at varying oxygen concentrations was determined by recording the increase in absorbance at 235 nm.
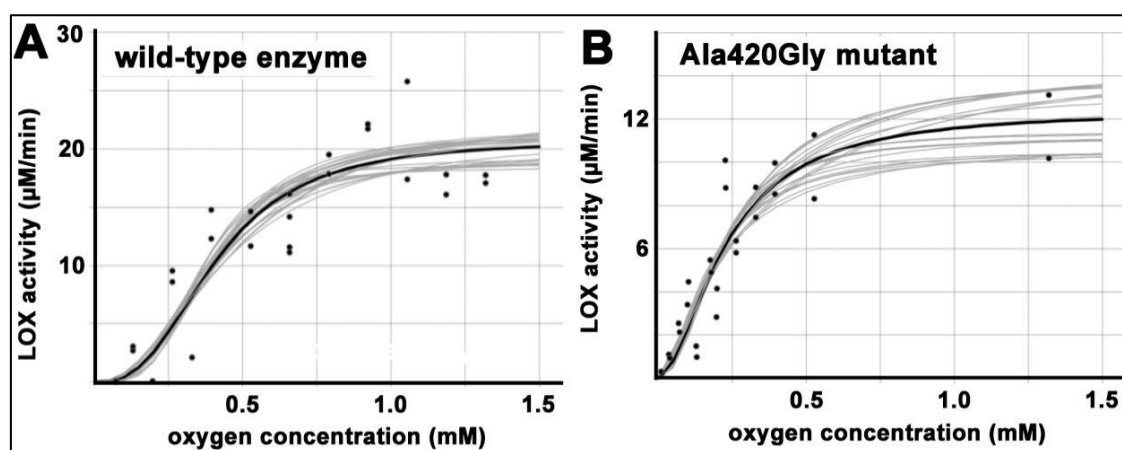
Figure 19: Comparison of oxygen affinity between wildtype- and Ala420Gly-PA-LOX. The arachidonic acid (328 µM) oxygenase activity of both the wildtype- (0.41 µg) and Ala420Gly (7.6 µg)-PA-LOX was measured at 12 different oxygen concentrations that were achieved by mixing different volumes of argon-flushed (anaerobic) and oxygen-flushed (hyperoxic) PBS. The increase in activity at each concentration was monitored spectrophotometrically for 3 min. The linear part of the progress curves were used to determine the catalytic activity that was then plotted against the different oxygen concentrations employed and fitted against a Hill-type rate equation (Kalms et al., 2017).

Quantitative evaluation of the Hills equation (Figure 19) indicated a Km value for oxygen of 406 µM for the wildtype enzyme (Table 14). This result was rather surprising since Km values for oxygen in the one digit µM range have previously been determined for other LOX-isoforms (Juránek et al., 1999; Yamamoto et al.,

2002). For the Ala420Gly mutant the oxygen Km was improved reaching a Km of 235 µM. These data suggests that oxygen diffusion within the enzyme might be altered by the Ala420Gly exchange. In order to confirm these differences in oxygen Km we determined the reaction rates of both wildtype-PA-LOX and its Ala420Gly mutant at 165 µM of arachidonic acid under normoxic (air saturation) and hyperoxic (oxygen saturation) conditions. From the hyperoxia/normoxia ratios given in Table 14, it can be concluded that the reaction rates under hyperoxic conditions were significantly higher when compared to those at normoxic conditions. The catalytic activity of the wildtype-PA-LOX at hyperoxic conditions was more than 3-fold higher. However, with Ala420Gly-PA-LOX, the hyperoxic/normoxic catalytic activity ratio was 1.6 confirming the previous finding that the mutant exhibits a higher oxygen affinity than the wildtype-PA-LOX. These data indicate that at normoxia (oxygen concentration of about 180 µM) the two enzyme species do not work at oxygen saturation.

Table 14: Kinetic parameters of wildtype- and its Ala420Gly-PA-LOX at different oxygen concentrations (Kalms et al., 2017). AA-Arachidonic acid

Parameter	PA-LOX type	
	Wildtype	**Ala420Gly**
Hyperoxia/normoxia ratio at 165 µM AA	3.4	1.6
K_M **(oxygen, µM)**	406 ± 37	235 ± 44
Vmax (µM/min)	20.5 ± 1.5	12.6 ± 1.7
Catalytic efficiency (min^{-1})	0.051	0.053

The physiological relevance of this unusually high oxygen Km has not been explored, but such kinetic properties are characteristic for sensor proteins. Thus, it might be possible that PA-LOX may be part of the oxygen sensor of *P. aeruginosa*.

Summary: The Ala420Gly exchange improves the oxygen affinity of the wildtype-PA-LOX.

3.3. Biological relevance of PA-LOX

3.3.1. Synthetic capacity for pro- and/or anti-inflammatory mediators

3.3.1.1. Leukotriene synthase activity

Previous literature reports indicated that several ALOX5 and ALOX15 orthologs are capable of catalyzing the conversion of 5- and 15-H(p)ETE (hydroperoxy fatty acid substrates) to epoxy leukotrienes, which constitute potent pro-inflammatory mediators (Bryant et al., 1985; Ueda et al., 1986; Brash et al., 1989). To quantify their leukotriene synthase activity, aliquots of both PA-LOX and rabbit ALOX15 were incubated with 15S-H(p)ETE under anaerobic conditions and the conjugated trienes formed were analyzed by RP-HPLC. Rabbit ALOX15 was used as a positive control as it has previously shown to convert 15S-H(p)ETE to 14,15-epoxyleukotriene A4 and its hydrolysis products (Bryant et al., 1985). As indicated in Figure 20A, rabbit ALOX15 catalyzed the conversion of 15S-H(p)ETE to conjugated trienes (absorbance at 270 nm). Corresponding incubations with 15S-HETE did not lead to the formation of such products and thus, one may conclude that the conjugated trienes did not originate from the double oxygenation pathway but rather from the hydrolysis of an epoxy leukotriene intermediate. With PA-LOX, conjugated trienes were only detected in small amounts although similar arachidonic acid oxygenase activities of the two enzymes were employed. These data suggest that 15-H(p)ETE is not efficiently converted to epoxy leukotrienes by recombinant PA-LOX, which is consistent with the previous findings (Deschamps et al., 2016) that 15-H(p)ETE is a poor substrate for PA-LOX. Thus, PA-LOX does not exhibit a sizeable leukotriene synthase activity.

Summary: PA-LOX unlike rabbit ALOX15 does not catalyze the synthesis of leukotrienes from 15S-H(p)ETE..

3.3.1.2. Lipoxin synthase activity

Lipoxins are a family of bioactive products generated from arachidonic acid and function as essential immunomodulatory and anti-inflammatory mediators (Romano, 2010). Pure rabbit ALOX15 catalyzes the conversion of 5,15-DiHETE

to conjugated tetraenes indicating its ability to synthesize lipoxins (Kuhn et al., 1984). In order to test the lipoxin synthase activity of PA-LOX, the enzyme was incubated with 5*S*-HETE and a 1:1 mixture of 5*S*,6*S*- and 5*S*,6*R*-DiHETE. The ability of PA-LOX to synthesize lipoxins was determined by measuring the formation of conjugated tetraenes with an absorbance maximum of 300 nm by RP-HPLC. From Figure 20B and C it can be seen that significant amounts of conjugated tetraenes were formed with PA-LOX.
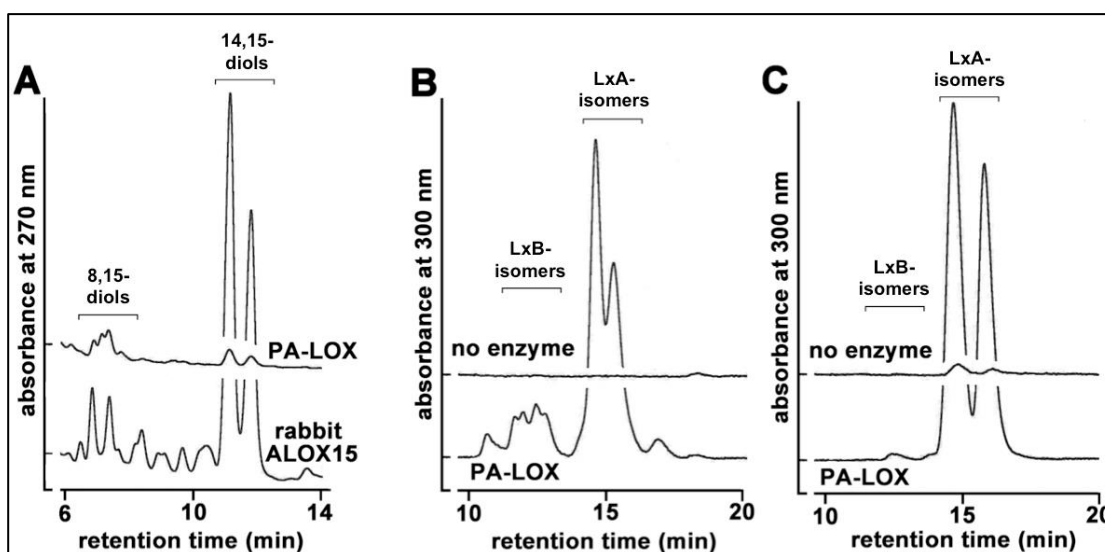
Figure 20: Ability of PA-LOX to synthesize leukotrienes and lipoxins. A) Leukotriene synthase activity: 52 µg of pure PA-LOX were incubated in 1 ml of PBS (pH 7.4) containing 25 µM of 15-H(p)ETE for 10 min at 25 °C. Similar incubations were carried out with 72 µg of purified rabbit ALOX15 (similar arachidonic acid activity as PA-LOX) as a positive control. The reactions products were reduced with sodium borohydride and the sample was acidified with acetic acid. The products were then analyzed by RP-HPLC to measure the conjugated trienes at an absorbance of 270 nm. B+C) Lipoxin synthase activity: 2 µg of purified PA-LOX were incubated in 500 µl of PBS (pH 7.4) containing 30 µM of 5S-HETE (panel B) and 5,6-DiHETE (panel C) for 10 min at 25 °C. To activate the enzyme, 3 µM of linoleic acid was added, which was quickly oxygenated to 13-H(p)ODE, which serves as an enzyme activator. The reaction products were reduced and analyzed by RP-HPLC recording the absorbance of 300 nm (Banthiya et al., 2016).

Although a previous study on PA-LOX suggested that this enzyme does not exhibit lipoxin synthase activity (Deschamps et al., 2016) our data clearly show the formation of conjugated tetraenes during the oxygenation of 5*S*-HETE and 5*S*,6*S*/*R*-DiHETE.

Summary: PA-LOX catalyzes the synthesis of the anti-inflammatory lipoxins from 5S-HETE and 5S,6S/R-DiHETE.

3.3.2. Phospholipids as PA-LOX substrates

3.3.2.1. PA-LOX oxygenates all the four classes of phospholipids

The ability to oxygenate phospholipids containing polyenoic acids led to the discovery of rabbit ALOX15 (Schewe et al., 1975). Recombinantly expressed PA-LOX has previously been crystallized and its substrate binding pocket contained a bound phospholipid molecule (Garreta et al., 2013). These data indicated that the enzyme is capable of binding phospholipids at the catalytic center and also suggests that it might be capable of oxidizing intact phospholipids without the preceding activity of a lipid-hydrolyzing enzyme.
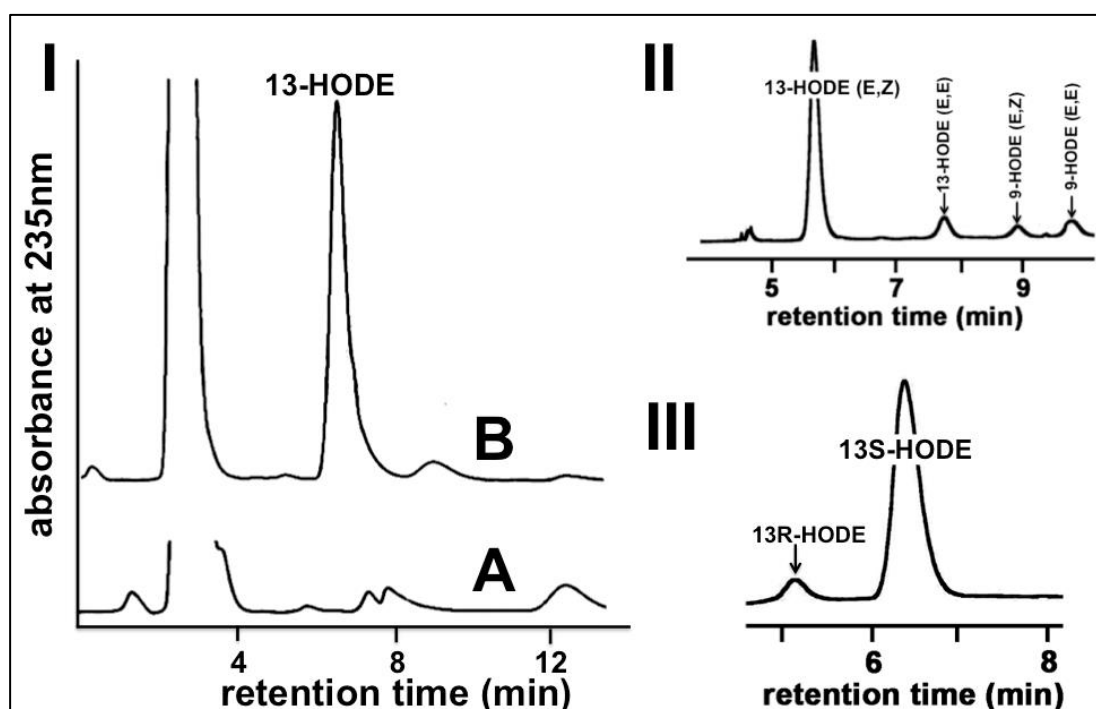
Figure 21: Phospholipid oxygenase activity of PA-LOX. 50 µg of PA-LOX was incubated with 1-palmitoyl-2-linoleoyl-phosphatidylethanolamine (dissolved in 0.5 % sodium cholate) in 1 ml of PBS (pH 7.4) for 5 min at 25 °C. The concentration of the phosphatidylethanolamine was adjusted to a linoleic acid concentration of 165 µM with a final detergent concentration of 0.5 %. The oxygenation products were reduced to the corresponding hydroxy-derivatives, the lipids were extracted and hydrolyzed under alkaline conditions. The major conjugated dienes of both A) no enzyme controls and B) PA-LOX containing samples were first separated on RP-HPLC (I) and the isomer composition of the PA-LOX containing samples were quantified by SP-HPLC (II) and CP-HPLC (III) (Banthiya et al., 2016).

To test this hypothesis, aliquots of purified PA-LOX and rabbit ALOX15 were incubated with different classes of pure phospholipids Table 15. The reaction products were extracted, hydrolyzed under alkaline conditions and the

hydrolysates were analyzed by HPLC for conjugated diene containing products formed during enzyme-phospholipid interaction (Figure 21). The conjugated dienes detected in RPHPLC co-migrated with the authentic standards of 13-HODE and 15-HETE. Since these compounds are not resolved in RP-HPLC, the conjugated dienes were prepared and further analyzed by SP-HPLC.

Table 15: Side-by-side comparison of the phospholipid oxygenase activity of PA-LOX with rabbit ALOX15: An aliquot of purified PA-LOX was incubated with the different classes of phospholipids for 15 min at room temperature. The concentration of the phospholipid was adjusted to a final linoleic acid concentration of 165 µM in 1 ml of PBS (pH 7.4) containing 0.5 % sodium cholate. The oxygenated products were recovered, reduced and subjected to lipid extraction and alkaline hydrolysis. The major product, 13-HODE, was prepared by RP- and SP-HPLC and enantiomer composition was then identified by CP-HPLC. Similar experiments were conducted with rabbit ALOX15 as a positive control. For the two LOXs, the peak area units obtained on the HPLC with no enzyme controls were subtracted from each substrate during the calculations of the percent relative activity. (Banthiya et al., 2016).

Substrate	PA-LOX		Rabbit ALOX15	
	Relative activity (%)	13S/13R-ratio (%)	Relative activity (%)	13S/13R ratio (%)
Linoleic acid	100	99:01	100	95:05
PE	0.06	93:07	8.3	95:05
PS	0.04	64:36	< 0.01	83:17
PI	0.05	95:05	0.5	88:12
PC	0.02	78:22	0.5	77:23

Co-chromatography of the major conjugated diene in SP-HPLC with an authentic standard of 13S-HODE indicated that the major oxygenation product was 13-HODE (Z,E).13-HODE (E,E), 9-HODE (E,Z) and 9-HODE (E,E) were also formed in small amounts. As expected, from CP-HPLC analysis, we confirmed that the major product with all the phospholipid substrates was 13S-HODE. Thus similar to rabbit ALOX15, purified PA-LOX is also capable of oxygenating *in vitro* pure phospholipids. After having shown that purified recombinant PA-LOX is capable of oxygenating phospholipids *in vitro*, we quantified the phospholipid oxygenase activity of PA-LOX and compared this catalytic activity with the phospholipid oxygenase activity of rabbit ALOX15 under comparable experimental conditions.

For this comparison the linoleic acid oxygenase activity of the two enzymes were quantified and then identical linoleic acid oxygenase activities of the two enzymes were used for the phospholipid oxygenase assay, which was carried out as described in the legend to Figure 21.

Table 15 indicates that both, rabbit ALOX15 and PA-LOX, are capable of oxygenating pure phospholipids *in vitro*. However, for both enzymes the ability to oxygenate free linoleic acid was much higher than their ability to oxygenate phospholipids. Rabbit ALOX15 exhibited a higher phospholipid oxygenase activity when compared with PA-LOX. On the other hand, the profile of oxygenation products with most phospholipid classes was comparable for the two enzymes and chiral 13*S*-HODE was always the major oxygenation product. The only exception was PS. Here a large share of the corresponding enantiomer (13*R*-HODE) was detected suggesting that the oxygenation of this substrate was not completely enzyme controlled.

Summary: PA-LOX exhibits a phospholipid oxygenase activity but this activity is more than 3 orders lower than its fatty acid oxygenase activity.

3.3.2.2. Fatty acid selectivity during phospholipid oxygenation

The crystal structure of PA-LOX indicated that the substrate-binding pocket consists of two sub-cavities, which join together in a lobby. Sub-cavity 1 involves the catalytic iron and the sn1 fatty acid of the endogenous phospholipid ligand ZPE. Sub-cavity 2 involves the sn2 fatty acid but this fatty acid cannot be oxygenated since the iron is not in this sub-cavity. In mammalian phospholipids the sn2 fatty acid is usually an unsaturated fatty acid. This leaves us with the dilemma that the unsaturated fatty acid of mammalian phospholipids is bound in the wrong sub-cavity. In other words, a phosphatidylethanolamine (PE) derivative with a linoleic acid at the sn1 position should be a more effective substrate for PA-LOX than a derivative with a linoleic acid at the sn2 position. Unfortunately, PE with linoleic acid at the sn1 position is not commercially available and thus comparison between PE-sn1-linoleate and PE-sn2-linoleate is not possible. However, PE derivatives with linoleate at both the sn1 and sn2 positions are available and can be used for comparative studies.

For such comparison, PA-LOX was incubated with 1-palmitoyl-2-linoleoyl-phosphatidylethanolamine (monolinoleoyl-PE) and 1,2-dilinoleoyl-phosphatidylethanolamine (dilinoleoyl-PE) side by side.
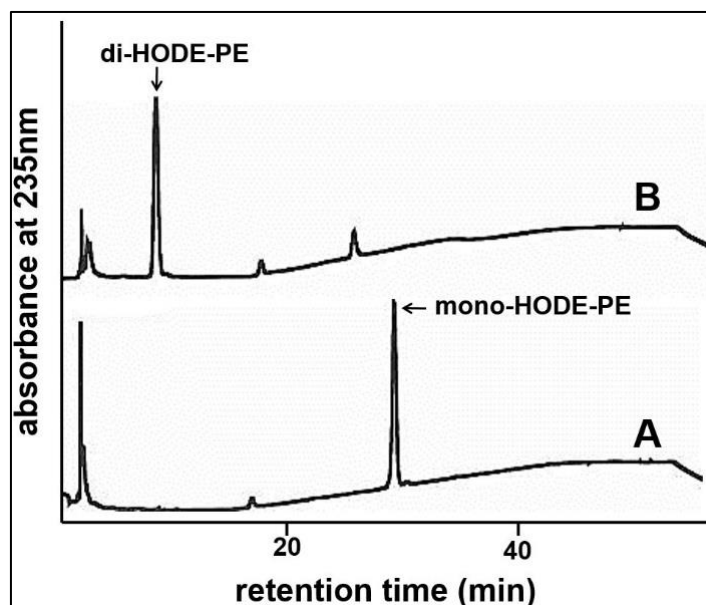
Figure 22: PA-LOX oxygenates fatty acids bound to both sn-1 and sn-2 positions of phospholipids. 12.5 µg of PA-LOX was incubated side by side with A) 1-palmitoyl-2-linoleoyl-phosphatidylethanolamine and B) 1,2-dilinoleoyl-phosphatidylethanolamine in 1 ml of PBS (pH 7.4) for 30 min at 25 °C. The concentration of the phosphatidylethanolamine was adjusted to a linoleic acid concentration of 165 µM with a final detergent concentration of 0.5 %. The lipids were extracted and the extracted phospholipids were analyzed on the RP-HPLC (gradient solution system) as indicated in Material and Methods (section 2.2.5.3.1.).

If these substrates were bound at the active site in the same way as the endogenous ligand (only the sn1 fatty acid is bound in proximity of the iron), one would expect oxygenation of only the sn1-linoleate. Therefore, HODE containing products must be seen only with dilinoleoyl-PE as monolinoleoyl-PE contains linoleic acid at sn2 position. However, from Figure 22A it can be seen that monolinoleoy-PE was oxygenated to mono-H(p)ODE-PE. This data indicates that the sn2 fatty acid can also be oxygenated. Thus, there must be the possibility for the sn2 fatty acid to be bound in the iron-containing subcavity 2 of the catalytic center. Moreover, when we employed dilinoeoyl-PE as substrate, the major product formed was di-HODE-PE (Figure 22B). This finding also indicates that the sn2 fatty acid is oxygenated by PA-LOX. Taken together, these data indicate that both the linoleic acids at sn1 and sn2 positions were oxygenated by PA-LOX.

Next, the total conjugated dienes formed with both the substrates were compared on RP-HPLC. From Figure 23, the products formed with the dilinoleoyl-PE are significantly higher than those formed with monolinoleoyl-PE.
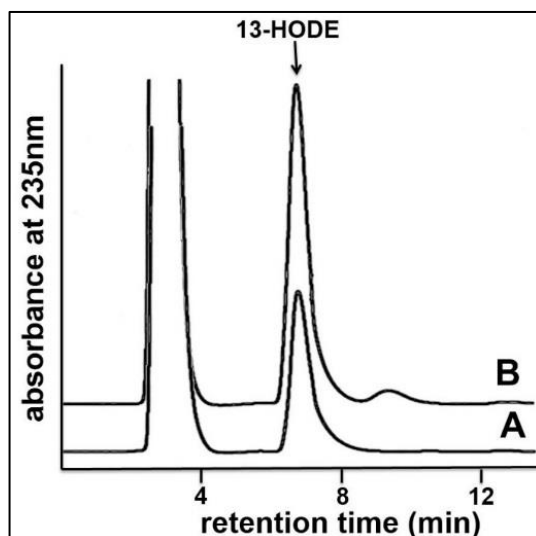
Figure 23: Comparision of the conugated dienes formed with monolinoleoyl-PE and dilinoleoyl-PE. 250 µg of PA-LOX was incubated with A) 1-palmitoyl-2-linoleoyl-phosphatidylethanolamine and B) 1,2-dilinoleoyl-phosphatidylethanolamine in 1 ml of PBS (pH 7.4) for 5 min at 25 °C. The concentration of the phosphatidylethanolamine was adjusted to a linoleic acid concentration of 165 µM with a final detergent concentration of 0.5 %. The oxygenation products were reduced to the corresponding hydroxy derivatives, the lipids were extracted and hydrolyzed under alkaline conditions. The major conjugated dienes with both the substrates were separated on RP-HPLC for quantification.

For statistical comparison, similar incubations of PA-LOX with the two substrates were carried out in triplicates. The mean amount of 13S-HODE formed with dilinoleoyl-PE was 7.2 ± 1.0-fold higher when compared with the monolinoleoyl-PE. These data strongly suggest that the phospholipid enzyme complex shown in the crystallographic data is one of several possible complexes. There is the possibility that the sn2 fatty acid is bound in the iron-containing sub-cavity.

Summary: PA-LOX is capable of oxygenating both the sn1 and sn2 fatty acids bound to phospholipids.

3.3.3. Biomembranes as PA-LOX substrates

In silico docking studies on rabbit ALOX15 indicated that its active site is too small to allow the binding of a complete phospholipid at its active site without steric

clashes (Ivanov et al., 2015). However, functional data clearly indicated that rabbit ALOX15 (Kuhn et al., 1990) as well as the orthologs from humans (Kühn et al., 1993) and pigs (Takahashi et al., 1993) are capable of oxygenating membrane and lipoprotein-bound phospholipids. PA-LOX on the other hand has an active site that is big enough to bind a complete phospholipid and oxygenates its bound polyenoic fatty acids (section 3.3.2). Also, PA-LOX is capable of oxygenating the most commonly occurring mammalian fatty acids, linoleic and arachidonic acid. Thus, it might also have the ability to oxygenate membrane bound phospholipids.

3.3.3.1. Oxygraphic measurements

To test this hypothesis, comparable linoleic acid oxygenase activities of PA-LOX and rabbit ALOX15 (positive control) were incubated with biomembranes in an oxygraphic assay chamber and the oxygen uptake was used as readout parameter for the membrane oxygenase activity of the two LOX-isoforms. As model membranes we used beef heart mitochondrial membranes, since previous studies indicated that these membranes are well oxygenated by rabbit ALOX15 (Kuhn et al., 1990).
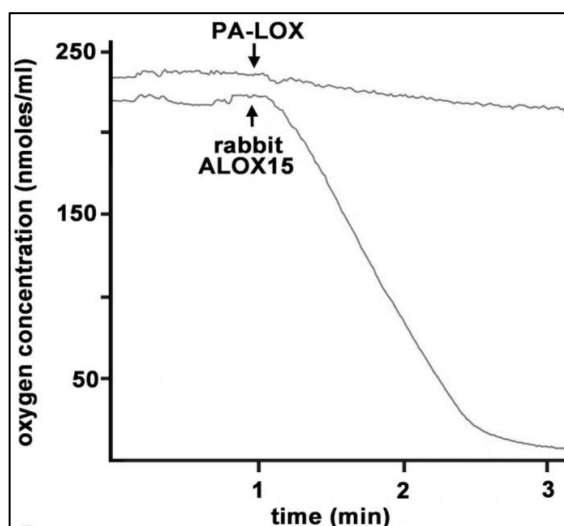
Figure 24: Comparison of membrane oxygenase activity of PA-LOX and rabbit ALOX15. 1 mg of beef heart mitochondrial membrane protein was incubated with PA-LOX and rabbit ALOX15 in 1 ml of PBS (pH 7.4) for 5 min at 25 °C in an oxygraphic assay chamber. The final concentration of PA-LOX and rabbit ALOX15 in the reaction mixture was adjusted to 92.8 nkat/ml and 9.9 nkat/ml linoleic acid oxygenase activity (determined oxygraphically) respectively. Efficiency of the membrane oxygenase activity was indicated by quantifying the decrease in the oxygen concentration in the reaction mixture in duplicates (Banthiya et al., 2015).

From Figure 24, it can be seen that addition of rabbit ALOX15 to the membrane suspension induced an oxygen consumption indicated by the time dependent decrease in the oxygen concentration in the assay chamber. To detect a measurable oxygen uptake with PA-LOX we had to increase the amount of enzyme so that linoleic acid oxygenase activity of PA-LOX was almost 10-fold higher than that of the rabbit enzyme. Thus, with rabbit ALOX15 this oxygen consumption was higher although only one tenth of linoleic acid oxygenase activity of this enzyme was added. From Table 16 it can be seen that the membrane oxygenase activity of rabbit ALOX15 was almost 25-times higher (7.4 s^{-1} vs. 0.3 s^{-1}) than that of PA-LOX.

Table 16: Comparison of membrane oxygenase activities of PA-LOX and rabbit ALOX15. Purified 1.2 µg of PA-LOX or 11.5 µg of rabbit ALOX15 were incubated in 1 ml of PBS (pH 7.4) containing 165 µM of linoleic acid or 1 mg of membrane protein. The reaction was monitored oxygraphically for 5 min at 25 °C to determine the consumption of oxygen by both PA-LOX and rabbit ALOX15 with the respective substrates. The molecular turn over ratios were then calculated from the maximal reaction rates (n=4) (Banthiya et al., 2015).

LOX type	Molecular turnover rates (s^{-1}) with	
	Linoleic acid	Mitochondrial membranes
Rabbit ALOX15	13.6 ± 2.6	7.4 ± 0.5
PA-LOX	162.4 ± 33.3	0.3 ± 0.1

Taken together, although PA-LOX and rabbit ALOX15 exhibit membrane oxygenase activities, both LOXs prefer free polyenoic fatty acids as substrates to biomembranes. Moreover, when normalized to similar linoleic acid oxygenase activity, rabbit ALOX15 oxygenates the mitochondrial membranes 289-times more efficiently than PA-LOX. This is surprising since the crystal structures of two enzymes would lead to inverse conclusions.

Summary: Oxygraphic measurements indicate the principle capability of PA-LOX to oxygenate membrane bound phospholipids. However, this ability of PA-LOX is more than 20-fold lower than membrane oxygenase activity exhibited by rabbit ALOX15.

3.3.3.2. Product structure

As second parameter to quantify the membrane oxygenase activity of PA-LOX, we analyzed the specific oxygenation products in the membrane ester lipids. For

this purpose PA-LOX and rabbit ALOX15 were incubated with the mitochondrial membranes for 15 min at 25 °C in PBS.
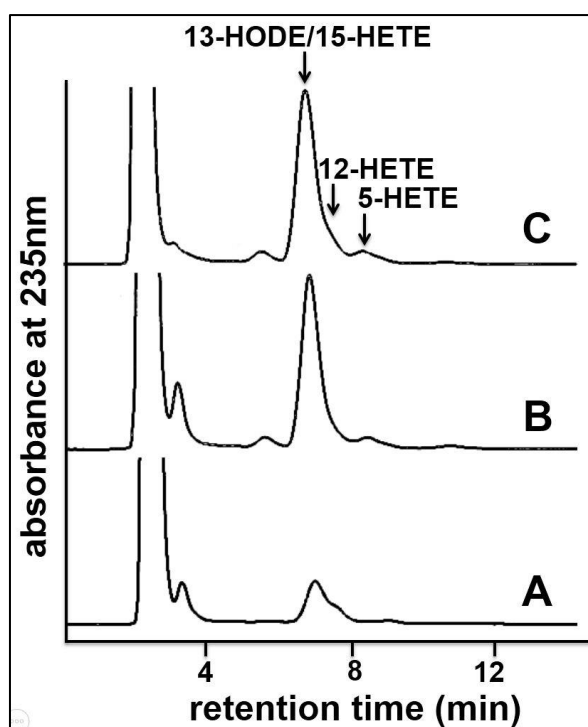
Figure 25: Formation of conjugated dienes during the interaction of pure PA-LOX, rabbit LOX with biomembranes. Beef heart mitochondrial membranes (5.3 mg/ml protein) in 1 ml of PBS (pH 7.4) were incubated with purified aliquot of PA-LOX and rabbit ALOX15 for 15 min at 25 °C in duplicates. To obtain almost similar amounts of products with both the enzymes, 50-fold higher linoleic acid oxygenase activity of PA-LOX was employed. After 15 min, the lipids were extracted and hydrolyzed under alkaline conditions. The hydrolyzed products of the mitochondrial membranes A) without any LOX, B) With PA-LOX and C) Rabbit ALOX15 were then analyzed on RP-HPLC to detect and collect the corresponding products.

The reaction was stopped by the addition of sodium borohydride, which reduces the hydroperoxy lipids to the corresponding alcohols. The membrane lipids were extracted, the ester lipids were hydrolyzed under alkaline conditions and the hydrolysates were subsequently analyzed by RP-HPLC. From RP-HPLC analysis (Figure 25) it can be seen that the hydrolyzed lipid extracts of membranes incubated in the absence of LOX contained only small amounts of conjugated dienes when compared with both PA-LOX and rabbit ALOX15. These data indicate that the enzymes are responsible for the formation of conjugated dienes. The major conjugated dienes formed during membrane-enzyme interaction co-migrated with 13-HODE and/or 15-HETE, which are not well separated under these chromatographic conditions. To obtain more details on the product

compositions formed by the two enzymes, the conjugated dienes were prepared by RP-HPLC and further analyzed on SP- and CP-HPLC. From Figure 26A, it can be seen that the major membrane oxygenase product of PA-LOX was 13-HODE(Z,E), while 15-HETE constituted a minor product.
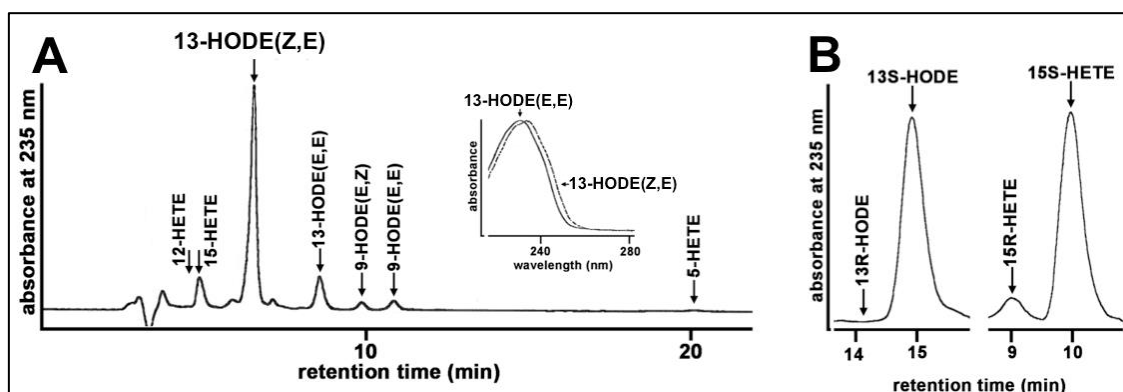
Figure 26: SP-HPLC and CP-HPLC analysis of the conjugated dienes formed during the interaction of PA-LOX with mitochondrial membranes. A) The conjugated dienes detected in Figure 25 with PA-LOX were collected, the solvent was evaporated, the remaining lipids were reconstituted in the SP-HPLC solvent and the conjugated dienes were analyzed by SP-HPLC. Inset: UV spectra of 13-HODE(E,E) and 13-HODE(Z,E) were recorded during the chromatographic run to confirm the supposed structure of the conjugated diene chromophore. B) The major conjugated dienes (15-HETE, 13-HODE(Z,E)) were prepared by SP-HPLC, the solvent was evaporated and the products were reconstituted in the CP-HPLC solvent and CP-HPLC was carried out as described in Material and Methods (2.2.5.3.3.). The arrows above the races indicate the retention times of authentic standards (Banthiya et al., 2015).

Thus, from all polyenoic fatty acids present in mitochondrial membranes linoleic acid was the major substrate. This result is not surprising since linoleic acid is the major polyenoic fatty acid present in inner mitochondrial membranes (Richardson et al., 1961). Additionally, traces of 13-HODE(E,E), 9-HODE(E,Z) were also seen (Figure 26A). A similar product pattern has previously been observed for rabbit ALOX15 (Kuhn et al., 1990). Determination of the enantiomer composition of 13-HODE and 15-HETE indicated a strong preponderance of the *S*-enantiomer. In contrast, the corresponding *R*-enantiomer was only present in small amounts indicating that the formation of these products was completely controlled by the enzyme (Figure 26B).

Summary: The predominant products formed when PA-LOX interacted with mitochondrial membranes are 13*S*-HODE and 15*S*-HETE confirming the membrane oxygenase activity of PA-LOX.

3.3.3.3. Time course of membrane oxygenation by PA-LOX

The kinetics of the membrane oxygenase activity of PA-LOX was determined by incubating the purified enzyme with beef heart mitochondrial membranes at 4 different time points: 5, 10, 15 and 30 min. The major conjugated dienes formed at each time point were quantified on RP-HPLC.
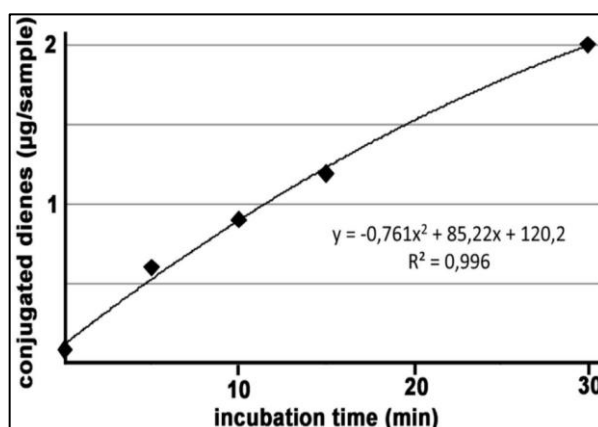
Figure 27: Time course of membrane oxygenase activity of PA-LOX. Purified and concentrated PA-LOX exhibiting a 13.3 nkat arachidonic acid activity/ml was incubated with 5.3 mg of beef heart mitochondrial membranes in 1 ml PBS at 25 °C for the respective incubation periods indicated in the graph. The lipids were extracted and then hydrolyzed under alkaline conditions. The conjugated dienes formed where then analysed on RP-HPLC (Banthiya et al., 2015).

Both linear and non-linear regressions were carried out on the kinetic data obtained, however, the non-linear data gave the best fit. From Figure 27 it can be seen that there is an almost linear increase in products up to 30 min. The curve does not intersect at zero because small amounts of conjugated dienes were already present in the biomembranes before incubation with the enzyme. Since linear regression analysis also fit the kinetic data well, it can be concluded that PA-LOX undergoes only a minor suicidal inactivation during its incubations with biomembranes. However, this was not the case with rabbit ALOX15. The majority of conjugated dienes formed with rabbit ALOX15 were seen within the first 5 min. At longer time periods, the amount of products formed decreased (data not shown). This might be due to the suicidal character of the oxygenase reaction.

Summary: PA-LOX exhibited only minor suicidal inactivation during incubation with biomembranes. On the other hand, rabbit ALOX15 exhausted its capacity within the first 5 minutes of incubation.

3.3.3.4. Phospholipid specificity during membrane oxygenation

In the previous sections (section 3.3.2), we have shown that when PA-LOX is incubated with the different phospholipid classes individually, it slightly prefers phosphatidylethanolamine (PE) as a substrate. To explore whether PE is also preferentially oxygenated when biomembranes are used as LOX substrates, the membranes were incubated with pure PA-LOX and rabbit ALOX15 (positive control) for 15 min, the reaction products were reduced to the corresponding alcohols and the membrane lipids were extracted. The major glycerophospholipid classes were then separated by SP-HPLC (Figure 28) and tested for the presence of conjugated dienes. For this purpose the different glycerophospholipid classes (PE, PC, PS/PI) were prepared, hydrolyzed and the hydroxy fatty acid/PUFA ratio was quantified by RP-HPLC as suitable measure for the degree of oxygenation. Table 17 indicates that in the no enzyme control incubations, the degree of oxygenation of all the phospholipid classes was very low (variation between 0.01 to 0.04 %).
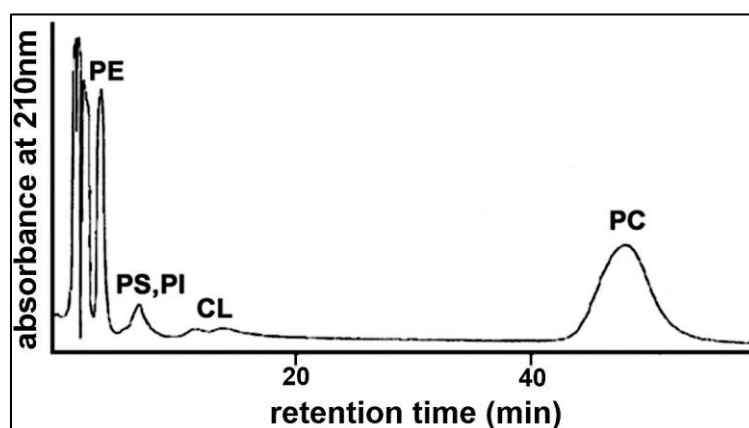
Figure 28: Separation of the major phospholipid classes from the mitochondrial membranes by SP-HPLC. Beef heart mitochondrial membranes (1 mg of membrane protein) in 1 ml of PBS (pH 7.4) were incubated in the absence and presence of PA-LOX and rabbit ALOX15 for 5 min at 25 °C. The final concentrations of PA-LOX and rabbit ALOX15 in the reaction mixture were 92.8 nkatal/ml and 9.9 nkatal/ml linoleic acid oxygenase activity (determined oxygraphically), respectively. The lipids were then extracted, evaporated and reconstituted in 1:1 mixture of chloroform/methanol for SP-HPLC analysis. Absorption at 210 nm detects the polyenoic fatty acid in the respective phospholipid class. The figure indicates the extracted lipids from biomembranes in the absence of enzyme (Banthiya et al., 2015).

The oxygenation degrees were significantly higher with both rabbit ALOX15 and PA-LOX catalysis. The degree of oxygenation of PE and PC with rabbit ALOX15

corresponded to 13.0 % and 7.4 %, while with PS/PI, the degree of oxygenation was only 1.5 %.

Table 17: Comparison of oxygenation degree of the different classes of phospholipids in biomembranes. The different glycerophospholipid classes were separated by SP-HPLC (Figure 28) and subjected to alkaline hydrolysis. The hydrolyzed products were then individually analyzed by RP-HPLC to determine the degree of oxygenation. For this purpose phospholipid classes were hydrolyzed under alkaline conditions and the resulting free fatty acids were analyzed by RP-HPLC for the occurrence of oxygenated derivatives. From the RP-HPLC traces the 13-HODE+15-HETE/linoleic acid + arachidonic acid ratio was calculated and this value was considered as a suitable measure for the degree of oxygenation of the different glycerophospholipid classes (Banthiya et al., 2015).

Enzyme	13-HODE+15-HETE / linoleic acid+arachidonic acid ratio (%)		
	PE	PS/PI	PC
No enzyme control	0.01	0.01	0.04
PA-LOX	1.1	0.3	0.22
Rabbit ALOX15	13	1.5	7.4

This data indicated that rabbit ALOX15 preferentially oxygenated PE followed by PC and PS/PI. PA-LOX also oxygenated PE (1.1 %) most efficiently. However, the oxygenation degree of all glycerophospholipid classes with PA-LOX was much lower than that determined for rabbit ALOX15. Since the membrane oxygenase activity of PA-LOX is low, 10-fold higher PA-LOX was employed for these incubations. This data is consistent with the oxygraphic measurements (Figure 24) indicating that, when normalized to identical linoleic acid oxygenase activities, the membrane oxygenase activity of PA-LOX is considerably lower.

Summary: PA-LOX and rabbit ALOX15 favor phosphatidylethanolamine as substrate among the different classes of phospholipids.

3.3.4. Intact erythrocytes as substrates for PA-LOX

3.3.4.1. Induction of hemolysis

As indicated above (section 3.3.3.), PA-LOX is capable of oxygenating mitochondrial membranes. However, it remained to be explored whether the enzyme also attacks plasma membranes of living cells. To test this, purified PA-

LOX was incubated with erythrocytes from healthy volunteers for different time periods. After the incubation times, the hemoglobin released due to lysis of the cells by LOXs, was quantified by measuring the absorbance at 410 nm (Soret band) in the supernatant after cells were spun down. To define 100 % hemolysis, red blood cells were completely hemolyzed by re-suspending them in water. From Figure 29 it can be seen that incubations with high amounts of PA-LOX (760 µg/ml PBS) induced gradual hemolysis. After 24 h more than 50 % of the erythrocytes were lyzed. At 10-fold lower enzyme concentration (76 µg/ml PBS) a lower degree of hemolysis was observed. Incubations with rabbit ALOX15 (the amount of enzyme added exhibited similar arachidonic oxygenase activity as that obtained with 760 µg of PA-LOX) induced less that 0.5 % of hemolysis during the first 4 hours. However, this value was significantly higher than the hemolysis induced in the no enzyme control.
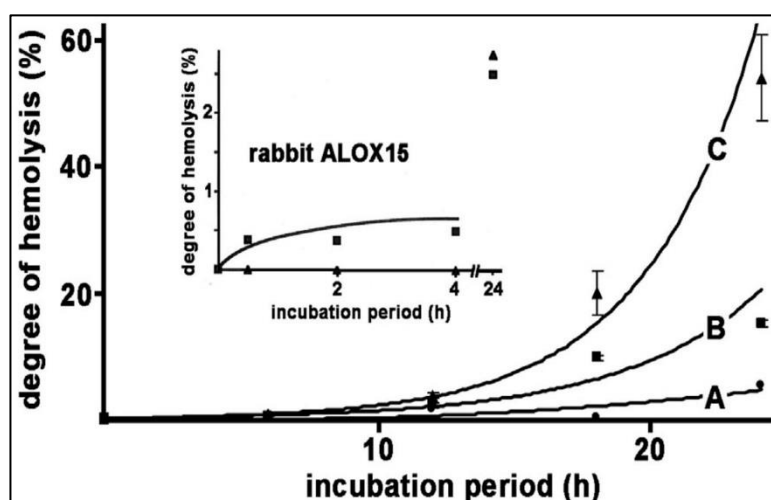
Figure 29: PA-LOX induces hemolysis in human erythrocytes. Freshly purified PA-LOX (76 µg/ml and 760 µg/ml) was incubated with 100 µl of erythrocytes in 1 ml of PBS (pH 7.4) for different time intervals (0, 6, 12, 18 and 24 h). Similar incubations were carried out with rabbit ALOX15 (1.2 mg/ml) and activity assays of the arachidonic acid oxygenase activities indicated similar catalytic activities of the two enzymes. As a negative control, a reaction mixture without any enzyme was also incubated. After the respective incubation periods, the erythrocytes were spun down and the supernatant was recovered. The cell pellets were subjected to osmotic hemolysis in 1 ml of ice-cold water (45 min) to induce complete (100 %) hemolysis. Absorption at 410 nm (in triplicates) of both the enzyme-induced lysis supernatant and the osmotic hemolysis supernatant was used to calculate the degree of hemolysis. The different values depicted above indicate the percentage of red blood cells of the reaction mixture that were hemolyzed by the different enzymes. A) No-enzyme control (circles) B) 76 µg of PA-LOX/ml C) 760 µg of PA-LOX/ml. Inset: Incubations with rabbit ALOX15 (solid squares: Rabbit ALOX15-incubations; triangles : No-enzyme control incubations) (Banthiya et al., 2015).

After 24 hours, the degree of hemolysis induced by PA-LOX was 20-fold higher than that induced by the rabbit enzyme (50 % hemolysis for PA-LOX vs. 2.5 % for rabbit ALOX15).

Summary: PA-LOX is capable of inducing hemolysis of intact erythrocytes, whereas rabbit ALOX15 is much less (20-fold lower) effective.

3.3.4.2. Lipidome analysis of erythrocyte lipids

HPLC analysis of the oxygenated polyenoic fatty acids formed during the incubation of PA-LOX with intact erythrocytes indicated that esterified 13-HODE and 15-HETE (not well separated under our analytical conditions) were formed during this interaction (Figure 30). Using a lipidomic approach (LC-MS/MS) we next intended to identify the intact oxygenated phospholipids formed during the PA-LOX-erythrocyte interaction. For this purpose 385 µg of freshly purified PA-LOX were incubated with intact erythrocytes for two different time periods (12 and 24 h). After the incubations the lipids were extracted and subjected to LC-MS analysis. Figure 31 compares the concentrations of selected phospholipid species in PA-LOX containing samples and the non-enzyme controls. The amounts of phospholipids containing monounsaturated fatty acids (not good substrates for PA-LOX) were comparable in both samples (Figure 31A). In contrast, the amounts of polyunsaturated fatty acid containing phospholipids were significantly lower in the samples treated with PA-LOX when compared to the non-enzymatic controls (Figure 31B). Next, we compared the amounts of phospholipids containing oxygenated derivatives of linoleic acid, arachidonic acid and docosahexaenoic acid such as HODEs, HETEs, KETEs and HDoHEs. Here we found that such phospholipids were mainly present LOX containing samples (Figure 31C). HODEs, HDoHEs, HETEs are the products of linoleic acid, docosahexaenoic acid and arachidonic acid peroxidation, respectively. KETE's are metabolites of arachidonic acid produced by the oxidation of HETE. Little or no of such oxygenated phospholipids (oxPLs) were seen in non-enzyme control incubations. Surprisingly, the levels of oxPLs were significantly higher in the 12 h incubations than at 24 h. This observation may be due to the fact that lipid hydroperoxides are unstable and may undergo decomposition during longer

incubation periods. One way of such secondary decomposition is fragmentation of the hydroperoxy fatty acid chain leading to phospholipids carrying shorter fatty acid chains (McIntyre, 2012). When searching for such truncated phospholipid species we found them in our incubation samples. However, they did not increase between 12 and 24 h (Figure 31D). The reason for this might be due to the fact that these short chain phospholipids may undergo secondary reactions at longer incubation periods. It has been reported that such short chain aldehydes form protein adducts (Michael and pyrole adducts) (Hoff et al., 2003) and thus, cannot be lipid extracted any more.
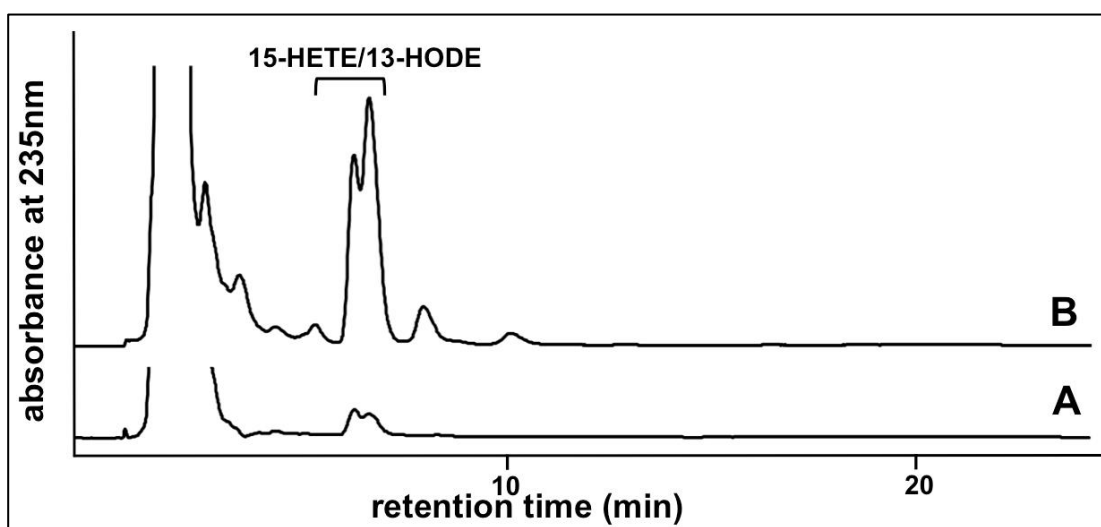
Figure 30: PA-LOX oxygenates linoleic acid and arachidonic acid esterified in the membrane phospholipids present in intact erythrocytes to 13-HODE and 15-HETE. 100 µl of packed erythrocytes in 1 ml of PBS (pH 7.4) were incubated with freshly purified PA-LOX (500 µg) at 25 °C for 24 h under continuous agitation. Similar incubations of the erythrocytes were carried out in the absence of PA-LOX as non-enzyme controls. After 24 h, the reaction mixture was subjected to lipid extraction. The bottom chloroform phase was recovered, the solvent was evaporated and the remaining lipids were reconstituted in methanol. The extracted lipids were then hydrolyzed under alkaline conditions and analyzed by RP-HPLC to determine the major oxygenation products formed in the A) non-enzymatic controls and B) PA-LOX containing samples.

Taken together, our lipidomic analyses indicate that pure recombinant PA-LOX oxidizes the membrane phospholipids of human erythrocytes. If such membrane oxidation proceeds during a *P. aeruginosa* infection, PA-LOX secreted from this bacterium is capable of inducing hemolysis of the hosts' erythrocytes by oxygenating their membrane bound phospholipids. Since it alters the integrity of the host cell membranes, PA-LOX may play a role as pathogenicity factor.
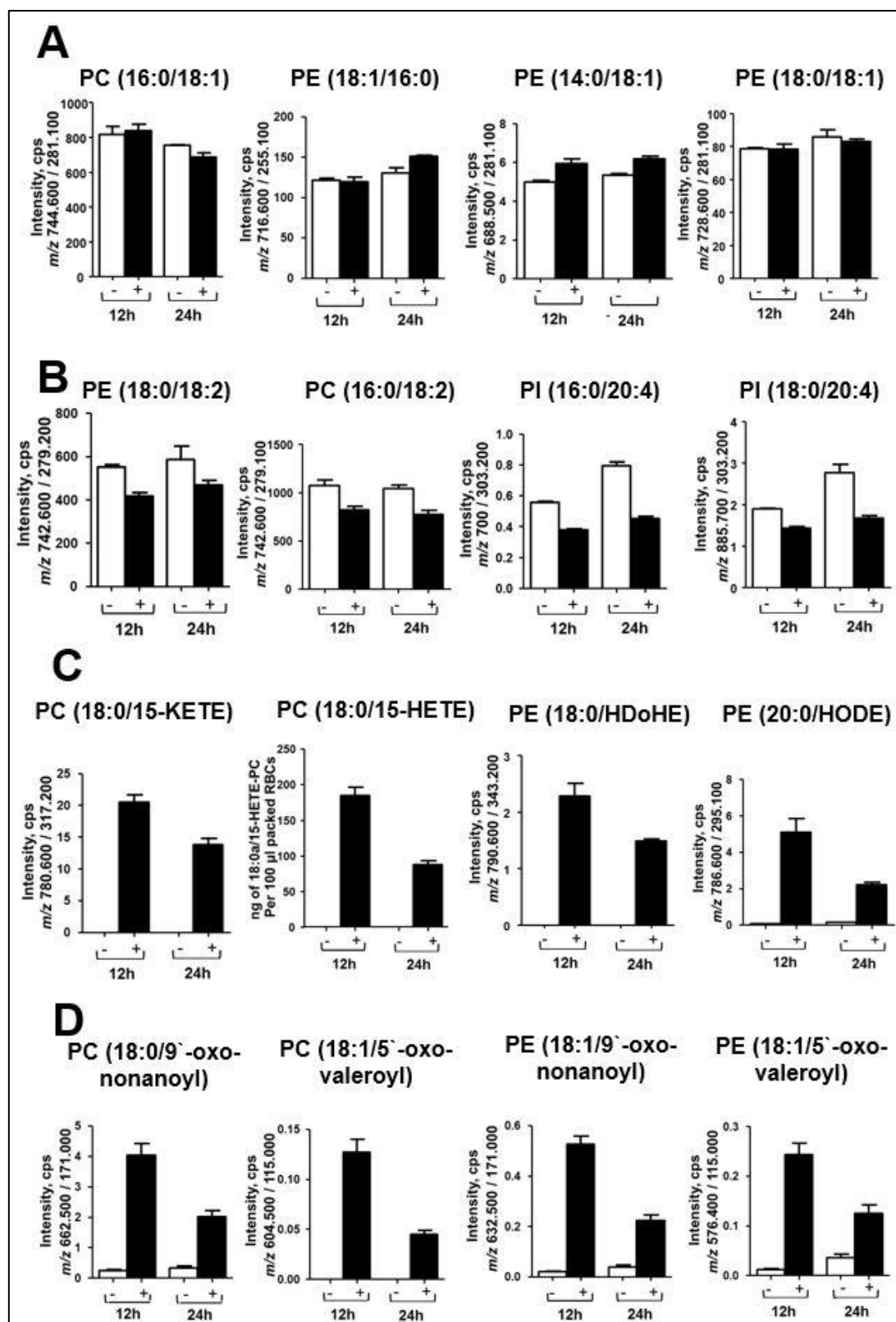
Figure 31: Lipidomic analysis of selected phospholipid species formed during in vitro incubation of intact human RBCs with purified PA-LOX. 100 µl of packed erythrocytes was incubated with 385 µg of freshly purified PA-LOX at 25 °C for 12 and 24 hours under continuous agitation. Similar incubations of the erythrocytes were carried out in the absence of PA-LOX as non-enzyme controls. The reaction mixture was subjected to lipid extraction. The bottom chloroform phase was recovered, the solvent was evaporated and the remaining lipids were reconstituted in methanol. These lipid extracts were

analyzed by reverse-phase LC-MS-MS. The levels of A) Saturated/monosaturated fatty acids containing phospholipids B) Polyunsaturated fatty acids containing phospholipids C) Oxygenated phospholipids and D) Truncated phospholipids were compared between the non-enzyme controls (-) and the PA-LOX (+) containing samples at both 12 and 24 hours of incubation. (white bars – non enzyme controls, n=2; black bars – PA-LOX containing samples, n=4).

Interestingly, a similar profile of oxygenated phospholipid species was analyzed when PA-LOX was incubated with cultured lung epithelial cells (A549 cells).

Summary: Lipidomic analysis of the extracted lipids indicates that PA-LOX induces hemolysis by oxygenating the plasma membrane phospholipids of intact erythrocytes.

4. DISCUSSION

4.1. Recombinant expression and purification of PA-LOX

4.1.1. PA-LOX sequence

Lipoxygenase in *Pseudomonas aeruginosa* (PA-LOX) was first discovered in mid-1960's (Shimahara, 1964). Unlike any other LOXs discovered so far, PA-LOX is a secretory protein (Vance et al., 2004). Using prediction algorithms, it was reported that the first 19 amino acids of the PA-LOX sequence involves a signal sequence, suggesting that PA-LOX might be a secreted protein (Vance et al., 2004). However, there is no direct experimental evidence supporting this hypothesis. One way of testing this would be by cleaving off the putative signal sequence and then testing the secretory ability of PA-LOX by measuring LOX-activity in the periplasm and cellular supernatant of the bacteria. Additionally, by fusing the cDNA of the signal sequence upstream of a reporter gene and then assaying secretion of the reporter, one can confirm the functionality of the predicted signal sequence.

For our expression strategy, we deleted the signal sequence but introduced a His$_6$-tag region at the N-terminus of the protein (Figure 5). We preferred intracellular recombinant expression for the following reasons: 1) A major problem with secreted recombinant proteins is proteolytic cleavage. A previous study has reported the isolation of a 45 kDa LOX from the periplasmic space of *P. aeruginosa* (Busquets et al., 2004). Although the sequence of this 45 kDa LOX is not yet available, the authors concluded that it might be a proteolysis product formed during secretion. Therefore, to avoid the isolation of such truncated versions of PA-LOX, we performed an intracellular recombinant expression. 2) Along with the signal sequence, N-terminal His$_6$-tag upstream of the signal peptide will also be cleaved off after translocation, thus lowering the efficiency of purification. 3) Other problems include incomplete translocation of proteins across the inner membrane of the *E. coli* due to the insufficient capacity of the export machinery. This reduces the total protein yield since the expressed recombinant protein in the cytoplasm is likely to accumulate in inclusion bodies (Mergulhão et al., 2005).

The putative N-terminal signal sequence was replaced by the His$_6$-tag sequence. The His$_6$-tag region is essential for convenient purification of the recombinant

protein. Thus, the N-terminal His$_6$-tag followed by 11 additional amino acids from the vector sequence preceded the coding region of PA-LOX. In principle, His$_6$-tag can be introduced either at the N-terminus or the C-terminus of recombinant proteins. However, when it comes to lipoxygenases, introduction of the His$_6$-tag at the C-terminus should be avoided since the C-terminal amino acid (Ile685 in case of PA-LOX) functions as ligand of the catalytic non-heme iron. Thus, elongation of the C-terminus, which will be achieved by the His$_6$-tag stretch, might alter the iron ligand sphere and thus inactivate the enzyme. Introduction of the His$_6$-tag at the N-terminus upstream of the signal sequence would neither be a good idea since the signal peptide is cleaved off after secretion, which would also remove the His$_6$-tag peptide, which makes it more difficult to purify the recombinant protein. Another possibility was to place the His$_6$-tag between the signal sequence and the remaining protein sequence. However, in this case, the His$_6$-tag might get folded into the protein structure, which might reduce the efficacy of purification by affinity chromatography. To avoid these problems and to get high expression yields of the recombinant enzyme for protein-chemical and enzymatic characterization, it was the most suitable expression strategy to place the His$_6$-tag at the N-terminus of the protein and remove the signal sequence.

4.1.2. Expression level

After sonication and removal of cell debris by centrifugation, the lysate supernatant was subjected to nickel agarose affinity chromatography to purify the His$_6$-tag fusion proteins. After this purification step, we got a total yield of 63 ± 5 mg of enzyme per liter of liquid culture, which was almost 5-fold higher than previously described (Deschamps et al., 2016). When we employed the same expression system for recombinant porcine ALOX15 a comparable yield (48 mg/L) was achieved. These data indicate that the expression system used here was very efficient for expression of LOX isoforms.

One of the major problems encountered during recombinant expression of proteins is aggregation in inclusion bodies (Singh et al., 2015). However, since our PA-LOX construct contained the N-terminal α-helix domain that is required for a soluble expression (Lu et al., 2016) and the total yield of the recombinantly expressed PA-LOX was high (63 mg/L), we did not test if PA-LOX is present in inclusion bodies so far.

4.1.3. Purity of PA-LOX

After affinity chromatographic purification of the His$_6$-tag fusion protein on a nickel agarose column a degree of purity >80 % of the enzyme preparation was obtained. SDS-PAGE indicated one major protein band migrating at the expected molecular weight of 70 kDa. In addition to the major band, two contaminating protein bands with approximate molecular weights of 25 kDa and 45 kDa were observed (Figure 6). Since these proteins could not be removed by affinity chromatography, it might be possible that the contaminating bands are also His$_6$-tag fusion proteins and may represent C-terminal truncation products of the PA-LOX, which might have been formed from the full-length enzyme by proteolysis or incomplete translation of the corresponding mRNA. However, westen blot analysis of our protein preparation using an anti-His$_6$-tag antibody indicated a single band at 70 kDa. No additional bands were seen at 25 kDa and 45 kDa. Thus, the chemical identity of these contaminating proteins is yet to be elucidated. In order to get rid of these contaminating bands, the nickel agarose elution fractions 1-3 were subjected to FPLC size exclusion chromatography, which separates proteins according to their molecular weight (Figure 7). Here we observed a major protein peak. When aliquots of this peak were analyzed by SDS-PAGE, we observed a single protein band migrating at 70 kDa without any contaminating protein bands. These data suggest a close to 100 % purity of the final enzyme preparation.

4.2. Chemical properties of enzyme preparation

4.2.1. Molecular weight of PA-LOX

First we compared the theoretical molecular weights (MW) of the native secretory PA-LOX (including the signal peptide), PA-LOX obtained from our expression system and PA-LOX expressed in the Deschamps study (Table 18). Here we found that the theoretical MW of our PA-LOX construct was similar to the native PA-LOX involving the signal sequence. On the other hand the molecular weight of the "Deschamps enzyme" (Deschamps et al., 2016) was higher because of the additional 14 amino acids from the vector sequence.

From SDS-PAGE, the experimental MW of our PA-LOX preparation was determined to be 70 kDa (Figure 6), which was in fair agreement with theoretical value deduced from the amino acid composition. The reason for the difference

between the theroretically predicted and SDS-displayed MW is unknown. However, an incomplete unfolding of PA-LOX might influence the electrophoretic mobility in SDS-PAGE. When the PA-LOX was expressed as secreted protein in *E. coli* using its endogenous signal peptide sequence, a similar molecular weight was determined (Lu et al., 2013). In the Deschamps study, PA-LOX was also expressed without its signal sequence but in SDS-PAGE it runs at an apparent MW of 76 kDa (Deschamps et al., 2016). This could be due to the 29 additional amino acids preceding the protein instead of the 19 amino acids of the signal peptide that was introduced in the expression plasmid between the His$_6$-tag and the native PA-LOX.

*Table 18: Comparison of the theoretical molecular weight of different PA-LOXs constructs. *(Deschamps et al., 2016), MW-Molecular weight.*

PA-LOX type	Theoretical MW (kDa)	Type of sequence	Sequence (No. of amino acids)
Native	74.53	Signal peptide	MKRRSVLLSGVALSGTALA (19)
This study	74.98	His$_6$-tag +vector	MGSSHHHHHHSSGLVPRGS HM (21)
Deschamps*	76.62	His$_6$-tag +vector	HHHHHHKPIPNPLLGLDSTEN LYFQGIDPFTEF (33)

Our construct was only 12 amino acids shorter than the protein expressed by the Deschamps study, which translates into a 1320 Da difference in MW between the two studies. However, from SDS-PAGE the difference in molecular weight is almost 6000 Da (70 kDa in ours vs. 76 kDa in (Deschamps et al., 2016)). The reason for this difference is unclear. However, the presence of excessive proline residues in the protein might affect its migration in SDS-PAGE. From Table 18, the vector sequence of the Deschamps study has four proline residues while our vector sequence has just one. Prolines introduce natural kinks in proteins making them structurally more rigid. Due to the compromised flexibility, there might be a reduction in the electrophoretic mobility of the protein (Kirkland et al., 1998). When PA-LOX was isolated from the periplasmic space of *Pseudomonas aeruginosa* 42A2, the enzyme exhibited a molecular weight of 45 kDa (Busquets et al., 2004). This value is much lower than the theoretical molecular weight of the native enzyme deduced from its amino acid composition. Thus, the enzyme

must have undergone proteolytic cleavage before or after it has been secreted into the periplasm. However, proteolytic removal of the signal sequence alone is not sufficient to explain the loss of 30 kDa. Cleavage in the C-terminal region of the native enzyme may not be a plausible explanation as this would result in the loss of three of the five non-heme iron ligands of the protein (His555, His559 and Ile685) and this would have inactivated the enzyme.

Figure 32: A) Predicted sequence of the periplasmic PA-LOX (black letters) from the native form containing all five iron ligands (bold and underlined amino acids) obtained from Sequence Manipulation Suite. B) Possible cleavage sites for trypsin (Tryps), chymotrypsin (Ch_hi) and Staphylococcus peptidase I (Staph) on the native PA-LOX around Ser273. (Arrow – Ser273) (Obtained from ExPASy peptide cutter program).

Thus, native PA-LOX should have lost the N-terminal sequence and such cleavage preserves all iron ligands. Using online prediction tools (Sequence Manipulation Suite), a 45 kDa protein is formed when proteolytic cleavage proceeded in the surrounding of Ser273 of native secretory PA-LOX (Figure 32A). The truncated protein starting from this position involves all the five amino acid

ligands for the non-heme iron, which are essential for the catalytic activity. To define the cleavage site more accurately, we employed the ExPASy peptide cutter program and observed several potential cleavage sites around Ser273 for trypsin-like and chymotrypsin-like proteases as well as for *Staphylococcus* peptidase I proteases (Figure 32B). Unfortunately, no direct analytical data are currently available on the N-terminal amino acid sequence of this 45 kDa native protein so that our theoretical considerations are somewhat speculative.

In contrast to PA-LOX, LOXs originating from other bacterial species such as *Thermoactinomyces vulguris* have a higher molecular weight of 160 kDa (Iny et al., 1993). Also, most plant LOXs have a molecular mass in the range of 94 – 104 kDa and LOXs from mammals in 75-80 kDa range (Brash, 1999).

4.2.2. The iron content of PA-LOX

Most lipoxygenases identified so far contain a non-heme iron at their active sites. The iron ion participates in the enzymatic reaction and is essential for the enzyme activity. However, some LOX isoforms contain a manganese ion instead. These enzymes include the LOX from *Gäumannomyces graminis* that contains 1 manganese ion per molecule enzyme. In contrast, its iron content was much lower (<0.15 iron ions per enzyme molecule (Su and Oliw, 1998)). Our PA-LOX preparation contains one-gram atom-iron per mole LOX. Thus, no iron supplementation of the expression system was required to meet the iron demand when expressing such high amounts of recombinant iron containing proteins. The PA-LOX isolated from the periplasmic space of *Pseudomonas aeruginosa* only contained 0.55 mol of iron per mol of protein and manganese was virtually absent (0.025 mol manganese per mol protein) (Busquets et al., 2004). When PA-LOX was expressed as recombinant His-tag fusion protein lacking the signal sequence, only 67 % metalation was observed (Deschamps et al., 2016). In other words, only two thirds of the enzyme molecules expressed under these conditions contain iron. This relatively low iron load might contribute to the lower specific activity of that particular PA-LOX preparation. Since lack of iron is likely to induce partial miss folding of the protein, a structural microheterogeneity of that enzyme preparation may be predicted, which might impact the crystallization behavior.

4.2.3. Crystal structure of wildtype-PA-LOX

The crystal structures of a number of different LOX-isoforms including PA-LOX have previously been solved and

Table 19 presents' details on the LOXs crystallized so far. We explored two crystal forms of wildtype-PA-LOX and solved the 3D-structure at a molecular resolution of up to 1.48 Å (Figure 8). PA-LOX has been crystallized before (1.75 Å and 2.0 Å) and superimposition of the two structures (Garreta et al., 2013) showed high degree of similarity. The prokaryotic PA-LOX displayed significantly different features when compared with the solved structures of eukaryotic LOXs: 1) PA-LOX lacks the N-terminal PLAT domain of the eukaryotic LOXs. Instead it involves a pair of long antiparallel helices (~100 amino acid residues) that acts as a lid for the entrance into the substrate-binding pocket. A similar observation was also made in the crystal structures of the fungal-LOXs obtained from *Magnaporthe oryzae* and *Gäumannomyces graminis*. The N-terminal PLAT domain is also absent in the structures of manganese containing LOXs (Chen et al., 2016; Wennman et al., 2016). A recent study has indicated that genetic truncation of the N-terminal alpha-helix lid-structure of the PA-LOX generated an enzyme, which was insoluble when expressed in *E. coli*. Moreover, proteolytic C-terminal truncation of the lid-structure (mini-LOX) improved the substrate affinity but lowered the catalytic activity and thermo stability. These data suggest that the N-terminus helix domain might impact the catalytic properties of the enzyme. However, the major effect of N-terminal truncation is that this manipulation renders the enzyme more insoluble (Lu et al., 2016). In eukaryotes, truncation of N-terminal domain reduced the catalytic efficiency of the enzyme leading to a rapid suicidal inactivation of the rabbit ALOX15. Moreover, in eukaryotes, the N-terminal β-domain was hypothesized to be involved in membrane binding and exhibits a regulatory importance (Walther et al., 2011).

2) The substrate binding pocket of PA-LOX is big, bifurcated and contains a complete phospholipid. The sn1 fatty acid moiety of this phospholipid occupies the sub-cavity that contains the non-heme iron, while the sn2 fatty acid occupies the second sub-cavity that does not have direct access to the non-heme iron. The polar head group occupies the 'lobby' region of the active site.

Table 19: Crystal data of LOXs from Protein data bank

LOX-isoform	PDB ID	Complex structures		Resolution (Å)	Reference
		Substrate	Inhibitor		
Glycine max LOX-1	2SBL			2.6	(Boyington et al., 1993)
	1YGE			1.4	(Minor et al., 1996)
Glycine max Thr756Arg LOX-1	5EEO			2.1	(Mikami et al., to be published)
Glycine max Leu546Ala/Leu754Ala LOX-1	4WHA			1.7	(Hu et al., 2014)
Glycine max Ile553Leu LOX-1	3BNB			1.45	(Meyer et al., 2008)
Glycine max Ile553Gly LOX-1	3BNC			1.65	
Glycine max Ile553Val LOX-1	3BND			1.6	
Glycine max Ile553Ala LOX-1	3BNE			1.4	
Glycine max Asn694Gly LOX-1	1Y4K			1.95	(Segraves et al., 2006)
Glycine max LOX-3	ILNH			2.6	(Skrzypczak-Jankun et al., 1997)
			1ROV/ 1HU9/ 1JNQ/ 1N8Q/ 1NO3/ 1IK3	2.0/2.2/2.1/ 2.1/2.15/2.0	(Skrzypczak-Jankun et al., 2001, 2003a, 2003b, 2004; Borbulevych et al., 2003; Vahedi-Faridi et al., 2004)
Glycine max LOX-B	2IUJ			2.4	(Youn et al., 2006)
Glycine max LOX-D	21UK			2.4	
Oryctolagus cuniculus 15LOX-1			1LOX	2.4	(Gillmor et al., 1997)
			2POM	2.4	(Choi et al., 2008)
Plexaura homomalla 8R-LOX		4QWT		2.0	(Neau et al., 2014)
	2FNQ			3.2	(Oldham et al., 2005)
	3FG1			1.85	(Neau et al., 2009)
Plexaura homomalla Ile805Tyr 8R-LOX	3FG3			1.9	
Plexaura homomalla Ile805Ala 8R-LOX	3FG4			2.31	
Homo sapiens 5LOX	3O8Y			2.39	(Gilbert et al., 2011)
Homo sapiens Ser663Ala 5LOX	3V92			2.74	(Gilbert et al., 2012)
Homo sapiens Ser663Asp 5LOX	3V98			2.07	
		3V99		2.25	
Gersemia fruticosa 11R-LOX	3VF1			2.47	(Eek et al., 2012)
Sus scrofa 12-LOX (Truncation)			3RDE	1.89	(Xu et al., 2012)
Homo sapiens 15LOX-2			4NRE	2.63	(Kobe et al., 2014)
Homo sapiens 12-LOX (truncation)	3D3L			2.6	(Tresaugues et al., to be published)
Gaeumannomyces graminis	5FX8			2.6	(Chen et al., 2016)
Magnaporthe oryzae	5FNO			2.04	(Wennman et al., 2016)
Pseudomonas aeruginosa			4G32	1.75	(Garreta et al., 2013)
			4G33	2.0	
Pseudomonas aeruginosa Gly186Glu			4RPE	1.6	(Carpena et al., to be published)
Cyanothece sp. PCC 8801	5EK8			2.7	(Newie et al., 2016)

In contrast, the substrate-binding pocket of the rabbit ALOX15 is a boot-shaped cavity, which is accessible from the surface (Gillmor et al., 1997; Choi et al., 2008). *In silico* docking studies have suggested that the substrate-binding pocket of this enzyme is too small to bind a complete phospholipid without steric clashes (Ivanov et al., 2015). However, small angle X-ray scattering experiments suggested that binding of a ligand at the active site of this enzyme induces major structural alterations that in turn might increase the overall volume of the binding pocket (Choi et al., 2008). The substrate-binding pocket of the coral 8R-LOX is a U-shaped channel, which may allow access to the non-heme iron from two different directions (Ivanov et al., 2010). Additionally, human ALOX5 involves an elongated substrate-binding cavity, which appears to be blocked at both ends. Phe177 and Tyr181 (FY-fork) guard one end, while Trp148 blocks the other end of the cavity. The authors suggest that the entry into such an active site requires a conformational change from either ends of the cavity (Gilbert et al., 2011). Taken together, the overall structure of PA-LOX clearly indicates that the substrate-binding pocket of this enzyme seems to be perfect to bind to a complete phospholipid thereby exhibiting a high binding affinity for phospholipids.

4.3. Enzymatic properties of wildtype-PA-LOX

4.3.1. Free fatty acids as substrates for PA-LOX

4.3.1.1. Kinetic parameters with arachidonic acid and linoleic acid

Arachidonic acid and linoleic acid are the two most abundant fatty acid LOX substrates in mammalian cells. However, these fatty acids rarely occur in *P. aeruginosa* (Oliver and Colwell, 1973). When PA-LOX oxygenates these substrates, n-6 hydroperoxy derivatives (15S-H(p)ETE and 13S-H(p)ODE) are formed. This finding is consistent with the literature data classifying PA-LOX as a secreted arachidonate15S-lipoxygenating enzyme (Vance et al., 2004).

The two LOX-isoforms from cyanobacteria, *Nostoc punctiforme* ATCC 29133, NpLOX1 and NpLOX2 also exhibited a similar linoleic acid oxygenation as PA-LOX (Koeduka et al., 2007) whereas the LOX isolated from *Nostoc sp.* PCC 7120 exhibited a 9R linoleic acid oxygenation (Lang et al., 2008). As prokaryotic LOXs, eukaryotic enzymes also exhibit variable reaction specificities and arachidonic acid is oxygenated to different product isomers (Table 20). To explore the reaction kinetics of arachidonic acid and linoleic acid oxygenation by PA-LOX,

spectrophotometric measurements were performed (Table 6 of Results sectio). PA-LOX exhibited a higher reaction rate with linoleic acid when compared with arachidonic acid (117.8 vs. 42.3 µM/min). Conversely, it exhibited higher affinity for arachidonic acid when compared to linoleic acid (Km of 48.9 vs. 174 µM).

Table 20: Product profile of several eukaryotic LOXs when subjected to arachidonic acid oxygenation.

Type of LOX	Products with arachidonic acid	Reference
Human ALOX15	15*S*-HETE and 12*S*-HETE (10:1)	(Sigal et al., 1988)
Human ALOX15b	15*S*-HETE	(Brash et al., 1997)
Rabbit ALOX15	15S-HETE	(Schewe et al., 1981)
Soybean LOX-1	15*S*-HETE	(Van Os et al., 1981)
Mouse alox15	12*S*-HETE	(Martínez-Clemente et al., 2010)
Mouse alox15b	8*S*-HETE	(Jisaka et al., 1997)
Rat alox15	12*S*-HETE and 15*S*-HETE (10:1)	(Watanabe et al., 1993)
Human ALOX12	12*S*-HETE	(Funk et al., 1990a)
Human ALOX12B	12*R*-HETE	(Boeglin et al., 1998)
Mouse alox12	12*S*-HETE	(Siebert et al., 2001)
Mouse alox12b	12*R*-HETE	(Krieg et al., 1999)
Porcine ALOX15	12*S*-HETE	(Yokoyama et al., 1986)
Zebrafish LOX	12*S*-HETE	(Jansen et al., 2011)
Coral LOX	8*R*-HETE	(Brash et al., 1996)
Human ALOX5	5*S*-HETE	(Funk et al., 1989)
Mouse alox5	5*S*-HETE	(Chen et al., 1995)

Interestingly, there is hardly any difference in the Kcat/Km ratio between the two substrates, indicating that the catalytic efficiency for both is similar. The molecular turnover rate of PA-LOX at 165 µM linoleic acid was determined to be 162 s^{-1} on the oxygraph. This value was more than 10-fold higher than the molecular turnover rate exhibited by rabbit ALOX15 (13.6 s^{-1}) under strictly comparable conditions. Simultaneous oxygraphic and spectrophotometric measurements of linoleic acid (165 µM) oxygenation indicated a deviation from 1:1 stoichiometry. In fact, under exactly comparable conditions, a molecular turnover rate 145 ± 14 s^{-1} was measured at the oxygraph and 76 ± 0.35 s^{-1} at the spectrophotometer.

Thus, the stoichiometry between oxygen consumption and conjugated diene formation was roughly 2:1. A 1.1 stoichiometry for rabbit ALOX15 has been reported earlier (Kühn et al., 1986). The lacking 1:1 stoichiometry between oxygen uptake and conjugated diene formation during PA-LOX catalyzed linoleic oxygenation may be due to the additional oxygen consuming secondary reactions (lipohydroperoxidase activity) or the decomposition of the conjugated dienes (e.g. formation of oxodienoic acid or short chain aldehydes) that might lead to an overestimation of PA-LOX mediated oxygen uptake. To address this question we recorded the UV-spectrum of the incubation mixture (range of 200-400 nm) during the time course of the oxygenation reaction but did not get any evidence for the formation of oxodienes. However, there is always the possibility for the formation of secondary lipid peroxidation products that do not show up in the spectrophotometer but such products need to be identified by MS/MS. In conclusion the molecular basis for the lack in stoichiometry between oxygen uptake and conjugated diene formation remains to be explored.

The Km value of eukaryotic LOXs for linoleic acid oxygenation vary in the lower micro molar range (Table 21).

Table 21: The Km values for linoleic acid oxygenation by eukaryotic LOXs

LOX-isoform	Km for linoleic acid (µM)	Reference
Human ALOX15	3	(Kühn et al., 1993)
Rabbit ALOX15	6.36	(Schewe et al., 1986b)
Soybean LOX-1	8.5	(Van Os et al., 1981)
Human ALOX12	10	(Chen et al., 1993)
Human ALOX5	12.2	(Soberman et al., 1985)

In contrast, the corresponding value for PA-LOX was more than 10-fold higher suggesting a low affinity of the enzyme for this fatty acid. It should however, be stressed that the Km strongly depends on the *in vitro* activity assay. Variations in the reaction conditions such as pH, buffer composition and reaction temperature as well as the presence or absence of detergents strongly impact the water solubility of fatty acid substrates and thus may impact the Km. Detergents strongly influence the monomer-micelle equilibrium of fatty acid substrates in the assay system and strongly impact the reaction kinetics. Thus, direct comparison

of Km values obtained in different kinetic assay systems can be misleading and side-by-side reactions are always recommended for direct comparison. The catalytic efficiency of the PA-LOX preparation with arachidonic acid as substrate from another study was significantly higher (16 $(\mu M \times s)^{-1}$) (Deschamps et al., 2016) than the corresponding value obtained with our enzyme preparation. The reason behind such a low catalytic efficiency of our enzyme preparation is the high Km (48.9 μM) and a low molecular turnover rate (23.5 s^{-1}) for arachidonic acid (Table 6). This may be due to the different buffer conditions used by this study. The activity assay in this study was carried out at a lower pH (6.5 vs. 7.4 in our study) and in the presence of detergents (0.01 % Triton X-100). In order to test the impact of detergents on the reaction kinetics we compared the rate of linoleic acid (165 μM) oxygenation by PA-LOX in the presence and absence of 0.01 % sodium cholate. Here we found a more than 70 % increase in the reaction rate in the presence of detergents. Since usually no detergents are present in biological environments we routinely explored the reaction kinetics in the absence of such additives. In the absence of detergents catalytic efficiencies (Kcat/Km) of 2 $(\mu M \times s)^{-1}$ and 0.10 $(\mu M \times s)^{-1}$ were determined for human ALOX15 and human ALOX15B (Wecksler et al., 2008) and these values are more similar to the data we determined for PA-LOX.

4.3.1.2. Kinetic parameters with other free fatty acid substrates

The polyenoic fatty acids present in mammalian cells can be subdivided with respect to their nutritional importance in two principle categories: omega-3 and omega-6. The major omega-3 polyenoic fatty acids, such as eicosapentaenoic (EPA) acid and docosahexaenoic acid (DHA), are biosynthesized via elongation and desaturation of alpha-linolenic acid. In contrast, omega-6 fatty acids, such as arachidonic acid (AA) and dihomo-γ-linolenic acid (DGLA), derive from linoleic acid (LA). In cellular systems several LOX-, COX- and cytochrome P450-isoenzymes compete for AA, EPA, DHA and DGLA to produce essential inflammatory mediators (Das, 2006). One of the main pre-requisite for a lipoxygenase catalyzed reaction is that the fatty acid substrates contain at least one 1,4-*cis,cis*-pentadiene structural unit (Haeggström and Funk, 2011). In order to explore the ability of PA-LOX to produce biologically relevant products, we tested the activity of PA-LOX with a number of polyunsaturated fatty acid

substrates with variable chain length and number of double bonds (Table 7). PA-LOX oxygenated almost all polyunsaturated fatty acid substrates at n-6th position irrespective of the chain length and the number of double bonds. However, among the free fatty acids tested, PA-LOX prefers DGLA and DHA. In addition, arachidonic acid and linoleic acid were also well oxygenated, while eicosapentaenoic acid was less effectively oxygenated.

DHA is found at high nanomolar concentrations in broncho-alveolar lavage fluid. Additionally, when DHA was added to cultures of *P. aeruginosa* PR3, the extracted lipids obtained after 72 h of bioconversion exhibited an antibacterial activity against both gram-positive and gram-negative bacteria (Shin et al., 2007). Cystic fibrosis patients exhibit abnormal blood and tissue levels of polyunsaturated fatty acids. Among others, the levels of DHA are reduced in ileum, lung and pancreas of cystic fibrosis mouse models. In contrast, the levels of the arachidonic acid are increased. Interestingly, these levels were normalized by dietary supplementation with DHA (Freedman et al., 1999; Mimoun et al., 2009). Using cell culture models, it has been demonstrated that the treatment of cystic fibrosis bronchial epithelial cells with exogenous DHA reverses this imbalance by down-regulating the expression of desaturase genes that function as catalysts during the conversion of linoleic acid to arachidonic acid (Njoroge et al., 2012). Thus, dietary supplementation of DHA has been recommended to improve the clinical conditions of some cystic fibrosis patients (Coste et al., 2007; Martinez et al., 2009). Here we report that PA-LOX prefers DHA as substrate and this finding suggests PA-LOX dependent metabolization of DHA might contribute to the reduction of DHA observed during the *P. aeruginosa* infections. Reducing the amounts of DHA in the host, the pathogen may delay its clearance from lungs. In another study on recombinantly expressed PA-LOX, it was suggested that arachidonic acid was the most preferred substrate for this enzyme (Deschamps et al., 2016). The reason behind this difference is unclear but the different assay conditions (substrate concentration 10 μM in the Deschamps study vs. 100 μM in our study, pH 7.0 in the Deschamps study vs. pH 7.4 in our study) may contribute. PA-LOX isolated from the periplasmic space of *P. aeruginosa* exhibited oleic acid oxygenase activity (Busquets et al., 2004) and a similar observation was later on also reported for the recombinant enzyme (Vidal-Mas et al., 2005). In the latter study it was reported that the oleic acid oxygenase activity of recombinant PA-

LOX amounted to about 30 %, when the rate of linoleic acid oxygenation was set to 100 % (Vidal-Mas et al., 2005). However, as indicated in Figure 33A, under similar enzyme amounts and assay conditions, we did not see an oleic acid oxygenase activity in our oxygraphic measurements.
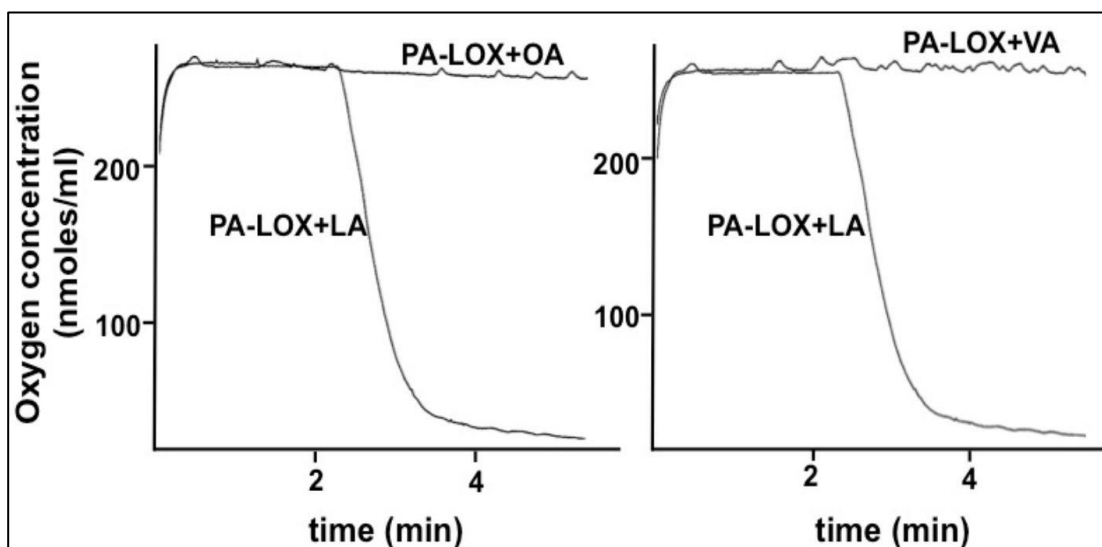
Figure 33: Testing the ability of PA-LOX to oxygenate oleic acid and vaccenic acid oxygraphically. 2.1 μg of freshly prepared PA-LOX was incubated with A) Oleic acid (OA) and B) Vaccenic acid (VA) in 1 ml of PBS (pH 7.4) for 5 min at 25 °C in an oxygraphic assay chamber. As a positive control, we also tested the linoleic acid (LA) oxygenase activity of PA-LOX side-by-side. The final concentration of the all the fatty acid substrates in the reaction mixture was adjusted to 165 μM. Ability of PA-LOX to oxygenate OA and VA was indicated by the decrease in the oxygen concentration in the reaction mixture.

The reasons for this discrepancy have not been explored. However, the activity assays in the Vidal-Mas study were differently structured. Compared with our standard assay Vidal-Mas incubated high amounts of recombinant PA-LOX (400 μg vs. 2.1 μg in our study) with more than 30-fold higher oleic acid concentrations (3.15 mM vs. 0.1 mM in our study). Moreover, the reaction mixture was incubated for longer time periods (2 hours vs. 3 min in our study) in 200 mM borate buffer (pH 8.0 vs. PBS with pH 7.4 in our study). The enzyme activity was monitored at 235 nm. This assay system is surprising since measurements at 235nm are based on the formation of conjugated dienes. Since oleic acid lacks the bisallylic methylene, it cannot be transformed to conjugated dienes (Vidal-Mas et al., 2005). Vaccenic acid is another monounsaturated fatty acid (C18: Δ11), which abundantly occurs in *P. aeruginosa* (Oliver and Colwell, 1973). Thus, we tested this fatty acid as substrate for PA-LOX. Comparative oxygraphic

measurements of purified PA-LOX with *cis*-vaccenic acid and linoleic acid (positive control) as substrate did not reveal any indications for a major vaccenic acid oxygenase activity of the enzyme. In fact, when compared with linoleic acid, we did not see any oxygen consumption with this monounsaturated fatty acid (Figure 33B).

In the literature the oleic acid oxygenase activity of PA-LOX was concluded from the analysis of the reaction products (Vidal-Mas et al., 2005), which is a very sensitive method. In contrast, oxygraphic measurements are not very sensitive but nevertheless, side-by-side comparative measurements with linoleic acid oxygenation suggest that under our experimental conditions, the vaccenic acid and oleic acid oxygenase activities are more than one order of magnitude lower than the enzyme's linoleic acid oxygenase activity.

4.3.1.3. Oxygen affinity of PA-LOX

Atmospheric dioxygen is the second substrate for all LOX-isoforms. The oxygen affinity of several mammalian LOXs has been studied before and the oxygen Km values are summarized in Table 22. The oxygen Km values for these LOXs range in the lower two-digit micromolar range. On the contrary, the wildtype-PA-LOX exhibits an unusually high Km value (406 µM) for oxygen indicating its low oxygen affinity (Table 14). Thus, under physiological conditions most mammalian LOXs are working in the range of oxygen saturation, where minor alterations in oxygen concentrations in the surrounding have negligible impact on the reaction rate. In contrast, at physiological conditions, PA-LOX is not oxygen saturated and thus, alterations in the oxygen concentration strongly impact the reaction rate.

Table 22: The oxygen affinity of various eukaryotic LOXs.

LOX-type	Oxygen affinity [µM]	Reference
Soybean LOX-1	20 ± 1.5	(Egmond et al., 1976)
Rabbit ALOX15	3.7 ± 0.2	(Ludwig et al., 1987)
Purified human ALOX12	14 ± 3.3	(Hada et al., 1991)
Crude human ALOX12	13 ± 4.1	(Juránek et al., 1999)
Purified human ALOX12	26 ± 6.0	(Takahashi et al., 1988)
Crude porcine ALOX15	26 ± 2.6	(Juránek et al., 1999)

In cystic fibrosis patients, who are frequently infected by *P. aeruginosa,* decreased oxygen concentrations were measured in the airways (Alvarez-Ortega and Harwood, 2007). Employing micro oxygen sensors, a pO2 as low as 2.5 mmHg was determined in the diseased lung region when compared with 180 mmHg in healthy airway lumen (Worlitzsch et al., 2002). Therefore, external oxygen supplementation is frequently employed for the treatment of acute episodes of respiratory failures (Madden et al., 2002). Our kinetic data suggest that during *P. aeruginosa* infections, an increase of the oxygen concentration would strongly activate PA-LOX activity but the clinical consequences of this enzyme activation remain to be explored. It may well be that this activation of PA-LOX might contribute to the deleterious effects of long-term oxygen therapy.

4.3.2. Thermal stability and activation energy of PA-LOX

When incubated at 4 °C, PA-LOX loses 60 % of its initial catalytic activity during the first 24 hours even if glycerol is present as stabilizing agent. After this incubation period, the enzyme was not completely inactive and after one week of incubation at 4 °C it still exhibited 20 % residual activity (Figure 15). However, a similar drop of the catalytic activity was not observed for the 45 kDA PA-LOX isolated from the periplasmic space of *P. aeruginosa*. This enzyme exhibited 100 % of its initial activity even after a week storage at 4 °C (Busquets et al., 2004). Thus, the truncated enzyme that is secreted from the bacterium appears to be more stable than its recombinant full-length isoform.

Temperature variations do not only impact enzyme stability but also the reaction rate and the reaction kinetics. In our hands, the temperature optimum (T_{opt}) of PA-LOX catalyzed linoleic acid oxygenation was 35 °C (Figure 14). In contrast, other study suggested a T_{opt} of about 25 °C (Lu et al., 2013; Deschamps et al., 2016). A similar T_{opt} (25 °C) was reported for oleic acid oxygenation catalyzed by the 45 kDa periplasmic PA-LOX (Busquets et al., 2004). From the Arrhenius plot, an activation energy for PA-LOX catalyzed linoleic acid oxygenation of 33.8 kJ/mol x K was calculated (Figure 14). This value is somewhat higher than that determined in side-by-side experiments with rabbit ALOX15 (14.3 kJ/mol x K). A similar activation energy of 18 kJ/mol x K was previously reported for soybean LOX (Tappel et al., 1953). Activation energy is the minimum amount of energy required to reach the catalytic transition state (Krishtalik, 1985). Thus,

both rabbit ALOX15 and soybean LOX require low initial energy to reach this threshold. However, at such low energies, reactions catalyzed by PA-LOX will not occur because they require almost 2 times higher energy to overcome this threshold.

4.4. Concepts for the reaction specificity of LOXs

4.4.1. Triad and Jisaka determinants

The positional specificity of LOXs mirrors the structure of the enzyme-substrate complex during a LOX catalyzed reaction. Several studies have been carried out to identify key amino acid residues that are essential for the reaction specificity of LOXs. The positional specificity of various ALOX15 and ALOX12 isoforms can be explained by the triad concept. According to this concept, a triad of amino acids, which align with Phe353 (Borngräber et al., 1996), Ile418/Met419 (Sloane et al., 1991a, 1995) and Ile593 (Borngräber et al., 1999) of rabbit ALOX15 function as sequence determinants for the positional specificity of LOXs. These residues are often clustered together in the 3-dimesional structures and form the bottom of the substrate-binding pocket. The bulkiness of their side chains appears to be of major importance since these side chains determine the depth of these pockets. The hydrogen abstractions of 15- and 12- lipoxygenating enzymes occur from C13 and C10 of the arachidonic acid, respectively. When the triad determinants of a 15-lipoxygenating LOX are replaced by less space-filling residues, the substrate penetrates deeper into the pocket, which approaches C10 of the arachidonic acid molecule closer to the non-heme iron resulting in a 12-lipoxygenation. On the contrary, larger residues at these positions favor arachidonate 15-lipoxygenation (Vogel et al., 2010). Conversion of a 15-lipoxygenating ALOX15 ortholog to a 12-lipoxygenating enzyme involves an alternative site for hydrogen abstraction (C-13 to C-10), while the radical rearrangement remains the same ([+2]-rearrangement of the radical electron towards the methylene end of the substrate in both 15- and 12-lipoxygenating enzymes). The 15-lipoxygenating ALOX15 orthologs from humans (Sloane et al., 1995) and rabbits (Borngräber et al., 1999) as well as the 12-lipoxygenating orthologs from pigs (Suzuki et al., 1994), rats (Pekárová et al., 2015), rhesus monkeys (Vogel et al., 2010) and gibbons (Adel et al., 2016) follow this triad concept. However, applicability of the triad concept has not yet been tested for

any bacterial LOXs. In order to identify the triad determinants of PA-LOX, we carried out multiple amino acid alignments of PA-LOX with mammalian ALOX15 orthologs and mutated the putative triad determinants of PA-LOX to smaller residues (Table 8). Unfortunately, we did not find convincing changes in the reaction specificity and these mutagenesis data indicate that PA-LOX does not follow the triad concept. Similar observations have been made for murine alox15b and its human ortholog. Instead of the triad determinants, Glu604 and Lys605 appeared to be positional determinants of human ALOX15B (Jisaka et al., 2000). Assuming a similar scenario for PA-LOX, we then mutated the corresponding amino acids of PA-LOX to residues of the murine alox15b (Table 9). However, the corresponding double mutant did neither show any alterations in the reaction specificity. The major product still remained 15S-H(p)ETE. Although mutations of the triad determinants did not induce major alterations in the positional specificity, the mutants exhibited altered catalytic efficiencies of arachidonic acid oxygenation. While the mutants, Met434Val and Leu612Val exhibited a reduced catalytic activity (35 % and 60 %, respectively) with arachidonic acid when compared to the wildtype-PA-LOX (100 %); the Glu369Ala and Phe435Leu mutants exhibited an increased catalytic activity (180 % and 240 % respectively). The Glu604Tyr+Lys605His double mutant exhibited a similar catalytic efficiency as the wildtype enzyme.

Exploring the 3D-structure of the wildtype-PA-LOX, we identified several other amino acid residues that might function as positional determinants since they might be involved in enzyme-substrate interaction.

Table 23: Analysis of the possible positional determinants of PA-LOX

Type of exchange	Mutant	Observation
Bulky amino acid to smaller amino acid	Met374Ala	<1% residual activity (inactive)
	Met434Ala	
	Phe435Ala	
	Tyr609Ala	
Smaller amino acid to bulky amino acid	Glu373Leu	>10% residual activity (active) No alteration in positional specificity
	Leu378Phe	
	Leu425Phe	
	Leu425Tyr	

These residues were mutated to either bulkier or lesser space filling residues (Table 23), expressed and the product profile of each of them was analyzed by HPLC. In addition to these amino acids, the structure of wildtype-PA-LOX indicated other residues, which might contribute to form the bottom of the substrate-binding pocket. These residues include Leu424, Phe430, Gln562 and Ile608. Testing these mutants in the future might help determine the positional determinants of PA-LOX.

4.4.2. Ala vs. Gly concept

4.4.2.1. Product profile after Ala to Gly exchange

We successfully identified the amino acid responsible for the enantioselectivity of PA-LOX. Multiple sequence alignments of several *S*- and *R*-LOXs with known reaction specificity have indicated that a single conserved amino acid residue at a critical position is different between these two types of enzyme subclasses. Most *S*-LOXs have an alanine at the critical position (so called 'Coffa Site'), while a glycine is present at the same position in most *R*-LOXs. Additionally, when the alanine is mutated to a glycine in human ALOX15B and mouse alox15b, these LOXs are converted to 11*R*- and 12*R*-lipoxygenating enzymes, respectively. Also, when the glycine of the human ALOX15B and coral 8*R*-LOX is mutated to alanine, these enzymes were transformed to 8*S*- and 12*S*-LOXs respectively (Coffa and Brash, 2004). However, similar mutations in ALOX15 orthologs from mice, rabbits, rhesus monkeys, orangutans and men induced only minor alterations in the reaction specificity, which do however point in the same direction (Jansen et al., 2011). Also, the 9*R*-LOX from the cyanobacterium *Nostoc sp.* PCC7120 carries an alanine at the 'Coffa Site'. When this Ala was mutated to a lesser bulky Gly, there was no significant alteration in the reaction specificity. However, when bulkier residues, such as Val or Ile, were introduced, 13*S*-HODE was the major oxygenation product (Andreou et al., 2008). On the other hand, there are exceptions from this concept such as zebrafish LOX-1. This enzyme carries a glycine at this position but functions as S-lipoxygenating (Jansen et al., 2011). PA-LOX is an *S*-lipoxygenating enzyme that carries an alanine at the 'Coffa Site' (Ala420). Targeted mutagenesis of this alanine to a lesser space filling glycine revealed partial changes in the enantioselectivity of the enzyme suggesting that PA-LOX adheres to the Ala vs. Gly concept of LOX-

specificity. An Ala420Gly-PA-LOX converted arachidonic acid to 11R-HETE and 15S-HETE in the ratio of about 1.5:1 (Figure 16). A similar 1.5:1 (11R-HETE:15S-HETE) ratio was obtained for the Ala416Gly of human ALOX15B (Coffa and Brash, 2004). Therefore, the S- or R-stereo control in LOXs is a joint contribution of both, the positional specificity and the enantioselectivity of LOXs.

This data indicates that PA-LOX adheres to the Ala-vs.-Gly concept of enantioselectivity. In order to obtain a structural explanation for the altered reaction specificity, we solved the crystal structure of the Ala420Gly mutant (1.8 Å) (Figure 17). The overall 3D-structures of wildtype and mutant PA-LOX were similar. Using the protein tunneling software Caver 3.0 (Kozlikova et al., 2014), a permanent tunnel that connects the protein surface with the catalytic center was detected and this tunnel might function as an intra-protein path for oxygen diffusion. Structural modeling of the enzyme-substrate complex suggested that when dioxygen employs this tunnel for intra-enzyme movement in the wildtype-PA-LOX, it is directed to C15 of the arachidonic acid backbone. However, the Ala420Gly-exchange redirects the intra-enzyme oxygen diffusion by bifurcating the putative oxygen access channel. Removal of the CH_3-group of Ala420 apparently opens a side channel so that atmospheric dioxygen can also reach C11 of arachidonic acid (Figure 18).

In an attempt to completely block arachidonic acid 15-lipoxygenation, amino acids that line the putative oxygen channel (towards C15 of arachidonic acid) were identified. One of them was Ile431, which is localized in the protein in such a way that its side chain narrows the putative oxygen channel for 15-lipoxygenation in wildtype-PA-LOX. We hypothesized that by replacing the Ile431 with a bulkier Phe, we might prevent oxygen molecules from reaching C15 of arachidonic acid during substrate oxygenation and force the oxygen molecules to travel along the new side channel, which was opened by Ala420Gly exchange. If this was the case, the double mutant Ile431Phe+Ala420Gly might strongly favor 11-lipoxygenation and the single mutant Ile431Phe might exhibit a strongly reduced reaction rate. As expected, the single mutant was inactive (residual activity ~0.3 %). However, the double mutant, Ile431Phe+Ala420Gly was also inactive. Since inactive mutants are difficult to interpret, these mutagenesis experiments did not advance our knowledge on the mechanistic basis of the functional alterations induced by Ala420Gly exchange. Additional mutagenesis

studies and crystallographic experiments under high oxygen pressure (oxygen pumping experiments) (Colloc'h et al., 2008) might help to shed light on this topic.

4.4.2.2. Ala420Gly and wildtype follow the antarafacial relationship

For most LOXs identified so far, hydrogen abstraction and oxygen insertion occur from opposite faces of the plane determined by the double bond system of the fatty acid substrate. Thus, these two steps of the LOX reaction follow an antarafacial relationship (Egmond et al., 1973; Kuhn, 2000). Although altered reaction specificity is seen with the Ala420Gly-PA-LOX, the products formed with both wildtype- (13S-HODE) and mutant-PA-LOX (9R- and 13S-HODE) involved the abstraction of pro$S$-hydrogen from C11 of the stereospecifically labeled linoleic acid (Table 12). Thus, during a PA-LOX catalyzed reaction, hydrogen abstraction and oxygen insertion follow the antarafacial paradigm of the LOX reaction. The prokaryotic *Anabaena LOX* also follows the antarafacial relationship. Similar to Ala420Gly-PA-LOX, this enzyme also involves abstraction of the pro$S$-hydrogen from C11 of linoleic acid during the formation of 9R-HODE (Zheng et al., 2008). An exception to this rule is the manganese containing 13R-MnLOX of *Gäumannomyces graminis* and the 9S-MnLOX of *Magnaporthe salvinii,* where hydrogen removal and oxygen insertion occur suprafacially (Hamberg et al., 1998). Experiments with stereospecifically labeled linoleic acid indicated that oxygenation of this substrate by soybean LOX-1, PA-LOX and 13R-MnLOX involves abstraction of the pro$S$-hydrogen from C11 of the linoleic acid. However, the site of oxygen insertion appears to be different. A direct comparison of the active site residues of the 13R-MnLOX and soybean LOX-1 suggested that the benzene ring of Phe337 of 13R-MnLOX (Leu407 in case of PA-LOX) is oriented in such a way that it shields the face of the 12Z double bond (of linoleic acid) which results in a 13R-oxygenation (Figure 34A). Multiple sequence alignment of different LOXs indicate that most iron containing LOXs contain an Ile or Val at this position (Wennman et al., 2012). In case of soybean LOX, the Ile547 at the same position favors a 13S-oxygenation (Figure 34B). Replacement of the Phe337 with an Ile retained the hydrogen abstraction of the 13R-MnLOX but completely flipped its oxidation process from suprafacial to mainly antarafacial resulting in a 13S-oxygenation (Wennman et al., 2012).
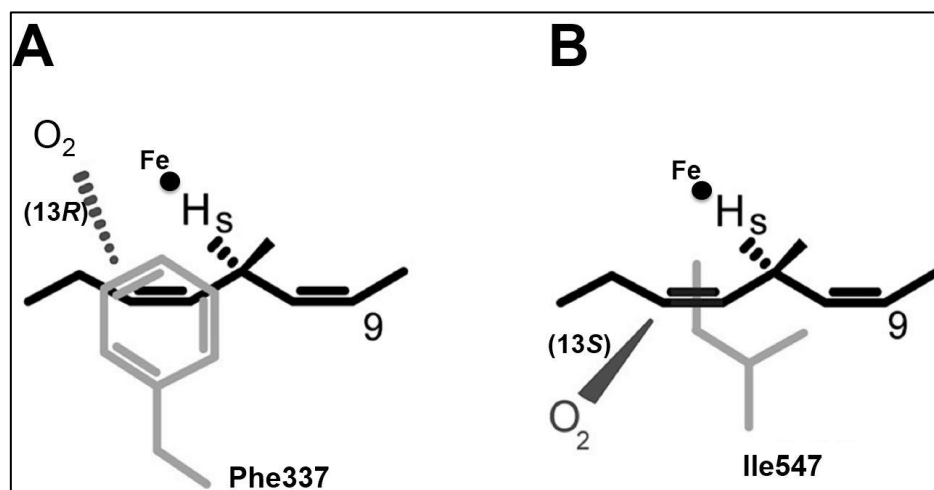
Figure 34: The predicted amino acids contributing towards the suprafacial and antarafacial relationship between hydrogen abstraction and oxygenation in A) 13R-lipoxygenating-Manganese LOX and B) 13S-lipoxygenating Soybean LOX-1 (modified from Wennman et al., 2012).

Thus, the authors concluded that a single amino acid residue controls the direction of oxygenation in the manganese LOXs. However, since the replacement of Phe337Ile opens the oxygen channel directed towards 13*S*-oxygenation, an additional amino acid residue/s must be involved in blocking the oxygen molecules migrating towards 13*R*-oxygenation. The authors' did not identify such residue/s both in the manganese and the soybean LOX-1 that actively blocks oxygen molecules from 13*R*-oxygenation during a dominant 13*S*-lipoxygenation.

The fatty acid in 13*R*-MnLOX is also aligned in the tail first orientation at the active site as in case of PA-LOX. Since 13*R*-MnLOX follows the suprafacial paradigm, the hydrogen abstraction and the oxygen insertion occur on the same plane (iron side) of the fatty acid determined by the double bonds (Figure 34A). However, in case of PA-LOX, hydrogen abstraction and oxygenation occurs antarafacially (as seen with soybean LOX-1 in Figure 34B), on the opposite sides of the fatty acid plane. Therefore, although the fatty acid substrates are aligned in a similar manner in both 13*R*-MnLOX and PA-LOX, oxygen insertions for the two LOXs occur on the opposite sides of the plane of the 1,4-pentadiene moiety.

4.4.2.3. Ala420Gly exchange lowers the catalytic efficiency of PA-LOX

Spectrophotometric analyses at different arachidonic acid concentrations were performed for direct comparison of the kinetics between the wildtype- PA-LOX

and its Ala420Gly-mutant (Table 10). After the Ala420Gly exchange, the Km (arachidonic acid) of the mutant enzyme (67.6 µM) was almost twice as high as that of the wildtype LOX (38.2 µM), indicating that the wildtype enzyme exhibits an almost 2-fold higher affinity for arachidonic acid than the mutant protein. Also, the wildtype-PA-LOX exhibited a 10-fold higher molecular turnover than the mutant-enzyme (21.45 s^{-1} vs. 1.6 s^{-1}). Previous studies have reported that the Ala to Gly exchange in the human ALOX15B, mouse 8S-LOX, coral 8R-LOX and human 12R-LOX resulted in a variable loss in the catalytic activity ranging from almost no impairment of catalytic activity to a ~15-fold drop in activity (Coffa and Brash, 2004). A similar reduction (13-fold) was observed when the Ala420 of our wildtype-PA-LOX was exchanged with Gly. The reason behind such a drop in activity is still unknown. However, one might speculate that substrate alignment at the active site is altered in such a way that the rate-limiting step of the LOX reaction might sterically be hindered. In other words, if the hydrogen to be abstracted is somewhat dislocated from the iron bound hydroxyl, hydrogen abstraction may be impaired. Modeling linoleic acid and arachidonic acid into the active site of both the wildtype- and Ala420Gly-PA-LOX suggested that the bisallylic methylenes (C11 of linoleic acid and C13 of arachidonic acid) were shifted away by 0.6 Å from the iron bound hydroxyl (Figure 17). This might be a plausible explanation for the observed lower catalytic activity of Ala420Gly-PA-LOX.

4.4.2.4. Ala420Gly improves the oxygen affinity of PA-LOX

The molecular basis for the altered reaction specificity induced by Ala-to-Gly exchange has not completely been clarified. From the crystallographic and structural modeling data, we concluded that the Ala420Gly-exchange bifurcated the putative oxygen diffusion channel of PA-LOX (Figure 18). The side chain of the Ala420 in the wildtype-PA-LOX prevents penetration of oxygen molecules to the 11R-position of arachidonic acid, which allows only 15S-lipoxygenation. In Ala420Gly-PA-LOX, this barrier is removed, which enables molecular dioxygen to reach both the C11 and C15 position of the substrate molecule explaining the dual specificity of the mutant enzyme. These structural data were consistent with kinetic measurements indicating that the Ala420Gly mutant exhibited a 2-fold higher oxygen affinity (Km for oxygen 406 µM for wildtype-PA-LOX vs. 235 µM

for Ala420Gly mutant) than the wildtype-PA-LOX (Table 14). These kinetic data are particularly remarkable since the oxygen affinity of both wildtype and mutant PA-LOX were much lower than the corresponding parameters of mammalian LOXs (Table 22).

4.5. Biological relevance of PA-LOX

4.5.1. Lipoxin and leukotriene synthase activity of PA-LOX

In addition to free polyenoic fatty acids, mammalian ALOX15 orthologs, such as rabbit ALOX15 (Bryant et al., 1985; Kuhn et al., 1987) and porcine ALOX15 (Ueda et al., 1987; Yamamoto et al., 1988), are also capable of oxygenating conjugated diene system containing hydroperoxy fatty acids to pro- and anti-inflammatory mediators such as leukotrienes and lipoxins. The ability of PA-LOX to synthesize leukotrienes was determined by quantifying the conjugated trienes formed when PA-LOX was incubated with 15S-H(p)ETE as substrate under anaerobic conditions. Unlike rabbit ALOX15, which was employed as positive control (Bryant et al., 1985), PA-LOX does not display major 14,15-leukotriene synthase activity (Figure 20). Translating into the *in vivo* situation these data suggest that PA-LOX might not contribute to induce a pro-inflammatory response directed against the pathogen. However, when PA-LOX was incubated with 5S-HETE (arachidonic acid oxygenation product of the ALOX5 pathway) and 5S,6S/R-DiHETE (5,6-leukotriene A4 hydrolysis product), it was capable of synthesizing lipoxin isomers, which constitute anti-inflammatory eicosanoids (Figure 20). In other words, PA-LOX might contribute to down-regulation of the host inflammatory reaction against the pathogen. A recent study, however, contradicted these findings (Deschamps et al., 2016). Here the authors reported that the recombinantly expressed PA-LOX does not exhibit any lipoxin synthase activity. This conclusion was made from kinetic *in vitro* incubations at enzymatic concentrations that were sufficient to catalyze free fatty acid oxygenation. In fact, at such low enzyme concentrations we did not detect major lipoxin formation under our experimental conditions either. However, at higher concentrations, substantial amounts of lipoxins could be detected in the incubation mixtures. Thus, taken together, the results of these two independent studies suggest that in principle PA-LOX is capable of catalyzing lipoxin formation from 5S-HETE and 5,6-DiHETE. However, the enzyme concentration must be high enough and 13-

H(p)ODE must be present as LOX activator in the incubation mixture. The biologically more relevant question is whether such high enzyme concentrations are actually reached *in vivo* and whether the amounts of lipoxins formed under *in vivo* conditions are sufficiently high to repress the inflammatory reaction. These questions cannot be answered at the moment.

P. aeruginosa infections frequently occur in cystic fibrosis (CF) and a recent study suggested that eicosanoid class switching during pathogenesis of CF is defective in pediatric CF patients. As a consequence of this defective eicosanoid class switching, the lipoxin A4 / leukotriene B4 ratio is reduced, which counteracts active resolution of inflammation in the lower airways of CF patients. The lipoxin A4 / leukotriene B4 ratio in the bronchoalveolar lavage (BAL) fluid of controls (children without CF undergoing bronchoscopy for clinical reasons) indicated that their eicosanoid balance was strongly in favor of lipoxin A4 rather than leukotriene B4 as seen in CF BAL fluid. The reduced levels of the pro-resolving lipoxins compared to the pro-inflammatory leukotrienes has directly been associated with decreased lung function (Ringholz et al., 2014). Several studies have suggested the application of lipoxin derivatives as a therapeutic strategy to improve the conditions of CF patients. In fact, lipoxin A4 improves the conditions of the lung by repairing epithelial barrier function, by restoring the ion transport and by improving the height of the airway surface liquid layer in bronchial epithelium of CF patients (Verrière et al., 2012). It also reduces the severity of inflammation in this disease (Urbach et al., 2013). These data indicate that in addition to contributing to the evasion strategy of the *P.* aeruginosa, the lipoxin synthase activity of PA-LOX might contribute to silence CF symptoms.

4.5.2. PA-LOX oxygenates complex lipid assemblies

4.5.2.1. Phospholipid and biomembrane oxygenase activity of PA-LOX

Several mammalian ALOX15 orthologs of different species (Kuhn et al., 1990; Kühn et al., 1993; Takahashi et al., 1993; Pekárová et al., 2015) oxygenate esterified polyenoic fatty acids bound to biomembranes and lipoproteins. So far, among the prokaryotic LOXs, *Anabaena* LOX has shown to exhibit the principle capability of oxygenating arachidonic acid containing phosphatidylcholine. However, the membrane oxygenase activity of prokaryotic LOXs has not yet been reported (Zheng et al., 2008). There are several evidences available in the

literature that made us conclude that the secretory PA-LOX might be capable of oxygenating membrane bound phospholipids: 1) The crystal structure of PA-LOX indicated a bifurcated active site, which contained a complete phosphatidylethanolamine molecule. This endogenous lipid ligand was co-purified with the recombinant enzyme during the multi-step purification procedure (Garreta et al., 2013). This data prompted us to conclude that PA-LOX has a high binding affinity for phospholipids. 2) Tryptophan florescence measurement and isothermal calorimetric analysis suggested that PA-LOX is capable of interacting with polyunsaturated fatty acids containing phospholipids (not phospholipids containing the monounsaturated oleic acid). As a matter of fact, when the enzyme was added to phospholipid vesicles, an endothermal peak was observed in isothermal microcalorimeter but the baseline did not return to its initial value. From these results, the authors concluded that PA-LOX is capable of modifying phospholipid vesicles (Garreta et al., 2013). 3) *In vivo* invasiveness analysis indicated that the invasive capacity of PA-LOX expressing *P. aeruginosa* strains was significantly higher when compared with PA-LOX deficient strains (Garreta et al., 2013). This data suggested a possible role of PA-LOX in *P. aeruginosa* infections. However, whether PA-LOX increases infectiousness of the bacteria by directly modifying the host cell membranes or by interfering with the hosts' immune system remains to be elucidated. To test the membrane oxygenase activity of the PA-LOX we applied different analytical methods: 1) We carried out oxygraphic measurements (Figure 24) during the incubation of PA-LOX with biological model membranes (vesicles of mitochondrial inner membrane). Here we observed a clear oxygen consumption suggesting oxygenation of membrane lipids and/or proteins. 2). Using HPLC we detected oxygenated polyenoic fatty acids in the membrane lipids after a 15 min incubation period (Figure 25, Figure 26). More detailed analysis of the reaction products indicated the presence of 13*S*-H(p)ODE and 15*S*-H(p)ETE, which were absent in control incubations without enzyme. It should, however, be stressed that the oxygenase activity of both PA-LOX and rabbit ALOX15 with free polyenoic fatty acids was at least one order of magnitude higher than the membrane oxygenase activities of the two enzymes.

Interestingly, under strictly comparable conditions, rabbit ALOX15 exhibited a higher membrane oxygenase activity than PA-LOX (molecular turnover rates of

7.4 s^{-1} for rabbit ALOX15 vs. 0.3 s^{-1} for PA-LOX) as concluded from oxygraphic measurements (Table 16). This was surprising because the X-ray structure of PA-LOX seems more suitable for oxygenating phospholipids than rabbit ALOX15. While the substrate binding pocket of PA-LOX is big enough to accommodate a complete phospholipid molecule (Garreta et al., 2013), rabbit ALOX15 cannot bind a complete phospholipid without major structural rearrangement (Ivanov et al., 2015).

4.5.2.2. PA-LOX oxygenates intact cells

After having shown that PA-LOX is capable of oxygenating disintegrated model membranes, we were interested to explore if PA-LOX is capable of oxygenating the membranes of intact cells without the preceding activity of any lipid hydrolyzing enzymes. To answer this question, we incubated PA-LOX with intact human erythrocytes *in vitro* and observed strong hemolysis (50 %) indicating decomposition of the erythrocyte membranes (Figure 29). Under strictly comparable conditions the degree of hemolysis induced by a rabbit ALOX15 only varied between 1 to 2 %. Since hemolysis induced by rabbit ALOX15 was even lower than in non-enzymatic control incubations, it was concluded that only PA-LOX oxygenates the membrane lipids, which disrupts the red cells. Lipidomic analysis (Figure 31) of the phospholipid content of the red cell membranes indicated that the levels of polyunsaturated fatty acids containing phospholipids were strongly decreased after incubations of the RBCs with PA-LOX. On the other hand, the levels of monosaturated phospholipids remained unchanged when PA-LOX containing and PA-LOX lacking incubation samples were compared. These data are plausible because all PA-LOX catalyzed reactions require the presence of a bisallylic methylene in the lipid substrates. In addition to the time dependent decrease in PUFA-containing phospholipids, we observed an anti-parallel increase in phospholipids containing 13-HODE, 15-HETE and 15-KETE. Here again, these oxygenated phospholipid species were absent in control incubations without the enzyme. Moreover, we observed a time dependent increase in phospholipid species carrying truncated PUFA derivatives. Such truncated PUFAs have previously been described as products of LOX-catalyzed oxygenation of free PUFAs (McIntyre, 2012). Similar observations were made when PA-LOX was incubated with cultured lung

epithelial cells and these data suggest that the enzyme might be capable of attacking different types of plasma membranes.

When we compared the extent of membrane oxygenase activity with the fatty acid oxygenase activity of PA-LOX *in vitro,* we found that the fatty acid oxygenase activity was more than 2 orders of magnitude higher. However, to explore whether the membrane oxygenase activity we described is of any *in vivo* relevance, direct experimental data quantifying the *in vivo* expression level of the enzyme in *P. aeruginosa* infected patients are required. Currently, there is no information on the local *in vivo* concentration of PA-LOX in any *P. aeruginosa* infection model or in any other human disease. Immunohistochemical staining employing a PA-LOX specific antibody is one way of addressing this question. Moreover, it would be of particular interest to explore whether oxygenated phospholipid can be detected in the erythrocyte membranes of *P. aeruginosa* infected patients. Under the oxidizing conditions in human erythrocytes (oxygen concentrations are more than 2 orders of magnitude higher when compared with other cells; iron concentrations are more than 3 orders of magnitude higher than in other cells) oxygenation of unsaturated membrane lipids frequently occur. Still, the levels of oxidized phospholipids are kept minimal by continuous phospholipid repair processes. However, if membrane lipid oxidation is suddenly upregulated because PA-LOX is present, the repair capacity may be overcome, which would lead to an accumulation of lipid peroxidation products. The presence of such products may alter the plasma membrane properties and such RBCs are rapidly removed from circulation (Fadok et al., 2001). In addition, oxidized phospholipids are also important regulators for toll-like receptor (TLR) signaling. It has been shown that 15-H(p)ETE containing phospholipids may function as agonists of TLR-4 and thus, activate the NF-κB pathway of the immune cells (Man ek-Keber et al., 2015). Thus, during a *P. aeruginosa* infection, PA-LOX induced oxygenation of red cell membrane phospholipids might induce clearance of oxygenated RBC from the blood stream. If this is the case, the average life expectancy of RBC, which is about 110 days in normal humans, might be reduced in *P. aeruginosa* infected-patients. As long as this reduced cellular life span is compensated by higher RBC production in the bone marrow, anemia would not occur. However, at severe *P. aeruginosa* infections, the compensatory capacity of the bone marrow may not be sufficient anymore and then anemia may develop.

In a recent mouse study it has been suggested that the amplified inflammatory response observed during cystic fibrosis may be due to the impaired clearance of phospholipid hydroperoxides (Trudel et al., 2009). Thus, in addition to damaging intact cells, the continuous production of oxidized phospholipids by PA-LOX might worsen the conditions of *P. aeruginosa* infected patients.

In addition to the possible biological functions of PA-LOX discussed above, a recent study implicated PA-LOX in bacterial biofilm formation. In order to mimic an infection setting, the authors cultured *P. aeruginosa* on the surface of lung epithelial cells. They observed a reduction in the bacterial biofilm growth in the absence of PA-LOX when compared with *P. aeruginosa* that expreses LOX. On the other hand, the authors showed that PA-LOX was not required for biofilm formation in an abiotic experimental setup (Deschamps et al., 2016). Unfortunately, the underlying molecular mechanism for this observation has not been elucidated.

Although the membrane oxygenase activity of PA-LOX suggests that the enzyme is capable of destroying red blood cells, it still remains to be proven whether PA-LOX constitutes a virulence factor of *P. aeruginosa*. In fact, for this bacterium a number of other secreted virulence factors (e.g. secreted elastase) have been identified, which allow the bacteria to attack and invade host cells (Bejarano et al., 1989; Lyczak et al., 2000; Ben Haj Khalifa et al., 2011). The principle capacity of secreted PA-LOX to oxidize membrane lipids may make the host cell membrane more permeable for the bacteria, which might favor cell invasion. In this respect, PA-LOX might function as virulence factor, but an *in vivo* proof for this hypothesis is still pending.

P. aeruginosa infections are difficult to treat because this bacterium has developed resistance to a large range of antibiotics (Hurley et al., 2012). Understanding and identifying bacterial virulence factors, which include both the cell associated and extracellular compounds is important in the future for the identification of potent anti-*P. aeruginosa* drugs. In addition to anti-microbial agents that are currently being developed, targeted therapies against PA-LOX might constitute a therapeutic strategy for *P. aeruginosa* infections. Among the inhibitors we tested so far, only nordihydroguaiaretic acid (NDGA) seemed to be effective (IC_{50} = 31.6 µM) against PA-LOX. Thus, identification of PA-LOX specific inhibitors might improve the efficacy of the therapeutic arsenal

continuously being developed against *P. aeruginosa*. The high yield expression system developed in this work provides the possibility for the development of a test hierarchy for effective PA-LOX inhibitors, which can further be developed as anti- *P. aeruginosa* drugs.

5. SUMMARY

LOXs are lipid-peroxidizing enzymes, the biological functions of which have extensively been studied in mammals, plants and lower eukaryotic organisms. The opportunistic pathogen *Pseudomonas aeruginosa* (PA), which causes life-threatening infections in immunocompromised individuals, is among the rare bacterial species, which expresses a secretory lipoxygenase (PA-LOX). Although the enzyme was already discovered in the mid-1960s, its biological relevance has not been explored. The aim of this dissertation was to characterize PA-LOX with respect to its structural and functional properties and to obtain experimental evidence for its biological role. To reach these goals PA-LOX was overexpressed as recombinant His_6-tag fusion protein in *E. coli* and purified to electrophoretic homogeneity by a combination of different chromatographic techniques. A molecular weight of 70 kDA was determined and each enzyme molecule contained 1 iron ion. PA-LOX functions as n-6 fatty acid dioxygenase and exhibits a similar catalytic efficiency with both, arachidonic acid and linoleic acid. The enzyme was crystallized and its 3D-structure (1.48 Å) indicated that the polypeptide chain folds into a single domain. The active site, which contains the non-heme iron, constitutes a bifurcated hydrophobic cavity, which involves a phospholipid molecule as endogenous lipid ligand. Multiple mutagenesis studies indicated that the reaction specificity of PA-LOX does not follow some classical concepts worked out for mammalian LOXs. However, Ala420Gly exchange altered the reaction specificity of the enzyme and the crystal structure of the mutant enzyme (1.8 Å) suggested an altered path of intra-enzyme oxygen diffusion as mechanistic basis for the observed functional changes. In contrast to most mammalian LOX-isoforms, PA-LOX was capable of oxidizing phospholipids to specific oxygenation products even if they were incorporated in biomembranes. Long term (24 h) *in vitro* incubations of PA-LOX with intact erythrocytes caused hemolysis and lipidomic analysis indicated that more than 50 % of the polyenoic fatty acids present in the membrane lipids were oxygenated. It might be speculated that the catalytic activity of the secreted enzyme on the membrane phospholipids of host cells may destabilize the membrane structure allowing the pathogen to enter the cell more easily. In this case the development of PA-LOX specific inhibitors might constitute a novel concept for anti-PA therapy. Moreover, PA-LOX is

capable of converting polyenoic fatty acids to anti-inflammatory and pro-resolving lipoxins. If this catalytic activity is of *in vivo* relevance, the pathogen can down-regulate the immune system of the host, which might be considered as part of an evasion strategy of this particular pathogen.

6. ZUSAMMENFASSUNG

Lipoxygenasen (LOX) sind lipidperoxidierende Enzyme, deren biologische Funktionen in Säugetieren, Pflanzen und niederen Eukaryoten umfassend untersucht wurden. Das Bakterium *Pseudomonas aeruginosa* (PA), welches lebensbedrohliche Infektionen bei Patienten mit geschwächtem Immunsystem hervorruft, gehört zu den seltenen Bakterienspezies, die eine sekretorische LOX (PA-LOX) exprimieren. Obwohl das Enzym bereits in den 1960er Jahren erstmals beschrieben wurde, konnte seine biologische Bedeutung bis heute nicht aufgeklärt werden. Die Ziele der vorliegenden Dissertation bestanden darin, die PA-LOX als rekombinantes Protein zu exprimieren und es hinsichtlich seiner strukturellen und funktionellen Eigenschaften zu charakterisieren. Die rekombinante PA-LOX weist ein Molekulargewicht von 70 kDa auf und jedes Enzymmolekül enthält ein Eisenion. Das Protein fungiert als n-6-Fettsäuredioxygenase und kann Linolsäure, Arachidonsäure und andere Polyenfettsäuren mit hoher Reaktionsrate oxygenieren. Das rekombinante Protein wurde kristallisiert und seine 3D-Struktur (1,48 Å) aufgeklärt. Die Polypeptidkette faltet sich zu einer einzigen Domäne, welche das katalytisch wirksame Nichthämeisen enthält. Das aktive Zentrum der PA-LOX wird von einem gabelförmigen hydrophoben Hohlraum gebildet, der ein Phospholipidmolekül als endogenen Lipidliganden enthält. Multiple Mutageneseuntersuchungen zeigten, dass die Reaktionsspezifität der PA-LOX nicht den klassischen Konzepten folgt, die für Säugetier-LOX ausgearbeitet wurden. Der Austausch von Ala420Gly veränderte die Reaktionsspezifität des Enzyms und die Kristallstruktur der Enzymmutante deutet darauf hin, dass die Diffussion von Sauerstoff innerhalb des Proteins durch die Mutation verändert wurde. Diese strukturelle Veränderung erklärt die beobachtete Modifizierung der Positionsspezifität. Im Gegensatz zu den meisten Säugetierlipoxygenasen ist die PA-LOX in der Lage, Phospholipide zu spezifischen Oxygenierungsprodukten umzuwandeln, selbst wenn diese in Biomembranen eingebaut sind. Langzeitnkubationen (24 h) der rekombinanten PA-LOX mit intakten Erythrozyten führten zur Hämolyse, wobei die Lipidom-Analyse zeigte, dass mehr als 50 % der in den Membranlipiden vorliegenden Polyenfettsäuren oxygeniert waren. Da PA in der Lage ist, eukaryotische Zellen zu infizieren, könnte man

spekulieren, dass die katalytische Aktivität des sezernierten Enzyms die Membranstruktur der Wirtszellen destabilisiert, wodurch das Pathogen leichter in die Zelle gelangen kann. Sollte dieser Mechansimus zutreffen, könnte die Entwicklung von PA-LOX-spezifischen Inhibitoren von großem medizinischen Interesse sein. Darüber hinaus ist PA-LOX in der Lage, Polyenfettsäuren zu entzündungshemmenden Lipoxinen umzuwandeln. Wenn diese katalytische Aktivität auch *in vivo* nachzuweisen wäre, kann das Bakterium das Immunsystem des Wirts herunterregulieren, was als Teil einer Evationsstrategie dieses Erregers angesehen werden kann.

7. BIBLIOGRAPHY

Adams, P. D.; Afonine, P. V.; Bunkóczi, G.; Chen, V. B.; Davis, I. W.; Echols, N.; Headd, J. J.; Hung, L.-W. W.; Kapral, G. J.; Grosse-Kunstleve, R. W.; et al. PHENIX: A Comprehensive Python-Based System for Macromolecular Structure Solution. *Acta Crystallogr. D. Biol. Crystallogr.* **2010**, *66* (Pt 2), 213–221.

Adel, S.; Karst, F.; González-Lafont, À.; Pekárová, M.; Saura, P.; Masgrau, L.; Lluch, J. M.; Stehling, S.; Horn, T.; Kuhn, H.; et al. Evolutionary Alteration of ALOX15 Specificity Optimizes the Biosynthesis of Antiinflammatory and Proresolving Lipoxins. *Proc. Natl. Acad. Sci. U. S. A.* **2016**, *113* (30), E4266-4275.

Alborn, H. T. An Elicitor of Plant Volatiles from Beet Armyworm Oral Secretion. *Science (80-.).* **1997**, *276* (5314), 945–949.

Alvarez-Ortega, C.; Harwood, C. S. Responses of Pseudomonas Aeruginosa to Low Oxygen Indicate That Growth in the Cystic Fibrosis Lung Is by Aerobic Respiration. *Mol. Microbiol.* **2007**, *65* (1), 153–165.

Andre, E.; Hou, K. W. The Presence of a Lipoid Oxidase in Soyabean, Glycine Soya. *Comptes rendus l'Académie des Sci.* **1932**, *194*, 645–647.

Andreou, A.; Vanko, M.; Bezakova, L.; Feussner, I. Properties of a Mini 9R-Lipoxygenase from Nostoc Sp. PCC 7120 and Its Mutant Forms. *Phytochemistry* **2008**, *69* (9), 1832–1837.

Bachmann, A.; Hause, B.; Maucher, H.; Garbe, E.; Vörös, K.; Weichert, H.; Wasternack, C.; Feussner, I. Jasmonate-Induced Lipid Peroxidation in Barley Leaves Initiated by Distinct 13-LOX Forms of Chloroplasts. *Biol. Chem.* **2002**, *383* (10), 1645–1657.

Banthiya, S.; Pekárová, M.; Kuhn, H.; Heydeck, D. Secreted Lipoxygenase from Pseudomonas Aeruginosa Exhibits Biomembrane Oxygenase Activity and Induces Hemolysis in Human Red Blood Cells. *Arch. Biochem. Biophys.* **2015**, *584*, 116–124.

Banthiya, S.; Kalms, J.; Yoga, E. G.; Ivanov, I.; Carpena, X.; Hamberg, M.; Kuhn, H.; Scheerer, P. Structural and Functional Basis of Phospholipid Oxygenase Activity of Bacterial Lipoxygenase from Pseudomonas Aeruginosa. *Biochim. Biophys. Acta - Mol. Cell Biol. Lipids* **2016**, *1861* (11), 1681–1692.

Bateman, A.; Sandford, R. The PLAT Domain: A New Piece in the PKD1 Puzzle. *Curr. Biol.* **1999**, *9* (16), R588-590.

Baysal, T.; Demirdoven, A. Lipoxygenase in Fruits and Vegetables: A Review. *Enzyme Microb. Technol.* **2007**, *40* (4), 491–496.

Bejarano, P. A.; Langeveld, J. P.; Hudson, B. G.; Noelken, M. E. Degradation of Basement Membranes by Pseudomonas Aeruginosa Elastase. *Infect. Immun.* **1989**, *57* (12), 3783–3787.

Le Bel, M.; Brunet, A.; Gosselin, J. Leukotriene B4, an Endogenous Stimulator of the Innate Immune Response against Pathogens. *J. Innate Immun.* **2014**, *6* (2), 159–168.

Belkner, J.; Wiesner, R.; Kühn, H.; Lankin, V. Z. The Oxygenation of Cholesterol Esters by the Reticulocyte Lipoxygenase. *FEBS Lett.* **1991**, *279* (1), 110–114.

Beloin, C.; Roux, A.; Ghigo, J. M. Escherichia Coli Biofilms. *Curr. Top. Microbiol. Immunol.* **2008**, *322*, 249–289.

Berman, H. M.; Westbrook, J.; Feng, Z.; Gilliland, G.; Bhat, T. N.; Weissig, H.; Shindyalov, I. N.; Bourne, P. E. The Protein Data Bank. *Nucleic Acids Res.* **2000**,

28 (1), 235–242.

Bligh, E. G.; Dyer, W. J. A Rapid Method of Total Lipid Extraction and Purification. *Can. J. Biochem. Physiol.* **1959**, *37* (8), 911–917.

Boeglin, W. E.; Kim, R. B.; Brash, A. R. A 12R-Lipoxygenase in Human Skin: Mechanistic Evidence, Molecular Cloning, and Expression. *Proc. Natl. Acad. Sci. U. S. A.* **1998**, *95* (12), 6744–6749.

Borbulevych, O. Y.; Jankun, J.; Selman, S. H.; Skrzypczak-Jankun, E. Lipoxygenase Interactions with Natural Flavonoid, Quercetin, Reveal a Complex with Protocatechuic Acid in Its X-Ray Structure at 2.1 Å Resolution. *Proteins Struct. Funct. Bioinforma.* **2003**, *54* (1), 13–19.

Borgeat, P.; Hamberg, M.; Samuelsson, B. Transformation of Arachidonic Acid and Homo-Gamma-Linolenic Acid by Rabbit Polymorphonuclear Leukocytes. Monohydroxy Acids from Novel Lipoxygenases. *J. Biol. Chem.* **1976**, *251* (24), 7816–7820.

Borngräber, S.; Kuban, R.-J.; Anton, M.; Kühn, H. Phenylalanine 353 Is a Primary Determinant for the Positional Specificity of Mammalian 15-Lipoxygenases. *J. Mol. Biol.* **1996**, *264* (5), 1145–1153.

Borngräber, S.; Grabenhorst, E.; Anton, M.; Conradt, H.; Kühn, H. Intra- and Extracellular Expression of Rabbit Reticulocyte 15-Lipoxygenase in the Baculovirus/insect Cell System. *Protein Expr. Purif.* **1998**, *14* (2), 237–246.

Borngräber, S.; Browner, M.; Gillmor, S.; Gerth, C.; Anton, M.; Fletterick, R.; Kühn, H. Shape and Specificity in Mammalian 15-Lipoxygenase Active Site. The Functional Interplay of Sequence Determinants for the Reaction Specificity. *J. Biol. Chem.* **1999**, *274* (52), 37345–37350.

Boyington, J. C.; Gaffney, B. J.; Amzel, L. M. The Three-Dimensional Structure of an Arachidonic Acid 15-Lipoxygenase. *Science* **1993**, *260* (5113), 1482–1486.

Bradford, M. M. A Rapid and Sensitive Method for the Quantitation of Microgram Quantities of Protein Utilizing the Principle of Protein-Dye Binding. *Anal. Biochem.* **1976**, *72* (1–2), 248–254.

Brash, A. R. Lipoxygenases: Occurrence, Functions, Catalysis, and Acquisition of Substrate. *J. Biol. Chem.* **1999**, *274* (34), 23679–23682.

Brash, A. R.; Ingram, C. D.; Harris, T. M. Analysis of a Specific Oxygenation Reaction of Soybean Lipoxygenase-1 with Fatty Acids Esterified in Phospholipids. *Biochemistry* **1987**, *26* (17), 5465–5471.

Brash, A. R.; Yokoyama, C.; Oates, J. A.; Yamamoto, S. Mechanistic Studies of the Dioxygenase and Leukotriene Synthase Activities of the Porcine Leukocyte 12S-Lipoxygenase. *Arch. Biochem. Biophys.* **1989**, *273* (2), 414–422.

Brash, A. R.; Hughes, M. A.; Hawkins, D. J.; Boeglin, W. E.; Song, W. C.; Meijer, L. Allene Oxide and Aldehyde Biosynthesis in Starfish Oocytes. *J. Biol. Chem.* **1991**, *266* (34), 22926–22931.

Brash, A. R.; Boeglin, W. E.; Chang, M. S.; Shieh, B. H. Purification and Molecular Cloning of an 8R-Lipoxygenase from the Coral Plexaura Homomalla Reveal the Related Primary Structures of R- and S- Lipoxygenases. *J. Biol. Chem.* **1996**, *271* (34), 20949–20957.

Brash, A. R.; Boeglin, W. E.; Chang, M. S. Discovery of a Second 15S-Lipoxygenase in Humans. *Proc. Natl. Acad. Sci. U. S. A.* **1997**, *94* (12), 6148–6152.

Brash, A. R.; Schneider, C.; Hamberg, M. Applications of Stereospecifically-Labeled Fatty Acids in Oxygenase and Desaturase Biochemistry. *Lipids* **2012**, *47* (2), 101–

116.

Brünger, A. T. Free R Value: A Novel Statistical Quantity for Assessing the Accuracy of Crystal Structures. *Nature* **1992**, *355* (6359), 472–475.

Bryant, R. W.; Bailey, J. M.; Schewe, T.; Rapoport, S. M. Positional Specificity of a Reticulocyte Lipoxygenase. Conversion of Arachidonic Acid to 15-S-Hydroperoxy-Eicosatetraenoic Acid. *J. Biol. Chem.* **1982**, *257* (11), 6050–6055.

Bryant, R. W.; Schewe, T.; Rapoport, S. M.; Bailey, J. M. Leukotriene Formation by a Purified Reticulocyte Lipoxygenase Enzyme. Conversion of Arachidonic Acid and 15-Hydroperoxyeicosatetraenoic Acid to 14,15-Leukotriene A4. *J. Biol. Chem.* **1985**, *260* (6), 3548–3555.

Burow, G. B.; Gardner, H. W.; Keller, N. P. A Peanut Seed Lipoxygenase Responsive to Aspergillus Colonization. *Plant Mol. Biol.* **2000**, *42* (5), 689–701.

Burrall, B. A.; Cheung, M.; Chiu, A.; Goetzl, E. J. Enzymatic Properties of the 15-Lipoxygenase of Human Cultured Keratinocytes. *J. Invest. Dermatol.* **1988**, *91* (4), 294–297.

Busquets, M.; Deroncele, V.; Vidal-Mas, J.; Rodriguez, E.; Guerrero, A.; Manresa, A. Isolation and Characterization of a Lipoxygenase from Pseudomonas 42A2 Responsible for the Biotransformation of Oleic Acid into (S)-(E)-10-Hydroxy-8-Octadecenoic Acid. *Antonie van Leeuwenhoek, Int. J. Gen. Mol. Microbiol.* **2004**, *85* (2), 129–139.

Chen, X. S.; Brash, A. R.; Funk, C. D. Purification and Characterization of Recombinant Histidine-Tagged Human Platelet 12-Lipoxygenase Expressed in a Baculovirus/insect Cell System. *Eur. J. Biochem.* **1993**, *214* (3), 845–852.

Chen, X. S.; Naumann, T. A.; Kurre, U.; Jenkins, N. A.; Copeland, N. G.; Funk, C. D. cDNA Cloning, Expression, Mutagenesis, Intracellular Localization, and Gene Chromosomal Assignment of Mouse 5-Lipoxygenase. *J. Biol. Chem.* **1995**, *270* (30), 17993–17999.

Chen, Y.; Wennman, A.; Karkehabadi, S.; Engström, Å.; Oliw, E. H. Crystal Structure of Linoleate 13R-Manganese Lipoxygenase in Complex with an Adhesion Protein. *J. Lipid Res.* **2016**, *57* (8), 1574–1588.

Choi, J.; Chon, J. K.; Kim, S.; Shin, W. Conformational Flexibility in Mammalian 15S-Lipoxygenase: Reinterpretation of the Crystallographic Data. *Proteins* **2008**, *70* (3), 1023–1032.

Chovancova, E.; Pavelka, A.; Benes, P.; Strnad, O.; Brezovsky, J.; Kozlikova, B.; Gora, A.; Sustr, V.; Klvana, M.; Medek, P.; et al. CAVER 3.0: A Tool for the Analysis of Transport Pathways in Dynamic Protein Structures. *PLoS Comput. Biol.* **2012**, *8* (10), e1002708.

Cobanoğlu, B.; Toskala, E.; Ural, A.; Cingi, C. Role of Leukotriene Antagonists and Antihistamines in the Treatment of Allergic Rhinitis. *Curr. Allergy Asthma Rep.* **2013**, *13* (2), 203–208.

Coffa, G.; Hill, E. M. Discovery of an 11 (R)- and 12(S)-Lipoxygenase Activity in Ovaries of the Mussel Mytilus Edulis. *Lipids* **2000**, *35* (11), 1195–1204.

Coffa, G.; Brash, A. R. A Single Active Site Residue Directs Oxygenation Stereospecificity in Lipoxygenases: Stereocontrol Is Linked to the Position of Oxygenation. *Proc. Natl. Acad. Sci. U. S. A.* **2004**, *101* (44), 15579–15584.

Coffa, G.; Schneider, C.; Brash, A. R. A Comprehensive Model of Positional and Stereo Control in Lipoxygenases. *Biochem. Biophys. Res. Commun.* **2005a**, *338* (1), 87–92.

Coffa, G.; Imber, A. N.; Maguire, B. C.; Laxmikanthan, G.; Schneider, C.; Gaffney, B. J.; Brash, A. R. On the Relationships of Substrate Orientation, Hydrogen Abstraction, and Product Stereochemistry in Single and Double Dioxygenations by Soybean Lipoxygenase-1 and Its Ala542Gly Mutant. *J. Biol. Chem.* **2005b**, *280* (46), 38756–38766.

Cohen, Y.; Gurevitz, M. The Cyanobacteria—ecology, Physiology and Molecular Genetics. *The Prokaryotes* **2006**, *4*, 1074–1098.

Cole, B. K.; Lieb, D. C.; Dobrian, A. D.; Nadler, J. L. 12- and 15-Lipoxygenases in Adipose Tissue Inflammation. *Prostaglandins Other Lipid Mediat.* **2013**, *104–105*, 84–92.

Collaborative Computational Project, N. 4. The CCP4 Suite: Programs for Protein Crystallography. *Acta Crystallogr. Sect. D Biol. Crystallogr.* **1994**, *50* (5), 760–763.

Colloc'h, N.; Gabison, L.; Monard, G.; Altarsha, M.; Chiadmi, M.; Marassio, G.; Sopkova-de Oliveira Santos, J.; El Hajji, M.; Castro, B.; Abraini, J. H.; et al. Oxygen Pressurized X-Ray Crystallography: Probing the Dioxygen Binding Site in Cofactorless Urate Oxidase and Implications for Its Catalytic Mechanism. *Biophys. J.* **2008**, *95* (5), 2415–2422.

Corey, E.; Lansbury, P. J. Stereochemical Course of 5-Lipoxygenation of Arachidonate by Rat Basophil Leukemic Cell (RBL-1) and Potato Enzymes. *J. Am. Chem. Soc.* **1983**, *105* (12), 4093–4094.

Coste, T. C.; Armand, M.; Lebacq, J.; Lebecque, P.; Wallemacq, P.; Leal, T. An Overview of Monitoring and Supplementation of Omega 3 Fatty Acids in Cystic Fibrosis. *Clin. Biochem.* **2007**, *40* (8), 511–520.

Crane, F.; Glenn, J.; Green, D. Studies on the Electron Transfer System IV. The Electron Transfer Particle. *Biochim. Biophys. Acta* **1956**, *22* (3), 475–487.

Das, U. N. Essential Fatty Acids: Biochemistry, Physiology and Pathology. *Biotechnol. J.* **2006**, *1* (4), 420–439.

Davis, I. W.; Leaver-Fay, A.; Chen, V. B.; Block, J. N.; Kapral, G. J.; Wang, X.; Murray, L. W.; Arendall, W. B.; Snoeyink, J.; Richardson, J. S.; et al. MolProbity: All-Atom Contacts and Structure Validation for Proteins and Nucleic Acids. *Nucleic Acids Res.* **2007**, *35* (Web Server issue), W375-383.

Dennis, E. A.; Norris, P. C. Eicosanoid Storm in Infection and Inflammation. *Nat. Rev. Immunol.* **2015**, *15* (8), 511–523.

Deschamps, J. D.; Ogunsola, A. F.; Jameson, J. B.; Yasgar, A.; Flitter, B. A.; Freedman, C. J.; Melvin, J. A.; Nguyen, J. V. M. H.; Maloney, D. J.; Jadhav, A.; et al. Biochemical and Cellular Characterization and Inhibitor Discovery of Pseudomonas Aeruginosa 15-Lipoxygenase. *Biochemistry* **2016**, *55* (23), 3329–3340.

Dubois, R. N.; Abramson, S. B.; Crofford, L.; Gupta, R. A.; Simon, L. S.; Van De Putte, L. B.; Lipsky, P. E. Cyclooxygenase in Biology and Disease. *FASEB J.* **1998**, *12* (12), 1063–1073.

Eek, P.; Jarving, R.; Jarving, I.; Gilbert, N. C.; Newcomer, M. E.; Samel, N. Structure of a Calcium-Dependent 11R-Lipoxygenase Suggests a Mechanism for Ca2+ Regulation. *J. Biol. Chem.* **2012**, *287* (26), 22377–22386.

Egmond, M. R.; Vliegenthart, J. F.; Boldingh, J. Stereospecificity of the Hydrogen Abstraction at Carbon Atom N-8 in the Oxygenation of Linoleic Acid by Lipoxygenases from Corn Germs and Soya Beans. *Biochem. Biophys. Res. Commun.* **1972**, *48* (5), 1055–1060.

Egmond, M. R.; Veldink, G. A.; Vliegenthart, J. F.; Boldingh, J. C-11 H-Abstraction from Linoleic Acid, the Rate-Limiting Step in Lipoxygenase Catalysis. *Biochem. Biophys. Res. Commun.* **1973**, *54* (3), 1178–1184.

Egmond, M. R.; Brunori, M.; Fasella, P. M. The Steady-State Kinetics of the Oxygenation of Linoleic Acid Catalysed by Soybean Lipoxygenase. *Eur. J. Biochem.* **1976**, *61* (1), 93–100.

Emsley, P.; Cowtan, K. Coot: Model-Building Tools for Molecular Graphics. *Acta Crystallogr. D. Biol. Crystallogr.* **2004**, *60* (Pt 12 Pt 1), 2126–2132.

Emsley, P.; Lohkamp, B.; Scott, W. G.; Cowtan, K. Features and Development of Coot. *Acta Crystallogr. D. Biol. Crystallogr.* **2010**, *66* (Pt 4), 486–501.

Epp, N.; Fürstenberger, G.; Müller, K.; de Juanes, S.; Leitges, M.; Hausser, I.; Thieme, F.; Liebisch, G.; Schmitz, G.; Krieg, P. 12R-Lipoxygenase Deficiency Disrupts Epidermal Barrier Function. *J. Cell Biol.* **2007**, *177* (1), 173–182.

Ereso, A. Q.; Cureton, E. L.; Cripps, M. W.; Sadjadi, J.; Dua, M. M.; Curran, B.; Victorino, G. P. Lipoxin A4 Attenuates Microvascular Fluid Leak during Inflammation. *J. Surg. Res.* **2009**, *156* (2), 183–188.

Eskin, N. A.; Grossman, S.; Pinsky, A. Biochemistry of Lipoxygenase in Relation to Food Quality. *CRC Crit. Rev. Food Sci. Nutr.* **1977**, *9* (1), 1–40.

Evans, P. Scaling and Assessment of Data Quality. *Acta Crystallogr. D. Biol. Crystallogr.* **2006**, *62* (Pt 1), 72–82.

Fadok, V. A.; de Cathelineau A; Daleke, D. L.; Henson, P. M.; Bratton, D. L. Loss of Phospholipid Asymmetry and Surface Exposure of Phosphatidylserine Is Required for Phagocytosis of Apoptotic Cells by Macrophages and Fibroblasts. *J. Biol. Chem.* **2001**, *276* (2), 1071–1077.

Fischer, A. M.; Dubbs, W. E.; Baker, R. A.; Fuller, M. A.; Stephenson, L. C.; Grimes, H. D. Protein Dynamics, Activity and Cellular Localization of Soybean Lipoxygenases Indicate Distinct Functional Roles for Individual Isoforms. *Plant J.* **1999**, *19* (5), 543–554.

Freedman, S. D.; Katz, M. H.; Parker, E. M.; Laposata, M.; Urman, M. Y.; Alvarez, J. G. A Membrane Lipid Imbalance Plays a Role in the Phenotypic Expression of Cystic Fibrosis in Cftr-/- Mice. *Proc. Natl. Acad. Sci.* **1999**, *96* (24), 13995–14000.

Freire-Moar, J.; Alavi-Nassab, A.; Ng, M.; Mulkins, M.; Sigal, E. Cloning and Characterization of a Murine Macrophage Lipoxygenase. *Biochim. Biophys. Acta* **1995**, *1254* (1), 112–116.

Funk, C. D.; Hoshiko, S.; Matsumoto, T.; Rdmark, O.; Samuelsson, B. Characterization of the Human 5-Lipoxygenase Gene. *Proc. Natl. Acad. Sci. U. S. A.* **1989**, *86* (8), 2587–2591.

Funk, C. D.; Furci, L.; FitzGerald, G. A. Molecular Cloning, Primary Structure, and Expression of the Human Platelet/erythroleukemia Cell 12-Lipoxygenase. *Proc. Natl. Acad. Sci. U. S. A.* **1990a**, *87* (15), 5638–5642.

Funk, C. D.; Chen, X. S.; Johnson, E. N.; Zhao, L. Lipoxygenase Genes and Their Targeted Disruption. *Prostaglandins Other Lipid Mediat.* **2002**, *68–69*, 303–312.

Funk, M. O.; Carroll, R. T.; Thompson, J. F.; Sands, R. H.; Dunham, W. R. Role of Iron in Lipoxygenase Catalysis. *J. Am. Chem. Soc.* **1990b**, *112* (13), 5375–5376.

Gabadinho, J.; Beteva, A.; Guijarro, M.; Rey-Bakaikoa, V.; Spruce, D.; Bowler, M. W.; Brockhauser, S.; Flot, D.; Gordon, E. J.; Hall, D. R.; et al. MxCuBE: A Synchrotron Beamline Control Environment Customized for Macromolecular Crystallography Experiments. *J. Synchrotron Radiat.* **2010**, *17* (5), 700–707.

Gane, J.; Buckley, R. Leukotriene Receptor Antagonists in Allergic Eye Disease: A Systematic Review and Meta-Analysis. *J. allergy Clin. Immunol. Pract.* **2013**, *1* (1), 65–74.

Garreta, A.; Carpena, X.; Busquets, M. Crystallization of the Lipoxygenase of Pseudomonas Aeruginosa 42A2 , Evolution and Phylogenetic Study of the Subfamilies of the Lipoxygenases. *Recent Adv. Pharm. Sci. (Cap. 11)* **2011**, *661* (2), 247–273.

Garreta, A.; Val-Moraes, S. P.; Garcia-Fernandez, Q.; Busquets, M.; Juan, C.; Oliver, A.; Ortiz, A.; Gaffney, B. J.; Fita, I.; Manresa, A.; et al. Structure and Interaction with Phospholipids of a Prokaryotic Lipoxygenase from Pseudomonas Aeruginosa. *FASEB J.* **2013**, *27* (12), 4811–4821.

Gellatly, S. L.; Hancock, R. E. W. Pseudomonas Aeruginosa: New Insights into Pathogenesis and Host Defenses. *Pathog. Dis.* **2013**, *67* (3), 159–173.

Gilbert, N. C.; Bartlett, S. G.; Waight, M. T.; Neau, D. B.; Boeglin, W. E.; Brash, A. R.; Newcomer, M. E. The Structure of Human 5-Lipoxygenase. *Science (80-.).* **2011**, *331* (6014), 217–219.

Gilbert, N. C.; Rui, Z.; Neau, D. B.; Waight, M. T.; Bartlett, S. G.; Boeglin, W. E.; Brash, A. R.; Newcomer, M. E. Conversion of Human 5-Lipoxygenase to a 15-Lipoxygenase by a Point Mutation to Mimic Phosphorylation at Serine-663. *FASEB J.* **2012**, *26* (8), 3222–3229.

Gillmor, S. A.; Villaseñor, A.; Fletterick, R.; Sigal, E.; Browner, M. F. The Structure of Mammalian 15-Lipoxygenase Reveals Similarity to the Lipases and the Determinants of Substrate Specificity. *Nat. Struct. Biol.* **1997**, *4* (12), 1003–1009.

Grechkin, A. Recent Developments in Biochemistry of the Plant Lipoxygenase Pathway. *Prog. Lipid Res.* **1998**, *37* (5), 317–352.

Griffiths, A.; Barry, C.; Alpuche-Solis, A. G.; Grierson, D. Ethylene and Developmental Signals Regulate Expression of Lipoxygenase Genes during Tomato Fruit Ripening. *J. Exp. Bot.* **1999**, *50* (335), 793–798.

Guerrero, A.; Casals, I.; Busquets, M.; Leon, Y.; Manresa, A. Oxydation of Oleic Acid to (E)-10-Hydroperoxy-8-Octadecenoic and (E)-10-Hydroxy-8-Octadecenoic Acids by Pseudomonas Sp. 42A2. *Biochim. Biophys. Acta* **1997**, *1347* (1), 75–81.

Gupta, S.; Srivastava, M.; Ahmad, N.; Sakamoto, K.; Bostwick, D. G.; Mukhtar, H. Lipoxygenase-5 Is Overexpressed in Prostate Adenocarcinoma. *Cancer* **2001**, *91* (4), 737–743.

Haas, U.; Raschperger, E.; Hamberg, M.; Samuelsson, B.; Tryggvason, K.; Haeggström, J. Z. Targeted Knock-down of a Structurally Atypical Zebrafish 12S-Lipoxygenase Leads to Severe Impairment of Embryonic Development. *Proc. Natl. Acad. Sci. U. S. A.* **2011**, *108* (51), 20479–20484.

Hada, T.; Ueda, N.; Takahashi, Y.; Yamamoto, S. Catalytic Properties of Human Platelet 12-Lipoxygenase as Compared with the Enzymes of Other Origins. *Biochim. Biophys. Acta - Lipids Lipid Metab.* **1991**, *1083* (1), 89–93.

Hada, T.; Swift, L. L.; Brash, A. R. Discovery of 5R-Lipoxygenase Activity in Oocytes of the Surf Clam, Spisula Solidissima. *Biochim. Biophys. Acta - Lipids Lipid Metab.* **1997**, *1346* (2), 109–119.

Haeggström, J. Z.; Funk, C. D. Lipoxygenase and Leukotriene Pathways: Biochemistry, Biology, and Roles in Disease. *Chem. Rev.* **2011**, *111* (10), 5866–5898.

Ben Haj Khalifa, A.; Moissenet, D.; Vu Thien, H.; Khedher, M. Virulence Factors in Pseudomonas Aeruginosa: Mechanisms and Modes of Regulation. *Ann. Biol. Clin.*

(Paris). **2011**, *69* (4), 393–403.

Hamberg, M. Steric Analysis of Hydroperoxides Formed by Lipoxygenase Oxygenation of Linoleic Acid. *Anal. Biochem.* **1971**, *43* (2), 515–526.

Hamberg, M. Stereochemistry of Oxygenation of Linoleic Acid Catalyzed by Prostaglandin – Endoperoxide H Synthase-2. *Lipids* **1998**, *46* (2), 201–206.

Hamberg, M. Stereochemistry of Hydrogen Removal During Oxygenation of Linoleic Acid by Singlet Oxygen and Synthesis of 11(S)-Deuterium-Labeled Linoleic Acid. *Lipids* **2011**, *46* (2), 201–206.

Hamberg, M.; Samuelsson, B. On the Specificity of the Oxygenation of Unsaturated Fatty Acids Catalyzed by Soybean Lipoxidase. *J. Biol. Chem.* **1967a**, *242* (22), 5329–5335.

Hamberg, M.; Samuelsson, B. Oxygenation of Unsaturated Fatty Acids by the Vesicular Gland of Sheep. *J. Biol. Chem.* **1967b**, *242* (22), 5344–5354.

Hamberg, M.; Samuelsson, B. Prostaglandin Endoperoxides. Novel Transformations of Arachidonic Acid in Human Platelets. *Proc. Natl. Acad. Sci. U. S. A.* **1974**, *71* (9), 3400–3404.

Hamberg, M.; Hamberg, G. On the Mechanism of the Oxygenation of Arachidonic Acid by Human Platelet Lipoxygenase. *Biochem. Biophys. Res. Commun.* **1980**, *95* (3), 1090–1097.

Hamberg, M.; Su, C.; Oliw, E. Manganese Lipoxygenase. Discovery of a Bis-Allylic Hydroperoxide as Product and Intermediate in a Lipoxygenase Reaction. *J. Biol. Chem.* **1998**, *273* (21), 13080–13088.

Hammerström, S.; Samuelsson, B. Detection of Leukotriene A4 as an Intermediate in the Biosynthesis of Leukotrienes C4 and D4. *FEBS Lett.* **1980**, *122* (1), 83–86.

Hansen, J.; Garreta, A.; Benincasa, M.; Fusté, M. C.; Busquets, M.; Manresa, A. Bacterial Lipoxygenases, a New Subfamily of Enzymes? A Phylogenetic Approach. *Appl. Microbiol. Biotechnol.* **2013**, *97* (11), 4737–4747.

Harel, Z. Cyclooxygenase-2 Specific Inhibitors in the Treatment of Dysmenorrhea. *J. Pediatr. Adolesc. Gynecol.* **2004**, *17* (2), 75–79.

Hawkins, D. J.; Brash, A. R. Eggs of the Sea Urchin, Strongylocentrotus Purpuratus, Contain a Prominent (11R) and (12R) Lipoxygenase Activity. *J. Biol. Chem.* **1987**, *262* (16), 7629–7634.

Hicks, A.; Monkarsh, S. P.; Hoffman, A. F.; Goodnow, R. Leukotriene B4 Receptor Antagonists as Therapeutics for Inflammatory Disease: Preclinical and Clinical Developments. *Expert Opin. Investig. Drugs* **2007**, *16* (12), 1909–1920.

Hoff, H. F.; O'Neil, J.; Wu, Z.; Hoppe, G.; Salomon, R. L. Phospholipid Hydroxyalkenals: Biological and Chemical Properties of Specific Oxidized Lipids Present in Atherosclerotic Lesions. *Arterioscler. Thromb. Vasc. Biol.* **2003**, *23* (2), 275–282.

Hooft, R. W. W.; Vriend, G.; Sander, C.; Abola, E. E. Errors in Protein Structures. *Nature.* 1996, pp 272–272.

Horn, T.; Adel, S.; Schumann, R.; Sur, S.; Kakularam, K. R.; Polamarasetty, A.; Redanna, P.; Kuhn, H.; Heydeck, D. Evolutionary Aspects of Lipoxygenases and Genetic Diversity of Human Leukotriene Signaling. *Prog. Lipid Res.* **2015**, *57*, 13–39.

Hu, S.; Sharma, S. C.; Scouras, A. D.; Soudackov, A. V; Carr, C. A. M.; Hammes-Schiffer, S.; Alber, T.; Klinman, J. P. Extremely Elevated Room-Temperature Kinetic Isotope Effects Quantify the Critical Role of Barrier Width in Enzymatic C-H Activation. *J. Am. Chem. Soc.* **2014**, *136* (23), 8157–8160.

Hurley, M. N.; Cámara, M.; Smyth, A. R. Novel Approaches to the Treatment of Pseudomonas Aeruginosa Infections in Cystic Fibrosis. *Eur. Respir. J.* **2012**, *40* (4), 1014–1023.

Incardona, M.-F. F.; Bourenkov, G. P.; Levik, K.; Pieritz, R. A.; Popov, A. N.; Svensson, O. EDNA: A Framework for Plugin-Based Applications Applied to X-Ray Experiment Online Data Analysis. *J. Synchrotron Radiat.* **2009**, *16* (6), 872–879.

Iny, D.; Pinsky, A.; Cojocoru, M.; Grossman, S. Lipoxygenase of Thermoactinomyces Vulgaris, Purification and Characterization of Reaction Products. *Int. J. Biochem.* **1993**, *25* (9), 1313–1323.

Ivanov, I.; Heydeck, D.; Hofheinz, K.; Roffeis, J.; O'Donnell, V. B.; Kuhn, H.; Walther, M. Molecular Enzymology of Lipoxygenases. *Arch. Biochem. Biophys.* **2010**, *503* (2), 161–174.

Ivanov, I.; Kuhn, H.; Heydeck, D. Structural and Functional Biology of Arachidonic Acid 15-Lipoxygenase-1 (ALOX15). *Gene* **2015**, *573* (1), 1–32.

Jansen, C.; Hofheinz, K.; Vogel, R.; Roffeis, J.; Anton, M.; Reddanna, P.; Kuhn, H.; Walther, M. Stereocontrol of Arachidonic Acid Oxygenation by Vertebrate Lipoxygenases: Newly Cloned Zebrafish Lipoxygenase 1 Does Not Follow the Ala-versus-Gly Concept. *J. Biol. Chem.* **2011**, *286* (43), 37804–37812.

Jisaka, M.; Kim, R. B.; Boeglin, W. E.; Nanney, L. B.; Brash, A. R. Molecular Cloning and Functional Expression of a Phorbol Ester-Inducible 8S-Lipoxygenase from Mouse Skin. *J. Biol. Chem.* **1997**, *272* (39), 24410–24416.

Jisaka, M.; Kim, R. B.; Boeglin, W. E.; Brash, A. R. Identification of Amino Acid Determinants of the Positional Specificity of Mouse 8S-Lipoxygenase and Human 15S-Lipoxygenase-2. *J. Biol. Chem.* **2000**, *275* (2), 1287–1293.

Juránek, I.; Suzuki, H.; Yamamoto, S. Affinities of Various Mammalian Arachidonate Lipoxygenases and Cyclooxygenases for Molecular Oxygen as Substrate. *Biochim. Biophys. Acta - Mol. Cell Biol. Lipids* **1999**, *1436* (3), 509–518.

Kabsch, W. Xds. *Acta Crystallogr. Sect. D Biol. Crystallogr.* **2010**, *66* (2), 125–132.

Kalms, J.; Banthiya, S.; Yoga, E. G.; Hamberg, M.; Holzhutter, H.-G.; Kuhn, H.; Scheerer, P. The Crystal Structure of Pseudomonas Aeruginosa Lipoxygenase Ala420Gly Mutant Explains the Improved Oxygen Affinity and the Altered Reaction Specificity. *Biochim. Biophys. Acta - Mol. Cell Biol. Lipids* **2017**.

Kandouz, M.; Nie, D.; Pidgeon, G. P.; Krishnamoorthy, S.; Maddipati, K. R.; Honn, K. V. Platelet-Type 12-Lipoxygenase Activates NF-kappaB in Prostate Cancer Cells. *Prostaglandins Other Lipid Mediat.* **2003**, *71* (3–4), 189–204.

El Kebir, D.; Filep, J. G. Modulation of Neutrophil Apoptosis and the Resolution of Inflammation through β2 Integrins. *Front. Immunol.* **2013**, *4*, 60.

Kelavkar, U. P.; Nixon, J. B.; Cohen, C.; Dillehay, D.; Eling, T. E.; Badr, K. F. Overexpression of 15-Lipoxygenase-1 in PC-3 Human Prostate Cancer Cells Increases Tumorigenesis. *Carcinogenesis* **2001**, *22* (11), 1765–1773.

Kelavkar, U. P.; Parwani, A. V; Shappell, S. B.; Martin, W. D. Conditional Expression of Human 15-Lipoxygenase-1 in Mouse Prostate Induces Prostatic Intraepithelial Neoplasia: The FLiMP Mouse Model. *Neoplasia* **2006**, *8* (6), 510–522.

Kinzig, A.; Fürstenberger, G.; Bürger, F.; Vogel, S.; Müller-Decker, K.; Mincheva, A.; Lichter, P.; Marks, F.; Krieg, P. Murine Epidermal Lipoxygenase (Aloxe) Encodes a 12-Lipoxygenase Isoform. *FEBS Lett.* **1997**, *402* (2–3), 162–166.

Kirkland, T. N.; Finley, F.; Orsborn, K. I.; Galgiani, J. N. Evaluation of the Proline-Rich Antigen of Coccidioides Immitis as a Vaccine Candidate in Mice. *Infect. Immun.*

1998, *66* (8), 3519–3522.

Knapp, M. J.; Seebeck, F. P.; Klinman, J. P. Steric Control of Oxygenation Regiochemistry in Soybean Lipoxygenase-1. *J. Am. Chem. Soc.* **2001**, *123* (12), 2931–2932.

Kobe, M. J.; Neau, D. B.; Mitchell, C. E.; Bartlett, S. G.; Newcomer, M. E. The Structure of Human 15-Lipoxygenase-2 with a Substrate Mimic. *J. Biol. Chem.* **2014**, *289* (12), 8562–8569.

Koeduka, T.; Kajiwara, T.; Matsui, K. Cloning of Lipoxygenase Genes from a Cyanobacterium, Nostoc Punctiforme, and Its Expression in Eschelichia Coli. *Curr. Microbiol.* **2007**, *54* (4), 315–319.

Koljak, R.; Boutaud, O.; Shieh, B. H.; Samel, N.; Brash, A. R. Identification of a Naturally Occurring Peroxidase-Lipoxygenase Fusion Protein. *Science* **1997**, *277* (5334), 1994–1996.

Kolomiets, M. V; Hannapel, D. J.; Chen, H.; Tymeson, M.; Gladon, R. J. Lipoxygenase Is Involved in the Control of Potato Tuber Development. *Plant Cell* **2001**, *13* (3), 613–626.

Kozlikova, B.; Sebestova, E.; Sustr, V.; Brezovsky, J.; Strnad, O.; Daniel, L.; Bednar, D.; Pavelka, A.; Manak, M.; Bezdeka, M.; et al. CAVER Analyst 1.0: Graphic Tool for Interactive Visualization and Analysis of Tunnels and Channels in Protein Structures. *Bioinformatics* **2014**, *30* (18), 2684–2685.

Krieg, P.; Siebert, M.; Kinzig, A.; Bettenhausen, R.; Marks, F.; Fürstenberger, G. Murine 12(R)-Lipoxygenase: Functional Expression, Genomic Structure and Chromosomal Localization 1. *FEBS Lett.* **1999**, *446* (1), 142–148.

Krieg, P.; Rosenberger, S.; de Juanes, S.; Latzko, S.; Hou, J.; Dick, A.; Kloz, U.; van der Hoeven, F.; Hausser, I.; Esposito, I.; et al. Aloxe3 Knockout Mice Reveal a Function of Epidermal Lipoxygenase-3 as Hepoxilin Synthase and Its Pivotal Role in Barrier Formation. *J. Invest. Dermatol.* **2013**, *133* (1), 172–180.

Krishtalik, L. I. Effective Activation Energy of Enzymatic and Nonenzymatic Reactions. Evolution-Imposed Requirements to Enzyme Structure. *J. Theor. Biol.* **1985**, *112* (2), 251–264.

Krönke, G.; Katzenbeisser, J.; Uderhardt, S.; Zaiss, M. M.; Scholtysek, C.; Schabbauer, G.; Zarbock, A.; Koenders, M. I.; Axmann, R.; Zwerina, J.; et al. 12/15-Lipoxygenase Counteracts Inflammation and Tissue Damage in Arthritis. *J. Immunol.* **2009a**, *183* (5), 3383–3389.

Krönke, G.; Uderhardt, S.; Katzenbeisser, J.; Schett, G. The 12/15-Lipoxygenase Pathway Promotes Osteoclast Development and Differentiation. *Autoimmunity* **2009b**, *42* (4), 383–385.

Kuhn, H. Structural Basis for the Positional Specificity of Lipoxygenases. *Prostaglandins Other Lipid Mediat.* **2000**, *62* (3), 255–270.

Kuhn, H.; Wiesner, R.; Stender, H. The Formation of Products Containing a Conjugated Tetraenoic System by Pure Reticulocyte Lipoxygenase. *FEBS Lett.* **1984**, *177* (2), 2–6.

Kuhn, H.; Wiesner, R.; Alder, L.; Fitzsimmons, B. J.; Rokach, J.; Brash, A. R. Formation of Lipoxin B by the Pure Reticulocyte Lipoxygenase via Sequential Oxygenation of the Substrate. *Eur J Biochem* **1987**, *169* (3), 593–601.

Kuhn, H.; Belkner, J.; Wiesner, R.; Brash, A. R. Oxygenation of Biological Membranes by the Pure Reticulocyte Lipoxygenase. *J. Biol. Chem.* **1990**, *265* (30), 18351–18361.

Kuhn, H.; Saam, J.; Eibach, S.; Holzhütter, H. G.; Ivanov, I.; Walther, M. Structural Biology of Mammalian Lipoxygenases: Enzymatic Consequences of Targeted Alterations of the Protein Structure. *Biochem. Biophys. Res. Commun.* **2005**, *338* (1), 93–101.

Kuhn, H.; Banthiya, S.; van Leyen, K. Mammalian Lipoxygenases and Their Biological Relevance. *Biochim. Biophys. Acta - Mol. Cell Biol. Lipids* **2015**, *1851* (4), 308–330.

Kühn, H.; Salzmann-Reinhardt, U.; Ludwig, P.; Pönicke, K.; Schewe, T.; Rapoport, S. The Stoichiometry of Oxygen Uptake and Conjugated Diene Formation during the Dioxygenation of Linoleic Acid by the Pure Reticulocyte Lipoxygenase. Evidence for Aerobic Hydroperoxidase Activity. *Biochim. Biophys. Acta - Lipids Lipid Metab.* **1986**, *876* (2), 187–193.

Kühn, H.; Barnett, J.; Grunberger, D.; Baecker, P.; Chow, J.; Nguyen, B.; Bursztyn-Pettegrew, H.; Chan, H.; Sigal, E. Overexpression, Purification and Characterization of Human Recombinant 15-Lipoxygenase. *Biochim. Biophys. Acta* **1993**, *1169* (1), 80–89.

Lang, I.; Obel, C.; Porzel, A.; Heilmann, I.; Feussner, I. A Lipoxygenase with Linoleate Diol Synthase Activity from Nostoc Sp. PCC 7120. *Biochem. J* **2008**, *410*, 347–357.

Laskowski, R. A.; MacArthur, M. W.; Moss, D. S.; Thornton, J. M. PROCHECK: A Program to Check the Stereochemical Quality of Protein Structures. *J. Appl. Crystallogr.* **1993**, *26* (November), 283–291.

Lehnert, N.; Solomon, E. I. Density-Functional Investigation on the Mechanism of H-Atom Abstraction by Lipoxygenase. *J. Biol. Inorg. Chem.* **2003**, *8* (3), 294–305.

Lõhelaid, H.; Järving, R.; Valmsen, K.; Varvas, K.; Kreen, M.; Järving, I.; Samel, N. Identification of a Functional Allene Oxide Synthase-Lipoxygenase Fusion Protein in the Soft Coral Gersemia Fruticosa Suggests the Generality of This Pathway in Octocorals. *Biochim. Biophys. Acta - Gen. Subj.* **2008**, *1780* (2), 315–321.

Lovell, S. C.; Davis, I. W.; Arendall, W. B.; de Bakker, P. I. W.; Word, J. M.; Prisant, M. G.; Richardson, J. S.; Richardson, D. C. Structure Validation by Cα Geometry: Φ,ψ and Cβ Deviation. *Proteins Struct. Funct. Bioinforma.* **2003**, *50* (3), 437–450.

Lu, X.; Zhang, J.; Liu, S.; Zhang, D.; Xu, Z.; Wu, J.; Li, J.; Du, G.; Chen, J. Overproduction, Purification, and Characterization of Extracellular Lipoxygenase of Pseudomonas Aeruginosa in Escherichia Coli. *Appl. Microbiol. Biotechnol.* **2013**, *97* (13), 5793–5800.

Lu, X.; Wang, G.; Feng, Y.; Liu, S.; Zhou, X.; Du, G.; Chen, J. The N-Terminal α-Helix Domain of Pseudomonas Aeruginosa Lipoxygenase Is Required for Its Soluble Expression in Escherichia Coli but Not for Catalysis. *J. Microbiol. Biotechnol.* **2016**, *26* (10), 1701–1707.

Ludwig, P.; Holzhütter, H. G.; Colosimo, A.; Silvestrini, M. C.; Schewe, T.; Rapoport, S. M. A Kinetic Model for Lipoxygenases Based on Experimental Data with the Lipoxygenase of Reticulocytes. *Eur. J. Biochem.* **1987**, *168* (2), 325–337.

Lyczak, J. B.; Cannon, C. L.; Pier, G. B. Establishment of Pseudomonas Aeruginosa Infection: Lessons from a Versatile Opportunist. *Microbes Infect.* **2000**, *2* (9), 1051–1060.

Madden, B. P.; Kariyawasam, H.; Siddiqi, A. J.; Machin, A.; Pryor, J. A.; Hodson, M. E. Noninvasive Ventilation in Cystic Fibrosis Patients with Acute or Chronic Respiratory Failure. *Eur. Respir. J.* **2002**, *19* (2), 310–313.

Man ek-Keber, M.; Frank-Bertoncelj, M.; Hafner-Bratkovi, I.; Smole, A.; Zorko, M.; Pirher, N.; Hayer, S.; Kralj-Igli, V.; Rozman, B.; Ilc, N.; et al. Toll-like Receptor 4 Senses Oxidative Stress Mediated by the Oxidation of Phospholipids in Extracellular Vesicles. *Sci. Signal.* **2015**, *8* (381), ra60-.

Martínez-Clemente, M.; Ferré, N.; Titos, E.; Horrillo, R.; González-Périz, A.; Morán-Salvador, E.; López-Vicario, C.; Miquel, R.; Arroyo, V.; D. Funk, C.; et al. Disruption of the 12/15-Lipoxygenase Gene (Alox15) Protects Hyperlipidemic Mice from Nonalcoholic Fatty Liver Disease. *Hepatology* **2010**, *52* (6), 1980–1991.

Martinez, J. G.; Waldon, M.; Huang, Q.; Alvarez, S.; Oren, A.; Sandoval, N.; Du, M.; Zhou, F.; Zenz, A.; Lohner, K.; et al. Membrane-Targeted Synergistic Activity of Docosahexaenoic Acid and Lysozyme against Pseudomonas Aeruginosa. *Biochem. J.* **2009**, *419* (1), 193–200.

De Marzo, N.; Sloane, D. L.; Dicharry, S.; Highland, E.; Sigal, E. Cloning and Expression of an Airway Epithelial 12-Lipoxygenase. *Am. J. Physiol.* **1992**, *262* (2 Pt 1), L198-207.

McCoy, A. J.; Grosse-Kunstleve, R. W.; Adams, P. D.; Winn, M. D.; Storoni, L. C.; Read, R. J. Phaser Crystallographic Software. *J. Appl. Crystallogr.* **2007**, *40* (4), 658–674.

McIntyre, T. M. Bioactive Oxidatively Truncated Phospholipids in Inflammation and Apoptosis: Formation, Targets, and Inactivation. *Biochim. Biophys. Acta - Biomembr.* **2012**, *1818* (10), 2456–2464.

Mei, G.; Di Venere, A.; Nicolai, E.; Angelucci, C. B.; Ivanov, I.; Sabatucci, A.; Dainese, E.; Kuhn, H.; Maccarrone, M. Structural Properties of Plant and Mammalian Lipoxygenases. Temperature-Dependent Conformational Alterations and Membrane Binding Ability. *Biochemistry* **2008**, *47* (35), 9234–9242.

Mergulhão, F. J. M.; Summers, D. K.; Monteiro, G. A. Recombinant Protein Secretion in Escherichia Coli. *Biotechnol. Adv.* **2005**, *23* (3), 177–202.

Meruvu, S.; Walther, M.; Ivanov, I.; Hammarstro, S.; Fu, G.; Krieg, P. Sequence Determinants for the Reaction Specificity of Murine (12 R) -Lipoxygenase. **2005**, *280* (44), 36633–36641.

Meyer, M. P.; Tomchick, D. R.; Klinman, J. P. Enzyme Structure and Dynamics Affect Hydrogen Tunneling: The Impact of a Remote Side Chain (I553) in Soybean Lipoxygenase-1. *Proc. Natl. Acad. Sci.* **2008**, *105* (4), 1146–1151.

Mimoun, M.; Coste, T. C.; Lebacq, J.; Lebecque, P.; Wallemacq, P.; Leal, T.; Armand, M. Increased Tissue Arachidonic Acid and Reduced Linoleic Acid in a Mouse Model of Cystic Fibrosis Are Reversed by Supplemental Glycerophospholipids Enriched in Docosahexaenoic Acid. *J. Nutr.* **2009**, *139* (12), 2358–2364.

Minor, W.; Steczko, J.; Stec, B.; Otwinowski, Z.; Bolin, J. T.; Walter, R.; Axelrod, B. Crystal Structure of Soybean Lipoxygenase L-1 at 1.4 A Resolution. *Biochemistry* **1996**, *35* (33), 10687–10701.

Mosblech, A.; Feussner, I.; Heilmann, I. Oxylipins: Structurally Diverse Metabolites from Fatty Acid Oxidation. *Plant Physiol. Biochem. PPB / Société Fr. Physiol. végétale* **2009**, *47* (6), 511–517.

Mueller, U.; Förster, R.; Hellmig, M.; Huschmann, F. U.; Kastner, A.; Malecki, P.; Pühringer, S.; Röwer, M.; Sparta, K.; Steffien, M.; et al. The Macromolecular Crystallography Beamlines at BESSY II of the Helmholtz-Zentrum Berlin: Current Status and Perspectives. *Eur. Phys. J. Plus* **2015**, *130*, 141.

Murshudov, G. N.; Vagin, A. A.; Dodson, E. J. Refinement of Macromolecular Structures

by the Maximum-Likelihood Method. *Acta Crystallogr. D. Biol. Crystallogr.* **1997**, *53* (Pt 3), 240–255.

Neau, D. B.; Gilbert, N. C.; Bartlett, S. G.; Boeglin, W.; Brash, A. R.; Newcomer, M. E. The 1.85 Å Structure of an 8 R -Lipoxygenase Suggests a General Model for Lipoxygenase Product Specificity. *Biochemistry* **2009**, *48* (33), 7906–7915.

Neau, D. B.; Bender, G.; Boeglin, W. E.; Bartlett, S. G.; Brash, A. R.; Newcomer, M. E. Crystal Structure of a Lipoxygenase in Complex with Substrate: The Arachidonic Acid-Bindind Site of 8R-Lipoxygenase. *J. Biol. Chem.* **2014**, *289* (46), 31905–31913.

Neitzel, J. J. Fatty Acid Molecules: A Role in Cell Signaling. *Nat. Educ.* **2010**, *3* (9), 57.

Newie, J.; Andreou, A.; Neumann, P.; Einsle, O.; Feussner, I.; Ficner, R. Crystal Structure of a Lipoxygenase from Cyanothece Sp. May Reveal Novel Features for Substrate Acquisition. *J. Lipid Res.* **2016**, *57* (2), 276–287.

Njoroge, S. W.; Laposata, M.; Katrangi, W.; Seegmiller, A. C. DHA and EPA Reverse Cystic Fibrosis-Related FA Abnormalities by Suppressing FA Desaturase Expression and Activity. *J. Lipid Res.* **2012**, *53* (2), 257–265.

Nugteren, D. H. Arachidonate Lipoxygenase in Blood Platelets. *Biochim. Biophys. Acta - Lipids Lipid Metab.* **1975**, *380* (2), 299–307.

Nurizzo, D.; Mairs, T.; Guijarro, M.; Rey, V.; Meyer, J.; Fajardo, P.; Chavanne, J.; Biasci, J.-C. C.; McSweeney, S.; Mitchell, E. The ID23-1 Structural Biology Beamline at the ESRF. *J. Synchrotron Radiat.* **2006**, *13* (3), 227–238.

Ohira, T.; Arita, M.; Omori, K.; Recchiuti, A.; Van Dyke, T. E.; Serhan, C. N. Resolvin E1 Receptor Activation Signals Phosphorylation and Phagocytosis. *J. Biol. Chem.* **2010**, *285* (5), 3451–3461.

Oldham, M. L.; Brash, A. R.; Newcomer, M. E. Insights from the X-Ray Crystal Structure of Coral 8R-Lipoxygenase: Calcium Activation via a C2-like Domain and a Structural Basis of Product Chirality. *J. Biol. Chem.* **2005**, *280* (47), 39545–39552.

Oliver, J. D.; Colwell, R. R. Extractable Lipids of Gram-Negative Marine Bacteria: Fatty-Acid Composition. *Int. J. Syst. Bacteriol.* **1973**, *23* (4), 442–458.

Van Os, C. P.; Rijke-Schilder, G. P.; Van Halbeek, H.; Verhagen, J.; Vliegenthart, J. F. Double Dioxygenation of Arachidonic Acid by Soybean Lipoxygenase-1. Kinetics and Regio-Stereo Specificities of the Reaction Steps. *Biochim. Biophys. Acta* **1981**, *663* (1), 177–193.

Pace-Asciak, C. R. The Hepoxilins and Some Analogues: A Review of Their Biology. *Br. J. Pharmacol.* **2009**, *158* (4), 972–981.

Pallast, S.; Arai, K.; Pekcec, A.; Yigitkanli, K.; Yu, Z.; Wang, X.; Lo, E. H.; van Leyen, K. Increased Nuclear Apoptosis-Inducing Factor after Transient Focal Ischemia: A 12/15-Lipoxygenase-Dependent Organelle Damage Pathway. *J. Cereb. Blood Flow Metab.* **2010**, *30* (6), 1157–1167.

Palmblad, J.; Malmsten, C. L.; Udén, A. M.; Rådmark, O.; Engstedt, L.; Samuelsson, B. Leukotriene B4 Is a Potent and Stereospecific Stimulator of Neutrophil Chemotaxis and Adherence. *Blood* **1981**, *58* (3), 658–661.

Pekárová, M.; Kuhn, H.; Bezáková, L.; Ufer, C.; Heydeck, D. Mutagenesis of Triad Determinants of Rat Alox15 Alters the Specificity of Fatty Acid and Phospholipid Oxygenation. *Arch. Biochem. Biophys.* **2015**, *571*, 50–57.

Pistorius, E. K.; Axelrod, B. Iron , an Essential Component of Lipoxygenase. **1974**, *249* (1973), 3183–3186.

Porta, H.; Rocha-Sosa, M. Lipoxygenase in Bacteria: A Horizontal Transfer Event?

Microbiology **2001**, *147* (Pt 12), 3199–3200.

Porta, H.; Rocha-Sosa, M. Plant Lipoxygenases. Physiological and Molecular Features. *Plant Physiol.* **2002**, *130* (1), 15–21.

Powell, W. S.; Rokach, J. The Eosinophil Chemoattractant 5-Oxo-ETE and the OXE Receptor. *Prog. Lipid Res.* **2013**, *52* (4), 651–665.

Rådmark, O.; Samuelsson, B. Regulation of the Activity of 5-Lipoxygenase, a Key Enzyme in Leukotriene Biosynthesis. *Biochem. Biophys. Res. Commun.* **2010**, *396* (1), 105–110.

Rådmark, O.; Werz, O.; Steinhilber, D.; Samuelsson, B. 5-Lipoxygenase: Regulation of Expression and Enzyme Activity. *Trends Biochem. Sci.* **2007**, *32* (7), 332–341.

Rapoport, S.; Gerischer-Mothes, W. Biochemical Preliminaries in the Maturation of Erythrocytes; an Inhibitor of the Succinic Oxidase System in the Reticulocytes. *Hoppe. Seylers. Z. Physiol. Chem.* **1955**, *302* (4–6), 167–178.

Rapoport, S. M.; Schewe, T.; Wiesner, R.; Halangk, W.; Ludwig, P.; Janicke-Höhne, M.; Tannert, C.; Hiebsch, C.; Klatt, D. The Lipoxygenase of Reticulocytes. Purification, Characterization and Biological Dynamics of the Lipoxygenase; Its Identity with the Respiratory Inhibitors of the Reticulocyte. *Eur. J. Biochem.* **1978**, *96* (3), 545–560.

Richardson, T.; Tappel, A. L.; Gruger, E. H. Essential Fatty Acids in Mitochondria. *Arch. Biochem. Biophys.* **1961**, *94*, 1–6.

Ringholz, F. C.; Buchanan, P. J.; Clarke, D. T.; Millar, R. G.; McDermott, M.; Linnane, B.; Harvey, B. J.; McNally, P.; Urbach, V. Reduced 15-Lipoxygenase 2 and Lipoxin A4/leukotriene B4 Ratio in Children with Cystic Fibrosis. *Eur. Respir. J.* **2014**, *44* (2), 394–404.

Robins, S. J.; Patton, G. M. Separation of Phospholipid Molecular Species by High Performance Liquid Chromatography: Potentials for Use in Metabolic Studies. *J. Lipid Res.* **1986**, *27* (2), 131–139.

Rodriguez, R.; Chinea, G.; Lopez, N.; Pons, T.; Vriend, G. Homology Modeling, Model and Software Evaluation: Three Related Resources. *Bioinformatics* **1998**, *14* (6), 523–528.

Romano, M. Lipoxin and Aspirin-Triggered Lipoxins. *ScientificWorldJournal.* **2010**, *10*, 1048–1064.

Sachs-Olsen, C.; Sanak, M.; Lang, A. M.; Gielicz, A.; Mowinckel, P.; Lødrup Carlsen, K. C.; Carlsen, K.-H.; Szczeklik, A. Eoxins: A New Inflammatory Pathway in Childhood Asthma. *J. Allergy Clin. Immunol.* **2010**, *126* (4), 859–867.e9.

Saravitz, D. M.; Siedow, J. N. The Lipoxygenase Isozymes in Soybean [Glycine Max (L.) Merr.] Leaves.Changes during Leaf Development, after Wounding, and Following Reproductive Sink Removal. *Plant Physiol.* **1995**, *107* (2), 535–543.

Savari, S.; Vinnakota, K.; Zhang, Y.; Sjölander, A. Cysteinyl Leukotrienes and Their Receptors: Bridging Inflammation and Colorectal Cancer. *World J. Gastroenterol.* **2014**, *20* (4), 968–977.

Schafer, A. I. Effects of Nonsteroidal Antiinflammatory Drugs on Platelet Function and Systemic Hemostasis. *J. Clin. Pharmacol.* **1995**, *35* (3), 209–219.

Schewe, T.; Halangk, W.; Hiebsch, C.; Rapoport, S. M. A Lipoxygenase in Rabbit Reticulocytes Which Attacks Phospholipids and Intact Mitochondria. *FEBS Lett.* **1975**, *60* (1), 149–152.

Schewe, T.; Halangk, W.; Hiebsch, C.; Rapoport, S. Degradation of Mitochondria by Cytosolic Factors in Reticulocytes. *Acta Biol. Med. Ger.* **1977**, *36* (3–4), 363–372.

Schewe, T.; Wiesner, R.; Rapoport, S. M. Lipoxygenase from Rabbit Reticulocytes.

Methods Enzymol. **1981**, *71 Pt C*, 430–441.

Schewe, T.; Rapoport, S. M.; Kühn, H. Enzymology and Physiology of Reticulocyte Lipoxygenase: Comparison with Other Lipoxygenases. *Adv. Enzymol. Relat. Areas Mol. Biol.* **1986a**, *58*, 191–272.

Schewe, T.; Rapoport, S. M.; Kühn, H. Enzymology and Physiology of Reticulocyte Lipoxygenase: Comparison with Other Lipoxygenases. *Adv. Enzymol. Relat. Areas Mol. Biol.* **1986b**, *58*, 191–272.

Schneider, C.; Pratt, D. A.; Porter, N. A.; Brash, A. R. Control of Oxygenation in Lipoxygenase and Cyclooxygenase Catalysis. *Chem. Biol.* **2007**, *14* (5), 473–488.

Schroepfer, G. J.; Bloch, K. The Stereospecific Conversion of Stearic Acid to Oleic Acid. *J. Biol. Chem.* **1965**, *240*, 54–63.

Segraves, E. N.; Chruszcz, M.; Neidig, M. L.; Ruddat, V.; Zhou, J.; Wecksler, A. T.; Minor, W.; Solomon, E. I.; Holman, T. R. Kinetic, Spectroscopic, and Structural Investigations of the Soybean Lipoxygenase-1 First-Coordination Sphere Mutant, Asn694Gly. *Biochemistry* **2006**, *45* (34), 10233–10242.

Senger, T.; Wichard, T.; Kunze, S.; Göbel, C.; Lerchl, J.; Pohnert, G.; Feussner, I. A Multifunctional Lipoxygenase with Fatty Acid Hydroperoxide Cleaving Activity from the Moss Physcomitrella Patens. *J. Biol. Chem.* **2005**, *280* (9), 7588–7596.

Serhan, C. N.; Petasis, N. A. Resolvins and Protectins in Inflammation Resolution. *Chem. Rev.* **2011**, *111* (10), 5922–5943.

Serhan, C. N.; Dalli, J.; Karamnov, S.; Choi, A.; Park, C.-K.; Xu, Z.-Z.; Ji, R.-R.; Zhu, M.; Petasis, N. A. Macrophage Proresolving Mediator Maresin 1 Stimulates Tissue Regeneration and Controls Pain. *FASEB J.* **2012**, *26* (4), 1755–1765.

Shimahara, K. Peroxidation of Soy Bean Oil by Lipoxygenase- Forming Bacteria (Gram-Negative, Rod-Shaped) Isolated from Garbage. *Kogio Kagaku Zasshi* **1964**, *67*, 1164–1168.

Shimahara, K.; Hashizume, Y. Properties of a Lipoxygenase-like Enzyme Produced by Pseudomonas Aeruginosa Strain A-4. *J. Ferment. Technol.* **1973**, *51*, 183–189.

Shin, S. Y.; Bajpai, V. K.; Kim, H. R.; Kang, S. C. Antibacterial Activity of Bioconverted Eicosapentaenoic (EPA) and Docosahexaenoic Acid (DHA) against Foodborne Pathogenic Bacteria. *Int. J. Food Microbiol.* **2007**, *113* (2), 233–236.

Siebert, M.; Krieg, P.; Lehmann, W. D.; Marks, F.; Fürstenberger, G. Enzymic Characterization of Epidermis-Derived 12-Lipoxygenase Isoenzymes. *Biochem. J.* **2001**, *355* (Pt 1), 97–104.

Siedow, J. N. Plant Lipoxygenase: Structure and Function. *Annu. Rev. Plant Physiol. Plant Mol. Biol.* **1991**, *42* (1), 145–188.

Sigal, E.; Craik, C. S.; Highland, E.; Grunberger, D.; Costello, L. L.; Dixon, R. A.; Nadel, J. A. Molecular Cloning and Primary Structure of Human 15-Lipoxygenase. *Biochem. Biophys. Res. Commun.* **1988**, *157* (2), 457–464.

Singh, A.; Upadhyay, V.; Upadhyay, A. K.; Singh, S. M.; Panda, A. K. Protein Recovery from Inclusion Bodies of Escherichia Coli Using Mild Solubilization Process. *Microb. Cell Fact.* **2015**, *14* (1), 41.

Singh, R. K.; Tandon, R.; Dastidar, S. G.; Ray, A. A Review on Leukotrienes and Their Receptors with Reference to Asthma. *J. Asthma* **2013**, *50* (9), 922–931.

Skrzypczak-Jankun, E.; Amzel, L. M.; Kroa, B. A.; Funk, M. O. Structure of Soybean Lipoxygenase L3 and a Comparison with Its L1 Isoenzyme. *Proteins* **1997**, *29* (1), 15–31.

Skrzypczak-Jankun, E.; Bross, R. A.; Carroll, R. T.; Dunham, W. R.; Funk, M. O. Three-

Dimensional Structure of a Purple Lipoxygenase. *J. Am. Chem. Soc.* **2001**, *123* (44), 10814–10820.

Skrzypczak-Jankun, E.; Zhou, K.; Jankun, J. Inhibition of Lipoxygenase by (-)-Epigallocatechin Gallate: X-Ray Analysis at 2.1 A Reveals Degradation of EGCG and Shows Soybean LOX-3 Complex with EGC Instead. *Int. J. Mol. Med.* **2003a**, *12* (4), 415–420.

Skrzypczak-Jankun, E.; Zhou, K.; McCabe, N. P.; Selman, S. H.; Jankun, J. Structure of Curcumin in Complex with Lipoxygenase and Its Significance in Cancer. *Int. J. Mol. Med.* **2003b**, *12* (1), 17–24.

Skrzypczak-Jankun, E.; Borbulevych, O. Y.; Jankun, J. Soybean Lipoxygenase-3 in Complex with 4-Nitrocatechol. *Acta Crystallogr. Sect. D Biol. Crystallogr.* **2004**, *60* (3), 613–615.

Sloane, D. L.; Leung, R.; Craik, C. S.; Sigal, E. A Primary Determinant for Lipoxygenase Positional Specificity. *Nature* **1991a**, *354* (6349), 149–152.

Sloane, D. L.; Dixon, R. A.; Craik, C. S.; Sigal, E. Expression of Cloned Human 15-Lipoxygenase in Eukaryotic and Prokaryotic Systems. *Adv. Prostaglandin. Thromboxane. Leukot. Res.* **1991b**, *21A*, 25–28.

Sloane, D. L.; Leung, R.; Barnett, J.; Craik, C. S.; Sigal, E. Conversion of Human 15-Lipoxygenase to an Efficient 12-Lipoxygenase: The Side-Chain Geometry of Amino Acids 417 and 418 Determine Positional Specificity. *Protein Eng.* **1995**, *8* (3), 275–282.

Soberman, R. J.; Harper, T. W.; Betteridge, D.; Lewis, R. A.; Austen, K. F. Characterization and Separation of the Arachidonic Acid 5-Lipoxygenase and Linoleic Acid Omega-6 Lipoxygenase (Arachidonic Acid 15-Lipoxygenase) of Human Polymorphonuclear Leukocytes. *J. Biol. Chem.* **1985**, *260* (7), 4508–4515.

Spector, A. A.; Kim, H.-Y. Cytochrome P450 Epoxygenase Pathway of Polyunsaturated Fatty Acid Metabolism. *Biochim. Biophys. Acta - Mol. Cell Biol. Lipids* **2015**, *1851* (4), 356–365.

Su, C.; Oliw, E. H. Manganese Lipoxygenase. Purification and Characterization. *J. Biol. Chem.* **1998**, *273* (21), 13072–13079.

Sumner, B.; Sumner, J. Oxidation by Carotene Oxidase. *J. Biol. Chem.* **1940**, *134* (1935), 531–533.

Sun, D.; Funk, C. D. Disruption of 12/15-Lipoxygenase Expression in Peritoneal Macrophages. Enhanced Utilization of the 5-Lipoxygenase Pathway and Diminished Oxidation of Low Density Lipoprotein. *J. Biol. Chem.* **1996**, *271* (39), 24055–24062.

Suzuki, H.; Kishimoto, K.; Yoshimoto, T.; Yamamoto, S.; Kanai, F.; Ebina, Y.; Miyatake, A.; Tanabe, T. Site-Directed Mutagenesis Studies on the Iron-Binding Domain and the Determinant for the Substrate Oxygenation Site of Porcine Leukocyte Arachidonate 12-Lipoxygenase. *Biochim. Biophys. Acta* **1994**, *1210* (3), 308–316.

Takahashi, Y.; Ueda, N.; Yamamoto, S. Two Immunologically and Catalytically Distinct Arachidonate 12-Lipoxygenases of Bovine Platelets and Leukocytes. *Arch. Biochem. Biophys.* **1988**, *266* (2), 613–621.

Takahashi, Y.; Glasgow, W. C.; Suzuki, H.; Taketani, Y.; Yamamoto, S.; Anton, M.; Kühn, H.; Brash, A. R. Investigation of the Oxygenation of Phospholipids by the Porcine Leukocyte and Human Platelet Arachidonate 12-Lipoxygenases. *Eur. J. Biochem.* **1993**, *218* (1), 165–171.

Tappel, A. L.; Lundberg, W. O.; Boyer, P. D. Effect of Temperature and Antioxidants

upon the Lipoxidase-Catalyzed Oxidation of Sodium Linoleate. *Arch. Biochem. Biophys.* **1953**, *42* (2), 293–304.

Theorell, H.; Holman, R. T.; Akeson, A. Crystalline Lipoxidase. *Acta Chem. Scand.* **1947**, *1* (6), 571–576.

Tranbarger, T. J.; Franceschi, V. R.; Hildebrand, D. F.; Grimes, H. D. The Soybean 94-Kilodalton Vegetative Storage Protein Is a Lipoxygenase That Is Localized in Paraveinal Mesophyll Cell Vacuoles. *Plant Cell* **1991**, *3* (9), 973–987.

Trudel, S.; Kelly, M.; Fritsch, J.; Nguyen-Khoa, T.; Thérond, P.; Couturier, M.; Dadlez, M.; Debski, J.; Touqui, L.; Vallée, B.; et al. Peroxiredoxin 6 Fails to Limit Phospholipid Peroxidation in Lung from Cftr-Knockout Mice Subjected to Oxidative Challenge. *PLoS One* **2009**, *4* (6), e6075.

Ueda, N.; Yamamoto, S.; Oates, J. A.; Brash, A. R. Stereoselective Hydrogen Abstraction in Leukotriene A4 Synthesis by Purified 5-Lipoxygenase of Porcine Leukocytes. *Prostaglandins* **1986**, *32* (1), 43–48.

Ueda, N.; Yokoyama, C.; Yamamoto, S.; Fitzsimmons, B. J.; Rokach, J.; Oates, J. A.; Brash, A. R. Lipoxin Synthesis by Arachidonate 12-Lipoxygenase Purified from Porcine Leukocytes. *Biochem. Biophys. Res. Commun.* **1987**, *149* (3), 1063–1069.

Urbach, V.; Higgins, G.; Buchanan, P.; Ringholz, F. The Role of Lipoxin A4 in Cystic Fibrosis Lung Disease. *Comput. Struct. Biotechnol. J.* **2013**, *6* (7), 1–5.

Vagin, A. A.; Steiner, R. A.; Lebedev, A. A.; Potterton, L.; McNicholas, S.; Long, F.; Murshudov, G. N. REFMAC 5 Dictionary: Organization of Prior Chemical Knowledge and Guidelines for Its Use. *Acta Crystallogr. Sect. D Biol. Crystallogr.* **2004**, *60* (12), 2184–2195.

Vaguine, A. A.; Richelle, J.; Wodak, S. J. SFCHECK: A Unified Set of Procedures for Evaluating the Quality of Macromolecular Structure-Factor Data and Their Agreement with the Atomic Model. *Acta Crystallogr. D. Biol. Crystallogr.* **1999**, *55*, 191–205.

Vahedi-Faridi, A.; Brault, P.-A.; Shah, P.; Kim, Y.-W.; Dunham, W. R.; Funk, M. O. Interaction between Non-Heme Iron of Lipoxygenases and Cumene Hydroperoxide: Basis for Enzyme Activation, Inactivation, and Inhibition. *J. Am. Chem. Soc.* **2004**, *126* (7), 2006–2015.

Vance, R. E.; Hong, S.; Gronert, K.; Serhan, C. N.; Mekalanos, J. J. The Opportunistic Pathogen Pseudomonas Aeruginosa Carries a Secretable Arachidonate 15-Lipoxygenase. *Proc. Natl. Acad. Sci. U. S. A.* **2004**, *101* (7), 2135–2139.

Verrière, V.; Higgins, G.; Al-Alawi, M.; Costello, R. W.; McNally, P.; Chiron, R.; Harvey, B. J.; Urbach, V. Lipoxin A4 Stimulates Calcium-Activated Chloride Currents and Increases Airway Surface Liquid Height in Normal and Cystic Fibrosis Airway Epithelia. *PLoS One* **2012**, *7* (5), e37746.

Vidal-Mas, J.; Busquets, M.; Manresa, A.; Busquets, M.; Manresa, A. Cloning and Expression of a Lipoxygenase from Pseudomonas Aeruginosa 42A2. *Antonie Van Leeuwenhoek* **2005**, *87* (3), 245–251.

Vogel, R.; Jansen, C.; Roffeis, J.; Reddanna, P.; Forsell, P.; Claesson, H.-E.; Kuhn, H.; Walther, M. Applicability of the Triad Concept for the Positional Specificity of Mammalian Lipoxygenases. *J. Biol. Chem.* **2010**, *285* (8), 5369–5376.

Walther, M.; Hofheinz, K.; Vogel, R.; Roffeis, J.; Kühn, H. The N-Terminal β-Barrel Domain of Mammalian Lipoxygenases Including Mouse 5-Lipoxygenase Is Not Essential for Catalytic Activity and Membrane Binding but Exhibits Regulatory Functions. *Arch. Biochem. Biophys.* **2011**, *516* (1), 1–9.

Wasilewicz, M. P.; Kołodziej, B.; Bojułko, T.; Kaczmarczyk, M.; Sulzyc-Bielicka, V.; Bielicki, D.; Ciepiela, K. Overexpression of 5-Lipoxygenase in Sporadic Colonic Adenomas and a Possible New Aspect of Colon Carcinogenesis. *Int. J. Colorectal Dis.* **2010**, *25* (9), 1079–1085.

Watanabe, T.; Haeggström, J. Z. Rat 12-Lipoxygenase: Mutations of Amino Acids Implicated in the Positional Specificity of 15- and 12-Lipoxygenases. *Biochem. Biophys. Res. Commun.* **1993**, *192* (3), 1023–1029.

Watanabe, T.; Medina, J. F.; Haeggström, J. Z.; Rådmark, O.; Samuelsson, B. Molecular Cloning of a 12-Lipoxygenase cDNA from Rat Brain. *Eur. J. Biochem.* **1993**, *212* (2), 605–612.

Watson, H. Biological Membranes. *Essays Biochem.* **2015**, *59*, 43–69.

Weber, H.; Chételat, A.; Caldelari, D.; Farmer, E. E. Divinyl Ether Fatty Acid Synthesis in Late Blight-Diseased Potato Leaves. *Plant Cell* **1999**, *11* (3), 485–494.

Wecksler, A. T.; Kenyon, V.; Deschamps, J. D.; Holman, T. R. Substrate Specificity Changes for Human Reticulocyte and Epithelial 15-Lipoxygenases Reveal Allosteric Product Regulation. *Biochemistry* **2008**, *47* (28), 7364–7375.

Wennman, A.; Jerneren, F.; Hamberg, M.; Oliw, E. H. Catalytic Convergence of Manganese and Iron Lipoxygenases by Replacement of a Single Amino Acid. *J. Biol. Chem.* **2012**, *287* (38), 31757–31765.

Wennman, A.; Oliw, E. H.; Karkehabadi, S.; Chen, Y. Crystal Structure of Manganese Lipoxygenase of the Rice Blast Fungus Magnaporthe Oryzae. *J. Biol. Chem.* **2016**, *291* (15), 8130–8139.

Winn, M. D.; Isupov, M. N.; Murshudov, G. N. Use of TLS Parameters to Model Anisotropic Displacements in Macromolecular Refinement. *Acta Crystallogr. Sect. D Biol. Crystallogr.* **2001**, *57* (1), 122–133.

Winn, M. D.; Ballard, C. C.; Cowtan, K. D.; Dodson, E. J.; Emsley, P.; Evans, P. R.; Keegan, R. M.; Krissinel, E. B.; Leslie, A. G. W.; McCoy, A.; et al. Overview of the CCP4 Suite and Current Developments. *Acta Crystallogr. Sect. D Biol. Crystallogr.* **2011**, *67* (4), 235–242.

Worlitzsch, D.; Tarran, R.; Ulrich, M.; Schwab, U.; Cekici, A.; Meyer, K. C.; Birrer, P.; Bellon, G.; Berger, J.; Weiss, T.; et al. Effects of Reduced Mucus Oxygen Concentration in Airway Pseudomonas Infections of Cystic Fibrosis Patients. *J. Clin. Invest.* **2002**, *109* (3), 317–325.

Xu, S.; Mueser, T. C.; Marnett, L. J.; Funk, M. O. Crystal Structure of 12-Lipoxygenase Catalytic-Domain-Inhibitor Complex Identifies a Substrate-Binding Channel for Catalysis. *Structure* **2012**, *20* (9), 1490–1497.

Yamamoto, S.; Ueda, N.; Yokoyama, C.; Fitzsimmons, B. J.; Rokach, J.; Oates, J. A.; Brash, A. R. Lipoxin Syntheses by Arachidonate 12- and 5-Lipoxygenases Purified from Porcine Leukocytes. *Adv. Exp. Med. Biol.* **1988**, *229*, 15–26.

Yamamoto, S.; Juranek, I.; Suzuki, H. Affinities of Mammalian Arachidonate Oxygenases for Molecular Oxygen. *Int. Congr. Ser.* **2002**, *1233* (September), 337–342.

Yokomizo, T. Leukotriene B4 Receptors: Novel Roles in Immunological Regulations. *Adv. Enzyme Regul.* **2011**, *51* (1), 59–64.

Yokoyama, C.; Shinjo, F.; Yoshimoto, T.; Yamamoto, S.; Oates, J. A.; Brash, A. R. Arachidonate 12-Lipoxygenase Purified from Porcine Leukocytes by Immunoaffinity Chromatography and Its Reactivity with Hydroperoxyeicosatetraenoic Acids. *J. Biol. Chem.* **1986**, *261* (35), 16714–16721.

Yoo, S.; Lim, J. Y.; Hwang, S. W. Resolvins: Endogenously-Generated Potent Painkilling

Substances and Their Therapeutic Perspectives. *Curr. Neuropharmacol.* **2013**, *11* (6), 664–676.

Yoshimoto, T.; Suzuki, H.; Yamamoto, S.; Takai, T.; Yokoyama, C.; Tanabe, T. Cloning and Sequence Analysis of the cDNA for Arachidonate 12-Lipoxygenase of Porcine Leukocytes. *Proc. Natl. Acad. Sci. U. S. A.* **1990**, *87* (6), 2142–2146.

Youn, B.; Sellhorn, G. E.; Mirchel, R. J.; Gaffney, B. J.; Grimes, H. D.; Kang, C. Crystal Structures of Vegetative Soybean Lipoxygenase VLX-B and VLX-D, and Comparisons with Seed Isoforms LOX-1 and LOX-3. *Proteins Struct. Funct. Bioinforma.* **2006**, *65* (4), 1008–1020.

Zhao, L.; Funk, C. D. Lipoxygenase Pathways in Atherogenesis. *Trends Cardiovasc. Med.* **2004**, *14* (5), 191–195.

Zheng, Y.; Boeglin, W. E.; Schneider, C.; Brash, A. R.; Lang, I.; Obel, C.; Porzel, A.; Heilmann, I.; Feussner, I. A 49-kDa Mini-Lipoxygenase from Anabaena Sp. PCC 7120 Retains Catalytically Complete Functionality. *J. Biol. Chem.* **2008**, *410* (8), 347–357.

Zimmerman, D. C.; Vick, B. A. Lipoxygenase in Chlorella Pyrenoidosa. *Lipids* **1973**, *8* (5), 264–266.

8. LIST OF PUBLICATIONS

Published articles/reviews

Kalms, J.; **Banthiya, S**.; Yoga, E. G.; Hamberg, M.; Holzhutter, H.-G.; Kuhn, H.; Scheerer, P. The Crystal Structure of Pseudomonas Aeruginosa Lipoxygenase Ala420Gly Mutant Explains the Improved Oxygen Affinity and the Altered Reaction Specificity. *Biochim. Biophys. Acta - Mol. Cell Biol. Lipids* **2017**, DOI: 10.1016/j.bbalip.2017.01.003.

Banthiya, S.; Kalms, J.; Yoga, E. G.; Ivanov, I.; Carpena, X.; Hamberg, M.; Kuhn, H.; Scheerer, P. Structural and Functional Basis of Phospholipid Oxygenase Activity of Bacterial Lipoxygenase from Pseudomonas Aeruginosa. *Biochim. Biophys. Acta - Mol. Cell Biol. Lipids* **2016**, *1861* (11), 1681–1692.

Banthiya, S.; Pekárová, M.; Kuhn, H.; Heydeck, D. Secreted Lipoxygenase from Pseudomonas Aeruginosa Exhibits Biomembrane Oxygenase Activity and Induces Hemolysis in Human Red Blood Cells. *Arch. Biochem. Biophys.* **2015**, *584*, 116–124.

Kuhn, H.; **Banthiya, S**.; van Leyen, K. Mammalian Lipoxygenases and Their Biological Relevance. *Biochim. Biophys. Acta* **2015**, *1851* (4), 308–330.

Articles in preparation

Banthiya, S.; Aldrovandi, M.; O'Donnell, V. B.; Kalms, J.; Yoga, E. G; Scheerer, P.; Heydeck, D.; Kuhn, H. Structural identification of the endogenous ligand of *Pseudomonas aeruginosa* lipoxygenase

Aldrovandi, M.; **Banthiya, S.**; O'Donnell, V. B.; Heydeck, D.; Kuhn, H. Lipidomic analysis of oxidized phospholipids generated in human erythrocytes when interacted with *Pseudomonas aeruginosa* lipoxygenase

<u>Poster presentations</u>

Expression and Characterization of Lipoxygenase Isoforms from Pseudomonas aeruginosa. Investigations into the Biological Role of this Enzyme for the Opportunistic Pathogen. **<u>Banthiya S.</u>**, Reddanna P. and Kühn H. (International Conference on Recent Advances in Research and Treatment of Human Diseases, January 2015, Hyderabad, India)

Expression and Characterization of Lipoxygenase Isoforms from Pseudomonas aeruginosa. **<u>Banthiya S.</u>**, Heydeck D., Kalms J., Scheerer P. and Kühn H (40th FEBS conference – The Biochemical Basis of Life 2015, July 2015, Berlin, Germany)

Structural and Functional Characterization of the Secreted Lipoxygenase from Pseudomonas aeruginosa. **<u>Banthiya S.</u>**, Heydeck D., Kalms J., Scheerer P. and Kühn H. (14th International conference - Bioactive Lipids in Cancer, Inflammation and related diseases, July 2015, Budapest, Hungary)

Structural and functional characterization of Pseudomonas aeruginosa lipoxygenase.Investigations into the Biological Role of this Enzyme for the Opportunistic Pathogen. **<u>Banthiya S.</u>**, Heydeck D., Kalms J., Scheerer P. and Kühn H (American Society of Microbiology Conference on Pseudomonas, September, 2015, Washington D.C., USA)

Potential role of pathogen lipoxygenase for Pseudomonas aeruginosa infections. **<u>Banthiya S.</u>**, Heydeck D., Kalms J., Yoga E.G., Scheerer P. and Kühn H. (6th European Workshop on Lipid Mediators, September 2016, Frankfurt, Germany)

9. CURRICULUM VITAE

For reasons of data protection, the curriculum vitae is not published in the electronic version

For reasons of data protection, the curriculum vitae is not published in the electronic version

10. APPENDIX

Primers

Val189Arg up – CGG GTC GGC CTG CTG **AGA** GAC GAC ATC CTC
Val189Arg do – GAG GAT GTC GTC **TCT** CAG CAG GCC GAC CCG

Val189Tyr up – CGG GTC GGC CTG CTG **TAC** GTC GAC GAC ATC
Val189Tyr do – GAT GTC GTC GAC **GTA** CAG CAG GCC GAC CCG

Glu369Ala up – CAG GTC GCC GAG **GCG** AAC TAC CAC GAG
Glu369Ala do – CTC GTG GTA GTT **CGC** CTC GGC GAC CTG

Glu373Asp up – GAG AAC TAC CAC **GAC** ATG TTC GTC CAC CTG
Glu373Asp do – CAG GTG GAC GAA CAT **GTC** GTG GTA GTT CTC

Glu373Leu up – GAG AAC TAC CAC **CTG** ATG TTC GTC CAC CTG
Glu373Leu do – CAG GTG GAC GAA CAT **CAG** GTG GTA GTT CTC

Met374Ala up – GAG AAC TAC CAC GAG **GCG** TTC GTC CAC CTG
Met374Ala do – CAG GTG GAC GAA **CGC** CTC GTG GTA GTT CTC

Leu378Phe up – GAG ATG TTC GTC CAC **TTC** GCC CAG ACC CAC
Leu378Phe do – GTG GGT CTG GGC **GAA** GTG GAC GAA CAT CTC

Leu378Tyr up – GAG ATG TTC GTC CAC **TAC** GCC CAG ACC CAC
Leu378Tyr do – GTG GGT CTG GGC **GTA** GTG GAC GAA CAT CTC

Ala420Gly up – TTC ATC AAC GAG GGG **GGG** GCG CGG ATC CTG
Ala420Gly do – CAG GAT CCG CGC **CCC** CCC CTC GTT GAT GAA

Leu425Phe up – GCG CGG ATC CTG **TTC** CCC AGC GCG GGC TTC
Leu425Phe do – GAA GCC CGC GCT GGG **GAA** CAG GAT CCG CGC

Leu425Tyr up – GCG CGG ATC CTG **TAC** CCC AGC GCG GGC TTC
Leu425Tyr do – GAA GCC CGC GCT GGG **GTA** CAG GAT CCG CGC

Ile431Ala up – CCC AGC GCG GGC TTC **GCC** GAC GTG ATG TTC
Ile431Ala do – GAA CAT CAC GTC **GGC** GAA GCC CGC GCT GGG

Ile431Glu up – CCC AGC GCG GGC TTC **GAA** GAC GTG ATG TTC
Ile431Glu do – GAA CAT CAC GTC **TTC** GAA GCC CGC GCT GGG

Ile431Phe up – CCC AGC GCG GGC TTC **TTC** GAC GTG ATG TTC
Ile431Phe do – GAA CAT CAC GTC **GAA** GAA GCC CGC GCT GGG

Ile431Tyr up – CCC AGC GCG GGC TTC **TAC** GAC GTG ATG TTC
Ile431Tyr do – GAA CAT CAC GTC **GTA** GAA GCC CGC GCT GGG

Met434Ala up – GGC TTC ATC GAC GTG **GCG** TTC GCC GCG CCG
Met434Ala do – CGG CGC GGC GAA **CGC** CAC GTC GAT GAA GCC

Met434Val up – GGC TTC ATC GAC GTG **GTG** TTC GCC GCG CCG
Met434Val do – CGG CGC GGC GAA **CAC** CAC GTC GAT GAA GCC

Phe435Ala up – TTC ATC GAC GTG ATG **GCC** GCC GCG CCG ATC
Phe435Ala do – GAT CGG CGC GGC **GGC** CAT CAC GTC GAT GAA

Phe435Leu up – TTC ATC GAC GTG ATG **TTA** GCC GCG CCG ATC
Phe435Leu do – GAT CGG CGC GGC **TAA** CAT CAC GTC GAT GAA

Met434Val+Phe435Leu up – GGC TTC ATC GAC GTG **GTG TTA** GCC GCG
CCG ATC CAG
Met434Val+Phe435Leu do – CTG GAT CGG CGC GGC **TAA CAC** CAC GTC
GAT GAA GCC

Glu604Tyr+Lys605His up – CTG GTG GCG CTG **TAC CAC** GTG AAC ATC TAT

Glu604Tyr+Lys605His do – ATA GAT GTT CAC **GTG GTA** CAG CGC CAC CAG

Tyr609Ala up – GAG AAG GTG AAC ATC **GCT** CAC CTG CTC GGT

Tyr609Ala do – ACC GAG CAG GTG **AGC** GAT GTT CAC CTT CTC

Leu612Val up – ATC TAT CAC CTG **GTC** GGT TCG GTC TAC

Leu612Val do – GTA GAC CGA ACC **GAC** CAG GTG ATA GAT